SCALE-UP AND CONTROL OF A MULTI-COMPONENT EMULSION POLYMERIZATION SYSTEM

by

JACOBUS PETRUS THERON

Thesis submitted in partial fulfilment of the requirements for the degree of
Master of Science in Engineering
at the
University of Stellenbosch

Supervisor:
Prof. J.H. Knoetze
Department of Chemical Engineering

Stellenbosch
January 2000

DECLARATION

I declare that this thesis is my own original work, except where specifically acknowledged in the text. Neither the present thesis nor any part thereof, has been submitted previously at any other university.

J.P. THERON

30 November 1999

ABSTRACT

A new emulsion (code name: NW 120) has been developed by Plascon on laboratory scale, for application in the paint industry. It is an environmentally friendly emulsion in which no coalescent solvent is used. It also has a core-shell morphology. Research was undertaken to scale-up (industrialize) the emulsion polymerization of NW 120.

The use of a suitable pilot plant was investigated. An available bench-scale pilot plant (RC1, Mettler Toledo) was found to be very expensive. The reactors were very small (≈1.8 l) and the reactor set-ups (reactor, baffles and stirrer configuration) were not similar to the industrial size reactors used by Plascon.

A fully computer controlled bench-scale pilot plant was subsequently designed and built at a fraction of the cost of the commercially available set-up. The reactor (5 l) was a scale-down replica (geometrically similar) of the industrial size reactors used by Plascon. The reactor was designed to also serve as a calorimeter.

Very good control was achieved over the reaction temperature and addition rates of the monomers and catalyst. Heat loss and heat capacity models were derived for a variation in the reaction temperature between 82.5 – 87.5 ^{0}C in order to perform accurate energy balances (calorimeter) around the reactor. The accuracy of the calorimeter was verified at a reaction temperature of 85 ^{0}C, by measuring the heat that evolved when a sodium hydroxide solution was diluted with water. The accuracy of the calorimeter was found to be extremely good.

The pilot plant was commissioned with an industrially manufactured emulsion (code name: AE 446), well known to Plascon. The results obtained in the pilot plant reactor were very similar to those obtained for the full-scale manufacturing of AE 446. It was determined that if geometrical similarity between the pilot plant reactor and the industrial size reactor is preserved and if the correct process conditions (stirring speed, reaction temperature and addition rates of the monomers/catalyst) are maintained, then the direct scale-up of the production of NW 120, from bench-scale to full-scale, would be possible.

The reaction conditions were varied over a wide range, in order to find the optimum process conditions.

The stirring speed was varied between 150 – 550 rpm. Shear sensitivity was observed at stirring speeds of 450 rpm and higher. The measured physical properties at 550 rpm were found to be unacceptable. The optimum stirring speed for the desired particle size and viscosity was found to lie between 150 rpm and 250 rpm.

The reaction temperature was varied between 70 and 90 ^{0}C. The optimum reaction temperature was found to lie between 80 and 90 ^{0}C. It was possible to successfully reduce the monomer addition time, and hence the reaction times, by increasing the addition rate of the monomers/catalyst, from 4 h to 2 $\frac{1}{2}$ h.

The method developed by Klein et al. (1996), for the scale-up of the stirring speed of emulsion polymerization reactions was used to determine the equivalent full-scale stirring speed.

The scale-up of NW 120 was subsequently conducted at 85 ^{0}C, at a stirring speed of 35 rpm and the monomers/catalyst were added over a period of 4 h. The use of reduced reaction times were not considered in the first scale-up run since at that stage it was not clear whether the heat removal capability of the industrial size reactor would be adequate to cope with the increase in the evolved heat, associated with an increase in the addition rates of the monomers/catalyst.

Very good results were obtained. The measured physical properties of NW 120 produced in the industrial size reactor were found to be almost exactly the same as in the pilot plant reactor.

OPSOMMING

'n Nuwe emulsie (kode naam NW 120) is deur Plascon op laboratorium skaal ontwikkel, vir die gebruik in die verfbedryf. Dit is 'n omgewingsvriendelike produk en geen oplosmiddels word gebruik vir die filmvormingsproses nie. Hierdie projek handel oor die opskalering (industrialisering) van die produksie van NW 120.

Die gebruik van 'n geskikte loodsaanleg is eers ondersoek. Daar is gevind dat die beskikbare laboratorium skaal loodsaanleg (RC1, Mettler Toledo) baie duur was. Die reaktore is baie klein (≈1.8 l). Die reaktoropstellings (reaktor, keerplate en roerder-konfigurasie) is ook nie in ooreenstemming met die industriële grootte reaktore wat deur Plascon gebruik word nie.

'n Ten volle rekenaarbeheerde loodsaanleg is ontwerp en gebou teen 'n breuk van die koste van soortgelyke kommersieel beskikbare opstellings. Die reaktor (5 l) is 'n skaalmodel (geometries gelykvormig) van die industriële grootte reaktore wat deur Plascon gebruik word. Die reaktor word ook aangewend as 'n kalorimeter.

Baie goeie beheer oor die reaktortemperatuur, sowel as die toevoertempo's van die monomere en die katalis is verkry. Hitteverlies en hittekapasiteits modelle is afgelei vir variasies in die reaktortemperatuur tussen 82.5 – 87.5 ^{0}C om dit moontlik te maak om akkurate energiebalanse te kan opstel (kalorimeter). Die akkuraatheid van die kalorimeter is getoets by 85 ^{0}C, deur die verdunningswarmte van 'n natrium-hidroksiedoplossing te meet. Daar is gevind dat die kalorimeter baie akkuraat is.

'n Industrieel vervaardigde (Plascon) emulsie (kode naam: AE 446) is gebruik om die loodsaanleg in bedryf te stel. Die resultate wat in die loodsaanleg verkry is, was ongeveer dieselfde as die resultate wat in die industriële reaktore verkry word.

Hierdie resultate toon dat indien die reaktore geometries gelykvormig is en indien die regte prosestoestande (roerspoed, reaksietemperatuur en toevoertempo's van die monomere/katalis) gebruik word, dit moontlik sou wees om NW 120 direk op te skaal van loodsaanleg tot volskaal.

Die reaksietoestande is gevarieer oor 'n wye bereik om die optimum prosestoestande te probeer verkry.

Die roerspoed is gevarieer tussen 150 – 550 opm. Daar is gevind dat die emulsie sleur sensitief is bokant 'n roerspoed van 450 opm. Die gemete fisiese

eienskappe by 'n roerspoed van 550 opm was onaanvaarbaar. Die optimum roerspoed in terme van partikelgrootte en viskositeit lê tussen 150 en 250 opm.

Die reaksietemperatuur is gevarieer tussen 90 – 70 ^{0}C. Die optimum temperatuur lê tussen 90 – 80 ^{0}C.

Dit was moontlik om die monomeer-toevoertyd, m.a.w die reaksietyd, te verminder deur die toevoertempo van die monomere/katalis te verhoog, van 4 tot $2\frac{1}{2}$ uur.

Die metode wat deur Klein et al. (1996) ontwikkel is vir die opskalering van die roerspoed van 'n emulsiepolimerisasie reaksie is gebruik om die ekwivalente roerspoed vir die opskalering te verkry.

Die opskalering van NW 120 is uitgevoer by 'n reaksietemperatuur van 85 ^{0}C en 'n roerspoed van 35 opm. Die monomere/katalis is toegevoer oor 'n tydperk van 4 uur. Die verkorte reaksietyd is nie oorweeg vir die opskaleringslopie nie omdat dit nog nie seker was of die hitteverwydering van die industriële reaktor effektief genoeg sou wees om die verhoging in die reaksiewarmte-ontwikkeling, wat geassosieer word met 'n verhoging in die toevoertempo van die monomere/katalis, te kan verwyder nie.

Baie goeie resultate is verkry. Die gemete fisiese eienskappe van NW 120 wat verkry is in die industriële reaktor was ongeveer dieselfde as dié wat verkry is op die loodsaanleg.

ACKNOWLEDGEMENTS

I would like to thank the following people and institutions for their contributions:

Prof. J.H. Knoetze, my study leader, for his advice, guidance and encouragement throughout this study

Plascon (Pty) Ltd, in particular, Dr. B. Cooray, Mr. J. Engelbrecht and Dr. D. De-Wet Roos for their help and financial support

Prof. R.D. Sanderson, for his motivation and support

The personnel of the workshop at the Department of Chemical Engineering, **J.M. Barnard, A.P. Cordier** and **V Carolissen.**

Special thanks to **Mr. F.P.J. Muller** (Electronic Engineer) for his help in setting up all the electronic equipment and their interfaces.

LIST OF CONTENTS

ABSTRACT iii

OPSOMMING v

ACKNOWLEDGEMENTS vii

LIST OF CONTENTS viii

LIST OF FIGURES xiii

LIST OF TABLES xvi

NOMENCLATURE xvii

CHAPER 1 INTRODUCTION AND OBJECTIVES

1.1 EMULSION POLYMERIZATION: AN OVERVIEW 1

1.2 NW 120 3

1.3 OBJECTIVES 3

CHAPTER 2 PROCESS BACKGROUND

2.1 CHEMISTRY 5

2.1.1 Introduction 5

2.1.2 Homo- and co- emulsion polymerizations 5

2.1.3 Core – shell morphology 7

2.1.4 The three intervals in batch emulsion polymerization 9

2.2 MONITORING AND CONTROL OF EMULSION POLYMERIZATION REACTIONS 11

2.2.1 Open-loop control strategies 11

2.2.1.1 The use of ultrasound for on-line conversion monitoring

2.2.1.2 Homopolymerization: The use of calorimetry for on-line conversion monitoring

2.2.1.3 Copolymerization: The use of calorimetry for on-line conversion monitoring

2.2.1.4 The use of densimetry for on-line conversion monitoring
2.2.2 Closed-loop control strategies 16
2.2.2.1 Quality control in emulsion polymerization systems by means of feedback control
2.3 EXPERIMENTAL SET-UPS USED TO STUDY EMULSION POLYMERIZATION REACTIONS 20
2.4 SCALE-UP CONSIDERATIONS FOR EMUSLION POLYMERIZATION REACTIONS 22

CHAPTER 3 EXPERIMENTAL SET-UP AND PROCEDURE

3.1 INTRODUCTION 25
3.2 EXPERIMENTAL SET-UP 25
3.2.1 Materials 25
3.2.2 Equipment 26
3.3 OUTLINE OF CONTROL SOFTWARE 36
3.4 CONTROL METHODOLOGY 39
3.4.1 Control action 39
3.4.2 Design of digital PID controller 39
3.4.2.1 Comparison between position and velocity algorithms
3.4.3 Control of process variables 41
3.5 CALIBRATION OF ELECTRONIC EQUIPMENT 42
3.5.1 Major equipment 42
3.6 CALORIMETRIC CALCULATIONS 43
3.6.1 Energy balance equations 43
3.6.2 Change in the heat capacity of the reacting liquid 46
3.6.3 Heat losses from the reactor 47
3.6.3.1 Calibration set-up
3.6.3.2 Calibration procedure
3.7 EXPERIMENTAL 52
3.7.1 Experimental procedure 52
3.7.1.1 Experimental routine

3.7.1.2 Sampling
3.7.1.3 Reactor clean-out
3.8 ANALYTICAL ANALYSIS 56
3.8.1 Conversion monitoring 56
3.8.1.1 Gas chromatograph set-up
3.8.1.2 Calculation of the response factor
3.8.1.3 Method
3.8.2 Viscosity analysis 59
3.8.1.1 Set-up
3.8.2.2 Procedure
3.8.3 Solids contents 60
3.8.3.1 Set-up
3.8.3.2 Procedure
3.8.4 Molecular weight 61
3.8.4.1 Set-up
3.8.4.2 Procedure
3.8.5 Particle size determination 61
3.8.5.1 Set-up
3.8.5.2 Procedure

CHAPTER 4 EVALUATION AND COMMISSIONING OF PILOT PLANT SET-UP

4.1 INTRODUCTION 63
4.2 CALIBRATION RESULTS 63
4.2.1 Heat capacity model 63
4.2.2 Heat loss model 65
4.2.3 Accuracy of calorimeter 69
4.3 EVALUATION OF PILOT PLANT REACTOR 70
4.3.1 Control of reactor temperature 70
4.3.2 Evaluation of torque measurements 72
4.3.3 Evaluation of the consistency of the reactants and catalyst addition rates 74
4.4 COMMISSIONING OF PILOT PLANT REACTOR 74

CHAPTER 5 LAB-SCALE EVALUATION OF NW 120

5.1 INTRODUCTION 76
5.2 CHANGE IN STIRRING SPEED 76
5.2.1 Effect of stirring speed on the time dependence of conversion 79
5.2.2 Effect of stirring speed on the time dependence of particle size 82
5.2.3 Effect of stirring speed on the time dependence on viscosity 84
5.2.4 Gravimetrical analysis of conversion 86
5.3 REACTION TEMPERATURE 86
5.3.1 Effect of reaction temperature on the time dependence of conversion 91
5.3.2 Effect of reaction temperature on the time dependence of particle size 93
5.3.3 Effect of reaction temperature on the time dependence of of viscosity 95
5.3.4 Effect of reaction temperature on the change in cumulative heat of reaction 96
5.3.5 Effect of reaction temperature on the change in molecular weight 97
5.4 REACTION TIME 98
5.4.1 Effect of reaction time on the time dependence of conversion 102
5.4.2 Effect of reaction time on the time dependence of particle size 104
5.4.3 Effect of reaction time on the time dependence on viscosity 106
5.4.4 Effect of reaction time on the change in cumulative heat of reaction 107
5.5 SAMPLING 109
5.6 CALCULATION OF THE TOTAL CONVERSION FROM CALORIMETRIC MEASUREMENTS 110

CHAPTER 6 SCALE-UP OF THE PRODUCTION OF NW 120

6.1 INTRODUCTION 112

6.2 SCALE-UP CONSIDERATIONS 112
6.3 PROCESS CONDITIONS 113
6.4 SCALE-UP RESULTS 114

CHAPTER 7 CONCLUSIONS

7.1 INTRODUCTION 119
7.2 IDENTIFICATION OF A SUITABLE AVAILABLE PILOT PLANT 119
7.3 EVALUATION OF NEWLY DEVELOPED BENCH-SCALE-SCALE PILOT PLANT 120
7.3.1 Design and construction 120
7.3.2 Commissioning of bench-scale pilot plant 120
7.4 LAB-SCALE EVALUATION OF NW 120 121
7.4.1 Effect of stirring speed 121
7.4.2 Effect of reaction temperature 122
7.4.3 Effect of reaction time 122
7.4.4 Sampling 123
7.5 SCALE-UP OF THE PRODUCTION OF NW 120 123
7.6 RECOMMENDATIONS AND FUTURE WORK 124

REFERENCES 126

APPENDIX A 130
APPENDIX B 158
APPENDIX C 162
APPENDIX D 165
APPENDIX E 172
APPENDIX F 181
APPENDIX G 193

LIST OF FIGURES

CHAPTER 2

FIGURE 2.1 Stabilized monomer drop and a micelle 6
FIGURE 2.2 Propagation of the oligomeric radical within the micelle 6
FIGURE 2.3 Latex particle 7
FIGURE 2.4 The three extreme 'core-shell-type' arrangements 8
FIGURE 2.5 Illustration of symbols used in the Young-Dupre equation 9
FIGURE 2.6 Three intervals in batch polymerization 10
FIGURE 2.7 Sensor used for ultrasonic measurements 12
FIGURE 2.8 Nonlinear inferential feedback control structure 18
FIGURE 2.9 RC 1 glass reactor (Mettler Toledo) 21

CHAPTER 3

FIGURE 3.1 Developed pilot plant set-up 27
FIGURE 3.2 Schematic representation of the experimental set-up 28
FIGURE 3.3 Monitoring and control of the reactant/dosing 29
FIGURE 3.4 Schematic diagram of reactor 30
FIGURE 3.5 Set-up used to measure torque exerted on motor 32
FIGURE 3.6 Illustration of reactor with peripheral devices 34
FIGURE 3.7 A typical calibration curve for the stirrer 43
FIGURE 3.8 Calibration heater set-up 48
FIGURE 3.9 Electronic layout of heater circuitry 50
FIGURE 3.10 Photograph of reactor inside 55
FIGURE 3.11 GC Chromatogram 58
FIGURE 3.12 Cup-and-spindle configuration of the Haake viscometer 59
FIGURE 3.13 Apparatus used for measuring solids content 60

CHAPTER 4

FIGURE 4.1 Model validation 64
FIGURE 4.2 Model of measured values 65
FIGURE 4.3 Model validation 68

FIGURE 4.4 Model of measured values 69
FIGURE 4.5 Measured cumulative heat of reaction 70
FIGURE 4.6 Reactor temperature profile (179 W step input) 71
FIGURE 4.7 Reactor temperature profile (NW 120) 72
FIGURE 4.8 Torque profiles 73
FIGURE 4.9 Addition profile for core catalyst (0.009 $^{g}/_{s}$) 74

CHAPTER 5

FIGURE 5.1 Change in particle size with change in stirring speed 78
FIGURE 5.2 Change in viscosity with change in stirring speed 79
FIGURE 5.3 Fractional conversion (150-350 rpm) 80
FIGURE 5.4 Fractional conversion (250, 450 and 550 rpm) 81
FIGURE 5.5 Effect of stirring speed on conversion (150 rpm) 81
FIGURE 5.6 Effect of stirring speed on conversion (550 rpm) 82
FIGURE 5.7 Effect of stirring speed on particle size (150-350 rpm) 83
FIGURE 5.8 Effect of stirring speed on particle size (150, 450, 550 rpm) 83
FIGURE 5.9 Effect of stirring speed on viscosity (150-450 rpm) 84
FIGURE 5.10 Effect of stirring speed on viscosity (250 and 550 rpm) 85
FIGURE 5.11 Gravimetrical validation of GC method 86
FIGURE 5.12 Change in particle size (core) 88
FIGURE 5.13 Change in particle size (End result) 88
FIGURE 5.14 Viscosity as a function of reaction temperature 89
FIGURE 5.15 Cumulative heat of reaction (core) 90
FIGURE 5.16 Cumulative heat of reaction (End result) 90
FIGURE 5.17 Fractional conversion (90-80 ^{0}C) 91
FIGURE 5.18 Fractional conversion (85, 75 and 70 ^{0}C) 92
FIGURE 5.19 Effect of reaction temperature on conversion (70 ^{0}C) 93
FIGURE 5.20 Effect of reaction temperature on particle size (Core) 94
FIGURE 5.21 Effect of reaction temperature on particle size (Shell) 94
FIGURE 5.22 Effect of reaction temperature on viscosity (85, 75, 70 ^{0}C) 95
FIGURE 5.23 Cumulative heat of reaction (85 and 70 ^{0}C) 96
FIGURE 5.24 Change in particle size (Core) 99
FIGURE 5.25 Change in particle size (End result) 100

FIGURE 5.26 Change in viscosity (End result) 100
FIGURE 5.27 Cumulative heat of reaction (Core) 101
FIGURE 5.28 Cumulative heat of reaction (End result) 101
FIGURE 5.29 Fractional conversion (Core) 102
FIGURE 5.30 Effect of 50% reduction in core reaction time on conversion 103
FIGURE 5.31 Fractional conversion 104
FIGURE 5.32 Effect of core reaction time on particle size profile (Shell) 105
FIGURE 5.33 Effect of shell reaction time on particle size (Shell) 106
FIGURE 5.34 Effect of normalized core reaction time on viscosity profile 106
FIGURE 5.35 Cumulative heat of reaction profiles 107
FIGURE 5.36 Cumulative heat of reaction profiles 108
FIGURE 5.37 Prediction of conversion from calorimetry 110
FIGURE 5.38 Prediction of conversion from calorimetry (Time Lag) 111

CHAPTER 6

FIGURE 6.1 Fractional conversion (150 rpm) 115
FIGURE 6.2 Fractional conversion (250 rpm) 116
FIGURE 6.3 Conversion (based on monomer feed) 116
FIGURE 6.4 Particle size profiles (150 rpm) 117
FIGURE 6.5 Particle size profiles (250 rpm) 117
FIGURE 6.6 Viscosity profiles (150 rpm) 118
FIGURE 6.7 Viscosity profiles (250 rpm) 118

LIST OF TABLES

CHAPTER 3

TABLE 3.1 Revised Recipe 26
TABLE 3.2 Exact dimensions of parts of the reactor (Figure 3.4) 31
TABLE 3.3 Summary of process inputs and outputs 38
TABLE 3.4 Response factors obtained 57
TABLE 3.5 Results obtained from method evaluation 58

CHAPTER 4

TABLE 4.1 Regression coefficient obtained for heat capacity model 64
TABLE 4.2 Summary of results obtained 65
TABLE 4.3 Regression coefficients obtained for heat loss model 67
TABLE 4.4 Linear and non-linear heat loss components 69
TABLE 4.5 Theoretical and measured heats of solution 69
TABLE 4.6 Torque measurements 73
TABLE 4.7 Summary of results obtained 75

CHAPTER 5

TABLE 5.1 Summary of results obtained 77
TABLE 5.2 Summary of results obtained 87
TABLE 5.3 Summary of results obtained from MW analyses 97
TABLE 5.4 Summary of results obtained 98
TABLE 5.5 Summary of heat dissipation 108
TABLE 5.6 Summary of results obtained 109

CHAPTER 6

TABLE 6.1 Summary of results obtained 114

NOMENCLATURE

A	:	Heat transfer area	$[m^2]$
A'	:	Densitometer constant	$[g/cm^3 s^2]$
$A_{standard}$	:	Integrated area of internal standard	$[mm^2]$
A_i	:	Integrated area of component, i	$[mm^2]$
a	:	Regression coefficient	$[kJ/kg^0C.s]$
B	:	Densitometer constant	$[s^2]$
B(t)	:	Measured analogue signal	[V]
B	:	regression coefficient	$[kJ/kg(^0C)^2]$
C_p	:	Heat capacity	$[kJ/kg^0C]$
$\overline{C}_p$	:	Average heat capacity	$[kJ/kg^0C]$
c	:	Regression coefficient	$[kJ/kg^0C]$
D_i	:	Inter particle distance	[m]
D_p	:	Particle diameter	[m]
D_s	:	Stirrer diameter	[m]
D_s'	:	Stirrer diameter	[ft]
$\dot{E}$	:	Energy	[kW]
e(t)	:	Error signal at time, t	[V]
F	:	Applied force	[N]
Fr	:	Froude number	[ ]
f_i	:	Response factor for component, i	[ ]
$f_{standard}$	:	Response factor of internal standard	[ ]
G_i	:	Mass of component, i	[g]
$G_{standard}$	:	Mass of internal standard	[g]
ΔH_p	:	Heat of polymerization	$[J/mol]$
h	:	Convection coefficient	$[kW/m^{2\,0}C]$

h_L	:	Convection coefficient for free convection	$[kW/m^{2\,0}C]$
I	:	Current	[A]
K_c	:	Controller gain	[ ]
k	:	Counter in time	[ ]
k	:	Conduction coefficient	$[kW/m^{2\,0}C]$
k1	:	regression coefficient	$[kW/^{0}C]$
k2	:	Regression coefficient	$[kW/K^{4}]$
k_d	:	Decomposition constant	$[1/s]$
k^*	:	Consistency factor	$[s^{n-1}]$
M	:	Reactor mass	[kg]
$\dot{m}$	:	Mass flowrate	$[kg/s]$
N	:	Stirring speed	$[1/s]$
N_{min}	:	Minimum rotational speed for dispersion	[rpm]
N_{Re}	:	Mixing Reynolds number	[ ]
Nu_L	:	Nusselt number for free convection	[ ]
n	:	Counter in time	[ ]
n^*	:	Flow index	[ ]
p	:	Instantaneous polymer properties	[ ]
$\hat{p}$	:	Estimated value for, p	[ ]
p(t)	:	Controller analogue output	[V]
$\bar{p}$	:	Bias value	[V]
Q(t)	:	Evolution of heat at time, t	[kW]
$\dot{Q}$	:	Heat transfer rate	[kW]
$\dot{Q}_r$	:	Heat of reaction evolved	[kW]
R	:	Gas constant	$[kJ/mol^{0}C]$
R_p	:	Rate of polymerization	$[mol/l.s]$
R(t)	:	Analogue setpoint	[V]
Ra_L	:	Rayleigh number for free convection	[ ]

r	:	Moment arm	[m]
T	:	Temperature	[^{0}C]
T'	:	Temperature	[K]
T_f'	:	Film temperature	[K]
t''	:	Period of oscillation	[s]
Δt	:	Sampling period	[s]
V	:	Potential difference	[V]
V_{H_2O}	:	Volume of water	[l]
W	:	Work applied	[kW]
$\hat{x}$	:	Estimated process model states	[ ]
$\bar{x}$	:	Vector of process model states	[ ]
y	:	Measurement vector	[ ]

GREEK SYMBOLS

ν	:	Fractional volume	[ ]
γ	:	Interfacial energy	[ ]
ρ	:	Density	$[g/cm^3]$
$\rho_{S.G}$	:	Specific density	[ ]
τ_I	:	Time constant (integral action)	[s]
τ_D	:	Time constant (derivative action)	[s]
τ	:	Torque	[Nm]
ε	:	Emissivity	[ ]
σ	:	Stefan Boltzman constant	$[kW/m^2K^4]$
μ_a	:	Apparent viscosity	[cP]
Φ	:	Latex volume fraction	[ ]

SUBSCRIPTS

A	:	Hydrophilic polymer
B	:	Hydrophobic polymer
W	:	Water phase
0	:	Initial value

set	:	Setpoint
t	:	Technical
r	:	Reactor
ref	:	Reference
jacket	:	Reactor jacket
cond	:	Reactor condensator
losses	:	Reactor heat losses
HR	:	Heat of reaction
avg	:	Average
cal	:	Calibration
ambient	:	Ambient conditions
reac,1	:	Reactor inner wall
reac,2	:	Reactor outer wall

CHAPTER 1

INTRODUCTION AND OBJECTIVES

1.1 EMULSION POLYMERIZATION: AN OVERVIEW

The production of polymer colloids, commonly called latexes, by means of emulsion polymerization is of great importance to industry, especially the paint industry. In the early 1990s the total production of all polymers in western countries was in excess of 10^8 tons per year, of which polymers made by emulsion polymerization constituted 12-15% (Gilbert, 1995). Some of the high value products of emulsion polymerization reactions include synthetic elastomer coatings and adhesives.

There are considerable incentives for obtaining a better understanding of, and developing, emulsion polymerization systems that will consistently produce high quality products, at competitive prices. A better understanding of the physical design of the reactors used in the manufacturing processes and the operational manufacturing procedures will thus be of great importance.

According to Poehlein (1996), the use of batch reaction systems for emulsion polymerization are not often used in industry because of heat transfer limitations, copolymer composition drift, a lack of control of particle morphology, size and concentration, and because of an enhanced tendency for high solid-content systems to coagulate.

Continuous reactors have been used in the production of styrene-butadiene rubber (SBR) for more than 40 years. More recent products made in continuous reactors include coatings, adhesives and other elastomers. A number of continuous reactor systems (single- pass tubes, loop reactors and a combination of continuous stirred tank reactors (CSTR)) have been used to manufacture polymer latexes. Some of the major advantages include the economical production of large volumes of products and large heat transfer surfaces (Poehlein, 1996). Some of these continuous reactor systems are, however, characterized by plugging, inadequate mixing, the requirement of excessive reactor lengths to achieve sufficiently high conversions and

some systems are not adequately flexible for the production of products with a narrow particle size distribution.

Some of these limitations can be minimized or overcome as the process is usually performed as a semi-batch reaction process that involves the initial charging of some of the reagents, followed by the programmed addition of the remaining reagents.

Some emulsion polymerization process variables include (Poehlein, 1996):

- composition of the initial charge in the reactor
- reaction conditions when the flow of the remaining reagents commence
- rate of reagent addition
- composition of the flow stream(s) as a function of time and/or reaction conditions
- reaction temperature
- stirrer speed and stirrer configuration
- reactor geometry
- reaction time.

These variables influence, and can sometimes be manipulated to control, the following reaction and product characteristics:

- reaction rate and therefore the heat load on the cooling system
- copolymer composition parameters
- particle characteristics: number, concentration and size distribution
- solids content
- particle morphology and surface characteristics
- molecular weights and molecular structure.

Emulsion polymerization involves the formation of a network of polymer chains, each with different molecular weights. The physical properties of the polymer mixture depend on the molecular weight distribution.

According to Brooks (1997) the fractionation of such mixtures is very difficult because the chemical differences between the various molecular sizes are not sufficiently great. Most polymers are also non-volatile and cannot be fractionated by distillation.

There is very little scope for changing the molecular size range once the reaction has been completed. Therefore, to obtain a product with a required molecular

weight distribution, particle size and particle size distribution, the reaction mixture must be very carefully manipulated during the reaction itself.

Because of their somewhat unusual physical features, polymerization reactions pose severe problems in terms of reactor design and in the choice of a mixing pattern. Low viscosity monomers can react to form polymer-containing liquids with sometimes very high viscosities. The high viscosity reaction mixtures not only inhibit mixing and heat transfer, but also affect the reaction kinetics. This, in turn, can result in a change in the rate determining step of the reaction (Brooks, 1997).

Detailed kinetic and chemical information are not always available for complex emulsion polymerization reactions. In order to successfully design a reactor it is sometimes necessary to first generate useful models which will account for important reaction phenomena, like fluid mixing, change in physical and morphological properties and temperature variations.

In certain paint formulations composite latex particles said to have "core-shell" morphology are often used, because of their excellent properties (Gilbert, 1995).

1.2 NW 120

A new, environmentally friendly emulsion (code name: NW120) was recently developed by Plascon, on laboratory scale, for use in the paint industry. NW 120 is a multi-component emulsion polymerization system.

It was selected as it had a core-shell morphology and low residual volatile organic compounds. The excellent properties of the shell meant that no coalescent solvent was necessary for film formation.

1.3 OBJECTIVES

A new emulsion process is usually first developed on laboratory or bench-scale equipment prior to possible industrialization. During the development it is often necessary to use several reactor systems of different sizes before it is possible to introduce the new emulsion process in a production plant. It is often difficult to establish the critical control parameters and control procedures in order to avoid too many reject lots. Transfer of the production technology from one size reactor to another is often problematic and expensive.

The main objectives of this project were therefore to:

1) Identify a suitable bench scale reactor system for the study of emulsion polymerization reactions under very controlled conditions. This was to be done by first surveying related, available equipment.
2) As nothing suitable was found a fully computer-controlled, bench-scale, 5 l reactor system (pilot plant) was designed, constructed and commissioned with an industrially-known emulsion product, AE 446.
3) Study the manufacture of the new core-shell type emulsion polymerization system (NW 120) under very controlled conditions in the above process-controlled 5 l reaction system. This would include the identification and manipulation of those process parameters that are important for the scale-up of the production of NW 120, such as stirring speed, reaction temperature and addition rates of reagents/catalyst.
4) Establish specific procedures for the scale-up of the manufacture of NW 120. This includes calculations of the equivalent stirring speeds for the industrial size reactors. This was also to include the tailor-making of the emulsion product, as could be required by industry.

Results of this study contributed to both the fields of scale-up (or industrialization) of a multi component emulsion polymerization system and process control in emulsion polymerization. The focus was not on the polymer chemistry of NW 120 involved, but rather on the engineering procedures that are important for the successful industrialization.

CHAPTER 2

POLYMERIZATION REACTIONS BACKGROUND

2.1 CHEMISTRY

2.1.1 INTRODUCTION

Emulsion polymerization reactions are very complex and the kinetics involved are only partly understood. The reactions and procedures used in most industrial emulsion polymerizations are very complex, and the mechanisms of the processes involved are also very complicated (NW 120). Much research has been conducted in efforts to obtain better understanding of emulsion polymerization reactions (Blackley, 1975; Eliseeva et al., 1976; Gilbert, 1995).

The possible mechanism involved at molecular level for the well-known styrene emulsion polymerization system will be described. As the objective of such is to aid in the understanding of emulsion polymerization the mechanistic description will be given without any experimental or theoretical justification. The mechanistic approach of Gilbert (1995) will be followed.

2.1.2 HOMO- AND CO- EMULSION POLYMERIZATIONS

In this scenario, monomer drops are dispersed in water. Emulsifier is required to stabilize the monomer drops (hydrophilic 'heads' pointing to the aqueous phase), leading to the formation of micelles (Figure 2.1). Small amounts of monomer dissolve in the water, and for styrene this is about $4\times10^{-3}\ mol/dm^3$ at 50 ^{0}C (Gilbert, 1995). The initiator decomposes in the aqueous phase to form free radicals. These radicals react, to form oligomeric radicals, with the small amounts of monomer dissolved in the aqueous phase, until they become "surface-active" (Gilbert, 1995). In other words, the oligomeric radicals grow to a certain chain length until they become thermodynamically unstable, and are unable to remain soluble.

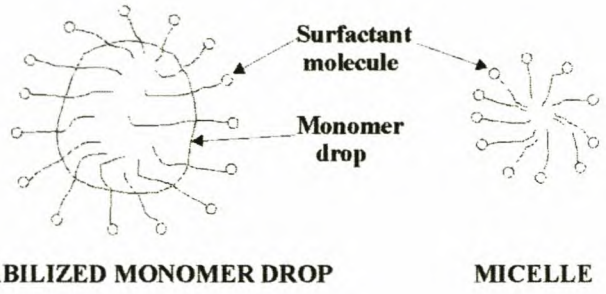

FIGURE 2.1 *Stabilized monomer drop and micelle (Gilbert, 1995)*

According to Gilbert (1995) the resulting species lead to the formation of primary particles, either by entering a pre-existing micelle or by aggregation with surfactant molecules in the aqueous phase. Propagation of the oligomeric radicals, which are enclosed in a micelle, now takes place (Figure 2.2) to form primary latex particles (Figure 2.3).

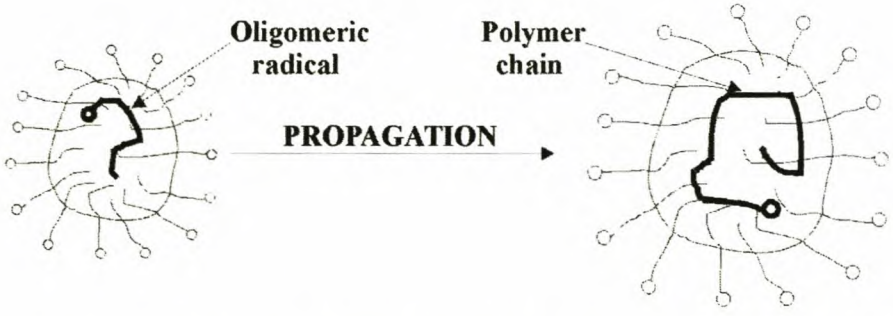

FIGURE 2.2 *Propagation of the oligomeric radical within the micelle (Gilbert, 1995).*

A wide particle size distribution can be obtained at this very early stage. Eventually, a sufficient number of particles will have formed and the new radicals that are produced in the aqueous phase then enter pre-existing particles, rather than nucleating new ones. It must be taken into account that there also exist surfactant balances, placing a limit on the total amount of particles that can be formed.

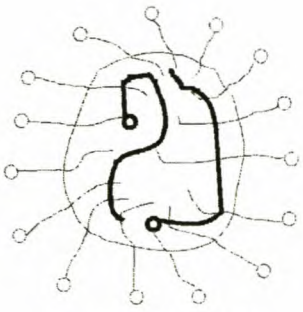

FIGURE 2.3 *Latex particle*

Propagation leads to an increase in the weight fraction of polymer and to an increase in the internal viscosity of the particle. Propagation will continue until all the monomer in the system is depleted.

When two monomers with different propagation rate constants and different reactivity ratios are added together a co-polymer, consisting of statistically alternating units of the two monomers, based on their concentration and reactivity is formed (Billmeyer, 1984). More recently, the ability to produce polymers containing long sequences of two or more different monomers (block and graft co-polymers) has led to new products with unique and valuable properties.

2.1.3 CORE – SHELL MORPHOLOGY

One type of (co) polymer (shell) can be grown around another type of (co) polymer (core) to form a composite latex particle with "core-shell" morphology. Emulsions with this morphology are often used in the formulation of paints. In paint applications, the core normally consists of a glassy polymer to give gloss and mechanical stability (hardness) and the shell, on the other hand, will consist of a rubbery polymer to enable the latex particle to form a uniform surface coating (e.g. NW 120) (Gilbert, 1995).

Three extreme 'core-shell-type' arrangements have been defined by Waters (1994) as, core-shell, inverted core-shell and separated core-shell (Figure 2.4).

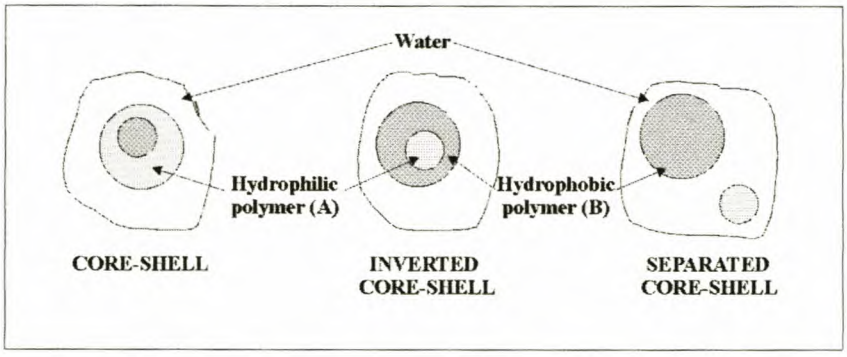

FIGURE 2.4 *Three extreme 'core-shell-type' arrangements (Waters, 1994)*

Generally speaking a latex particle with core-shell morphology has the more hydrophilic polymer (A) as the shell and the more hydrophobic polymer (B) as the core. However, there exist instances in which the hydrophilic polymer phase can be the core by either adjusting the kinetics of the polymerization reaction to "freeze" in the hydrophilic core, or by presenting a barrier to inversion by increasing the molecular mass of the hydrophilic core by crosslinking it. Such is the case with NW 120.

Such an arrangement as described above leads to a lower interfacial energy and will thus be more stable over separated core-shell, if:

$$\frac{\gamma_{B-W} - \gamma_{A-B}}{\gamma_{A-W}} > \frac{1 - v_A^{2/3}}{v_B^{2/3}} \qquad \text{.....2.1}$$

where the subscripts A and B refer to the hydrophilic and hydrophobic polymer, respectively and subscripts W refers to the water phase (Figure 2.4). The interfacial energy for the respective interfaces is denoted by γ. The fractional volume is here denoted by v (Waters, 1994).

Inverted core-shell will only be favored over core-shell when the volume of the hydrophilic polymer (A) is small. Inverted core-shell will thus be favored if:

$$\frac{\gamma_{B-W} - \gamma_{A-W}}{\gamma_{A-B}} < v_B^{2/3} - v_A^{2/3} \qquad \text{.....2.2}$$

According to Waters (1994) Eq. 2.1 is the same as that of the well-known Young-Dupre equation (Equation 2.2). The symbols used in Eq. 2.2 are illustrated in Figure 2.5. Complete engulfment (core-shell) and inverted core-shell is favored when $\cos\theta = 1$

$$\frac{\gamma_{B-W} - \gamma_{A-B}}{\gamma_{A-W}} = \cos\theta \qquad \text{.....2.3}$$

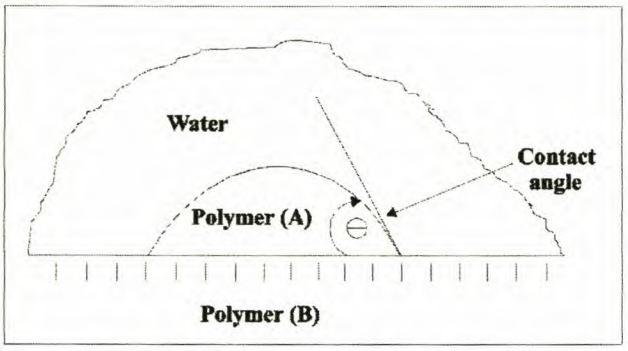

FIGURE 2.5 *Illustration of symbols used in the Young-Dupre equation (Waters, 1994).*

2.1.4 THE THREE INTERVALS IN BATCH EMULSION POLYMERIZATION

Batch emulsion polymerization is generally divided into three stages or Intervals (Figure 2.6). The three stages will be discussed very briefly here. The description given by Gilbert (1995) will be used.

INTERVAL 1: *Ab initio* emulsion polymerization commences with this rapid transitory period. The rate of polymerization increases (Figure 2.6) as new particles are nucleated i.e. the number of particles increases.

INTERVAL 2: In an *ab initio* system Interval 2 commences when particle nucleation ceases. All three possible phases are present: an aqueous phase, latex particles and monomer droplets. The latex particles maintain an approximately constant $^{monomer}/_{polymer}$ ratio (i.e. steady state exist). Monomer diffuses from the emulsion droplets, through the aqueous phase, into the latex particles. Particles are continually replenished with monomer as polymerization occurs within them.

INTERVAL 3: Monomer droplets eventually become exhausted and disappear, as polymerization progresses and monomer is consumed. Only latex particles and the aqueous phase are present during this period, with the majority of the remaining monomer being confined to the latex particles, with a small amount dissolved in the continuous phase. The rate of the polymerization reaction decreases as the

concentration of monomer, present only in the polymer particles, decreases (De La Rosa et al., 1996).

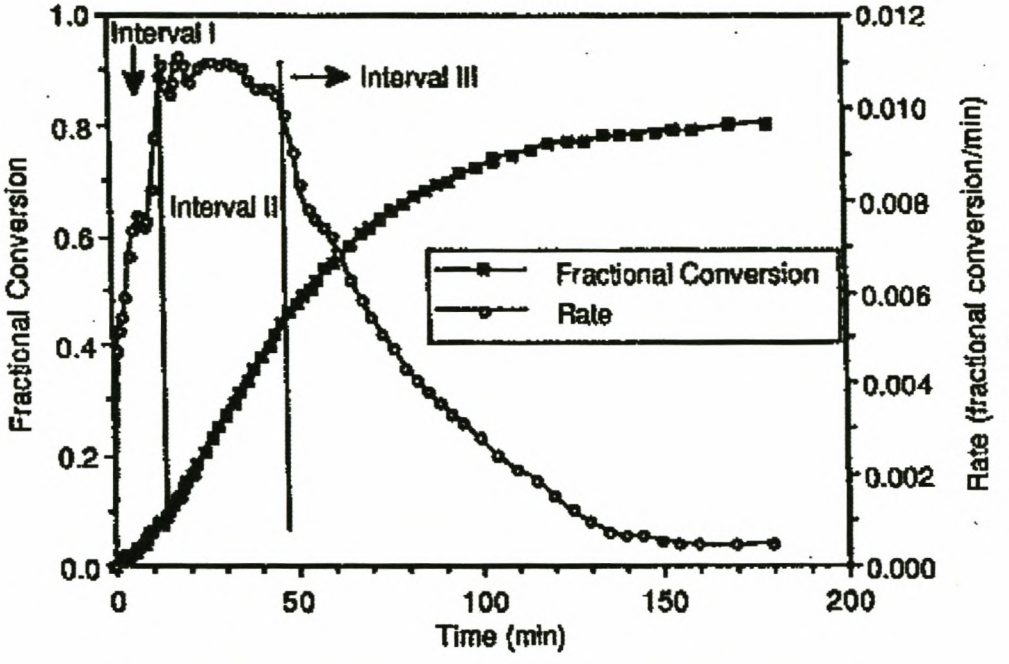

FIGURE 2.6 *Three intervals in batch emulsion polymerization (Gilbert, 1995)*

2.2 MONITORING AND CONTROL OF EMULSION POLYMERIZATION REACTIONS

The implementation of accurate monitoring and control strategies in emulsion polymerization systems are very difficult because of inherent modeling limitations and on-line measurement problems.

Only simple fundamental properties (temperature, pressure and pH) can at present be measured on-line. More sophisticated analyses are not possible on-line, due to limited robustness and accuracy of the instrumentation. Long retention times are also associated with complex analyses (e.g. particle size, particle size distribution and conversion).

The latex is a thermodynamically unstable multiphase system and this results in the clogging of sampling loops due to coagulation (Urretabizkaia et al., 1993). Special preparation of the samples is therefore required (Dimitratos et al., 1991).

A full characterization of the dynamic behavior of emulsion polymerization systems is thus not possible, because most of the process states cannot be measured on-line (Dimitratos et al., 1991).

The feasibility of open and closed loop control strategies have been investigated. The modes of operation and the models that were used were derived for very specific emulsion polymerization systems. Some of these methods will be reviewed here.

2.2.1 OPEN - LOOP CONTROL STRATEGIES

On-line estimates of the individual monomer conversions, from energy and mass balance equations and other techniques like ultrasound propagation, calorimetry and densimetry have been used to predict polymer properties, such as molecular weight distribution, glass transition temperatures and copolymer composition, and also to predict the optimum feed rate profiles of the monomers and catalysts to be added.

In an open-loop control strategy, accurate models of the reaction system are required for the calculation of the control trajectories of the manipulated variables, to produce a polymer with certain qualities.

2.2.1.1 THE USE OF ULTRASOUND FOR ON-LINE CONVERSION MONITORING

Monomer conversion can be estimated by measurements of the ultrasound propagation velocity in the emulsion polymerization reaction system

In homogeneous systems the velocity is proportional to the inverse of the square root of the product of density and compressibility. As both the latter change as monomer is converted into polymer, it provides a relationship between sound propagation velocity and monomer conversion (Canegallo et al., 1995).

Canegallo has also reported on methods in which both sound velocity and attenuation were measured, using a sensor based on the "pulse travelling technique". With the use of this technique it is possible to obtain information about the nucleation process as well as measuring high conversion values.

The sensor used by Canagallo was a prototype manufactured by Labor für Messtechnik of Graze (Austria) (Figure 2.7). The time needed for an ultrasonic pulse to travel between two piezoelectric transducers, E and R, at a fixed distance, L is measured. A thermocouple T was used to measure the temperature. It was reported that the sensor operates at a 3 MHz pulse frequency with a sound path length less than 1 cm and it provided 5 measurements per minute. Experiments were conducted on methyl methacrylate (MMA) and vinylacetate (VAc) homopolymerization reactions.

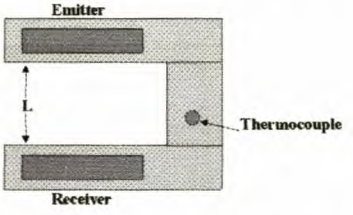

FIGURE 2.7 *Sensor used for ultrasonic measurements (Canegallo et al., 1995).*

One of the main advantages using this set-up is that the measuring probe can be directly plugged into the reacting mixture, without requiring a sampling device, thus making it particularly simple and suitable for industrial applications.

Unfortunately, the proposed set-up, using ultrasound for on-line conversion monitoring, has some rather distinct disadvantages. In order to evaluate the velocity of sound propagation in a multiphase system such as an emulsion, a full characterization of the relative amount and composition of each phase is required. Empirical

calibration of the system is dependent on the combination of reagents used and a new calibration curve should be derived if the monomer-to-water ratio is modified. It was also reported by Canegallo et al. (1995) that the sensitivity of the instrumentation is very low while monomer droplets are still present in the reaction mixture.

Canegallo et al. (1995) have proposed a model based calibration method. The disperse nature of the system as well as variations of the polymer compressibility during the reaction was accounted for in the model (Canegallo et al., 1995).

2.2.1.2 THE USE OF CALORIMETRY FOR ON-LINE CONVERSION MONITORING

HOMOPOLYMERIZATION

The application of calorimetry to homopolymerization on laboratory-scale and its theoretical application have been reported in the open literature (McKenna et al., 1996; Schuler et al., 1992; De La Rosa et al., 1996). A reaction calorimeter (RC1), designed and built by the Mettler Corp., was used for the experimental on-line conversion monitoring of styrene homopolymerization reactions (De La Rosa et al., 1996). Energy and material balances were used to calculate the overall conversion.

The rate of reaction (Eq. 2.4), in homo- emulsion polymerization ($\dot{Q}_r$) is directly proportional to the measured heat evolved.

$$\dot{Q}_r = V_{H_2O} \Delta H_p R_p \qquad \text{.....2.4}$$

where V_{H_2O} is the volume of water in the system; ΔH_p is the heat of polymerization of the monomer ($^{J}/_{mol}$) used; and R_p is the rate of polymerization ($^{mol}/_{l(water).s}$). The conversion can easily be obtained by looking at the rate-of-polymerization curve, which is obtained directly from the heat of reaction curve, or the conversion can directly be calculated, at time t, from the measured heat evolved (Eq. 2.5).

$$X_r(t) = \frac{\int_0^t Q_r dt}{\int_o^{t_f} Q_r dt} \qquad \text{.....2.5}$$

where $X_r(t)$ is the relative calorimetric conversion at time t, which is obtained by the relation between the partial heat of reaction evolved at time t, and the total heat evolved at the end, at time t_f, of the polymerization.

Although this is an important application of the calorimetric technique, it is not of much use in multi-component polymerization, where the conversion is not directly proportional to the heat evolved.

COPOLYMERIZATION

The use of reaction calorimetry for monitoring and, eventually controlling emulsion copolymerization systems is made difficult and in some cases virtually impossible because the estimation of the individual monomer conversions from the overall heat generation rate is not straightforward.

A number of authors (Gugliotta et al., 1995a; Gugliotta et al., 1995b; Urettabizkaia et al., 1993 and Leiza et al., 1993) have proposed methods whereby calorimetric data have been used for the on-line estimation of conversion and copolymer composition in semi-continuous emulsion polymerization reactors. The methods are however very strongly model-based. Such a method has been developed by Gugliotta et al. (1995a).

An automated laboratory reaction set-up (RC1), designed and manufactured by Mettler-Toledo, was used for the experiments. It was equipped with a 1.8l stainless steel reactor (Hp 60 Mettler-Toledo). The copolymerizations of 1) vinyl-acetate (VAc) and butyl acrylate (BuA) and 2) butyl acrylate (BuA) and styrene (St) were studied.

The mixture of monomers was fed into the reactor at a constant flow rate. The evolution of the overall heat rate of polymerization $\dot{Q}_r$ was measured. The conversion was calculated from the heat of polymerization. Samples were withdrawn from the reactor and the overall conversion and copolymer composition were verified by gravimetry and by gas chromatographic analysis, respectively.

According to the authors, good agreement was obtained between the calculated conversion and the cumulative copolymer composition and those verified by gas chromatographic analysis, respectively.

Gugliotta et al. (1995b) have used an optimum feed rate profile approach, derived by Arzamendi and Asua (1989) to produce a polymer with a desired composition, Y_A. Experiments were conducted with the copolymerization of VAc and BuA.

All of the less reactive monomer was charged into the reactor, followed by a certain amount of the more reactive monomer needed to initially produce a copolymer with the desired composition. The amount of more reactive monomer initially charged into reactor, as well as its feed rate profile was calculated, using the mathematical model derived by Arzamendi and Asua (1989). Good agreement was obtained between the calculated and the experimental compositions of the copolymer.

The above mentioned methods are heavily based on iterative mathematical models. Experiments were carried out on well-known and well-defined copolymer reactions. For such copolymer systems of which the reactivity ratios, the heat of homopolymerization, partition coefficients and propagation rate constants are freely available in the literature. These methods will thus be of very little use for ill-defined copolymer systems. The possible utilization of this method for multi-component polymerization has not been reported.

2.2.1.3 THE USE OF DENSIOMETRY FOR ON-LINE CONVERSION MONITORING

In the research conducted by Canegallo et al. (1993), a digital densitometer manufactured by Anton Paar (DMA 40) was used to study homopolymerization - (Styrene and Methyl Methacrylate) as well as copolymerization reactions (Styrene/ Methyl Methacrylate and Vinyl Acetate/ Methyl Methacrylate). The measuring cell was kept at a constant temperature. The natural period of oscillation (t'') of a sample in a U-type tube was used to obtain the density (Equation 2.6)

$$\rho = A' \times ((t'')^2 - B) \qquad \text{.....2.6}$$

where A and B are respective constants that depend on the temperature and the instrument used. The value of the constants were obtained by calibration of the instrument with reference to 'standard fluids' (e.g. water). The period of oscillation was measured as 43.2 times per minute.

The main drawback of this set-up is the lack of thermal stability of the sample stream. It has been reported that fluctuations of the sample temperature can produce fictitious oscillations in the evaluated conversion values (Canegallo et al., 1993). Bubbles in the sample cause scattering of density data. At high conversions problems have been found with fouling of the sampling circuit, which results in a decrease in the measured reliability.

The polymer density depends, in the case of copolymerization, upon its composition. There is no one-to-one relationship between latex density and polymer conversion as in the case of homopolymerization. The authors reported that this problem was overcome by combining the density measurements with a "simple reliable" model for predicting polymer composition as a function of conversion. McKenna et al. (1996) have used the combination of on-line densiometric measurements and a computer model of the process.

An open-loop control strategy provides for a very simple and effective way of controlling well-known and well-defined emulsion homopolymerizations and some emulsion copolymerization reaction systems. In some cases very complex or oversimplified models first need to be solved iteratively, before any control can be applied to the reaction system. In the absence of sensitive and robust instruments, techniques like calorimetry, densimetry and ultrasound have been developed that utilize such models for the on-line prediction of the physical and chemical properties of the polymer formed. In multi-component systems these methods are not of much use, because a full characterization of the relative amounts and compositions of each phase are still required. Open-loop control will fail when unexpected process disturbances occur.

2.2.2 CLOSED – LOOP CONTROL STRATEGIES

Progress in the optimal control of polymerization reactors, by means of a closed-loop control strategy has been slower than in certain industries (e.g. the petrochemical industry). This is mainly due to the unavailability of reliable and robust on-line polymerization characterization instruments. Closed-loop control of polymerization reactors has generally been limited to temperature and pressure controls only (Ponnuswamy et al., 1987).

Recent development of new analytical techniques for the measurement of polymer quality, as well as advances in computer control techniques have increased the scope of monitoring and controlling polymer quality by means of closed-loop control (Ponnuswamy et al., 1987).

2.2.2.1 QUALITY CONTROL IN EMULSION POLYMERIZATION SYSTEMS BY MEANS OF FEEDBACK CONTROL

In the application of feedback control in emulsion polymerization systems it is not acceptable to apply control that will drive the states back to their precomputed trajectories. Emulsion polymerization reactions are not reversible. It is therefore not possible to try and drive the equilibrium in a certain direction in order to try and compensate for deviations that have occurred, neither is it acceptable to mix good batches with poor quality batches to achieve a good average.

Particular applications for the feedback control schemes of Kravaris et al. (1989) and Ponnuswamy et al. (1987) have been reported. Kozub et al. (1992) and Urretabizkaia et al. (1994) investigated the feasibility of using different feedback controllers for the quality control of co-polymerization and multi-component polymerization systems, respectively.

Ponnuswamy et al. (1987) investigated the homopolymerization of methyl methacrylate in a batch reactor. Different open-loop optimum control policies were derived. Experimental results were compared with the theoretical predictions. A linear feedback controller was designed to maintain the process variables along their established open-loop optimal state trajectories in the presence of process disturbances. The linear feedback controller was successfully used only in simulated runs.

Non-ideal operating conditions, which normally arise from model mismatches and other disturbances can be compensated for by some correction to the optimal control trajectory. Such a nonlinear inferential feedback control strategy for semi-batch emulsion co-polymerization reactors was proposed by Kozub et al. (1992). The emulsion copolymerization of styrene/butadiene rubber was studied. The proposed control structure is illustrated in Figure 2.8, by means of a block diagram.

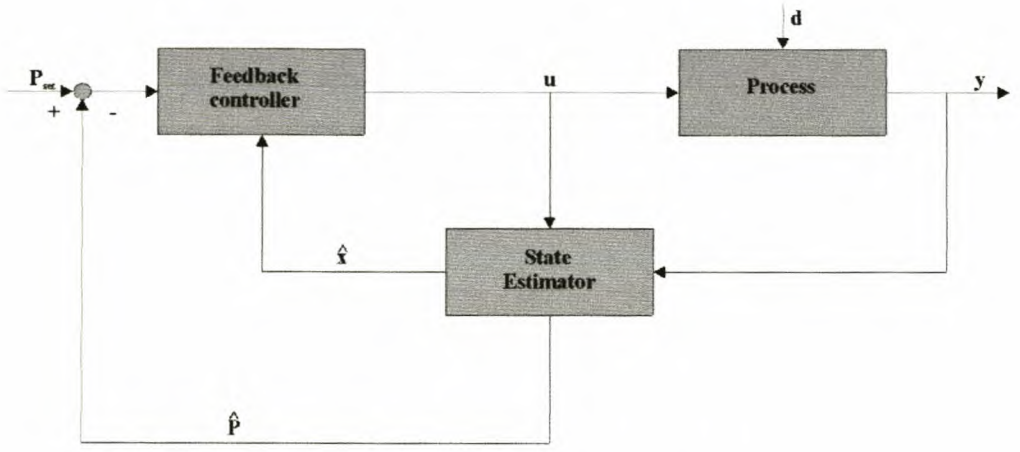

FIGURE 2.8 *Nonlinear inferential feedback control structure (Kozub et al., 1992)*

A non-linear state estimator uses the available measurement (y) to infer the state (x) and the instantaneous copolymer property (p) to be controlled. A non-linear controller recomputes the control action, based on the inferred instantaneous condition ($\hat{x}$) within the reactor and on the deviation of the inferred instantaneous property ($\hat{p}$) from their set points.

The information needed to calculate the copolymer properties of interest (p), for feedback control, such as monomer conversion, latex composition, average molecular weight and branching are provided by the state vector (x) (Kozub et al., 1992). The control methodology of Kozub et al. (1992) can be summarized as follows:

Measurements are obtained at discrete time intervals $y(t_k)$. It is used with the model to provide estimates of x and p. Corrections to the x and p open-loop trajectories are necessary, as a consequence of non-ideal operating conditions arising from model mismatches and disturbances. The largest errors occurred at the start of the reaction, due to uncertainty in the disturbances and model parameter information of the initial state estimate vector x_0. A trajectory for u is recomputed in order to reach the desired set point for p (p_{set}) when non-ideal process conditions are encountered. x and p are estimated, given discrete measurements $y(t_k)$, by the use of extended Kalman filters.

Open-loop control strategies provided an input trajectory in order for the co-polymer or reactor conditions to maintain their estimated values. Experiments were

conducted on well-known co-polymer reaction systems, ones for which the degree of branching and crosslinking for example are well defined.

A nonlinear adaptive plus proportional-integral control strategy was developed by Urretabizkaia et al. (1994) for the emulsion terpolymerization of vinyl acetate, methyl methacrylate and butyl acrylate.

A non-linear optimization algorithm was used to predict the amounts of monomer in the polymer particles. The prediction of the nonlinear adaptive part of the controller was updated and the parameter related to the polymerization rate (flow rates of the monomer streams) adjusted. The mathematical model in the nonlinear adaptive controller was also updated. An on-line gas chromatograph was used to measure the amounts of unreacted monomer in the reactor. The amount of unreacted monomer in the reactor was also calculated by means of a mathematical model of the process. The nonlinear optimization scheme minimizes the difference between the calculated and the measured amounts of unreacted monomer in the reactor. The desired terpolymer composition (set point) was compared with the estimated value, by means of the proportional-integral (PI) controller. The PI controller, which is a conventional feedback controller, adds its action to the output of the nonlinear part of the controller.

The flow rates could only be calculated every 9 min, when the simulated measurements were available. Gas chromatographic analysis took 18 min, during which time the flow rates were kept constant. The first control action could only be taken after 27 min and thereafter, only every 18 min. The time delay associated with this control strategy proposed by Urretabizkaia et al. (1994) renders itself of very little use in practical applications. The effects of process disturbances other than that of variations in the monomer flow rate were not included in the experimental work. It was also found that the addition of the proportional-integral part to the nonlinear adaptive controller does not offer any noticeable advantage.

A closed-loop control strategy provides a better and more accurate way of controlling emulsion polymerization reaction systems than that of just an open-loop control strategy does, although the optimum control strategies are still derived through open-loop techniques. The accuracy of the feedback part of the controller depends on the accuracy and reliability of the on-line sensors. Dead times of up to 27 min are also associated with certain feedback control strategies. No mention could be found as to where a feedback control strategy had been successfully used in a multi-component emulsion polymerization system.

2.3 EXPERIMENTAL SET-UPS USED TO STUDY EMULSION POLYMERIZATION REACTIONS

A pilot plant is an essential step between the laboratory investigations and the investigation of a new process or the optimization of an existing process. The pilot plant reactor needs to be a small-scale model of the full-scale process equipment, although the full-scale equipment that works best is not known yet (Dickey at al., 1993).

The pilot plant must therefore be more versatile than the anticipated production equipment and it must be able to operate over a wider range of temperatures, while handling a broader range of polymer viscosities and densities.

An integral part of any pilot plant set-up is the instrumentation and the control. Accurate and stable control over the reaction temperature, stirring speed and the addition rates of the reactants/catalysts are thus very important. Versatility is essential, both to conduct tests in the pilot plant reactor and to collect data useful for design and scale-up (Dickey at al., 1993). In the following section some experimental set-ups that have been used to study emulsion polymerization reactions will be reviewed.

Urretabizkaia (1994) used a 2l stainless steel, semi-batch reactor to study the terpolymerization of vinyl acetate, methyl methacrylate and butyl acrylate. It was equipped with a reflux condenser, stainless steel stirrer, two reagent inlets and an on-line sampling outlet. Hot water was circulated through the jacket of the reactor. A proportional controller was used to maintain the desired temperature inside the reactor by manipulating the flowrate of the cold water through the coil placed inside the reactor. The reactants were fed to the reactor by positive displacement pumps (FMI Metering pumps). Balances served as accurate mass flow-meters. The experimental set-up was controlled with a personal computer.

The research conducted by Arzamendi et al. (1991) on the polymerization of vinyl acetate and methyl acrylate was carried out in a 2l semi-batch reactor. The reactor was equipped with a stainless steel stirrer, reagent inlet and a condenser. The reactor was placed into a water bath at constant temperature and it was assumed that the heat losses from the reactor would be negligible. The flowrate and difference between the temperature of cold water flowing through a coil, placed inside the reactor and the reactor temperature, was used to calculate the heat of reaction. The

change in the heat capacity of the reacting liquid, as well as the accumulation of mass, was ignored.

The RC1 bench-scale pilot plant, manufactured by Mettler Toledo, is one of the most widely used in the study of emulsion polymerization (De La Rosa et al., 1996; Gugliotta et al., 1995; Urretabizkaia et al., 1993). Different size reactors are available. The largest stainless steel reactor has a capacity of 1.8l. The largest glass reactor has a capacity of 2l (Figure 2.9). Four balances are used for the accurate addition of the reactants and catalyst streams. The RC1 was designed to serve as a calorimeter.

FIGURE 2.9 *RC1 glass reactor (Mettler Toledo)*

Unfortunately, the RC1 is very expensive. (A quote for approximately R1.5 million was received at the end of 1998.) Further available reactors are very small and also not necessarily geometrically similar to the industrial reactor under investigation. It is not possible to change the stirrer and baffle configuration. The RC1 have very

prominent measuring probes (Figure 2.9), which act as baffles, and its effect is very difficult to scale-up.

The study of emulsion polymerization reactions is very difficult when such small reactors (1-2 l) are used. Physical disturbances such as the use of internal cooling coils and large prominent measuring probes pose severe problems, since its baffle effect is very difficult to scale-up successfully.

2.4 SCALE-UP CONSIDERATIONS FOR EMULSION POLYMERIZATION REACTIONS

It has been recognized by those practicing emulsion polymerization (De La Rosa et al., 1996; Poehlein, 1996; Gugliotta et al., 1995; Urretabizkaia et al., 1993) that the product quality is dependent on the manufacturing process. Emulsion polymerization inherently consists of a large number of process variables. Two of the most important variables identified by Klein et al. (1996) are the choice of a reactor (batch, semi-batch and continuous) and the large number of permutations of the contacting of the reagents feed streams.

The contacting of the feed streams is strongly affected by the type of mixing. The agitation characteristics in large industrial-size reactors or large pilot plant reactors are very different from those, which exist in laboratory-size reactors (1-2 l). The scale-up of the mixing process is, in many cases, paramount in reproducing end-use properties developed on bench scale (Klein et al., 1996).

Uhl et al. (1986) recommended the use of a dimensionless-number correlation for the scale-up of mixing vessels. In facilitating calculations of the mixing Reynolds number, the authors recommended the use of the following dimensionless form of the Reynolds number (N_{Re}):

$$N_{\mathrm{Re}} = 1480(D_s')^2 N\rho_{S.G} \Big/ \mu \qquad \text{.....2.7}$$

The stirrer diameter (D_s') has units of ft, while the stirrer speed is given in revolutions per minute (rpm). The specific gravity ($\rho_{S.G}$) is required and the viscosity has units of cP.

A power-per-volume-approach has been recommended to calculate the minimum rotational speed of the stirrer necessary for the suspension of particles in the

turbulent regime (Ullman's Encyclopedia of Industrial Chemistry, 1990). In this approach the Froude number (Fr) is used as scale-up criterion, where:

$$Fr = N^2 D_s / g \qquad \text{.....2.8}$$

$$Fr \approx (N^2 D_s) \qquad \text{.....2.9}$$

The stirring speed is given in, revolutions per minute (rpm) and the stirrer diameter in units of m.

The methods described above have been successfully used in the scale-up of mixing vessels, rather than the scale-up of the agitation of an emulsion polymerization system. Klein et al. (1996) however, proposed a method, which was useful as scale-up criteria in emulsion polymerization.

The method involves the calculation of the minimum rotational speed of an impeller (N_{min}) necessary to disperse the emulsion system. If the fluid parameters (density and viscosity) are constant and if geometric similarity exists it follows that the minimum rotational speed for the liquid system can be given as:

$$N_{min}(D_s)^{0.765} = \text{constant} \qquad \text{.....2.10}$$

The stirrer diameter is given in units of m.

The kinetics involved in emulsion polymerization reactions are very complex and not yet fully understood. Much research has already been conducted in efforts to understand homo- and co- emulsion polymerization reactions, in order for such reactions to be industrialized successfully.

Calorimetry, densimetry and ultrasound have been used successfully in the calculations of the open-loop control trajectories of some manipulated variables in certain well-known and well-defined homo- and co- emulsion polymerization reactions.

As emulsion polymerization reactions are not reversible it is not possible to try and shift the equilibrium in a certain direction, in order to compensate for deviations that might have occurred, as is the case in some other industries (e.g. oil refining) with a classic feedback control strategy. Nor is it possible to develop an adaptive type controller that depends on open-loop techniques in the calculation of the optimal control strategy for large complex or new emulsion reaction systems where no or very little reaction data are available.

The first step in the successful scale-up of any new emulsion polymerization system, especially one as complicated as a multi – component core-shell system, is a sound understanding of the interactions that exist between the various process variables and the process characteristics. This can only be achieved when the reactions are performed under very strictly controlled conditions in a laboratory or on a pilot plant. Calorimetry could be used to further aid in the understanding of the process interactions. The use of calorimetry alone, however, would render itself useless where very complex emulsion polymerization systems are investigated. It should rather be used in parallel with other measurements (e.g. conversion), for example to assist in the explanation of the changes in the morphology.

CHAPTER 3

EXPERIMENTAL SET-UP AND PROCEDURE

3.1 INTRODUCTION

A comprehensive understanding of the interactions that exist between the process variables (stirrer speed, reaction temperature, dosing program, etc.) and the product characteristics (viscosity, % solids, particle size and distribution, etc.) is needed for the successful scale-up and control of any emulsion polymerization reaction system, especially the ones resulting in products with complex morphologies (core-shell).

The process variables that are of critical importance first need to be identified, they then need to be varied and the responses measured / calculated / analyzed. The process variables can then be optimized, to form the basis for the scale-up and control of NW120 (or other possible complex emulsions), with minor modifications.

In this study a jacketed, semi-batch, reactor (5l) was designed and built. The reactor was a scaled down replica of an industrial size (10 ton) reactor. The reactor was designed to serve as a very accurate calorimeter. It was therefore equipped with very accurate measurement and control devices, which were coupled to a computer for on-line data acquisition and control purposes. The computer software needed was specifically developed for the experimental set-up. The experimental set-up and associated computer software were designed to be sufficient for it also to be used in the study of other reaction schemes, with minor modifications.

A multi-component, core-shell type, emulsion polymerization reaction system was studied. The core constituted 5 components and the shell 3 components. A two-step catalyst-dosing program was used.

3.2 EXPERIMENTAL SET-UP

3.2.1 MATERIALS

All experiments were carried out with industrial grade chemicals. Deionized water was used throughout. Due to confidentiality agreements, neither the names of

the monomers nor the catalysts may be published. A revised recipe for the preparation of NW 120 is summarized in Table 3.1.

TABLE 3.1 *Revised Recipe*

CHEMICALS	QUANTITY (g)
Initial Aqueous Phase	
Deionised Water	1986.2
Surfactant	93.0
Buffer	9.4
Initial Catalyst	
Deionised Water	9.5
Initiator	0.7
Initial Feed (Core)	
Monomer A	236.5
Monomer B	216.3
Monomer C	81.5
Monomer D	17.5
Crosslinker	34.0
Secondary Feed (Shell)	
Monomer B	494.0
Monomer C	927.5
Monomer D	43.0
Delayed Catalyst	
Deionised Water	174.6
Initiator	5.7
Surfactant	47.1

3.2.2 EQUIPMENT

The experimental set-up, a schematic diagram of which is shown in Figure 3.1.1, consisted of four main sections a dosing section (1) from which all the chemicals were fed into the reactor (2). The temperature in the reactor was kept constant by means of a heat removal/addition section (3). A computer (4) was used for control and on-line data acquisition.

FIGURE 3.1 *Developed pilot plant set-up*

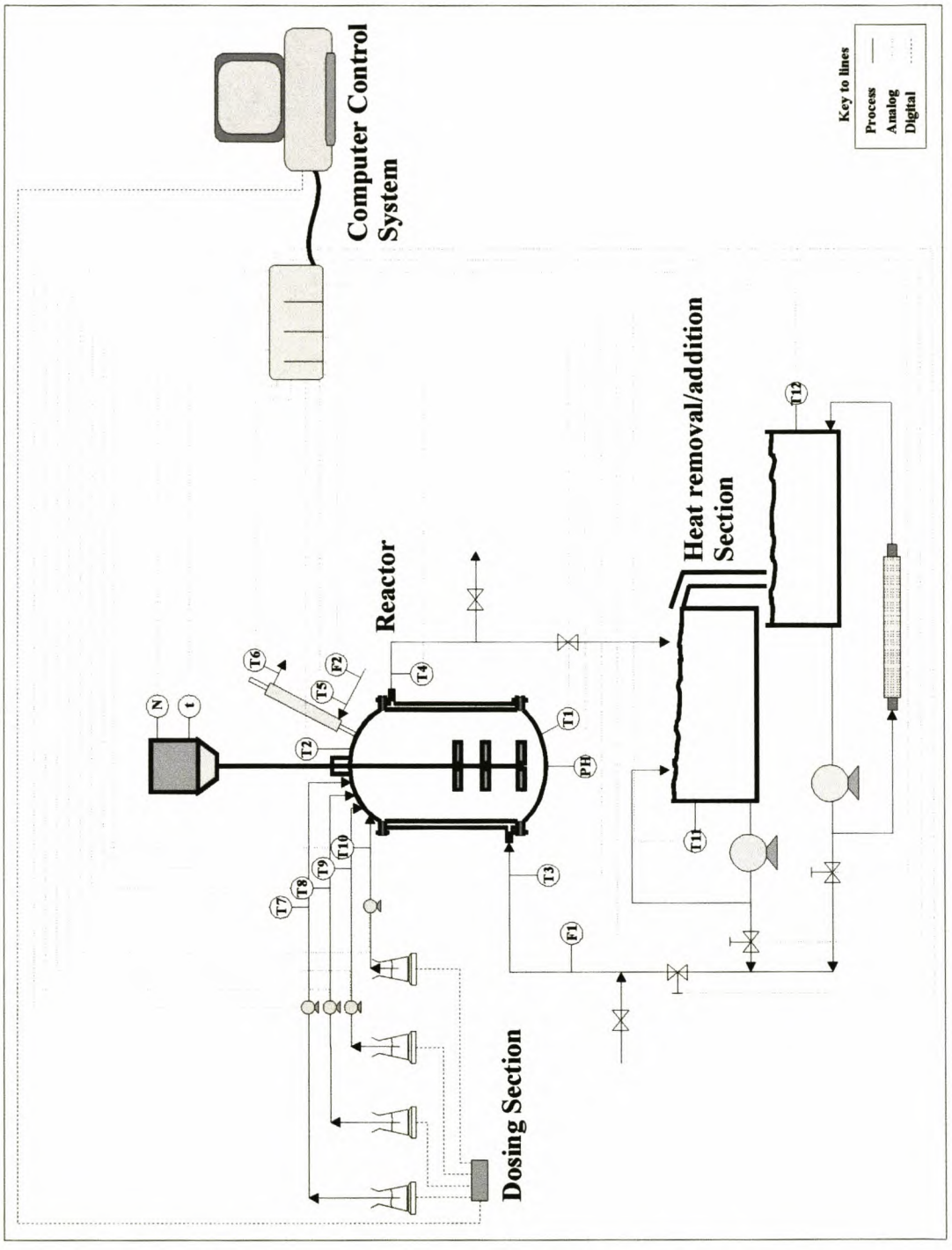

FIGURE 3.2 *Schematic representation of the experimental set-up*

DOSING SECTION

Four positive displacement pumps (FMI Metering, RHV 00 CKC) were used, to feed the reactants into the reactor. The pistons as well as the cylinder liners were manufactured from a ceramic material, and the cylinder casing from a fluorocarbon (PVDF). The frequency of the pistons, and hence the flowrate, was controlled, by means of a special pump controller, by a 4 –20 mA analog signal. It was further

possible to manually set the stroke length of the pistons. Very low and accurate flowrates could thus be achieved. $\frac{1}{4}''$ Teflon tubing was used to feed the reactants and catalyst to the reactor. The temperatures in each dosing line were measured with RTD's (3 wire, PT100) (T7 – T10).

The initial (core) and secondary (shell) reagents, as well as the delayed catalysts were pre-mixed and placed on three different balances, although provision was made for a fourth balance (Figure 3.3). The pump intakes were then connected to the mixtures by the Teflon tubing. The balances served as very accurate mass flow meters. A digital network was set up and the balance readings were transmitted to the RS232 port of the computer.

The three balances (Mettler Toledo, PB 5001F) used had a weighing capacity of 5100 g each. Provision was made for a fourth balance and dosing pump. All the balances had readabilities of 0.1 g and repeatabilities of 0.05 g.

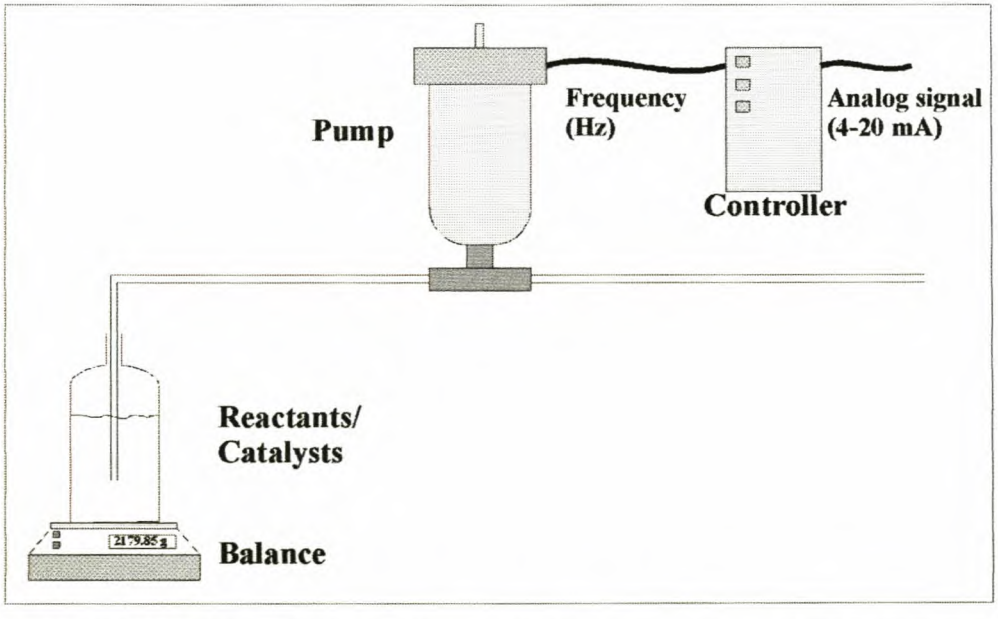

FIGURE 3.3 *Monitoring and control of the reactant/catalyst dosing.*

REACTOR

The pilot plant reactor (5 l) was a scaled-down version of an industrial-size (10 000 l) reactor, used by Plascon, to manufacture emulsions. The ratio between the reactor length and the inside diameter of the industrial size reactor, was used to obtain

the corresponding length and inside diameter of the pilot plant reactor (5 l). A constant length-to-inside diameter was thus used as scale factor.

A schematic diagram of the reactor appears in Figure 3.4, with exact dimensions summarized in Table 3.2. The reactor was manufactured from stainless steel (AISI 316 L) and the walls were 3 mm thick. A jacket was placed around the reactor, with a 6-mm clearance from the outer wall. Baffles on the inside of the jacket served to increase the residence time distribution of the heating/cooling fluid through the jackets.

The top and bottom domes were fitted to the reactor by 8-mm flanges. The domes had 10% torusspherical geometries. A set of removable, vertically aligned baffles were fixed to the inside of the reactor. Each set had four separate blades, which were aligned at right angles to the reactor wall.

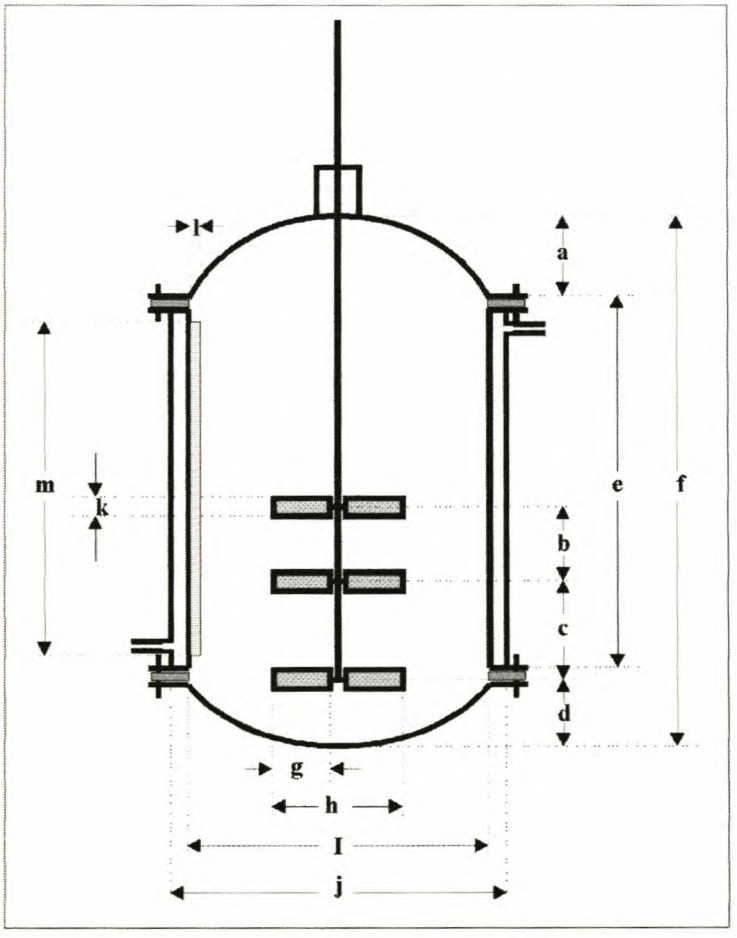

FIGURE 3.4 *Schematic diagram of reactor*

The ratios that exist between the reactor dimensions of the industrial-size reactor and its inside diameter (I) (Figure 3.4) were calculated. These ratios were kept constant, to

yield the dimensions for the pilot plant reactor as presented in Table 3.3. For example the height of the top reactor dome of the pilot plant reactor (a) (Table 3.2) was obtained as follows : $\left(a/I\right)_{Pilot\,Reactor} = \left(a/I\right)_{Full-scale\,Reactor}$

TABLE 3.2 *Exact dimensions of parts of the reactor (Figure 3.4)*

SYMBOLS	DIMENSIONS (mm)
a	44
b	43
c	58
d	46
e	200
f	295
g	39
h	92
I	174
j	194
k	17
l	12
m	161

The stirrer consisted of three sets of paddles that were fitted to the stirrer shaft (12 mm stainless steel). Each set comprised four individual, 45^0 pitch back, paddles.

A lip seal (Viton) was used to seal the stirrer shaft from the reactor. The stirrer was powered by a 550W, 4 pole, electrical motor. The motor was mounted on a set of ball bearings, to enable it to turn freely. A variable speed drive-type controller (XCB B09 4, High performance VS Mini) controlled the motor. It was possible to make very small changes to the stirring speed (N). The controller also compensated for, possible drift in stirring speed and slip losses. The torque exerted on the motor (t) by the reaction mixture, ball bearings and mechanical seal was measured by strain gauges, as illustrated in Figure 3.5.

A piece of stainless steel (AE 32 b) was machined to the following dimensions: length 90 mm, width 12 mm, thickness 2.97 mm. It was mounted 127 mm from the middle of the stirrer motor. Two strain gauges (CFC-11-5-gfgf) were placed on either side of the piece of machined stainless steel and 60 mm from its tip. A lever was machined from a piece of mild steel bar. The one end was machined into a U-shape. This end fitted loosely over the piece of stainless steel that housed the stain gauges. The mild steel bar was fitted to the motor. A constant force was hence exerted

on the piece of stainless steel when the motor was turning. The strain gauges were then coupled in closed loop and calibrated. The torque was measured as a 4 – 20 mA signal.

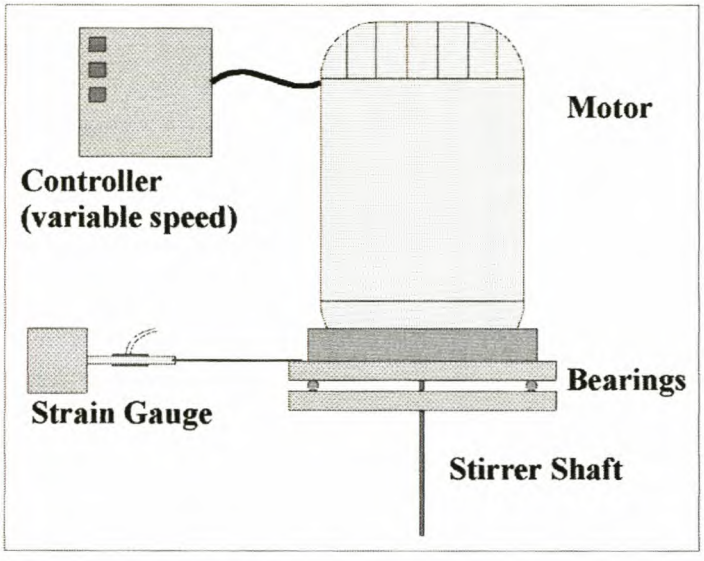

FIGURE 3.5 *Set-up used to measure torque exerted on motor*

Provision was made for four $\frac{1}{4}''$ tube, dosing lines into the reactor. Two were used for the reagents, and one for the catalysts. The other dosing line was not used in this study. Two sight glasses were fitted to the top of the reactor. An external light source was fitted to the one sight-glass hole.

A cooler/condenser was placed on the top of the reactor (Figure 3.6). It was a double-pipe-type heat exchanger (effective exchange area of 0.118 m^2). Tap water flowing through the annulus was used as coolant. The temperature and flowrate of the water were measured (T5, T6 and F2) (Figure 3.2) with RTD's (4 wire-type Pt 100's) and a flowmeter (Trimec MP 25S) respectively. The accuracy of the flowmeter was better than 0.5% of the measured flowrate. The heat load on the cooler/condenser could then be calculated. The heat load on the condenser was very small, i.e. the temperature difference of the coolant flowing through the annulus was very small, even at a very low flowrate (0.005 l/s). Special electronic circuitry had to be designed, whereby the two Pt100's measuring the inlet and outlet temperatures of the coolant were coupled in an electronic bridge, to measure the temperature difference to within 0.02 ^{0}C.

Two RTD's (3 wire Pt 100) were placed at the top and bottom of each reactor, to measure the temperature of the vapor (T2) and liquid (T1) (Figure 3.2) mixture. A sampling port, 6 mm in diameter, was placed on the top of the reactor and close to the reactor wall. This was done to minimize any disturbances to the reaction, while sampling.

The temperature difference and flowrate (T3, T4 and F1) (Figure 3.2) of the heating/cooling fluid flowing through the jacket of the reactor were measured by RTD's (4 wire Pt 100) and a very accurate flowmeter, respectively. A positive-displacement-type flowmeter (Trimec MP 25S) was used. Special electronic circuitry was also developed for the 2 Pt100's (4 wire), measuring the temperature difference of the fluid flowing through the jacket of the reactor. It was coupled in an electronic bridge. More stable and accurate temperature difference measurements were obtained. The reactor was designed to serve as a calorimeter. The accuracy of the calorimetry could be greatly improved by insulating the reactor effectively. The whole reactor was first painted with a ceramic-based paint (Ceratec, CTE 350) a further 25 mm of insulating material (ceramic blanket) was placed over the top dome, and 50 mm of the same material over the bottom dome of the reactor. 75 mm of *Thermasheet* foam was also placed around the reactor.

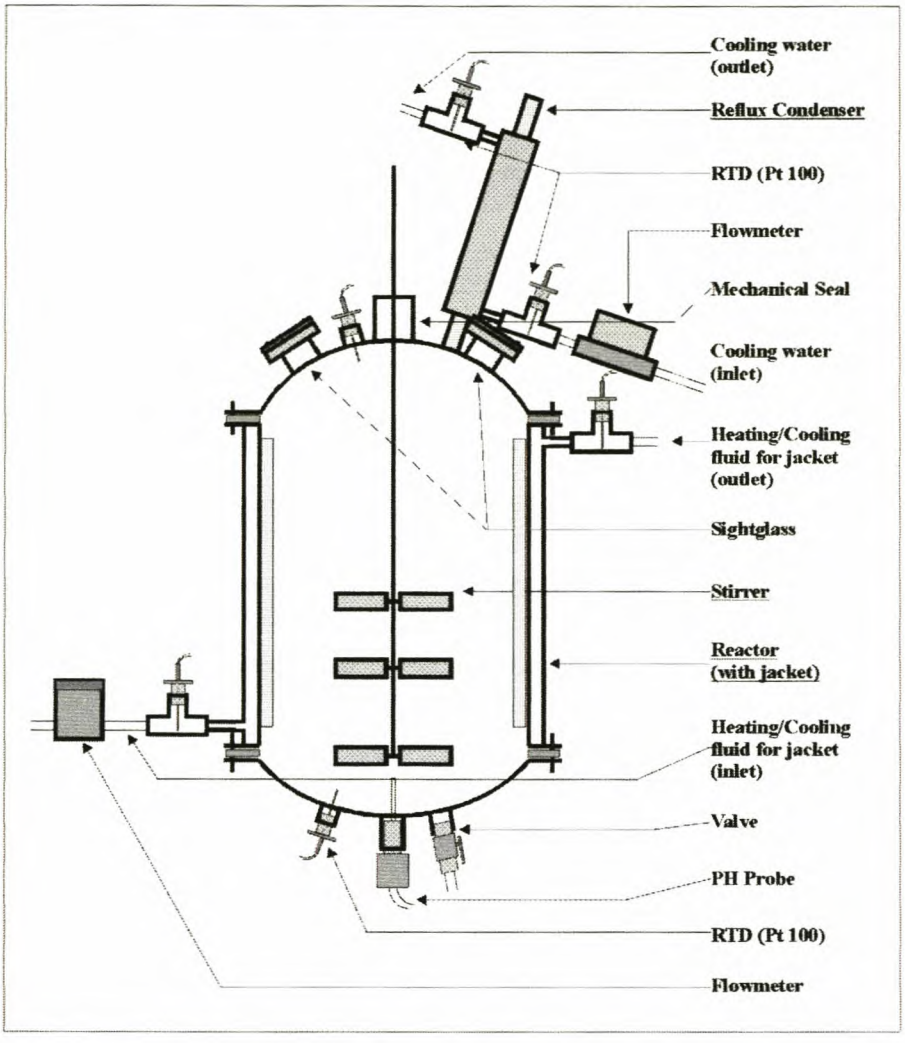

FIGURE 3.6 *Illustration of reactor with peripheral devices*

HEATING/COOLING SECTION

The temperature in the reactor was kept constant by the recirculation of a 5% mixture of water and ethylene glycol through the jacket of the reactor. The ethylene glycol was added to increase the boiling point of the water. Two reservoir tanks were used. A 3 kW heater kept the temperature in the one at an elevated temperature (≈ 92 °C) (T11), while the temperature in the other tank was kept much lower (≈ 23-25 °C) (T12). The system was designed so that the water/ethylene glycol mixture could be replaced by an oil if research needed to be conducted at elevated temperatures (90-120 ^{0}C).

A centrifugal pump, with maximum delivery of 2 m^3/h and a head of 3 bar, was connected to each tank, by means of a $1/2''$ stainless steel pipe. A recirculating

line, that ran back to each tank, was placed on the delivery side of each pump (See Figure 3.2). A gate valve in each of these lines ensured that the pumps operated at constant pressure. A shell-and-tube heat exchanger, with an effective heat transfer area of 0.70 m^2, was also placed in the recirculating line that ran back to the cold water tank. The temperature in that tank was thus kept at a reasonably constant low temperature.

Two electronically operated control valves were synchronized to regulate the flow from each tank. The hot and cold streams then joined to maintain the required temperature in the jacket, and thus in the reactor.

A third control valve and flowmeter were used to regulate the flowrate, of the circulating fluid through the jacket and into the warm water tank. The liquid level in the warm water tank was kept constant by means of an overflow to the cold water tank.

A 'normally open' solenoid valve was placed in the stream running to the jacket, and connected to an open tap. A second 'normally open' solenoid valve was placed in the stream running from the jacket, and connected to a drain. A third 'normally closed' solenoid valve was placed in the stream running from the jacket and just after the 'normally open' solenoid valve. In the event of a power failure, cold tap water was used to cool down the reactor, to prevent a possible run-a-way reaction.

CONTROL SYSTEM

An IBM compatible PC (Pentium II, 266 MHz) with a LX4 motherboard was used to control the pilot plant set-up. The motherboard housed 3 A/D and D/A PC cards respectively.

Two A/D cards were used, an Eagle Electric PC30G and an Eagle Electric PC30GA. These cards allowed for 16 single-ended or 8 differential inputs, and could be configured for unipolar (input range of 0 – 10 V) or bipolar (input range of ±5V and ±10V) operations. In this study a unipolar configuration was used, in which case the output code was straight binary. The resolution of the cards was 12 bits. Non-linearity of less than ± 0.75 LSB (least significant bit) is one of the key features of the PC30G and PC30GA cards.

One Eagle Electric PC66C D/A card was also used. It provided 12 channels of remote sensing capability, which compensates for voltage drops over long leads. DAC

settling times of less than 2 μs for a 10V-output swing is also associated with the PC66C. The DAC output voltage (span of 10 V) was variable by a reference voltage from -5V- (+)5V or from 0 – (+)10V or 0 – (-)10V. In this set-up an output voltage of 0 – 10V was used.

Software drivers (EDR software package) for the cards were available from the supplier. Some of the major features of the software package included:

- Polled, interrupt, single channel DMA and dual channel DMA data acquisition were fully supported at full throughput.
- Speed critical routines, such as polled sampling, have been coded in assembler for maximum speed.
- Streaming to disk and memory require only one DMA channel
- IRQ functions made it easy to write and install interrupt handlers from Pascal under DOS and Windows

The communication with the balances could only be achieved digitally (RS232), and it was thus necessary to set up an external digital network to interface with the balances. Some of the digital I/O lines of the PC30GA card were used to multiplex between the 3 balances, since only 2 RS232 ports are available on a PC. The digital interfaces of the balances were very slow and it took approximately 0.25 seconds to interface with each balance.

3.3 OUTLINE OF CONTROL SOFTWARE

A computer program, for the real time acquisition of data and for control purposes was written in Turbo Pascal. The computer program and a flow diagram thereof are presented in Addendum A. The program was run under DOS, to ensure dedicated processing by the computer, and hence maximum stability. This would not have been possible in a Windows environment, since Windows executes every program in a timeslice. The same stability would not have been possible. The program was structured in the form of different repeat loops and no interrupts were used.

The 3 PC cards were first initialized. That included the 3 PC cards, as well as the 4 balances. Each PC card was allocated to a baseaddres and given a board handle. The input and output ranges of the channels on the PC30G, PC30GA and the PC66C cards were set to a span of 0 -10V. This was achieved with specific calls to the drivers of the respective cards. A separate unit (weeg.pas) (Appendix B) was used to establish

serial communication with the balances. During initialization the port number, as well as the baudrate (19200 bits/s), were set.

Two data files, a calibration file (kal.dat) and an initial value file (init.dat) (Appendix C), were then initialized. The calibration file was used to convert all the input voltages to engineering units. The initial value file was used to set all the process setpoints, for example the reactor temperature, stirrer speed and dosing rates of the reactants and catalysts.

The program then proceeded to a warm-up cycle. In the first part of the warm-up, the valve controlling the flowrate of the heating/cooling fluid was set to open approximately 80% and that of the cooling fluid to open approximately 20%. The flowrate of the water flowing through the condenser (0.005 l/s) was set manually and kept constant for the duration of an experiment. The flowrate of heating/cooling fluid flowing through the jacket was set to approximately 0.07 l/s. This continued until the reactor temperature reached 99.99 % of its setpoint value. In the second part of the warm-up cycle the reactor was then controlled to within a 1 ^{0}C band around its setpoint and the flowrate of heating/cooling fluid through the jacket to its setpoint value (0.045 l/s). A further 24 min was allowed for the temperature inside the reactor to reach its setpoint value. Once the warm-up conditions were reached the program then proceeded to its main control loop.

In the main control loop, which repeated every 2 seconds, the readings from the balances were first obtained. All the other process inputs were then obtained (Table 3.3). The control action of the final control elements (valves, pumps, etc.) was then calculated whereafter control action was taken. All calorimetric and other relevant calculations then proceeded.

TABLE 3.3 *Summary of process inputs and outputs*

	PROCESS MEASUREMENTS
1	Balance reading 1 (Core)
2	Balance reading 2 (Shell)
3	Balance reading 3 (Catalyst)
4	Temperature of monomer: feed 1 (Core)
5	Temperature of monomer: feed 2 (Shell)
6	Temperature of catalyst: feed 3 (Catalyst)
7	Temperature of warm water tank
8	Temperature of cold water tank
9	Temperature of reacting vapour
10	Temperature of reacting liquid
11	Temperature at jacket inlet
12	Ambient temperature
13	Temperaure difference across jacket
14	Temperaure difference across condenser
15	Flowrate of recirculating fluid
16	Flowrate of condenser coolant
17	Torque
18	Calibration heater: Current
19	Calibration heater: Volt
	CONTROL OUTPUTS
1	Dosing pump 1 (Core)
2	Dosing pump 2 (Shell)
3	Dosing pump 3 (Catalyst)
4	Stirrer
5	Valve 1 (Warm water tank)
6	Valve 2 (Cold water tank)
7	Valve 3 (Jacket flowrate)

All the values of the input variables were then updated on the computer screen as well as written to file (plascon.txt). The main control loop repeated itself for the duration of the experiments ($2\frac{3}{4} - 4\frac{1}{4}$ hours). In the last part of the control program, the reactor temperature was kept constant for a further 30 min, to ensure the reaction was completed. The reactor temperature was then reduced to 70 ^{0}C where some of the post-treatment chemicals were added.

The reactor was then cooled down to 35 ^{0}C, all of the post-treatment chemicals were added, and all the boardhandles were released.

3.4 CONTROL METHODOLOGY

3.4.1 CONTROL ACTION

The flowrate of the circulating heating/cooling liquid through the jacket of the reactor was kept very low (0.045 l/s) to thereby try to increase the sensitivity of the calorimeter. This was a definitive control problem.

Proportional control algorithms were developed. A scheduled-gain-approach to the proportional controller was first tried. Stable control was only achieved for the flowrate of the heating/cooling liquid, as well as the dosing rates of the pumps. Good control over the temperature in the reactor could not be achieved. The temperature in the reactor oscillated within a 3-4 °C band around the reactor setpoint. No improvement was obtained even after extensive tuning. Adding integral and derivative control to the existing proportional controller then developed a digital PID controller. The design methodology of Seborg et al. (1989, pp.183-196, pp.614-627), was followed.

3.4.2 DESIGN OF A DIGITAL PID CONTROLLER

The ideal continuous (analog) PID controller is given by Seborg et al:

$$p(t) = \bar{p} + K_c\left[e(t) + \frac{1}{\tau_I}\int_0^t e(t')dt' + \tau_D\frac{de(t)}{dt}\right] \qquad .....3.1$$

where,

$$e(t) = R(t) - B(t) \qquad .....3.2$$

and p(t) = controller output

$\bar{p}$ = bias value

K_c = controller gain

e(t) = error signal

R(t) = setpoint

B(t) = measured value of the controlled variable

τ_I = time constant (integral action)

τ_D = time constant (derivative action)

The integral term in Eq. 3.1 is converted to a digital equivalent by using a trapezoidal finite difference approximation:

$$\int_0^t e(t')dt' \approx \sum_{k=1}^{n}\left(\frac{e_k + e_{k-1}}{2}\right)\Delta t \qquad \text{.....3.3}$$

$$\frac{de}{dt} \approx \frac{e_n - e_{n-1}}{\Delta t} \qquad \text{.....3.4}$$

where, Δt = sampling period

p_n = controller output at the n^{th} sampling period

e_n = error at the n^{th} sampling period

It is important to note that the summation begins at k = 1, since it is assumed that the system is at the desired steady state for $k \leq 0$, that is, $e_k = 0$ for $k \leq 0$.

The digital PID controller equation can be written in two ways, the position form and the velocity form. The position form (Eq. 3.5) can be obtained by substituting Eq.3.3 and Eq.3.4 into Eq.3.1.

POSITION ALGORITHM

$$p_n = \bar{p} + K_c\left[e_n + \frac{\Delta t}{2\tau_I}\sum_{k=1}^{n}(e_k + e_{k-1}) + \frac{\tau_D}{\Delta t}(e_n - e_{n-1})\right] \qquad \text{.....3.5}$$

The controller output is calculated directly from Eq.3.5 and is therefore referred to as the position form of the control law.

VELOCITY ALGORITHM

In the velocity form of the PID controller the computation of the summation in Eq.3.5 is avoided, making it an attractive alternative to the position form. The velocity form is obtained by writing Eq.3.5 for the (n-1) sampling instant (Eq.3.6) and then subtracting it from Eq.3.5:

$$p_{n-1} = \bar{p} + K_c\left[e_{n-1} + \frac{\Delta t}{2\tau_I}\sum_{k=1}^{n-1}(e_k + e_{k-1}) + \frac{\tau_D}{\Delta t}(e_{n-1} - e_{n-2})\right] \qquad \text{.....3.6}$$

$$\Delta p_n = p_n - p_{n-1} = K_c\left[(e_n - e_{n-1}) + \frac{\Delta t}{2\tau_I}(e_n + e_{n-1}) + \frac{\tau_D}{\Delta t}(e_n - 2e_{n-1} + e_{n-2})\right] \qquad \text{.....3.7}$$

3.4.2.1 COMPARISON BETWEEN POSITION AND VELOCITY ALGORITHMS

The position form of the PID controller explicitly requires specification of the steady state value of the controller output (bias term, $\bar{p}$), which is not the case with

the velocity form, where only the previous controller output value is required. The velocity form is also less prone to reset windup. Since manual operation of the control system usually precedes the transfer to automatic control, the initialization of the position form is just as easy as that of the velocity form, because $\bar{p}$, or p_{n-1} for the velocity form, is taken as the signal to the final control element at the time of transfer.

3.4.3 CONTROL OF PROCESS VARIABLES

The flowrate of the circulating heating/cooling fluid through the jacket of the reactor was measured every 2 seconds. A control valve served as a final control element. It was an electronically operated non-linear acting control valve. Very good control was obtained over the flowrate, which was kept very constant throughout an experimental run.

Two electronically operated, non-linear acting control valves served as final control elements in controlling the temperature in the reactor. The valves controlled the flowrate of the hot and cold circulating fluids. The two valves were synchronized (§3.2.2). If $p_n(1)$ represented the control action of valve 1, the control action of valve 2 could be given as: $p_n(2) = - p_n(1)$, so that the sum of their analogue output signals would always add up to 10V. A slow response was obtained, due to the very low flowrate of the circulating heating/cooling fluid. Very good and stable control was possible when very little derivative action was used and a sufficiently small controller gain was used.

The delivery rate of each dosing pump remained very stable over long periods of time. Each dosing pump was carefully calibrated to ensure as little overshoot as possible, especially at start-up. Control action was taken every four seconds and this further aided in establishing a very smooth and constant dosing profile.

A calibration profile was obtained for the stirrer. A linear acting controller was used to control the stirring speed. The stirring speed stayed very stable and no drift was encountered. The stirrer was calibrated regularly.

3.5 CALIBRATION OF ELECTRONIC EQUIPMENT

3.5.1 MAJOR EQUIPMENT

The temperature sensors and transmitters were calibrated for a temperature range of 0 – 100 °C. The transmitters of the 4 wire Pt 100's were factory calibrated. It was however possible to change the zero and the span of the 3 wire Pt 100's transmitters on the transmitters themselves.

All the electronic equipment was switched on and left for at least 2 days, for it to reach operating temperature. The temperature probes of the Pt 100's were disconnected. A high precision Field Calibrator (Unomat, TRX) was connected to the transmitters. A 100 Ω (0 °C) resistance was simulated and the zero of the transmitters were set. A 138.5 Ω (100 °C) resistance was then simulated and the span of the transmitters were set. The accuracy of the calibration was verified by simulating 3 temperatures between 0 – 100 °C. The same procedure was repeated for the 4-wire Pt 100's and any deviations that occurred were taken into account in the calibration data file (kal.dat) (Addendum C). This calibration procedure was repeated regularly.

Calibration certificates were included with each of the two flowmeters. It was necessary to set up the transmitters for the flowmeters in order to convert the frequency output to a volt output. The transmitters were set up to operate between 0 – 40 Hz input frequency, where 0 Hz represented 0 V and 40 Hz represented 10 V. The linearity of the transmitters were verified with an oscilloscope. The flowmeters and transmitters were then installed and calibrated by measuring the time it took to fill a fixed volume. The results obtained were compared with the factory's calibration results. The results agreed well.

The pH probe and transmitter were calibrated as a unit, by using the built-in calibration procedure of the transmitter. Buffer 4 and buffer 10 solutions were used for calibration purposes. The calibration procedure was verified by using a buffer 7 solution. The analogue output signal of the transmitter was calibrated accordingly, where 0 V represented pH 0 and 10 V represented pH 14.

The stirrer was calibrated, using a tachometer (SPM TAC-10). A calibration curve was drawn up, by measuring the stirrer speed for different analogue output signals to the motor. Very linear curves were obtained. A typical calibration curve for the stirrer is shown in Figure 3.7.

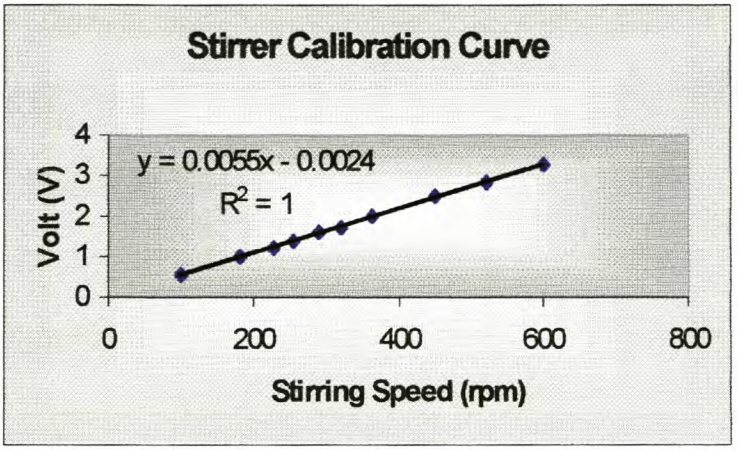

FIGURE 3.7 *A typical calibration curve for the stirrer*

The strain gauges were calibrated by applying a constant force and measuring the analogue output signal. A piece of Nylon string was fixed to the top of the metal bar. The string was kept perpendicular to the metal bar and was allowed to move freely over a thin polished stainless steel rod. Different weights were placed on the end of the string, to simulate a different magnitude of force applied and the analogue signal was then measured. The torque was calculated using the following relation:

$$\tau = \mathrm{F} \times r \times \sin\theta \qquad \text{.....3.8}$$

where the torque (τ) is given in units of Nm, the force applied (F) in units of Newton the moment arm (r) in units of meter and the angle (θ) at which the force is applied in units of radians. The moment arm was fixed at 0.147 m in the experimental set-up. A linear relation existed between the applied torque and the analogue output signal.

3.6 CALORIMETRIC CALCULATIONS

3.6.1 ENERGY BALANCE EQUATIONS

In order for the reactor to be used as a calorimeter the heat flow over the system boundaries needed to be known for any given time interval. The heat of reaction could be calculated by performing an accurate energy balance around the system boundaries (reactor):

$$\frac{dE}{dt} = \dot{E}_{in} - \dot{E}_{out} + \dot{Q} - W_t \qquad \text{.....3.9}$$

where,

$$\frac{dE}{dt} = MC_p \frac{dT_r}{dt} + M(T_r - T_{ref})\frac{dC_p}{dt} + C_p(T_r - T_{ref})\frac{dM}{dt} \qquad \text{.....3.10}$$

and M : reactor mass (kg)

C_p : heat capacity ($kJ/kg.^oC$)

T_r : reactor temperature (°C)

T_{ref} : reference temperature (25 °C)

$\frac{dE}{dt}$: energy accumulation (kW)

$\dot{E}_{in}$: energy flowing into the system (kW)

$\dot{E}_{out}$: energy flowing out of the system (kW)

$\dot{Q}$: energy generation (kW)

W_t : work applied to the system by the stirrer (kW).

Experiments were conducted in a semi-batch reactor. No mass was thus flowing out of the system, i.e. $\dot{E}_{out} = 0$. Eq.3.9 can be expanded by the following relationships:

$$\dot{E}_{in} = \sum_{i=1}^{n} m_i C_{p,i} (T_{in,i} - T_{ref}) \quad .....3.11$$

$$W_t = N \tau_r \quad .....3.12$$

$$\dot{Q} = \dot{Q}_{jacket} + \dot{Q}_{cond} + \dot{Q}_{losses} + \dot{Q}_{HR} \quad .....3.13$$

where,

$$\dot{Q}_{jacket} = \dot{m}_{jacket} C_p (T_{jacket,in} - T_{jacket,out}) \quad .....3.14$$

$$\dot{Q}_{cond} = \dot{m}_{cond} C_p (T_{cond,in} - T_{cond,out}) \quad .....3.15$$

and m_i : mass flowrate of component i into the reactor (kg/s)

$C_{p,i}$: heat capacity of component i ($kJ/kg.^oC$)

$T_{in,i}$: inlet temperature of component i (°C)

n : number of components fed to the reactor (n = 3)

N : stirrer speed ($1/s$)

τ_r : measured torque exerted by the reacting mixture on the motor (N.m)

$\dot{Q}_{jacket}$: heat duty on the jacket (kW)

$\dot{Q}_{cond}$: heat duty on the condenser (kW)

$\dot{Q}_{losses}$: heat losses from the reactor (kW)

$\dot{Q}_{HR}$: heat of reaction (kW)

$\dot{m}_{jacket}$: mass of liquid flowing through the jacket per unit of time ($^{kg}/_{s}$)

$\dot{m}_{cond}$: mass of liquid flowing through the condenser per unit of time ($^{kg}/_{s}$)

The subscripts jacket and cond refer to the jacket and the condenser of the reactor respectively (e.g. $T_{jacket,in}$ refers to the inlet temperature of the fluid flowing through the jacket of the reactor). Substituting Eq. 3.13 into Eq. 3.9 and using the fact that $\dot{E}_{out} = 0$ leads to the following:

$$\frac{dE}{dt} = \dot{E}_{in} + \dot{Q}_{jacket} + \dot{Q}_{cond} + \dot{Q}_{losses} + \dot{Q}_{HR} - W_t \qquad \text{.....3.16}$$

The heat of reaction can be obtained explicitly by rearranging Eq.3.16 and ignoring the work done on the system by the stirrer. The work done by the stirrer contributed less than 0.5% (≈ 6 kJ) of the total accumulated heat of reaction (≈1100 kJ).

$$\dot{Q}_{HR} = \frac{dE}{dt} - \dot{E}_{in} - \dot{Q}_{jacket} - \dot{Q}_{cond} - \dot{Q}_{losses} \qquad \text{.....3.17}$$

Substituting Eq.3.13 and 3.14 into Eq.3.17 and using the following conventions:

Heat added to the system : (+)Q ; *Heat removed from the system* : (-)Q

Work done on the system : (-)W; *Work done by the system* : (+)W

Heat was removed from the system ($\dot{Q}_{jacket}$ and $\dot{Q}_{cond}$) and a certain amount of heat was also lost ($\dot{Q}_{losses}$) to the surroundings. By definition (Eq. 3.11), heat was added to the system by the addition of the monomers and catalyst ($\dot{E}_{in}$). Hence Eq. 3.17 can be expanded to Eq. 3.18.

$$\dot{Q}_{HR} = \frac{dE}{dt} - \dot{E}_{in} + \dot{Q}_{losses} + \dot{m}_{jacket} C_p (T_{jacket,out} - T_{jacket,in}) + \dot{m}_{cond} C_p (T_{cond,out} - T_{cond,in})$$

.....3.18

In Eq.3.18 the heat loss term ($\dot{Q}_{losses}$), as well as the change in the heat capacity of the reacting liquid are yet unknown. In order to use Eq.3.18, to calculate

the heat of reaction, independent experiments had to be performed to evaluate the unknown term $\frac{dC_p}{dt}$.

3.6.2 CHANGE IN THE HEAT CAPACITY OF THE REACTING LIQUID

It is virtually impossible to calculate the heat capacity of complex latex particles, in an emulsion, because the exact polymer composition is not always known. The extent of co-polymerization and crosslinking, in the case of multi component latex particles, render any type of calculation worthless. The heat capacities for such polymer particles have to be measured.

In the experiments conducted approximately 13 samples (approximately 8 ml each) were withdrawn at fixed intervals over the period of reaction. The samples of the reaction mixture were terminated with the aid of a 1% Hydroquinone solution and then placed on ice. The samples were then stored in a fridge at 4 °C for further analysis.

A technique was developed by which to measure the heat capacity of complex latex particles, using Diffractional Scanning Calorimetry (DSC). The instrument (DSC) (Perkin Elmer, Pyris 1) with a Thermal Analyzer Controller (TAC 7/DX) (thermal gravimetrical analysis) was used to run the "wet" samples in open pans. Preliminary thermal gravimetrical analyses (TGA) revealed that experiments on the DSC could be conducted to a maximum temperature of 45 °C. This was done to prevent possible corrosion of the oven of the DSC.

The instrument was calibrated before each run. Two empty aluminum pans were weighed and placed in the oven. One of the pans served as a reference pan. The empty sample pans were then heated from 20 °C to 45 °C at a rate of 5 $^{\circ C}/_{\min}$. The amount of heat needed to heat the sample pan in relation to the reference pan was measured and plotted against temperature. Calibration curves were generated for each empty sample pan. It was found that there existed a very linear relationship between the amount of heat needed to heat the sample pan relative to the reference pan and the temperature of the sample pan.

Each sample pan was then filled with a known mass (10-20 mg) of emulsion. The amount of heat needed to heat the sample and sample pan relative to the reference

pan was plotted against the temperature. A very linear relationship existed between the heat input and the temperature in the temperature range 20-35 °C. The slight non-linearity that existed at the higher temperature could partly be explained by evaporation of the more volatile organic compounds present in the emulsion.

The instruments software made it possible to calculate the heat input for small temperature differences very accurately. This procedure was repeated at different temperature intervals for each sample. The calibration curves were used to calculate the absolute amount of heat necessary to heat the sample over a certain temperature interval. The average heat capacity ($\bar{C}_p^{ij}$) could then be calculated over the small temperature interval, using Eq.3.19.

$$(\dot{Q}_{avg}^{ij} - \dot{Q}_{cal}^{ij}) \times \Delta t = m\bar{C}_p^{ij}(T_j - T_i) \qquad \text{.....3.19}$$

where $\dot{Q}_{avg}^{ij}$ represents the average amount of heat necessary to heat a sample of mass, m, and the sample pan from an initial temperature, T_i to a final temperature, T_j, over a period of, Δt. The average amount of heat necessary to heat the sample pan in relation to the reference pan is represented by $\dot{Q}_{cal}^{ij}$ (obtained from the calibration curve).

Linear regression was used and a mathematical model of the form:

$$C_p = at + bT + c$$

was derived, describing the temperature (T) and time (t) dependence on the heat capacity of the emulsion. a, b and c represent regression coefficients. An example of a typical calibration curve and a sample curve are included in Appendix D.

3.6.3 HEAT LOSSES FROM THE REACTOR

3.6.3.1 CALIBRATION SET-UP

Small reaction vessels depict large $^{area}/_{volume}$ ratios and thus large heat losses. Increasing the amount of insulation around the reaction vessel will decrease the heat losses, but the exact amount of heat loss to the surroundings needs to be known exactly in order to perform an accurate energy balance around a reactor.

The heat losses can be calculated by performing a simple energy balance around the reactor. Two options were available. The first involved the addition of a known amount of heat to a non-reacting liquid inside the reactor (calibration heater),

and the second involved the use of a reacting system with a known heat of reaction (e.g. acid/base dilution), and then performing an energy balance around the reactor. The resulting heat removed by the condenser and jacket are measured and the respective heat losses calculated. The first option was used to set up a model for the heat losses and the second option was then used to quantify its accuracy.

The reactor was loaded with 3.174 kg of a 42.5% (mass base) sodium hydroxide solution. Distilled water was added to the reactor over a period of 1 h. The main control program (Plascon.txt) was used and the reactor temperature as well as the stirring speed were kept constant at 85 ^{0}C and 250 rpm, respectively. The cumulative heat of solution was obtained on-line. The theoretical heat of solution was calculated and compared with the experimental value obtained. The results are given in Chapter 4 (§ 4.2.3).

A 750 W (24 V, AC) heater was specially manufactured to fit onto the top of the reactor, by utilizing one of the sight glass holes. The heater was extended (Figure 3.8) using special Teflon insulating material. This was done in order to minimize the possible heat transfer to the fitting, as well as to its surroundings, through possible convection and radiation. The heater was placed in the bottom part of the reactor, without touching the walls, but deep enough as to be covered by the initial reactor charge (2.099 kg).

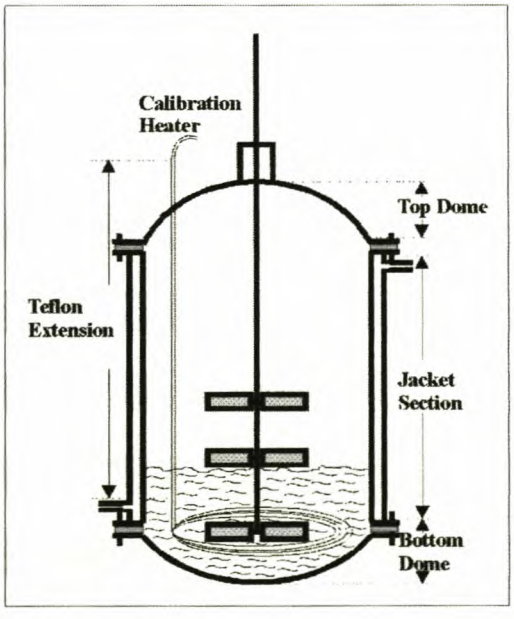

FIGURE 3.8 *Calibration heater set-up*

The heat added to the reactor by the calibration heater was calculated by measuring the potential difference across the heater as well as the current flowing through it.

$$\dot{Q}_{heater} = {}^{(I \times V)}\!/_{1000} \qquad \text{.....3.20}$$

where $\dot{Q}_{heater}$ represents the heat added to the liquid within the reactor by the calibration heater in units of kW and I donates the current flowing through the heater and V the potential difference across the heater in units of Ampère (A) and Volts (V) respectively.

There existed no cheap and accurate way of measuring alternating current (AC). A set-up was hence developed, a brief description of which is included in the next paragraph, to transform the alternating current to direct current (DC) and then to smooth it, for accurate measurements.

The 1000 VA transformer (XF 1) had tap points at 4 Volt increments (Figure 3.9), up to 24 Volt. A diode bridge, DB 1, restricted the AC current and basic voltage smoothing was carried out by two large capacitors, C1 (33000 μF) and C2 (33000 μF). The transistors T1, T2, T3 and T4 (type 2N3055) were employed, because it is difficult to smooth a large current with capacitors alone. Each transistor could handle a maximum of 10 Amp, and four were thus used in parallel. The 4 resistors R2 – R5 (0.01 Ω) were included in the circuit to ensure an even distribution of the total current between the 4 transistors. At full transistor (2N3055) gain (50) the output current was 35 Ampere, while the base current flowing through R1 was only 0.7 Ampere. R1 was chosen to ensure a maximum drop in voltage across the transistors of 3 Volt, at maximum current.

The voltage at the base of the transistors was smoothed by capacitor C3 (20000 μF). The relatively low base current ensured that efficient smoothing be obtained with a relatively small capacitor.

The output voltage was adjusted by changing the tap points on the transformer. Experiments were conducted in which the first 2 tap points were used to produce power output of approximately 24W and 90W. The output current was determined by measuring the voltage drop across R6 (0.03Ω), while the output voltage was measured across the heater element, H. Instantaneous power was calculated using Eq.3.20.

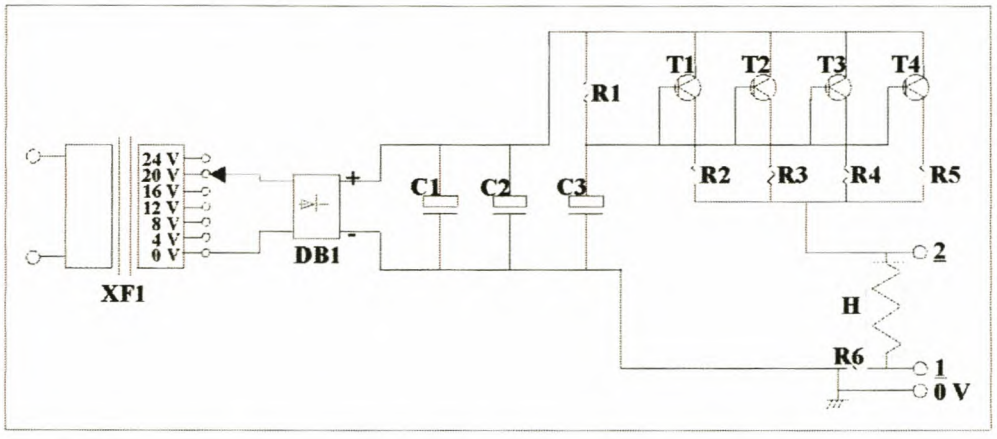

FIGURE 3.9 *Electronic layout of heater circuitry*

Eqs. 3.9, 3.10 and 3.13 (derived in Section 3.5.1) were simplified and used to calculate the heat losses from the reactor. It was assumed that the work done by the stirrer on the liquid inside the reactor as well as its change in heat capacity due to variations off its setpoint be neglected. No reactants were added to the reactor during a calibration run and therefore $\dot{E}_{in} = 0$ and $\frac{dM}{dt} = 0$. $\dot{E}_{out} = 0$ for the same reason as in Section 3.5.1. The following simplified equations could hence be derived:

$$\frac{dE}{dt} = \dot{Q} \qquad \text{.....3.21}$$

where

$$\frac{dE}{dt} = MC_p \frac{dT_r}{dt} \qquad \text{.....3.22}$$

and

$$\dot{Q} = \dot{Q}_{jacket} + \dot{Q}_{cond} + \dot{Q}_{losses} \qquad \text{.....3.23}$$

The heat losses could be calculated by substituting Eq.3.23 and Eq.3.22 into Eq.3.21 and using Eq.3.14 and Eq.3.15 to obtain the heat loss term explicitly:

$$\dot{Q}_{losses} = \frac{dE}{dt} + \dot{m}_{jacket} C_p (T_{jacket,out} - T_{jacket,in}) + \dot{m}_{cond} C_p (T_{cond,out} - T_{cond,in})$$

.....3.24

3.6.3.2 CALIBRATION PROCEDURE

The flowrate of the liquid flowing through the jacket of the reactor (0.045 l/s), as well as the flowrate of the coolant (water) flowing through the annulus of the condenser (0.005 l/s) were kept constant throughout all experiments.

Water was used in most of the calibration runs. Experimental results (Chapter 4) proved that the physical properties of the liquid within the reactor, as well as its level within the reactor, would have no effect on the heat losses from the reactor.

Experiments were conducted with different reactor loadings. The reactor was first charged with a loading equal to the initial loading (2.099 kg) of the recipe (Table 3.1). Experiments were then conducted in which full reactor loadings were used. Different stirring speeds (125, 250 and 375 rpm) were used. The reactor was also run at different temperatures (82.5, 85, 87.5 °C). Certain experiments were then repeated with a finished emulsion product, instead of pure water. The software used (reactor.pas) was specifically developed for the heat-loss-calibration-procedure.

The reactor was charged with a known mass of liquid and brought to operating temperature, wereafter the calibration heater was switched on. The process outputs (e.g. reactor temperature and flowrate of liquid through the jacket of the reactor) were written to the hard drive of the computer as a text file (output.txt). The calibration runs lasted at least 75 minutes, which is considerably longer than the 10 minutes allowed by De La Rosa et al., (1996). The average heat loss from the reactor could then be calculated. It was found that the heat losses were strongly influenced by the reactor and ambient temperatures.

The heat transfer from the reactor can be given as (Incropera & De Witt, 1990):

$$\dot{Q}_{losses} = \dot{Q}_{conduction} + \dot{Q}_{convection} + \dot{Q}_{radiation} \qquad \text{.....3.25}$$

$$\dot{Q}_{losses} = kA(T_{reac,1} - T_{reac,2}) + hA(T_{reac,2} - T_{ambient}) + \varepsilon A\sigma((T'_{reac,2})^4 - (T'_{ambient})^4) \qquad \text{.....3.26}$$

where $(\dot{Q}_{conduction}, \dot{Q}_{convection}, \dot{Q}_{radiation})$ refer to the heat transfer by conduction, convection and radiation, and in units of kW.

k : conduction coefficient $(kW/m^2.^oC)$

A : heat transfer area (m^2)

h : convection coefficient ($^{kW}/_{m^2.^oC}$);

ε : emissivity ( )

σ : Stefan Boltzman constant ($5.67 \times 10^{-11}\ ^{kW}/_{m^2.K^4}$).

T' refers to the temperature in units of Kelvin. The subscripts reac,1 and reac,2 refer to the inner wall and outer wall of the reactor and ambient, to the surroundings, respectively.

Linear regression was used to derived a heat loss model of the form :

$$\dot{Q}_{losses} = k_1(T_r - T_{ambient}) + k_2((T_r')^4 - (T_{ambient}')^4) \qquad .....3.27$$

3.7 EXPERIMENTAL

3.7.1 EXPERIMENTAL PROCEDURE

3.7.1.1 EXPERIMENTAL ROUTINE

The electronic equipment was switched on at the beginning of the experimental section of the project and left on. This was done so that the electronic equipment could stabilize. The flowrate of the coolant (water) flowing through the annulus of the condenser was set well before the start of an experimental run. The windows in the laboratory were kept closed and the extractor fans on.

The respective monomers used to manufacture the core and shell were pre-weighed in two separate glass tanks. The mixture in each tank was carefully stirred. The same procedure was followed for the delayed catalyst. The three tanks were then placed on their respective balances. The ball valves, which were placed just before the inlet to the reactor, were used to close the dosing lines and then each dosing line's purge valve was opened. The dosing pumps were set to manual, whereafter the dosing lines was filled with reactant/catalyst. The dosing pumps were set back to analogue control, the purge valves were closed and the valves on the main dosing lines opened. The balances were then zeroed.

The initial reactor load was charged to the reactor, with the exception of the initial catalyst. Updating the init.dat file set the reaction conditions. The main control program was initialized and the reactor was switched over to full computer control.

It took approximately 30 minutes for the temperature inside the reactor to reach its setpoint value. A further 24 minutes was allowed for the reactor and its peripheral devices to reach steady state. The initial catalyst was then added and the hatch on the reactor closed. Activation of the initial catalyst took approximately 6 minutes immediately whereafter dosing of the core monomers and delayed catalyst was started. Addition of the core monomers and its delayed catalyst proceeded over a maximum period of 2 hours. Addition of the shell monomers and its delayed catalyst were started immediately thereafter, and lasted a further maximum period of 2 – and $2\,1/4$ hours. All monomers were thus added to the reactor over a maximum period of 4 hours. The catalyst was, however, added over a maximum period of $4\,1/4$ hours, ensuring the reaction of most of the free monomers possibly still present. A further 30 minutes was allowed to ensure the depletion of all monomer and catalyst.

The emulsion was then cooled to approximately 35 °C, whereafter the addition of the post-treatment chemicals could commence. Constant stirring was applied throughout.

The $1/2''$ - ball valve, situated on the bottom of the reactor, was used to drain the emulsion. Immediate cleaning of the reactor was then started. The polymer present in the emulsion has a thermosetting character, hence cold tap water was used for this purpose. The monomer and catalyst tanks and dosing lines were cleaned. Water was then pumped through the lines. This procedure was repeated after each run. In spite of the very thorough cleaning technique used, fouling of the reactor walls still occurred.

Three main process variables were identified; these were stirring speed, reaction temperature and reaction time. Experiments were carried out in which the stirring speed was varied between (150 – 550) rpm, while the reactor temperature (85 ^{0}C) and addition time of the monomers was kept constant (4 hrs).

Experiments were then conducted in which the reaction temperature was varied between (90 – 70) ^{0}C, during which time the stirring speed and monomer addition time was kept constant at 250 rpm and 4 hrs, respectively.

Experiments were then conducted in which the time of monomer addition and hence the time of reaction was varied. The total time of reaction was reduced up to a maximum of 37.5%. In these reactions the stirring speed and reactor temperature were kept constant at 250 rpm and 85 ^{0}C, respectively.

3.7.1.2 SAMPLING

The sample port at the top of the reactor was initially used for sample taking. A 10-ml gas tight syringe, with a 110 mm needle, specifically manufactured for the purpose, was used to withdraw samples. The initial reactor loading constituted only 41% of the total reactor capacity. It was impossible to reach the reaction mixture with the syringe and needle, only. In order therefore to reach the liquid in the bottom part of the reactor a long (450 mm) thin Teflon tube was placed over the needle of the syringe. This arrangement was not successful because the Teflon tube got entangled in the top set of paddles. The Teflon tube was then replaced with a piece of stainless steel tubing, which proved to be more successful.

As the viscosity of the reacting liquid increased, sampling by the method described above, became very difficult. It became virtually impossible to withdraw samples towards the end of the reaction, due to the increase in viscosity. The sampling time also became very long. It took more than 2 minutes to withdraw a 10-ml sample. Cleaning of the needle and length of tubing was extremely difficult. The tubing also frequently clogged up. It was then decided to withdraw samples, using the $\frac{1}{2}''$-base valve.

Purging 10-15 ml of the reaction mixture first drained the valve. It was however immediately returned to the reactor, whereafter a sample was taken. The reaction in each sample was immediately terminated by 2 drops of a 1% Hydroquinone solution. The samples were then placed on ice and stored in a fridge at 4 °C.

Initially 20 samples were taken during the course of the reaction. It was found that the reaction could be successfully characterized by withdrawing only 15 samples. 8 Samples of 6-ml each and 9 samples of 20-ml each were withdrawn from the reactor, per run.

The influence of sample taking on the emulsion polymerization of NW 120 was determined by repeating a run in which no samples were withdrawn from the reactor during the course of the reaction. The physical properties (density, % solids, viscosity and particle size) of the products were compared. In the open literature, no mention could be found of the influence of sample taking, on emulsion polymerization systems. The results obtained in this study are included in Chapter 4 (§ 4.3.4).

3.7.1.3 REACTOR CLEAN-OUT

Experiments were conducted in which the process variables ranged from very low to very high upper limits. A certain amount of fouling of the inner walls of the reactor was hence experienced. A photograph of the inside of the reactor (Figure 3.10) was taken after the completion of a series of 9 experiments. Some of the experimental work involved reactor temperature variations ranging between 90 – 70 ^{0}C.

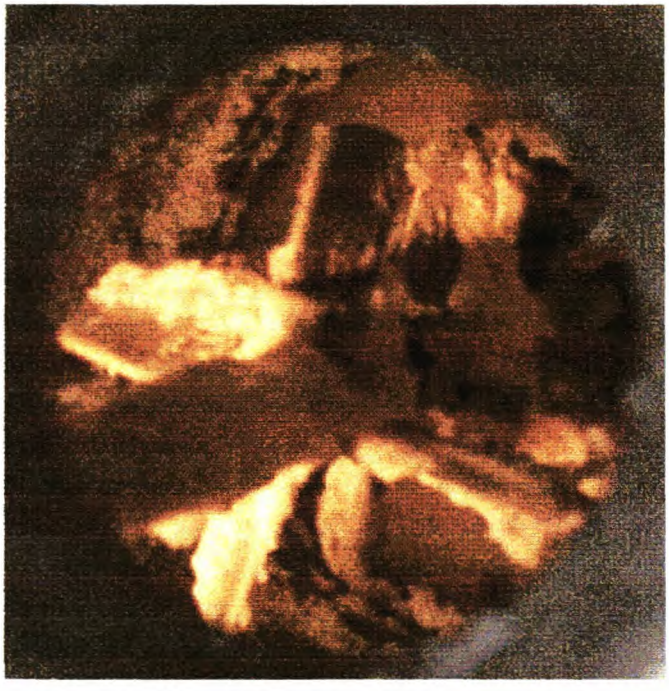

FIGURE 3.10 *Photograph of reactor inside*

Industrial reactors are normally 'boiled out' with solvents. Mixture of solvents are frequently used and the composition will vary from plant to plant. A similar technique was used to clean the newly developed pilot plant reactor.

The reactor was filled with a mixture of solvents and heated to 85 ^{0}C. The stirring speed was set at 250 rpm. The reactor temperature and stirring speed were maintained for at least 3 –5 hrs. The temperature of the solvent mixture inside the reactor was allowed to cool down naturally and then left inside the reactor for at least 48 hrs. The 'boilout' procedure was repeated with water. The reactor was then repeatedly rinsed with water to ensure that it was clean and free of all solvents.

3.8 ANALYTICAL ANALYSIS

The conversion, viscosity particle size and solids content of each sample, withdrawn from the reactor, were measured/analyzed. The particle size distribution was obtained at the end of the core phase, as well for the product. The molecular weights were also determined, for two selected experiments.

3.8.1 CONVERSION MONITORING

3.8.1.1 GAS CHROMATOGRAPH SET-UP

A Gas Chromatograph (Varian 2000) was used to study the conversion of the reactants. A 25 m capillary column (BPX5) that comprised 5% Phenyl was used to separates the free Monomers A, B, and C present in each sample. Silanized glass wool was placed in the injector liner to ensure that no polymer would be injected into the column. A 5 m pre-column was also used to further aid in the protection of the capillary column.

Helium gas, with a purity of 99.999%, was used as carrier gas. The split flowrate was set at approximately 42 ml/min. The temperature of the column was kept constant at 80 ^{0}C for 6 min. Good separation of all the components was achieved. The temperature of the column was then increased to 140 ^{0}C at a rate of 20 $^{\circ C}/_{\min}$. and kept, at the elevated temperature, for a further 1 min. This was done to protect the column against the possible build-up of monomer and water. The temperature of the injector and detector were kept constant, at 220 ^{0}C and 250 ^{0}C respectively.

3.8.1.2 CALCULATION OF THE RESPONSE FACTORS

An internal-standard method was used to calculate the conversion achieved from the free monomers present in each sample. DMF was used as internal standard. In order to calculate the conversion, the response factors of the different monomers first needed to be known.

Three different samples, comprising 0.5g, 1g and 3g of monomer were added to 0.5g DMF. This was done to verify the linearity of the calibration. This was repeated for the three monomers to be separated. The samples were diluted with ethylene chloride. The analysis of the response factors was carried out in duplicate and calculated using the following relationship:

$$f_i = \frac{A_{s\,tan\,dard}.G_i.f_{s\,tan\,dard}}{A_i.G_{s\,tan\,dard}} \qquad .....3.28$$

,where f_i : response factor of monomer i

$A_{standard}$: integrated area of internal standard

A_i : integrated area of component i

G_i : mass of monomer i

$G_{standard}$: mass of internal standard

$f_{standard}$: response factor of internal standard set to unity

Some of the results obtained are summarized in Table 3.4.

TABLE 3.4 *Response factors obtained*

MONOMER A			
Sample	**$G_{(standard)}$ (g)**	**$G_{(A)}$ (g)**	**Response Factor**
1	0.4858	0.5171	0.279
2	0.5072	1.1049	0.284
3	0.5141	2.9958	0.284
		Average:	**0.281**
MONOMER B			
Sample	**$G_{(standard)}$ (g)**	**$G_{(B)}$ (g)**	**Response Factor**
1	0.5172	0.4979	0.573
2	0.5049	1.0878	0.576
3	0.5020	2.9770	0.576
		Average:	**0.575**
MONOMER C			
Sample	**$G_{(standard)}$ (g)**	**$G_{(C)}$ (g)**	**Response Factor**
1	0.5256	0.5063	0.476
2	0.5050	1.0052	0.476
3	0.6805	2.9678	0.484
		Average:	**0.478**

3.8.1.3 METHOD

The validity as well as the accuracy of the method that was developed had to be evaluated. This was done by the addition of small quantities of the monomers to be separated, to a known amount of emulsion. The resulting mixture was left overnight under constant stirring to ensure full absorption of the monomers by the latex particles. Samples were withdrawn and analyzed. The results obtained are summarized in Table 3.5

TABLE 3.5 *Results obtained from method evaluation*

SAMPLE MAKE-UP	
Mass of Monomer added (g)	**17.50 g**
Mass of Emulsion added (g)	**603.40 g**
Mass of Monomer Calculated (GC) (g)	**15.74 g**

This procedure was repeated twice and it was found that the accuracy of the method was within 10%.

Approximately 1.5 – 2.0g of each sample withdrawn from the reactor was diluted with ≈2g of a 2% DMF/water solution. The amount (mass) of free monomer present in each sample was calculated, by rearranging Eq.3.28 and using the response factors obtained:

$$G_i = \frac{G_{s\,\mathrm{tan}\,dard} \cdot A_i \cdot f_i}{A_{s\,\mathrm{tan}\,dard} \cdot f_{s\,\mathrm{tan}\,dard}} \qquad \text{.....3.29}$$

A typical chromatogram to illustrate the good separation that was achieved, is shown in Figure 3.11.

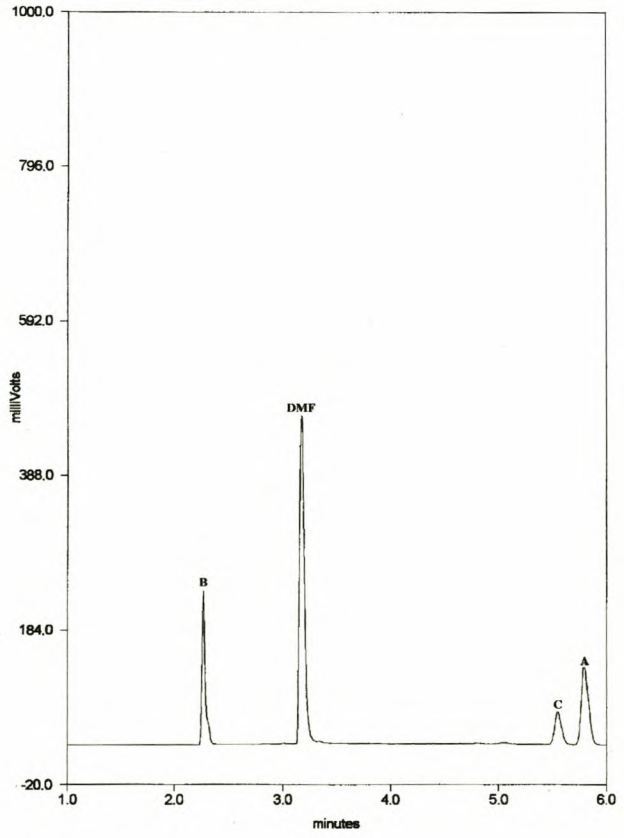

FIGURE 3.11 *GC Chromatogram*

3.8.2 VISCOSITY ANALYSIS

3.8.2.1 SET-UP

Preliminary viscosity analyses were performed with a Haake (Rheostress, RS 150) viscometer. It had a plate-and-cone configuration. No satisfactory results were obtained. The viscosity of the samples withdrawn from the reactor during the first part of the reaction (up to 2 ½ hrs) were very low (1.95-3.00 cps). It was found that at high shear rates, very little sample remained between the plate and the cone of the viscometer. Unreliable data were hence obtained and the plate-and-cone configuration was thus not suitable.

Analyses were then performed, with a different viscometer (Haake, RV 12, Rotoviscometer) which had a cup-and-spindle (NVSt) configuration (Figure 3.12). Deionized water and standard calibration oil (300 cP) were used to investigate the suitability of the cup-and-spindle configuration and to calibrate it. All analyses were performed at 30 ^{0}C. Water was kept in an external tank and kept at constant temperature. The water was pumped through the internal cavity that existed within the cup. The turning speed of the spindle had to be set manually. The torque exerted on the motor by the sample was measured at each turning speed.

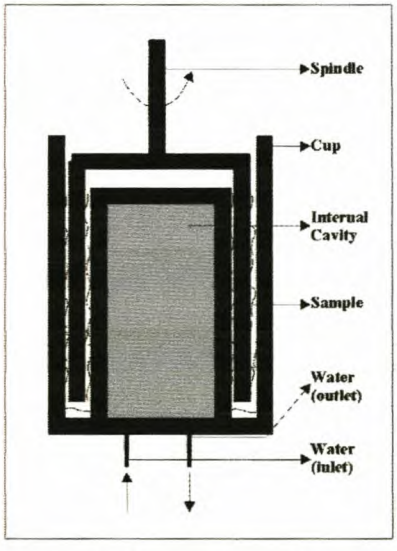

FIGURE 3.12 *Cup-and-spindle configuration of the Haake viscometer*

3.8.2.2 PROCEDURE

The cavity of the cup was filled with approximately 10 ml of sample. The spindle was then carefully slid into the cup. Any excess sample that might have

accumulated in the top part of the cavity was sucked out with a Pasteur pipette. The cup and the spindle were then fitted to the motor-drive-unit of the viscometer. Water was pumped through the internal cavity of the cup and enough time was allowed for the sample to reach equilibrium temperature.

At low viscosities (< 50 cP) the torque was measured at four different turning speeds (32-256 rpm). At medium viscosities (50 – 200 cP), 5 different spindle turning speeds were used, varying between 1.6 – 25.6 rpm. At a further increase in viscosity a third set of turning speeds had to be used (0.04 - 1.25 rpm).

It was found that the emulsion reaction demonstrated non-Newtonian behavior. The power law (Coulson & Richerson, Vol.3, 1982, pp. 415-419) was used to calculate the apparent viscosity (μ_a). A curve was fitted to the data obtained for each sample to obtain the consistency factor (k^*) and the flow index (n). The apparent viscosity could then be calculated for each sample using Eq. 3.30.

$$\mu_a = k^* \left(\frac{du}{dy} \right)^{n-1} \qquad \text{.....3.30}$$

The apparent viscosities are reported at a shear rate of 3.14 1/s. This was done to make the results obtained in this research comparable with results obtained by Plascon. The non-Newtonian behavior of NW 120 is illustrated in Addendum G.

3.8.3 SOLIDS CONTENT

3.8.3.1 SET-UP

A Halogen moisture analyzer (Mettler Toledo, HR 73), was used to analyze the solids content in each sample gravimetrically. The solids content represents the fraction of polymer already formed. The results were used to verify the accuracy of the GC method developed to obtain the conversion. A Halogen lamp served as heat source (Figure 3.13)

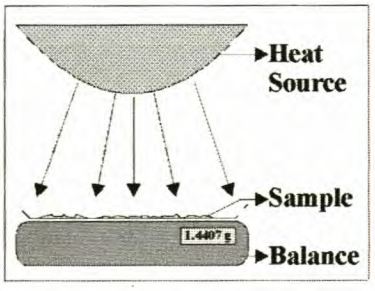

FIGURE 3.13 *Apparatus used for measuring solids content*

3.8.3.2 PROCEDURE

An Aluminum pan, weighing approximately 2.5g, was placed on the balance of the moister analyzer and then zeroed. The pan was removed and about 1.3 - 1.9g of sample was placed on the pan. The sample was spread evenly to ensure even drying. The pan with the sample was then replaced on the balance.

The Halogen moisture analyzer was programmed to dry the sample at a temperature of 180 ^{0}C until the balance reading remained constant. The solids content present in each sample was reported as a percentage. This procedure was repeated for each sample.

3.8.4 MOLECULAR WEIGHT

3.8.4.1 APPARATUS

The molecular weight (MW) of the polymer was measured by Gel Permeation Chromatography (GPC). The set-up was equipped with a system controller (Waters 600E) and a differential refractometer (Waters 410). An auto-sampler was used. All analyses were conducted at 30 ^{0}C.

3.8.4.2 PROCEDURE

Approximately 20 – 25g of the sample were used. Breaking down the stabilizing system (surfactant) coagulated the latex. This was achieved with methanol and a very small quantity of sodium chloride. The coagulated latex was then dried in a vacuum oven at a temperature of 60 ^{0}C for 12 h.

The polymer was dissolved with a suitable solvent (THF). A non-solvent (methanol) was added to coagulate the polymer again. The polymer was then separated from the supernatant fluid and dried at 60 ^{0}C for 12 h.

A 6 g/l solution of THF was used to dissolve the resulting polymer. The polymer/THF solution was filtered with a 0.22 μm filter prior to introduction into the GPC.

3.8.5 PARTICLE SIZE DETERMINATION

3.8.5.1 APPARATUS

Photon Correlation Spectroscopy (PCS) was used to measure the particle size (PS) of the latex particles. The method of Photon Correlation Spectroscopy (also

referred to as Dynamic Light Scattering) is especially suitable for measurements in the sub-micron region, i.e. below 1 μm. The only major competing technique is electron microscopy. Electron microscopy 'experiments' are slow, sample preparation is tedious and only a small amount of sample is analyzed, which may be unrepresentative (Malvern, PCS Training manual, 1996). De Wet-Roos (1999) proved that, with the use of Transmission Electron Microscopy (TEM), the particle sizes obtained with the Malvern Zetasizer are indeed representative of the "real" particle sizes obtained in an emulsion. A set-up comprised a correlator (Malvern Instruments, Series 7032 Multi 8) and a Zetasizer (Malvern Instruments, Zetasizer 4), which were coupled to an IBM compatible PC.

3.8.5.2 PROCEDURE

Filtered water (0.22 μm filter) was used to make up a 1mmol solution of NaCl. Approximately 20 ml of the NaCl solution was poured into a small glass cup, using a syringe fitted with a 0.45 μm syringe-type filter. Just enough emulsion was then added for the resulting solution to turn milky white. A Pasteur pipette was used to introduce some of the milky white solution into the glass civet of the Zetasizer. The sample was left for 3 min. to reach equilibrium temperature.

All particle size analyses were carried out at 30 ^{0}C and at an angle of 90°. Five sub-runs, each consisting of 10 individual runs, were carried out on each sample. The Zetasizer was set to 'Bi-modal' mode to investigate the presence of possible bi-modal distributions. A calibration run was completed with a special calibration fluid that contained particles with an average particle size (Z_{avg}) of 35 nm. This procedure was repeated twice weekly. The accuracy of the particle size (Z_{avg}) measurements was within ± 1.5 nm.

The particle size (nm) of the latex particles was reported as a Z-average ($Z_{avg.}$). The mean particle size was also reported. The measured laser intensity was plotted against particle size (nm). The particle size distribution (PSD) was reported as the width of the resulting peak at 50% of its height.

CHAPTER 4

EVALUATION AND COMMISSIONING OF PILOT PLANT SET-UP

4.1 INTRODUCTION

A fully computer controlled pilot plant was designed and built, to study the emulsion polymerization of NW 120. The accuracy of the calorimeter first needed to be verified and the accuracy and stability of the controls evaluated, before the pilot plant reactor could be commissioned.

The experimental results presented in this chapter consist of 3 main sections. In the first part, results are presented which were obtained from the calorimetric 'calibration' runs (4.2). Models were derived, using linear regression, for the change in the heat capacity of the reaction mixture (NW 120), as well as for the heat losses from the reactor. This was done to enable the performance of an accurate energy balance around the reactor and hence to calculate the heat of reaction on-line. The accuracy of the calorimetry was also quantified.

In the second part results are presented that were obtained from the evaluation of the pilot plant reactor (4.3). The stability of the control over the reactor temperature is investigated. Some results that were obtained from the torque measurements are also discussed.

In the last part of this chapter the physical performance of the reactor is investigated (4.4). The reactor was commissioned with an emulsion that is well known to Plascon (AE 446). AE 446 was selected because a lot of plant data was available.

4.2 CALIBRATION RESULTS

4.2.1 HEAT CAPACITY MODEL

Only the time (t) and temperature (T) dependence on the heat capacity were investigated. Due to limitations that existed with the DSC (§ 3.5.2) the temperature dependence on the heat capacity could only be analyzed to a maximum temperature of

40 ^{0}C. It is a well-known fact that there exists a non-linear relationship between the heat capacity and temperature. It was however decided to fit a linear model to the change in heat capacity with change in temperature, to enable extrapolation of the data to be made with greater confidence.

Linear regression was used (Addendum D, Table D3-1) and a mathematical model of the form:

$$C_p = at + bT + c \qquad \text{.....4.1}$$

was derived, with regression coefficients presented in Table 4.1.

TABLE 4.1 *Regression coefficients obtained for heat capacity model*

a	b	c
-8.6E-05	-0.00287	4.4298

The values predicted by the model were plotted against the measured values and a trendline was fitted through the data (Figure 4.1), using MS Excel 97. A straight line, with a gradient almost equal to 1 (0.9936) was obtained.

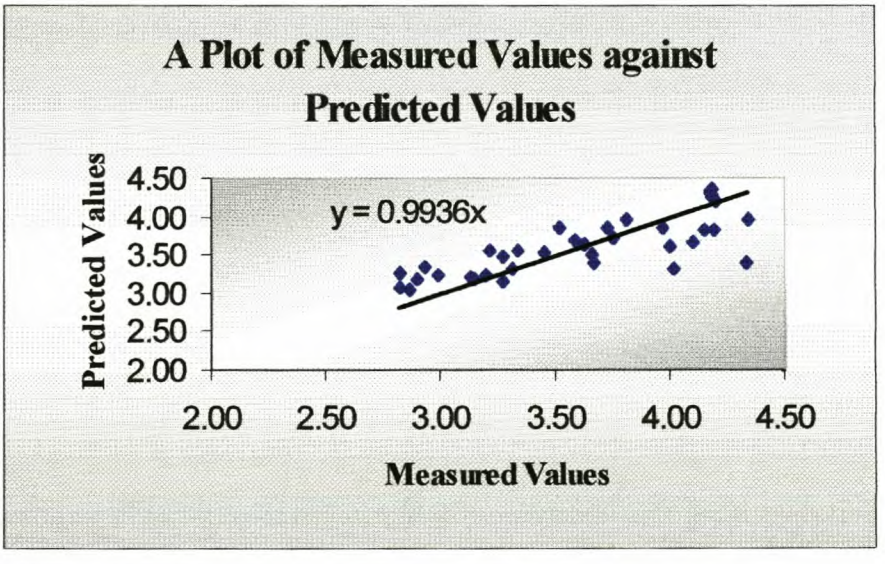

FIGURE 4.1 *Model validation*

In Figure 4.2 the derived model and the measured values were plotted on the same graph. It is clear how well the model predicts the experimental values. The accuracy of the derived model was 6.31% (Addendum D), which could result in a maximum uncertainty in the calorimetry measurements of ≈0.4 W (6.2 kJ)

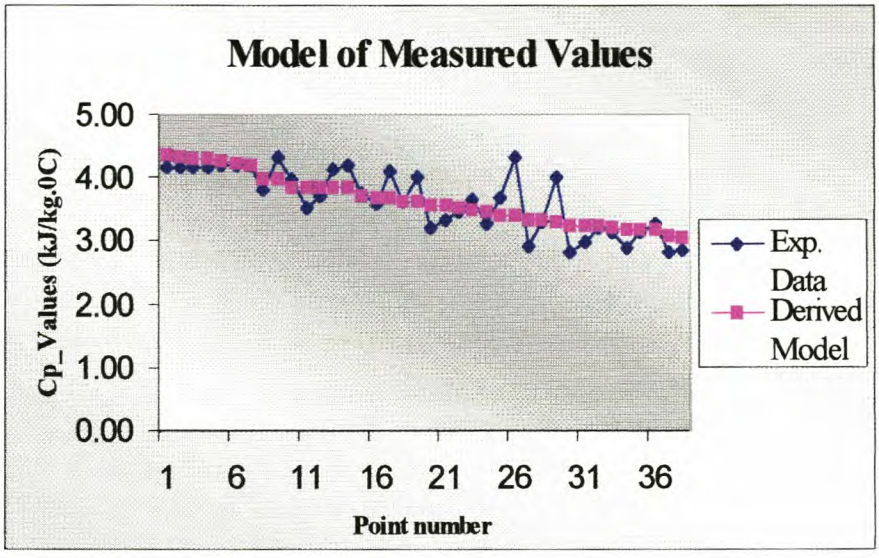

FIGURE 4.2 *Model of measured values*

4.2.2 HEAT LOSS MODEL

Experiments were carried out over a wide spectrum of reaction conditions, the results of which are presented in Addendum D (Table D4-1). A summary of a selected few appear in Table 4.2.

TABLE 4.2 *Summary of results obtained*

	Stirring speed	Reactor temp	Reactor loading	Ambient temp	Heat losses
Run	Rpm	Treac	Mass	Tsurr	Qloss
	(1/min)	(^{0}C)	(kg)	(^{0}C)	(W)
1	250	85.0	4500	28.5	55.2
2	125	85.0	4500	28.6	54.5
3	375	85.0	4500	28.5	54.0
7	250	82.5	4500	24.6	55.8
12	250	82.5	2099	25.1	56.3
8	250	85.0	2099	22.5	65.2
14	250	85	4500	21.6	63.6
5	250	87.5	4500	24.6	62.9
10	250	87.5	2099	24.5	63.4
5	250	87.5	4500	24.6	62.9
6	250	85.0	4500	24.6	59.6
7	250	82.5	4500	24.6	55.8
1	250	85.0	4500	28.5	55.2
6	250	85.0	4500	24.6	59.6
17	250	85.0	4500	19.1	67.0

The effect of stirring speed (Rpm) on the heat loss term (Q_{losses}) was first investigated. Experiments (Run 1 – Run 3) were conducted at a reactor temperature (T_r) of 85 ^{0}C, with a reactor loading (Mass) equal to 4.5 kg. During the experiments the ambient temperature ($T_{ambient}$) in the laboratory remained very constant at 28.5 ^{0}C. It is clear from the results presented in Table 4.2 that there was no real change in the heat losses with change in the stirring speed.

The influence of different reactor temperatures (82.5 – 87.5 ^{0}C) was investigated (Run 5 – Run 7). Results are presented in Table 4.2 at a constant ambient temperature of 24.6 ^{0}C. The heat losses seemed to be strongly dependent on the reactor temperature.

The influence that the ambient temperature has on the heat losses from the reactor was investigated. A few were included in Table 4.2 (Run 1, Run 6 and Run 17). An increase in the heat losses was experienced with a decrease in ambient temperature. Very little control was possible over the ambient temperature and experiments were hence restricted to time of day.

Experiments were then conducted to study the influence of different reactor loading (Mass) on the heat loss term. Experiments were carried out with loads equal to the initial reactor charge, and with loads equal to a full reactor, of an emulsion polymerization experiment. It is clear, especially from Runs 7&12 and Runs 5&10, that there exists very little change in the heat losses with change in reactor loading. The slight variation that existed between Runs 8&14 with change in reactor loading could be attributed to possible measurement error, but it is still well within experimental accuracy.

Three experiments (Run 17, Run 18 and Run 19) were then repeated, where the reactor was filled with an emulsion rather than with water (Addendum D, Table D4-1). The results that were obtained were included in the model that was derived. The squared error values (Table D4-2), that were obtained for the three respective experiments, indicate that they deviate very little, if any, from the model that was primarily derived with water. Linear regression was used (Addendum D, Table D4-2) and a model of the form:

$$\dot{Q}_{losses} = k_1(T_r - T_{ambient}) + k_2\sigma((T_r')^4 - (T_{ambient}')^4) \quad \text{.....4.2}$$

was derived, where k1 and k2 represent the regression coefficients of the linear and non-linear part of the heat losses. T_r and $T_{ambient}$ refer to the reactor and ambient

temperatures, respectively, in ^{0}C. The superscript to the symbols just described e.g. T_r', refer to the reactor temperature in units of Kelvin.

The regression coefficients that were obtained are presented in Table 4.3.

TABLE 4.3 *Regression coefficients obtained for heat loss model*

k1	k2
0.82468	0.02036

It was difficult to accurately measure the surface temperature of the outer wall of the reactor. The temperature within the reactor was hence used to develop a heat loss model. The model was derived for application over a small temperature range of approximately 5 ^{0}C (82.5 – 87.5 ^{0}C).

The first term in the model that was derived represents the heat losses due to free convection, where k_1 equals h' A. h' represents the simplified convection coefficient and A the heat transfer area. The heat transfer effect to the top and bottom domes, for example, can be investigated if it is assumed that it would act as a heated horizontal plate. The following relationships will thus hold (Incropera & De Witt, 1990):

$$Nu_L \propto (Ra_L)^a \qquad \text{.....4.3}$$

and from the definition of the Nusselt number for free convection (Nu_L) it further follows

$$h_L \propto (Ra_L)^a \qquad \text{.....4.4}$$

where h_L represents the convection heat transfer coefficient and Ra_L, the dimensionless Rayleigh number. The value of the constant a used depends upon the geometry of the object under investigation and can vary between 0.1-0.33. From the definition of the Rayleigh number it further follows:

$$h_L \propto \left(\frac{\left(T'_{reac,2} - T'_{ambient}\right)}{T'_f} \right)^a \qquad \text{.....4.5}$$

where

$$T'_f = f\left(T'_{reac,2}, T'_{ambient}\right) \qquad \text{.....4.6}$$

The film temperature ($T_f^{'}$) is a function of the outer surface temperature of the reactor ($T_{reac,2}^{'}$) and the ambient temperature ($T_{ambient}^{'}$).

The heat loss model was derived to study reactions at 85 ^{0}C. Extrapolation of the model is not recommended because of the non-linearity that exists in the calculation of the free convection heat transfer coefficient. Extrapolation of the model from a reactor temperature of 85 ^{0}C to 70 ^{0}C revealed a possible uncertainty in the model of approximately 4.6 W and could amount to ≈75 kJ over a $4\frac{1}{4}$ h reaction period and was not considered. Extrapolation of the model from a reactor temperature of 87.5 ^{0}C to 90 could amount to ≈40 kJ over a $4\frac{1}{4}$ h reaction period.

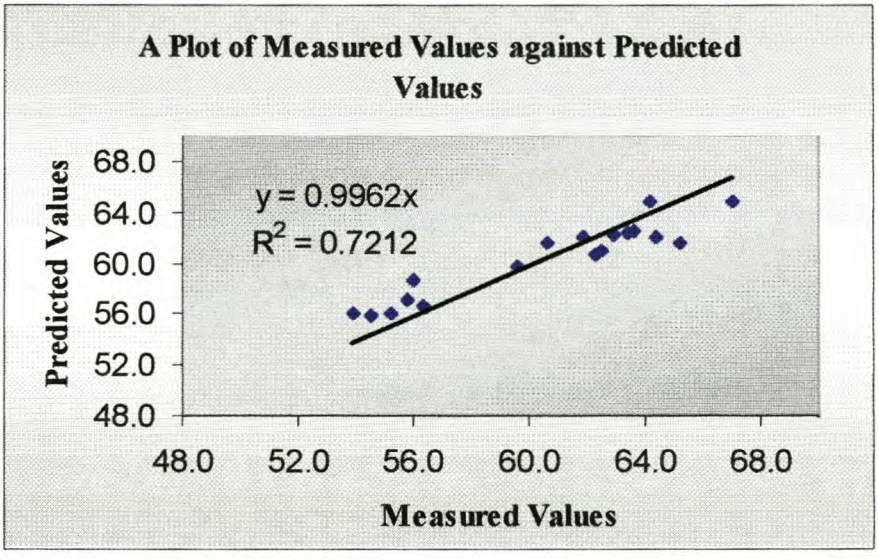

FIGURE 4.3 *Model validation*

The heat losses predicted by the model were plotted against the measured values and a trendline was fitted through the data (Figure 4.3), using MS Excel 97. A straight line with gradient almost equal to 1 (0.9962) was obtained. Figure 4.4 was included to illustrate how well the model predicts the experimental data. The accuracy of the derived model was 2.29%, which could result in a maximum uncertainty in the calorimetry measurements of ≈1.5 W (23 kJ).

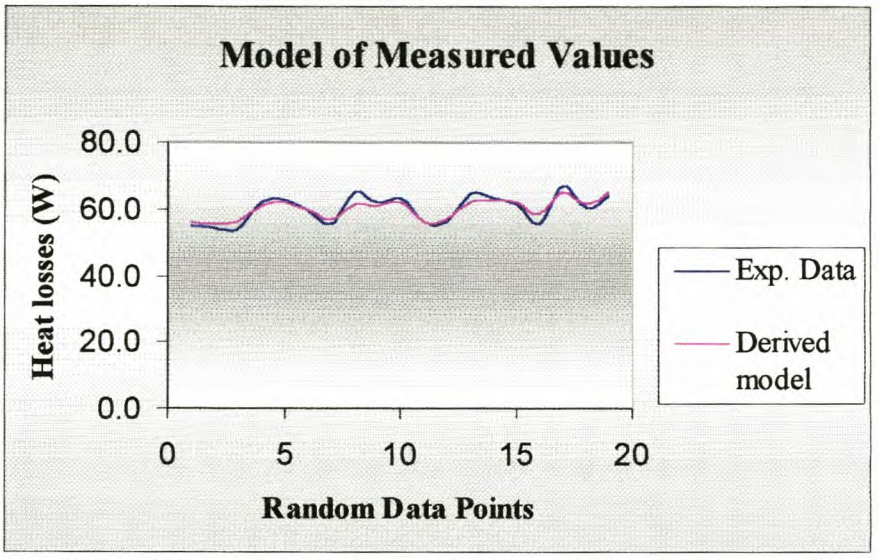

FIGURE 4.4 *Model of measured values*

The regression model was used to calculate the average linear and non-linear parts of the heat loss model. The results are presented in Table 4.4.

TABLE 4.4 *Linear and non-linear heat loss components*

Linear	Non-linear
50.1 W	9.9 W

The linear part of the model presented 83.5%, and the non-linear part 16.5% of the total heat losses.

4.2.3 ACCURACY OF CALORIMETER

The dilution of 3.174 kg of a 42.5% (mass base) sodium hydroxide solution was used to qualify the accuracy of the calorimetric set-up (electronic measurements and heat loss model). The theoretical heat of solution was calculated (Himmelblau, 1989) and compared with the measured heat of solution (Table 4.5).

TABLE 4.5 *Theoretical and measured heats of solution*

Theoretical Heat of Solution :	268.9 kJ
Measured Heat of Solution :	269.8 kJ

The theoretically calculated heat of solution compared very well with the heat of solution measured on-line, the graph of which is included in Figure4.5.

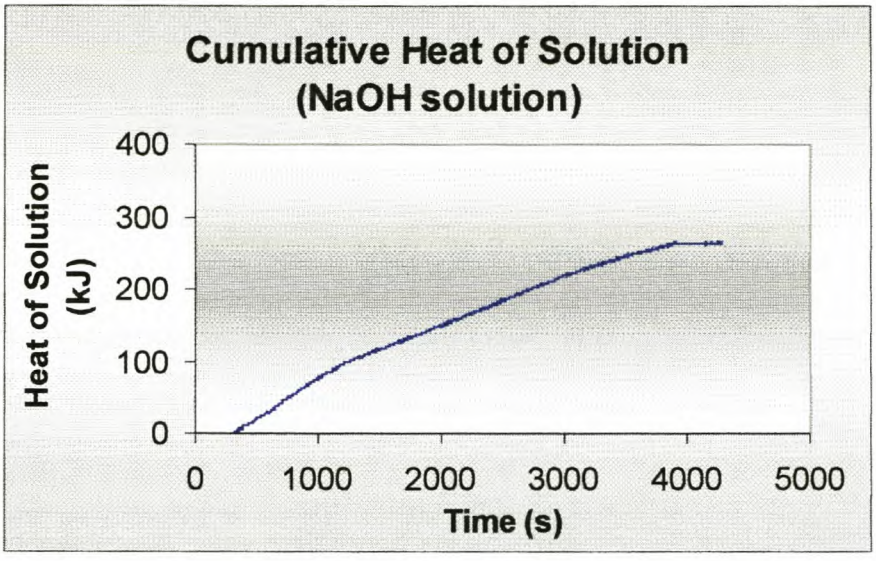

FIGURE 4.5 *Measured cumulative heat of solution*

4.3 EVALUATION OF PILOT PLANT REACTOR

4.3.1 CONTROL OF REACTOR TEMPERATURE

The research conducted in this study involved the variation of the process variables over extreme ranges. Stable control of the reactor temperature was thus of critical importance. The stability of the temperature control was tested with the use of a calibration heater.

The reactor was filled with water. The reactor temperature and stirring speed were set at 85 ^{0}C and 250 rpm, respectively. A 179 W step input was first introduced to the reactor at time 0 s. The response of the reactor temperature with time is given in Figure 4.6. The response for a 26 W step input is included in Addendum D (Figure D5-1).

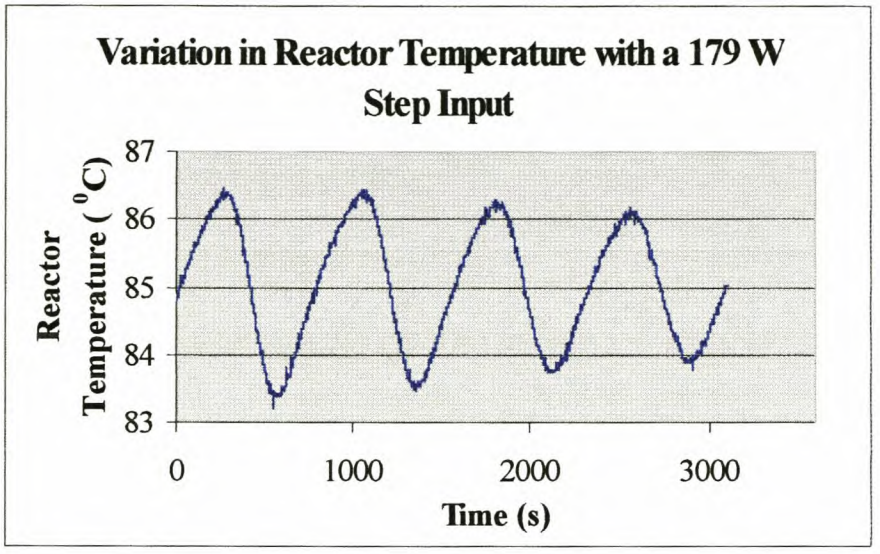

FIGURE 4.6 *Reactor temperature profile (179 W step input)*

Very good and stable control was achieved over the reactor temperature range. The good control was maintained even after the introduction of a large disturbance (179 W step input). The reactor temperature initially oscillated (± 1.3 ^{0}C) around its setpoint (85 ^{0}C), but converged to a less than ±1 ^{0}C band after approximately 48 min.

The results obtained for control over the reactor temperature, were much better than the results obtained by Litz (1998), who conducted research in a 15 l reactor at 46 ^{0}C. Litz reported fluctuations in the reactor temperature of more than ± 2 ^{0}C after just 2 ½ min and a temperature variation exceeding a ± 4 ^{0}C band after 12 min for a 30 W step input.

Figure 4.7 is an example to illustrate the variation in the reactor temperature for a preliminary emulsion polymerization experiment conducted on NW 120.

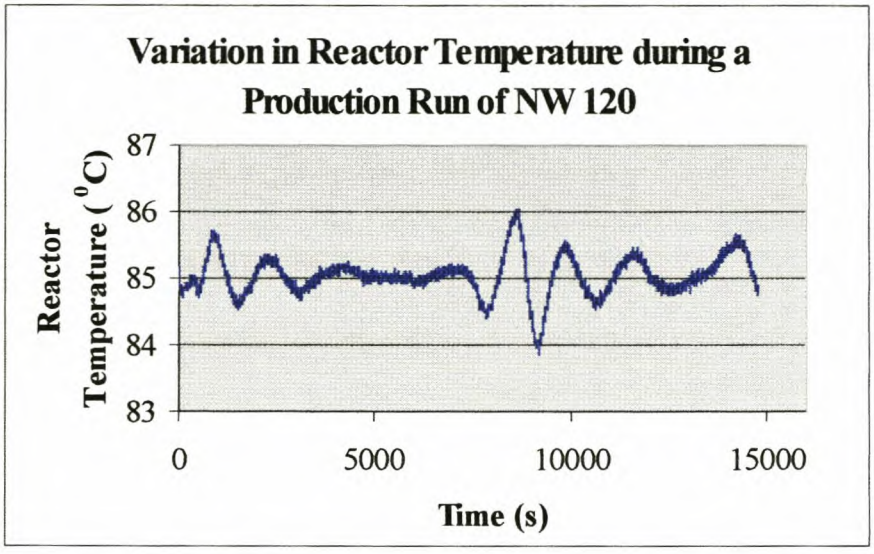

FIGURE 4.7 *Reactor temperature profile (NW 120)*

The sudden fluctuations in the reactor temperature after approximately 120 s and again after 7200 s are attributed to exotherms experienced with the reaction of the core (≈ 41 W) and shell (≈ 100 W) monomers. Very good convergence over the reactor temperature, to its setpoint value, was however achieved.

4.3.2 EVALUATION OF TORQUE MEASUREMENTS

The torque was measured at different stirring speeds with an empty reactor to determine the effect of the bearing and lip-seal on the torque measurements. It was found that the torque measurement stayed very constant (< 0.002 N.m) with variation in stirring speed. The torque exerted on the motor by the reacting liquid was obtained by subtracting the nearly constant value, obtained in an empty reactor, from the measured torque.

Two torque profiles, obtained at 85 ^{0}C and at 70 ^{0}C and at a stirring speed of 250 rpm, are presented in Figure 4.8.

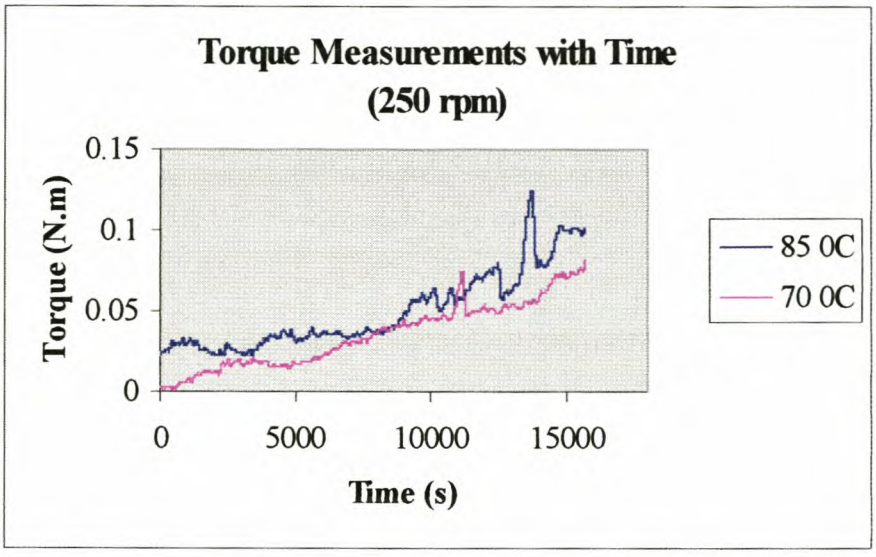

FIGURE 4.8 *Torque profiles*

The torque measurements were very noisy. The reproducibility of the measurements obtained was also not very good. The profiles presented in Figure 4.8 were smoothed by calculating a 50 point running average. 'Spikes' in the measurements were observed after 3 h (70 ^{0}C) and after $3\frac{3}{4}$ h (85 ^{0}C). This could be explained by the top set of paddles touching the rising level of reacting liquid.

A summary of the torque measurements, as well as their respective viscosities, obtained for 3 experimental runs are presented in Table 4.6.

TABLE 4.6 *Torque measurements*

RUN		**Run 02**	**Run 08**	**Run 11**
Temp.	**^{0}C**	**85 ^{0}C**	**85 ^{0}C**	**70 ^{0}C**
Rpm	1/min	350	250	250
Torque	N.m	1.1	1.0	0.7
Viscosity	cP	5610	4550	1220

From the results obtained at the end of the reaction, presented in Table 4.6, the increase in the torque with increase in the viscosity is clearly visible.

4.3.3 EVALUATION OF THE CONSISTENCY OF THE REACTANTS AND CATALYST ADDITION RATES

Balances were used as very accurate mass flow meters (Chapter 3) for the addition of the monomers and catalysts. Very stable and accurate addition profiles were obtained, even at very low mass flowrates. The mass flowrate of the core catalyst, when added to the reactor over a 2 hr period, was the lowest at 0.009 $^{g}/_{s}$. A typical addition rate profile obtained for the core catalyst is presented in Figure 4.9.

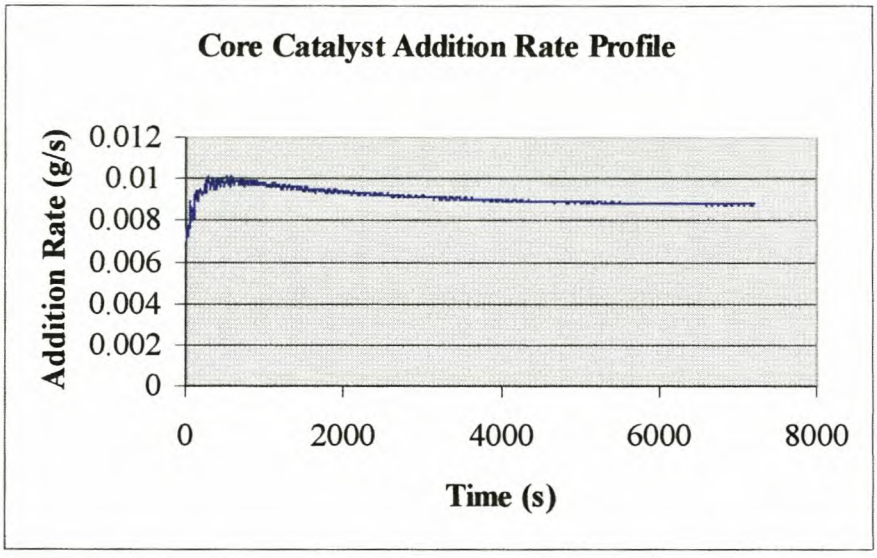

FIGURE 4.9 *Addition profile for core catalyst (0.009* $^{g}/_{s}$*)*

Smoother control, over the addition rates, was achieved when dosing pumps were started at 20% under their setpoint value. The very stable and accurate addition rate, even at an extremely low mass flowrate, of the core catalyst is clearly visible in figure 4.9.

4.4 COMMISSIONING OF PILOT PLANT REACTOR

The pilot plant reactor was commissioned with an emulsion (AE 446) that is well known to Plascon. Plascon has manufactured it for more than 7 years, and much data on the industrial performance of AE 446 is available. The performance of the pilot plant reactor could hence be compared with the performance of the industrial size (10 ton) reactor.

AE 446 is manufactured industrially at 85 ^{0}C and at a stirring speed of 35 rpm. All the monomers are added to the reactor over a period of 3 hrs. An order of magnitude calculation was carried out to obtain the equivalent stirring speed for the pilot plant reactor. A mixing-power-per-unit-volume approach, for mixing vessels (Eq. 2.8) was used (Ullman's Encyclopedia of Industrial Chemistry, 1990). The equivalent stirring speed was determined to be ≈ 136 rpm.

The minimum rotational speed of an impeller (N_{min}) necessary to disperse an emulsion (Eq. 2.9) was also used to calculate the equivalent stirring speed for the pilot plant reactor (Klein et al., 1996).

$$\left((D_s)^{0.765}.N_{\min}\right)_{Full-scale} = \left((D_s)^{0.765}.N_{\min}\right)_{Pilot-plant}$$

$$\left((1.21)^{0.765}.35\right)_{Full-scale} = \left((0.092)^{0.765}.N_{\min}\right)_{Pilot-plant}$$

$$\Rightarrow (N_{\min})_{Pilot-plant} = 251 \text{ rpm}$$

It was subsequently decided to conduct the commissioning run at a stirring speed of 250 rpm.

Very good results were obtained; the physical properties (density, % solids, viscosity and particle size) of AE 446 manufactured in the pilot plant reactor were within specification. A summary of the results obtained is given in Table 4.7.

TABLE 4.7 *Summary of results obtained*

Properties		Industrial Reactor	Pilot Reactor
Density	kg/l	1.042	1.051
Solids	%	46.1	46.2
Viscosity	cP	3700	4000
Particle Size	nm	79.8	79.2

The reported particle sizes (Z_{avg}), specific gravity and solids content of AE 446, manufactured in the industrial size reactor (10 ton) compare very well with the results obtained in the pilot plant reactor. The viscosities were measured with a Brookfield viscometer. The small differences that exist could possible be due to measurement inaccuracy, or to a difference in particle size distribution, which was not mentioned by the staff of the quality control laboratories at Plascon.

CHAPTER 5

LAB-SCALE EVALUATION OF THE PRODUCTION OF NW 120

5.1 INTRODUCTION

Models were derived for the change in the heat capacity of NW 120 and the heat losses associated with the reactor. These have enabled the on-line measurement of the heat of the reaction to be made, which could be used to aid further in the investigation of the scale-up of the production of NW 120. As mentioned in section 4.4 the pilot plant reactor was successfully commissioned with a well-known emulsion of Plascon, AE 446. The scale-down results that were obtained, in the pilot plant reactor compared very well with the results obtained in an industrial size (10 ton) reactor of Plascon.

The pilot plant could hence be used, with confidence, in the lab-scale evaluation of the production of NW 120. The effect that a change in the stirring speed had on the emulsion will first be described. The stirring speed was varied within the range 150 – 550 rpm. The sensitivity of the emulsion to change in the reaction temperature (70 – 90 ^{0}C) was also investigated. Experiments were also conducted in efforts to decrease the time of reaction by increasing the addition rates of the reactants and catalysts.

5.2 CHANGE IN STIRRING SPEED

The stirring speed was varied between (150 – 550) rpm (Addendum E, Run 01 – Run 05), while the reactor temperature was kept constant at 85 ^{0}C throughout. The monomer addition times of the core and shell phases were also kept constant for all 5 runs at 2 hrs, respectively. A summary of the results obtained at the end of the reaction is presented in Table 5.1.

TABLE 5.1 *Summary of results obtained*

		PRODUCT				
Run		Run 03	Run 01	Run 02	Run 04	Run 05
Rpm	1/min	150	250	350	450	550
Peak1						
Mean	nm	79.1	76.7	76.8	79.8	97.8
Width	nm	43.4	41.4	38.2	42.6	43.6
Z_{avg}	nm	71.9	69.8	70.4	73.7	91.0
Viscosity	cP	4400	4870	5610	4280	690
Solids	%	47.44	47.82	48.25	48.22	48.00
S.G.	kg/l	1.049	1.045	1.041	1.045	1.037

Figure 5.1 was obtained from a plot of particle size (Z_{avg}) against stirring speed. The particle size, as well as the mean particle size (Mean) (Table 5.1) remained nearly constant for variation in stirring speed (Rpm) between (150 – 450) rpm. The width of the distribution (Width), reported at 50% of the peak height, decreased slightly from a stirring speed of 150 rpm to 350 rpm.

There was an approximate 17 nm increase in the particle size (Z_{avg}) with an increase in the stirring speed from 450 rpm to 550 rpm, during which the particle size distribution remained almost constant.

The ionically charged surfactant, which serves to stabilize the latex particles, could have been stripped off, due to high shear forces, and lead to agglomeration, at the introduction of such a high stirring speed of 550 rpm. Much less loci for polymerization would then have been available, especially at the start of the reaction. These effects could have lead to a lower rate of polymerization and hence a lower conversion (Figure 5.4), increase in the particle size, as well as the particle size distribution of the emulsion with increase in stirring speed from 450 rpm to 550 rpm.

The solids content (Solids) of the emulsion (product) remained almost constant with change in the stirring speed, which indicates nearly full conversion. There seemed to be very little variation in the specific gravity (S.G.) with change in stirring speed (Table 5.1), which indicates that the emulsions were not aerated.

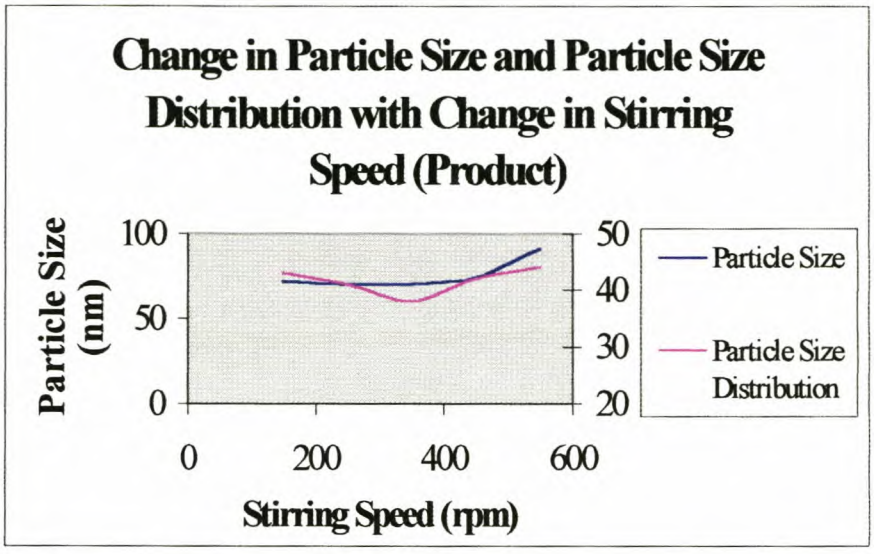

FIGURE 5.1 *Change in particle size with change in stirring speed*

The effect that a change in the stirring speed has on the viscosity is illustrated in Figure 5.2 where the results obtained at the end of the reaction are compared. There seemed to be an increase in the viscosity with an increase in the stirring speed from 150 rpm to 350 rpm, with a maximum value reported at 350 rpm. There existed a significant decrease in the viscosity with increase in the stirring speed from 450 rpm to 550 rpm.

The decrease in the viscosity is due to an increase in the particle size, as well as a slightly wider particle size distribution (Parsons, 1993), rather than possible aeration normally experienced at such high shear rates. The forces (London and Van der Waals) acting on the latex particles are directly proportional to $1/D_p$. A larger particle diameter (D_p) would therefore result in smaller interacting forces and hence a lower viscosity.

The smallest particle size was obtained at a stirring speed of 250 rpm, while the lowest viscosity was obtained at a stirring speed of 150 rpm, for the experiments carried out at a stirring speed ranging between (150 – 350) rpm.

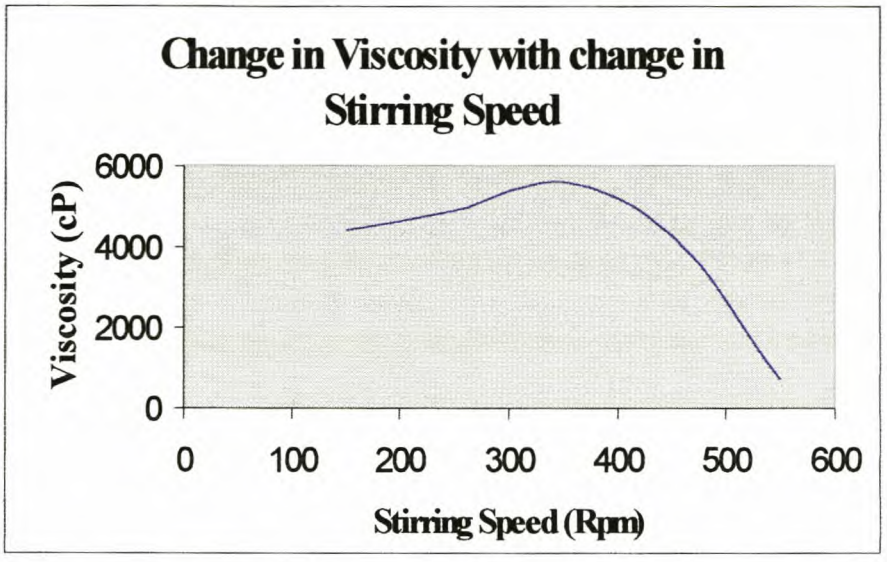

FIGURE 5.2 *Change in viscosity with change in stirring speed*

5.2.1 EFFECT OF STIRRING SPEED ON THE TIME DEPENDENCE OF CONVERSION

The overall conversion of monomer, at a given time, was calculated using the GC method that was developed (§ 3.7.1). Low conversions were observed for approximately the first 10 min. (600 s) of monomer addition. This effect was observed for all the reactions studied in this thesis.

The slightly lower conversion in the beginning of the reaction could be explained by occurrences associated with start-up, as well as inherent emulsion polymerization characteristics (initiation and particle formation, as well as possible inhibition due to the presence of small amounts of oxygen). Cold monomer ($\approx 25\ ^{0}C$) was added to the already warm reaction mixture ($70 - 90\ ^{0}C$), at which the condensator duty increased typically by 55 – 60 %. The sharp increase in the condensator duty was experienced in the first 2 – 3 min. of monomer addition.

There also existed a slight decrease in the overall conversion that lasted 25–35 min., with the start of the shell monomer addition. This effect was observed for all the experiments studied in this thesis.

The shell monomers were added to the reaction mixture under 'flooded' conditions. The condenser duty typically increased by 40 – 45 %. The increase in the condenser duty was experienced for the first 2 – 3 min. of shell monomer addition.

The fractional conversions are plotted against time for 3 different stirring speeds (150, 250 and 350 rpm) and are presented on one graph (Figure 5.3). The

overall conversion for the experiments presented in Figure 5.4 was very high throughout the experiments.

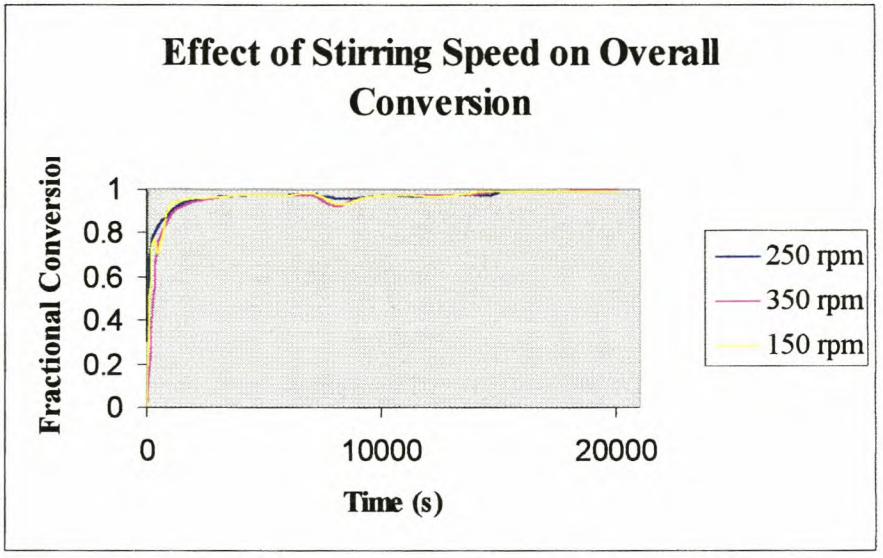

FIGURE 5.3 *Fractional conversion (150-350 rpm)*

The change in the fractional conversion with time for another set of stirring speeds (250, 450 and 550 rpm) is presented in Figure 5.4. The overall conversion for the experiment conducted at 550 rpm was much lower throughout the experiment than the experiments carried out e.g. at 250 rpm or 450 rpm.

At such very high shear rates the radical flux could have been influenced by the reducing loci for polymerization. This effect is known as hetero-termination (Gilbert, 1995).

Changes in the stirring speed seemed to have no effect on the final overall conversion. Reported changes in the monomer conversion were only experienced during the run. The residual free monomer of the product varied between (900 – 2500) ppm.

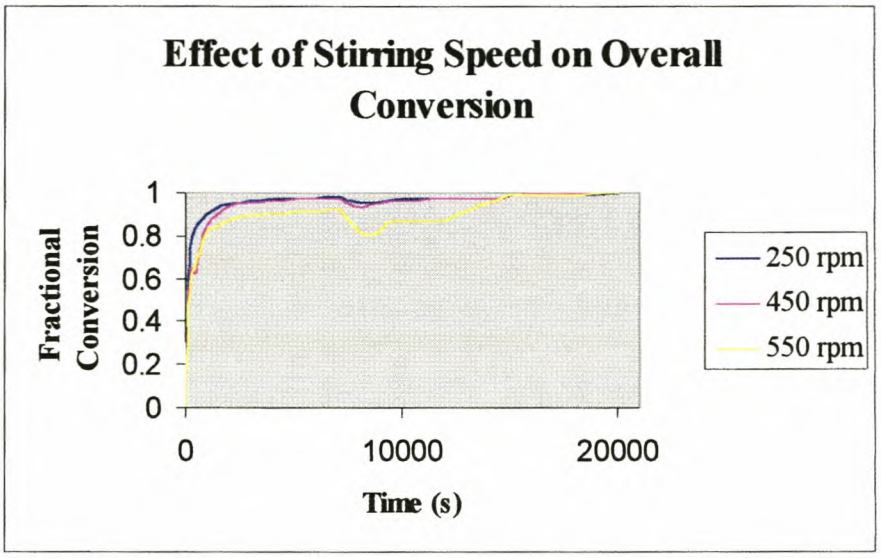

FIGURE 5.4 *Fractional conversion (250, 450 and 550 rpm)*

The effect of variation in stirring speed on the conversion (based on monomer feed) of the total reactor mass, is compared to the maximum theoretical conversion possible and are presented for the 2 extreme cases, 150 rpm (Figure 5.5) and 550 rpm (Figure 5.6).

The much lower conversion that was obtained for the experiment conducted at 550 rpm is clearly visible in Figure 5.6.

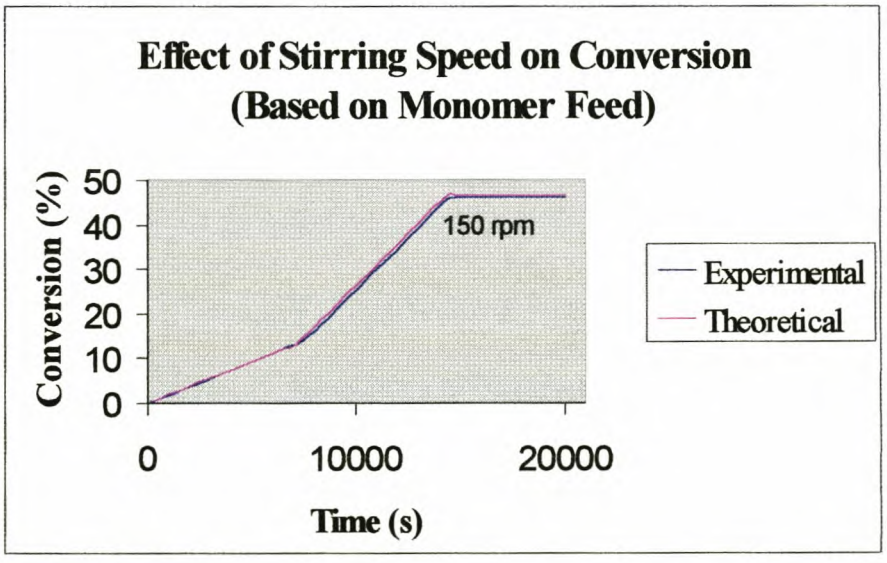

FIGURE 5.5 *Effect of stirring speed on conversion (150 rpm)*

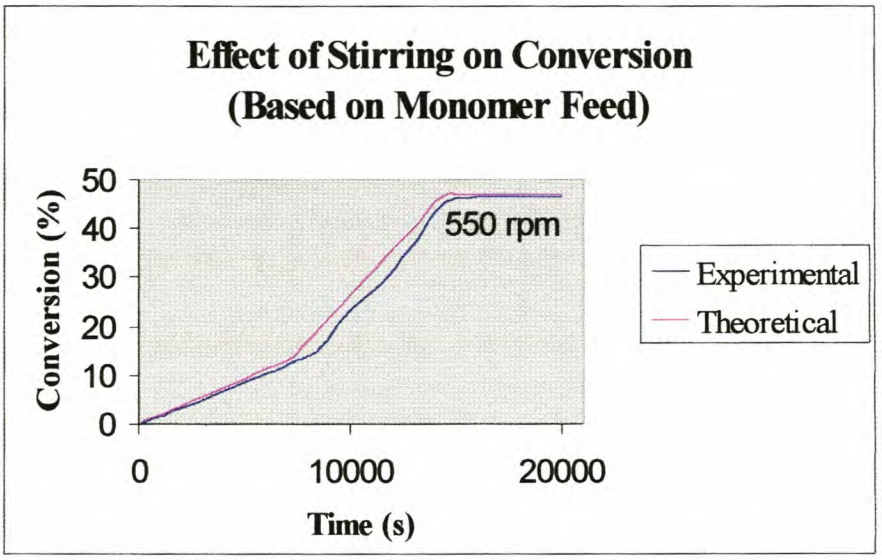

FIGURE 5.6 *Effect of stirring speed on conversion (550 rpm)*

5.2.2 EFFECT OF STIRRING SPEED ON THE TIME DEPENDENCE OF PARTICLE SIZE

The different particle sizes obtained were plotted against time. Trendlines were fitted through the data points, using MS Excel 97. This procedure was carried out merely to identify possible trends in the growth of the latex particle and this procedure was used throughout. It was impossible to measure particle sizes under 22 nm. The size measurements of the core particle could only be started after approximately 35% of the core monomer had already been added. Much more data points were available in the shell phase than in the core phase.

The effect of stirring speed on the particle sizes, during the core phase of the reaction, for the stirring speeds, ranging between (150 – 450) rpm, and for the 3 cases (150, 250 rpm and 550) rpm are included in Addendum F (Figure F1-4 and Figure F1-5).

The effect of stirring speed on the particle sizes, during the shell phase of the reaction, for the stirring speeds ranging between (150 – 350) rpm and (150, 450 and 550) rpm are presented in Figure 5.7 and Figure 5.8, respectively.

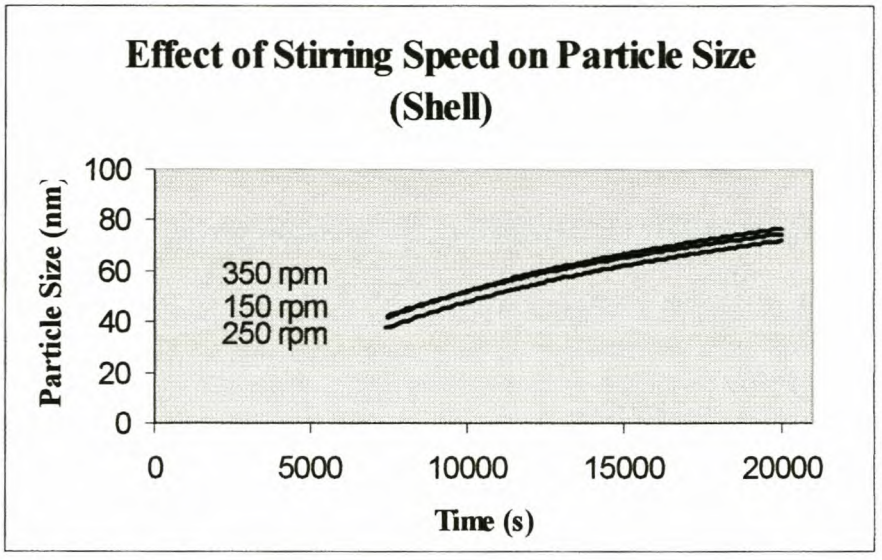

FIGURE 5.7 *Effect of stirring speed on particle size (150-350 rpm)*

There seemed to be very little change in the measured particle sizes with time, for the experiments conducted at stirring speeds ranging between (150 – 450) rpm during the core phase of the reaction (Figure F1-4), as well as during the shell phase of the reaction (Figure 5.7 and Figure 5.8).

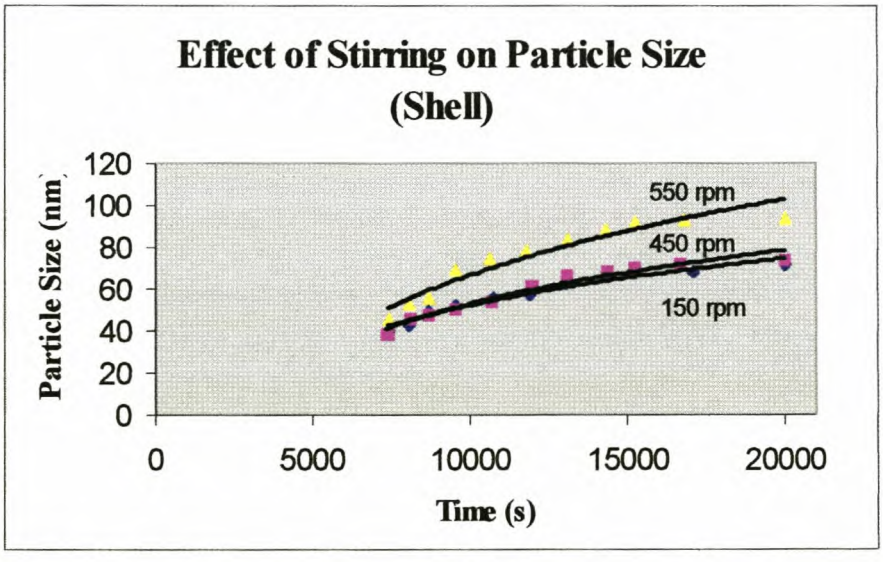

FIGURE 5.8 *Effect of stirring speed on particle size (150, 450 and 550 rpm)*

The experimental data points obtained, were included in Figure 5.8, but to increase readability it will be omitted in all the other graphs presented in this thesis. The particle sizes of the experiment conducted at 450 rpm (Figure 5.8) seemed to

have become larger than the experiment conducted at 150 rpm, towards the end of the reaction. The tremendous increase in the particle sizes of the experiment carried out at 550 rpm is clearly visible when the profile obtained is compared with any other experiment carried out in the series.

5.2.3 EFFECT OF STIRRING SPEED ON THE TIME DEPENDENCE ON VISCOSITY

The effect that different stirring speeds have on the viscosity profiles, for the stirring speeds ranging between (150 – 450) rpm is illustrated in Figure 5.9.

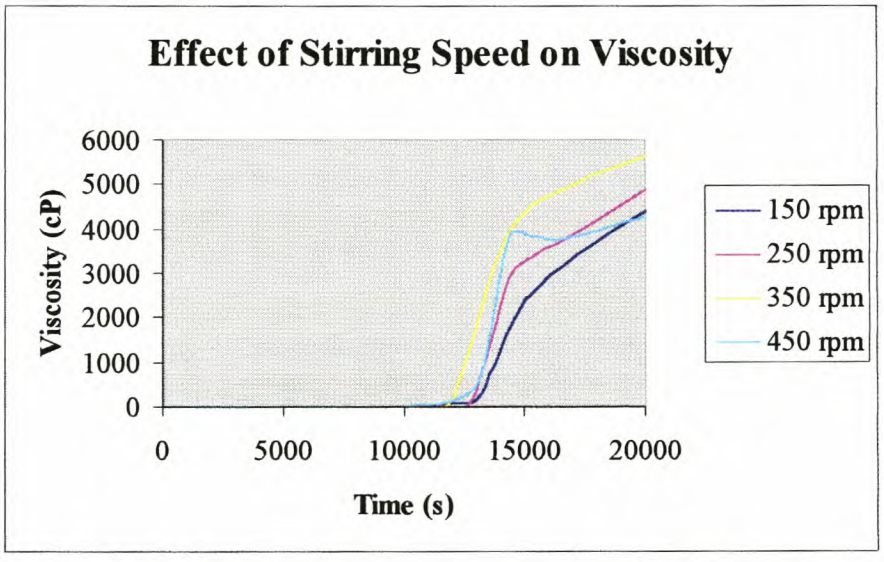

FIGURE 5.9 *Effect of stirring speed on viscosity (150-450 rpm)*

There seemed to be a sudden sharp increase in the viscosity during the last 15 minutes of shell monomer addition, whereafter the increase seemed lower, for all the reactions studied in this series (Figure 5.9 and Figure 5.10).

According to Schaller (1996), at high latex concentrations ($\Phi > 0.25$) the particle interactions start to dominate. The particle packing becomes a factor and leads to a sharp increase in the viscosity of the emulsion. The closer the particles are packed together the greater the interactions.

The interparticle distance is a function of the particle size (Eq. 5.1).

$$D_i = \left[\left[0.74/\Phi\right]^{1/3} - 1\right] \times D_p \qquad \text{.....5.1}$$

where D_i and D_p represent the interparticle distance and the particle size, respectively. The latex concentration or volume fraction is denoted by Φ. Larger particles are associated with larger interparticle distances (Eq. 5.1) and thus lower viscosity.

The viscosity profile obtained for the reaction carried out at a stirring speed of 350 rpm seemed to be the highest. The viscosity of the experiment conducted at a stirring speed of 450 rpm seemed to stay very constant after its initial increase. This could be due to a possible instability observed in the latex properties. Larger particles were obtained towards the end of the reaction (Figure 5.8), as well as a slight increase in the particle size distribution of the product (Table 5.1).

The viscosity profiles obtained at stirring speeds of 250 and 550 rpm are presented in Figure 5.10.

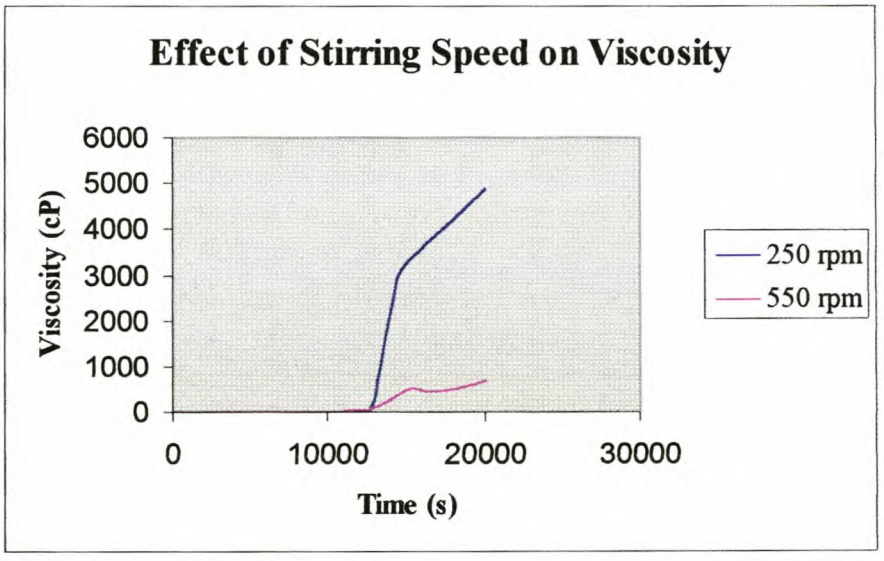

FIGURE 5.10 *Effect of stirring speed on viscosity (250 and 550 rpm)*

The viscosity profile obtained at 550 rpm is clearly much lower than the profile obtained at 250 rpm and it is mainly due to the larger particle sizes, as well as the wider particle size distribution, obtained at 550 rpm.

5.2.4 GRAVIMETRICAL ANALYSIS OF CONVERSION

An overall conversion profile was also obtained gravimetrically, and compared with a profile obtained using a GC method (Figure 5.11).

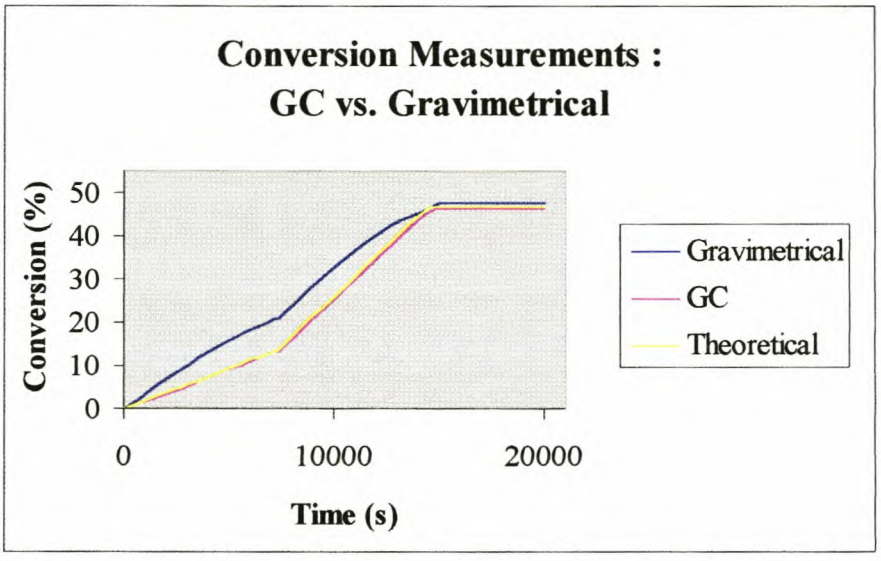

FIGURE 5.11 *Gravimetrical validation of GC method*

The conversion that was obtained using a gravimetrical method was much higher than the maximum theoretical conversion that was possible. The presence of the crosslinking agent in the core formed a probable barrier (skin) during drying that inhibited the evaporation of all the monomers. The use of a gravimetrical method, as used, to verify the accuracy of the conversion measured with the GC revealed poor and inaccurate results.

5.3 REACTION TEMPERATURE

The reaction temperatures were varied between 90 – 70 ^{0}C (Addendum E, Run 07 – Run 12), while the stirring speed was kept constant at 250 rpm for all 5 runs. The core and shell reaction times (monomer addition time) were also kept constant at 2h.

A summary of the results obtained at the end of the addition of the core monomers, as well as at the end of the reaction, is presented in Table 5.2

TABLE 5.2 *Summary of results obtained*

				CORE		
Run		Run 07	Run 08	Run 09	Run 10	Run 11
Temp.	^{0}C	90 ^{0}C	85 ^{0}C	80 ^{0}C	75 ^{0}C	70 ^{0}C
Peak1						
Mean	nm	30.1	36.4	36.6	40.8	50.4
Width	nm	11.6	19.1	17.1	17.3	21.0
Peak2						
Mean	nm	59.9	*	75.7	83.1	102.4
Width	nm	9.0	*	23.4	11.6	22.5
Z_{avg}	nm	36.1	35.0	35.8	39.8	48.9
CHR	kJ	255	250	270	-	-
				PRODUCT		
Run		Run 07	Run 08	Run 09	Run 10	Run 11
Temp	^{0}C	90 ^{0}C	85 ^{0}C	80 ^{0}C	75 ^{0}C	70 ^{0}C
Peak1						
Mean	nm	73.7	73.6	73.6	77.7	80.6
Width	nm	28.3	28.9	28.1	30.0	45.0
Z_{avg}	nm	70.6	70.9	70.8	75.1	76.4
CHR	kJ	1050	1103	1100	-	-
Viscosity	cps	4400	4550	4500	4380	1440
Solids	%	47.02	47.31	47.48	46.93	46.94
S.G.	kg/l	1.051	1.051	1.053	1.051	1.051

The changes in the particle sizes as a function of reaction temperature, at the end of the core phase as well as for the end results, is presented in Figure 5.12 and Figure 5.13, respectively.

All particle size measurements, carried out in this study, were conducted with a Malvern, Zetasizer, set in 'Bi-modal mode'. The second peak (Peak 2) that was observed (Table 5.2) could have been due to the stabilized monomer drops or other possible impurities.

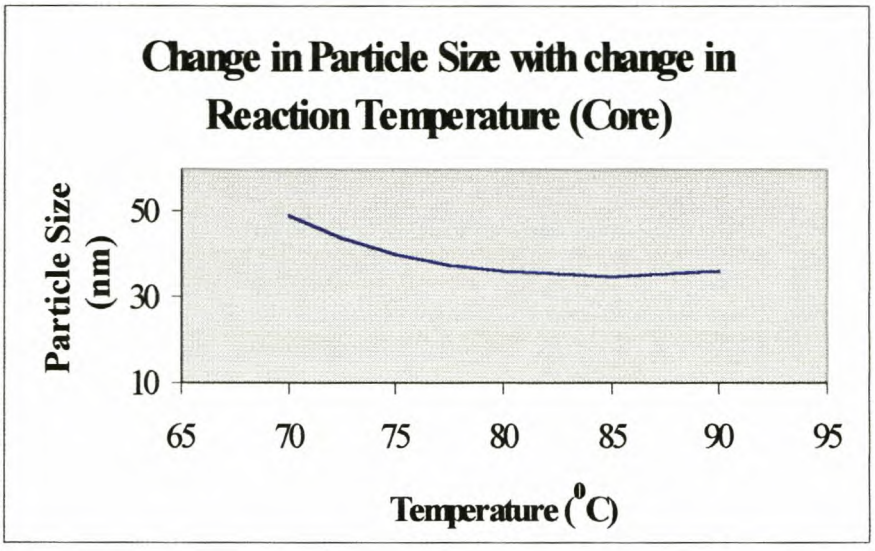

FIGURE 5.12 *Change in the particle size (Core)*

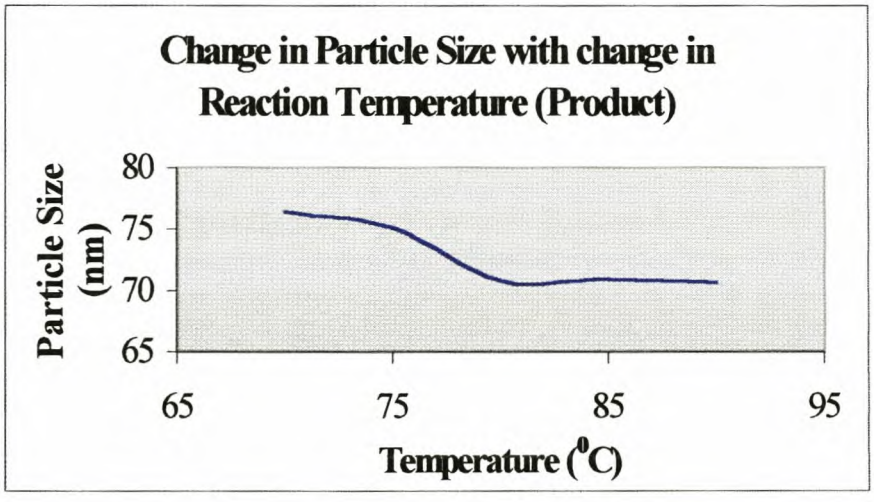

FIGURE 5.13 *Change in the particle size (End results)*

The particle size (Z_{avg}) remained constant with change in the reaction temperature within the temperature range 90 – 80 ^{0}C. This was observed for the analysis performed after the addition of the core monomers, as well as at the end of the reaction. There was an increase in the particle size with a further decrease in the reaction temperature from 80 ^{0}C to 70 ^{0}C, after the core phase (Figure 5.12), as well as at the end of the reaction (Figure 5.13).

The width of the particle size distribution (Width) seemed to have remained very constant for the temperature ranging between 90 – 75 ^{0}C, with a sudden increase at 70 ^{0}C.

There was very little change in the solids content (Solids) of the emulsion (Table 5.2) with change in reaction temperature. Nearly full conversion was achieved in all the reactions carried out in this series. There was no trend detected in the residual free monomer contents of the product (1000 – 1600 ppm) for the temperatures ranging from 90 – 70 ^{0}C. The specific gravity (S.G.) also seemed to have remained very constant throughout. The emulsions were therefore not aerated.

The change in the viscosity as a function of reaction temperature, for the results obtained at the end of the reaction, is presented in Figure 5.14.

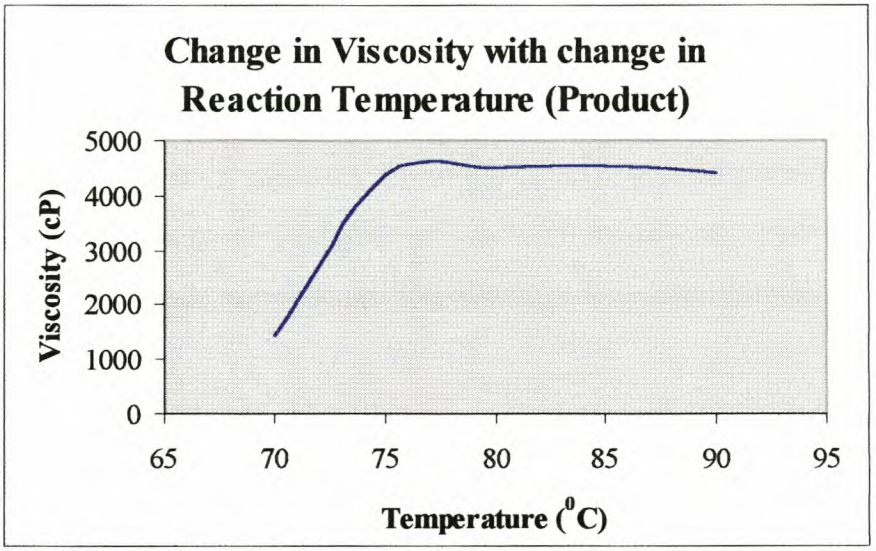

FIGURE 5.14 *Viscosity as a function of reaction temperature*

The viscosity remained almost constant for the temperature ranging from 90 – 75 ^{0}C, with a sudden decrease at 70 ^{0}C (Figure 5.14). This was a result of the much larger particle size and particle size distribution obtained at 70 ^{0}C.

The changes in the cumulative heat of reaction (CHR) obtained at the end of the core phase, as well as at the end of the reaction, are presented in Figure 5.15 and Figure 5.16, respectively.

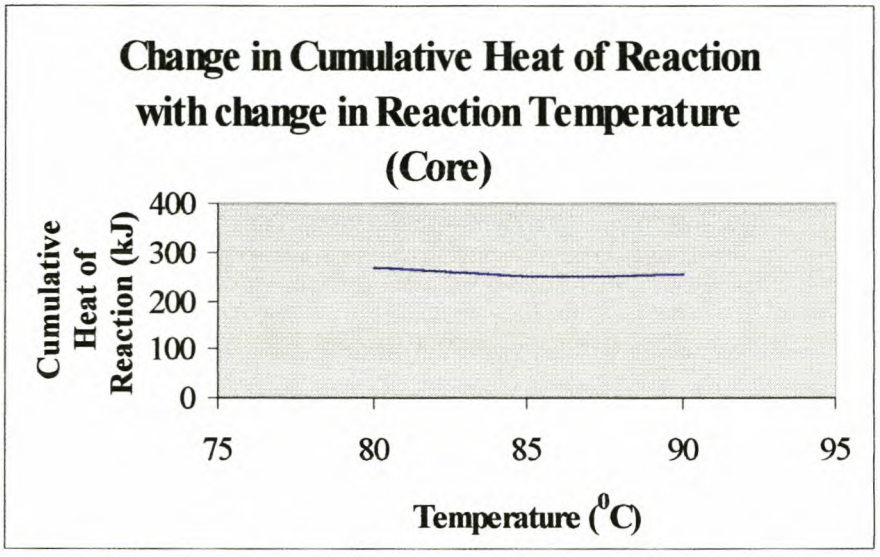

FIGURE 5.15 *Cumulative heat of reaction (Core)*

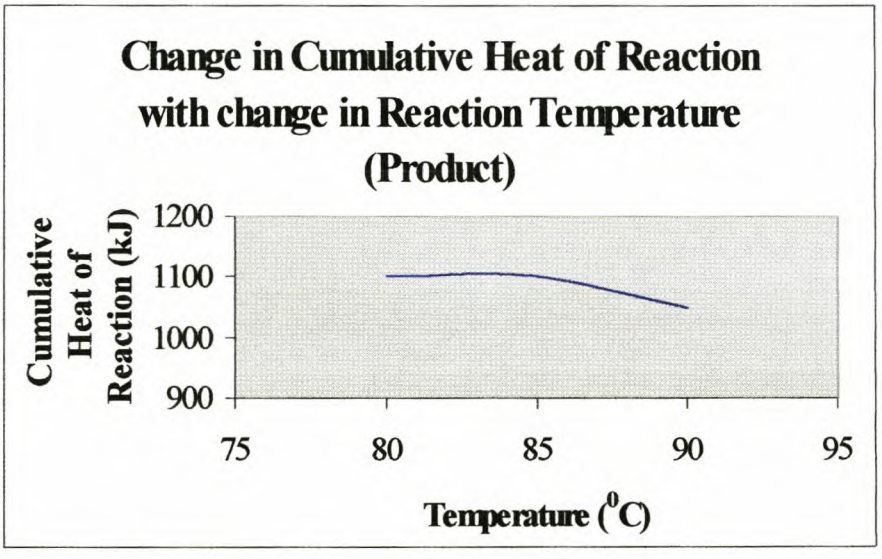

FIGURE 5.16 *Cumulative heat of reaction (End result)*

A heat loss model was derived (Chapter 4, §4.2.2) to predict the heat losses from the reactor for a reactor temperature ranging between 87.5 and 82.5 ^{0}C. The inaccuracies involved in extrapolating the heat loss model, due to the non-linearity that exist in the calculation of the free convection heat transfer coefficient, was discussed (§ 4.2.2). Inaccuracies in the results obtained at 90 ^{0}C and at 80 ^{0}C could amount to ≈40 kJ over a $4\frac{1}{4}$ h reaction period. These inaccuracies were taken into account in the results presented in Table 5.2, Figure 5.15 and Figure 5.16.

There was a slight increase in the cumulative heat of the reaction with a decrease in reaction temperature from 85 ^{0}C to 80 ^{0}C, for results obtained after the core phase (Figure 5.15), while there existed no difference between the results obtained at 85 ^{0}C to 90 ^{0}C.

The cumulative heat of reaction, obtained at the end of the reaction, for the experiment conducted at 90 ^{0}C was visibly lower (Figure 5.16) than for the experiments carried out at 85 ^{0}C and 80 ^{0}C.

The differences that exist in the cumulative heat for the experiments carried out at 85 and 90 ^{0}C, cannot be explained and was considered to be beyond the scope of this project.

5.3.1 EFFECT OF REACTION TEMPERATURE ON THE TIME DEPENDENCE OF CONVERSION

The overall monomer conversion (as a function of time), at different reaction temperatures, was plotted against reaction time. They are presented for the reaction temperatures ranging between 90 and 80 ^{0}C (Figure 5.17) as well as for the temperatures 85, 75 and 70 ^{0}C (Figure 5.18).

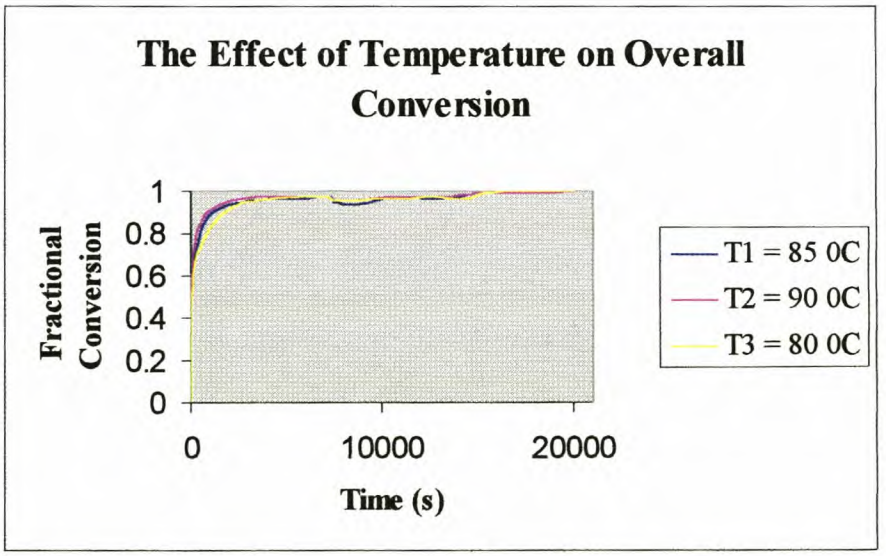

FIGURE 5.17 *Fractional conversion (90-80 ^{0}C)*

There seemed to be very little variation in overall monomer conversion with changes in the reaction temperature between 90 and 80 ^{0}C (Figure 5.17). This is also seen in Figure F2-1 – Figure F2-3 (Addendum F) in which the experimentally

obtained conversion (based on monomer feed) of the total reactor mass and the theoretically calculated conversions are compared.

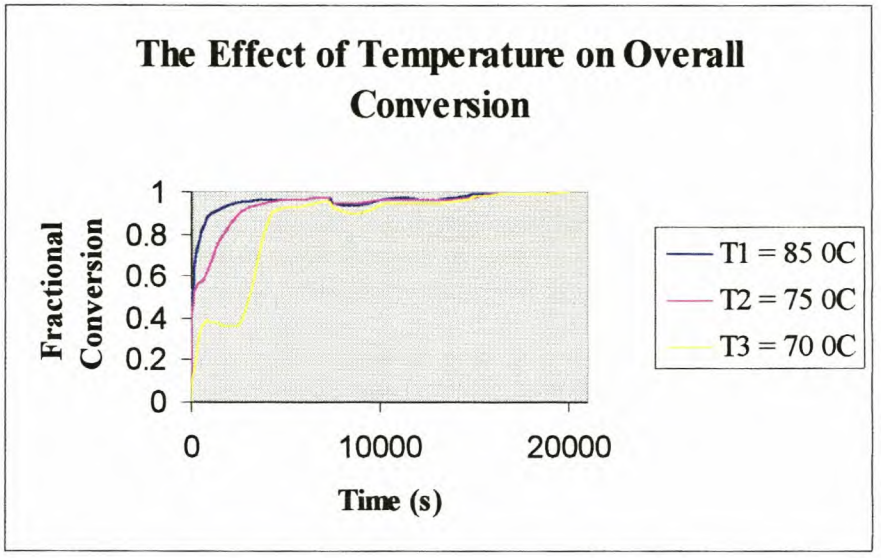

FIGURE 5.18 *Fractional conversion (85, 75 and 70 ^{0}C)*

There was a decrease in the overall conversion with a decrease in the reaction temperature (75 and 70 ^{0}C), during the first hour of monomer addition (Figure 5.18). This effect was much more pronounced for the experiment conducted at 70 ^{0}C. There seemed to have been an initial increase in the conversion, whereafter it remained constant, for more than 30 min.

Ammonium persulfate, as initiator, is normally used at elevated temperatures 1) because the decomposition constant for ammonium persulfate (k_d(persulfate)) is strongly favored at elevated temperatures and 2) to keep oxygen out of the reacting system and thus to eliminate possible deactivation of the persulfate.

The Arrhenius parameters for the persulfate decomposition are given by (Gilbert, 1995):

$$k_d(persulfate) = 8 \times 10^{15} e^{-135/RT} \qquad .....5.2$$

The calculated decomposition constant at 70 ^{0}C is ≈85% lower than the calculated constant at 85 ^{0}C. The overall conversion of the experiment carried out at 70 ^{0}C could thus have stagnated because of the inhibiting effect of dissolved oxygen that may have been present in the reacting liquid at such a low reaction temperature, as well as the lower overall decomposition of persulfate.

The effect that the reaction temperature at 70 ^{0}C (extreme) has on the conversion (based on monomer feed) of the total reactor mass is presented in Figure 5.19.

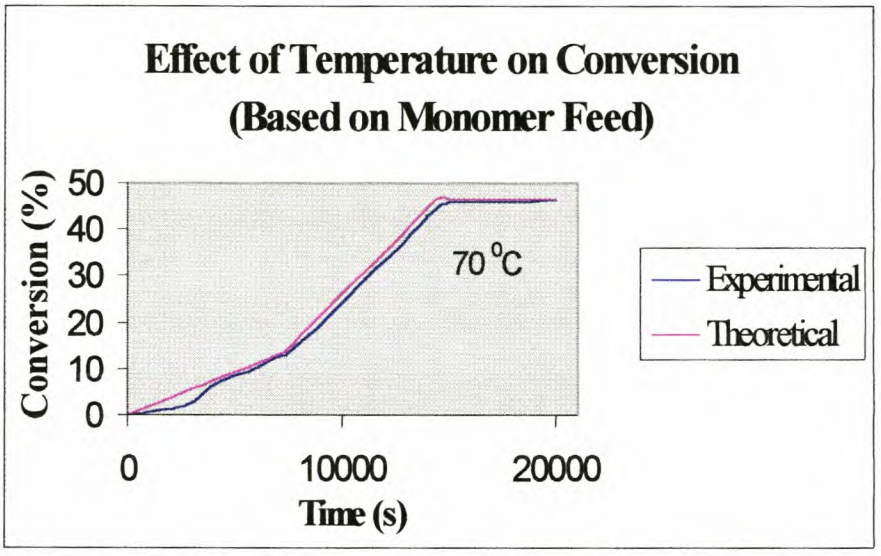

FIGURE 5.19 *Effect of reaction temperature on conversion (70 ^{0}C)*

The decrease in the conversion is barely visible in Figure F2-4 (Addendum F), for a reaction temperature of 75 ^{0}C, but at 70 ^{0}C it is clearly visible in Figure 5.19 .

5.3.2 EFFECT OF REACTION TEMPERATURE ON THE TIME DEPENDENCE OF PARTICLE SIZE

Particle size profiles as a function of time, that were obtained by varying the reaction temperature between 80 and 70 ^{0}C, during the core phase and shell phase of the reaction, are presented in Figure 5.20 and Figure 5.21, respectively. Particle size profiles as a function of time for the core and shell phase of the reaction, for variations in the reaction temperature between 90 and 80 ^{0}C are included in Addendum F (Figures F2-5 and F2-6)

There existed very little variation in the particle size profiles for the temperature ranging from 90 – 80 ^{0}C during the core phase, but especially during the shell phase of the reaction (Figures F2-5 and F2-6).

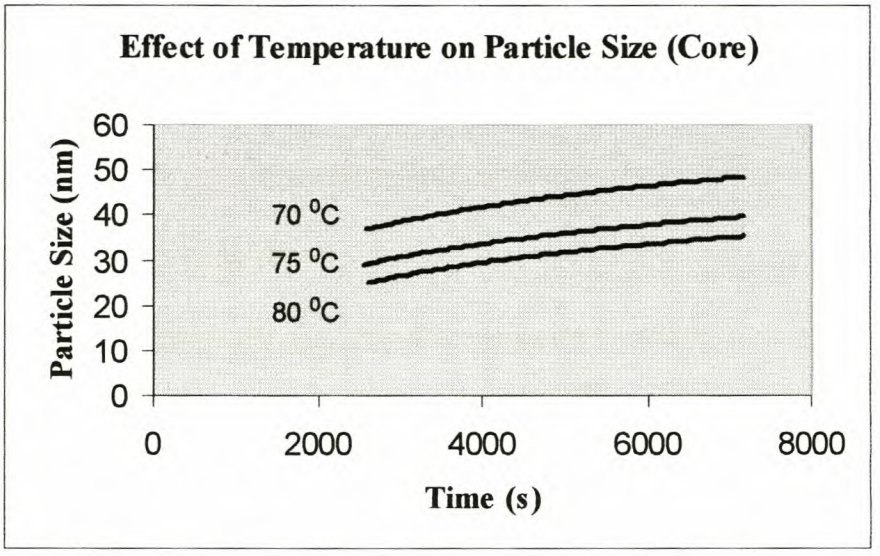

FIGURE 5.20 *Effect of reaction temperature on particle size (Core)*

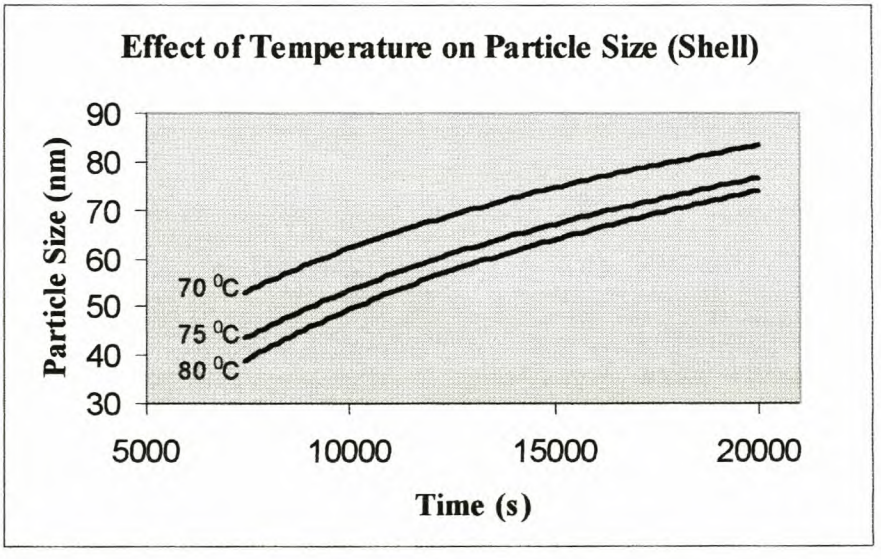

FIGURE 5.21 *Effect of reaction temperature on particle size (Shell)*

A further decrease in the reaction temperature from 80 to 70 ^{0}C resulted in a visible increase in the particle size during the respective, core and shell phases of the reaction.

In all the cases i.e. (80 – 70 ^{0}C) the small desired core is obtained. What this data does present is an opportunity to tailor the size of the core and the shell. More satisfactory is that the growth of the cores are nicely described by the curves presented, showing that electrostatic stability is maintained throughout the reaction when the correct stirring speed is maintained. The reason for the difference in particle

size, for the reaction temperature ranging from 80 - 90 ^{0}C, need not be explained, as electrostatic stabilization resulting from surfactant self-assemblies is temperature dependent.

5.3.3 EFFECT OF REACTION TEMPERATURE ON THE TIME DEPENDENCE OF VISCOSITY

Viscosity, as a function of time, for variations in the reaction temperature (85, 75 and 70) ^{0}C is presented in Figure 5.22, while the viscosity profiles obtained for reaction temperature variations ranging from 90 to 80 ^{0}C are included in Addendum F (Figure F2-7).

The viscosity profiles obtained for the experiments conducted at reaction temperatures between 90 and 80 ^{0}C were very similar (Figure F2-7).

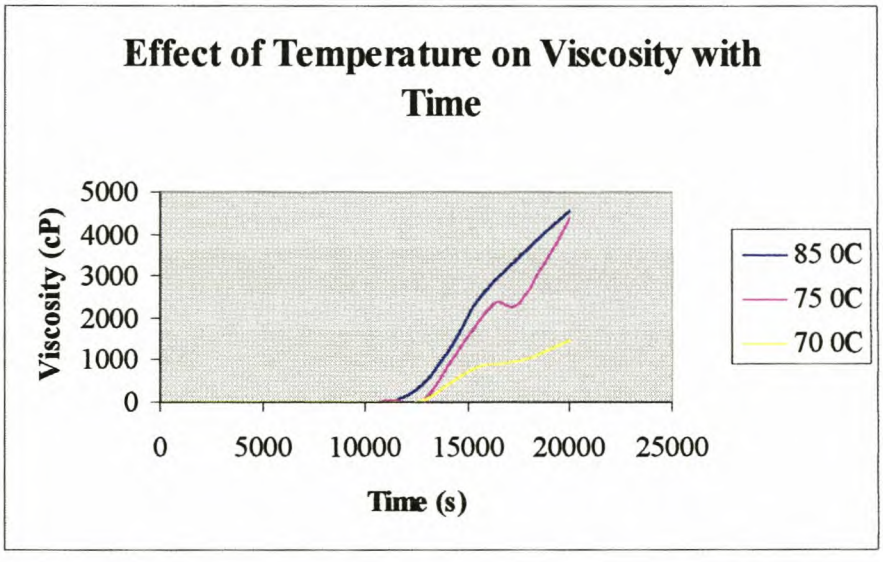

FIGURE 5.22 *Effect of reaction temperature on viscosity (85, 75 and 70 ^{0}C)*

The viscosity increased sharply during the last 15 minutes of monomer addition (Figure 5.22 and Figure F2-7). The increase in the viscosity at a reaction temperature of 70 ^{0}C was not nearly as sharp as for any other experiment conducted in this series. This is possibly due to the larger particle sizes as well as the larger distribution thereof. The point of inflection observed in Figure 5.22 for the experiment conducted at 75 ^{0}C was a result of one data point and could be due to a possible measurement error.

5.3.4 EFFECT OF REACTION TEMPERATURE ON THE CHANGE IN CUMULATIVE HEAT OF REACTION

The data obtained from the on-line calculation of the heat of reaction was further processed using MS Excel 97 to obtain presentable graphs. The cumulative heat of reaction profiles for the reaction temperatures (85 and 70) ^{0}C are presented on one graph (Figure 5.23). The cumulative heat of reaction profiles for the reaction temperature ranging from 90 to 75 ^{0}C are included in Addendum F (Figure F2-8).

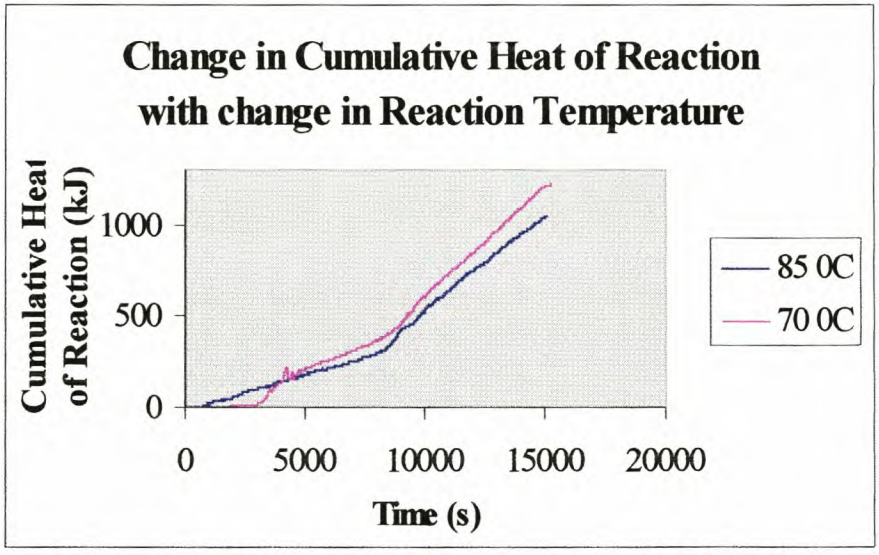

FIGURE 5.23 *Cumulative heat of reaction (85 and 70 ^{0}C)*

From Figure 5.23 it can be seen that there was very little or no reaction for approximately the first 30 min of the reaction, as was also observed in Figure 5.18, in the stagnancy that existed in the overall conversion during the same time.

The core (before the point of inflection) and the shell phase (after the point of inflection) are observed in Figure 5.23, for the experiment conducted at 85 ^{0}C. There was a significant increase in the heat of reaction between the core ($\approx$ 40 W) and the shell phase ($\approx$ 100 W), due to the addition profile of the reactants and catalysts. The core monomers were added under starved conditions (monomer addition rate < rate of reaction), while the shell monomers were added under flooded conditions (monomer addition rate $\geq$ rate of reaction).

5.3.5 EFFECT OF REACTION TEMPERATURE ON THE CHANGE IN MOLECULAR WEIGHT

Two experiments were repeated at 85 and 75 ^{0}C in which the crosslinking agent was left out of the recipe to investigate the influence that the reaction temperature has on the molecular weight (MW) of the polymer. The results obtained are shown in Table 5.3.

There was an increase in the MW with a decrease in the reaction temperature from 85 ^{0}C to 75 ^{0}C. This effect was observed for analyses performed at the end of the core phase, as well as at the end of the reaction.

The observed variations in the MW are explained by the following hypothesis: At the lower temperature (75 ^{0}C) fewer oligomeric radicals are produced in the water phase and it is therefore assumed that if the other variables such as solids content and latex volume, remain constant, less entry of the oligomeric radicals will take place and therefore fewer terminations will take place. The calculated number of particles decreased by ≈22%, while the decomposition constant for ammonium persulfate decreased by 73% with decrease in reaction temperature from 85 – 75 ^{0}C, i.e. less radicals per particle were present at 75 ^{0}C than at 85 ^{0}C. It is therefore possible that propagation be favored and that could result in the formation of longer polymer chains.

TABLE 5.3 *Summary of results obtained from MW analyses*

Temp	^{0}C	**85 ^{0}C**	**75 ^{0}C**
Width	nm	28.6	29.3
Zavg	nm	70.5	77.8
Viscosity	cP	5350	4095
Solids	%	46.98	46.77
MW	**CORE**	181000	311650
(g/mol)	**SHELL**	288000	500000

The viscosity obtained for the experiment conducted at 75 ^{0}C was much lower than the viscosity obtained at 85 ^{0}C. This was a result of the larger particle size (Z_{avg}) obtained at 75 ^{0}C, since the particle size distributions (Width) were almost the same.

5.4 REACTION TIME

Five reactions were carried out for which the total reaction time was reduced by up to 1 ½ h (Addendum E, Run 12 – Run 16), by increasing the addition rate of the monomers and catalysts. The total amounts of monomer and catalyst fed to the reactor were as described in the recipe for NW 120 (Chapter 3, Table 3.1). The reaction temperature and stirring speed were kept constant throughout, at 85 ^{0}C and 250 rpm, respectively.

A summary of the results obtained at the end of the core phase of the reaction, as well as at the end of reaction, is presented in Table 5.4.

TABLE 5.4 *Summary of results obtained*

		CORE				
Run		Run 12	Run 13	Run 14	Run 15	Run 16
Time	Core	2 hrs	1.5 hrs	1 hr	2 hrs	1 hr
Time	Shell	2 hrs	2 hrs	2 hrs	1.5 hrs	1.5 hrs
Peak1						
Mean	nm	*	3.9	3.3	3.4	3.8
Width	nm	*	0.4	0.4	0.4	0.4
Peak2						
Mean	nm	38.9	41.5	44.4	39.6	42.8
Width	nm	21.8	20.1	24.1	23.2	22.2
Z_{avg}	nm	36.5	38.3	40.6	35.9	38.4
CHR	kJ	299	288	285	262	267
		PRODUCT				
Run		Run 12	Run 13	Run 14	Run 15	Run 16
Time	Core	2 hrs	1.5 hrs	1 hr	2 hrs	1 hr
Time	Shell	2 hrs	2 hrs	2 hrs	1.5 hrs	1.5 hrs
Peak1						
Mean	nm	75.2	78.0	78.8	79.4	80.7
Width	nm	27.4	40.0	39.8	34.7	44.6
Z_{avg}	nm	72.6	72.7	74.1	76.9	74.0
CHR	kJ	1110	1063	1068	1065	1070
Viscosity	cP	4490	4290	4240	3840	2670
Solids	%	47.04	47.04	46.58	46.72	46.28
S.G.	kg/l	1.047	1.048	1.05	1.047	1.047

The change in the particle size (Z_{avg}) at the end of the core phase, as well as at the end of the reaction, after a reduction in the core reaction time are presented in Figure 5.24 and Figure 5.25, respectively.

The second peak (Peak 2) that was observed (Table 5.4) could have been due to possible impurities present in the sample.

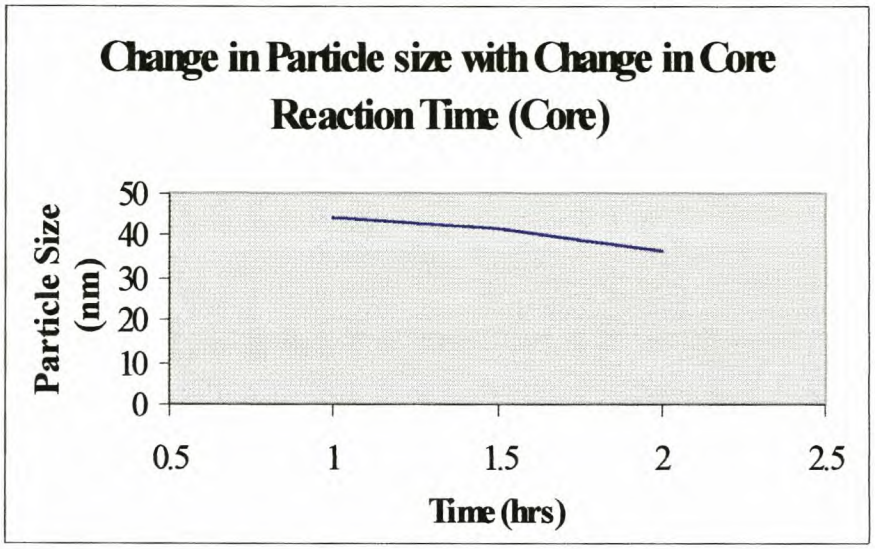

FIGURE 5.24 *Change in particle size (Core)*

There was a slight increase in the particle size (Z_{avg}) with a reduction in the core reaction time. This effect was more prominent in the core phase (Figure 5.24) than in the final results (Figure 5.25), where the difference in the particle size was less than 1.4 nm, which is well within the experimental accuracy of the instrument used (Malvern, §3.7.5).

The reproducibility of the particle sizes obtained at the end of the core phase, between Runs 12 & 15 and Runs 14 & 16 were very good.

There was an increase in the particle size and the particle size distribution (Width), and hence a decrease in viscosity, with a 25% ($\frac{1}{2}$ h) reduction in the shell reaction times (Run 15 and Run 12). A very similar effect was observed when the shell reaction time was reduced after a 1 hr (50%) reduction in the core reaction time (Run 14 & 16), except that the particle size distribution seemed the widest, and hence the viscosity the lowest, with a simultaneous reduction in core and shell reaction time (Run 16)

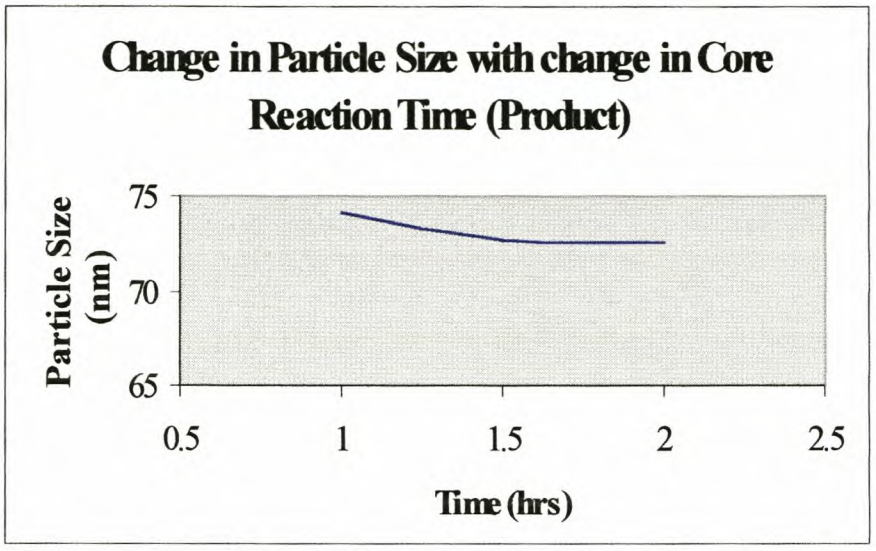

FIGURE 5.25 *Change in particle size (End result)*

A change in the viscosity as a function of core reaction time, for the results obtained at the end of the reaction, is presented in Figure 5.26.

There was a small reduction in the viscosity (Figure5.26) after a 25% ($\frac{1}{2}$ h) reduction in the core reaction time. The viscosity remained constant after a further reduction (50%) in core reaction time. The change in the viscosity can be correlated to the particle size distribution (Width) that revealed the same changes.

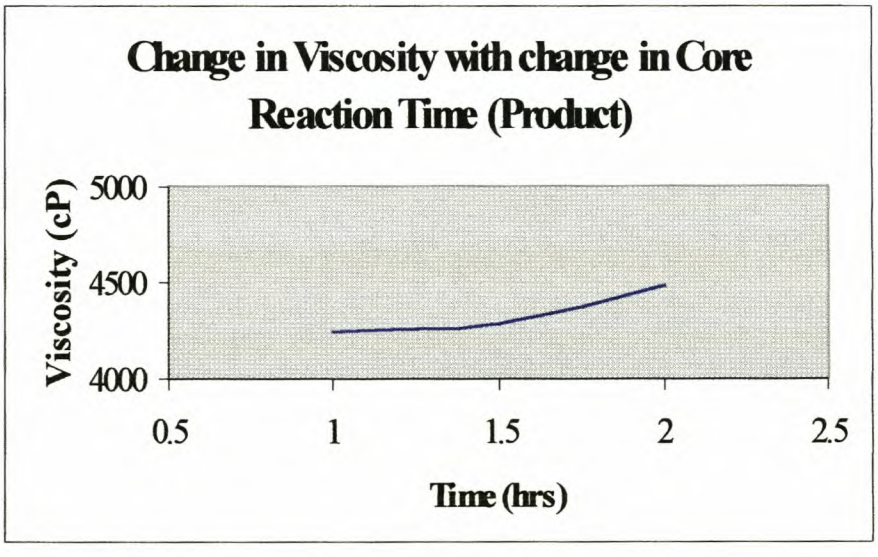

FIGURE 5.26 *Change in viscosity (End result)*

Changes in the cumulative heat of reaction, as a function of core reaction time obtained at the end of the core phase as well as at the end of the reaction, are presented in Figure 5.27 and Figure 5.28.

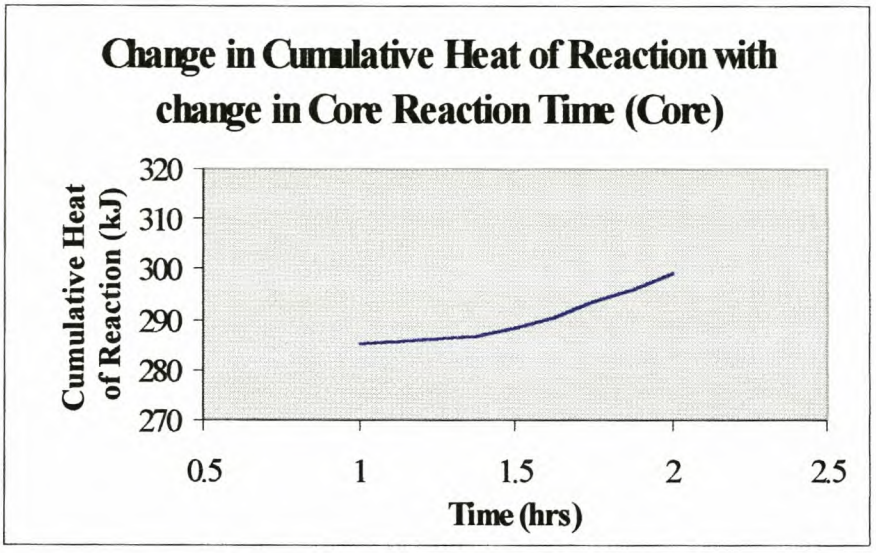

FIGURE 5.27 *Cumulative heat of reaction (Core)*

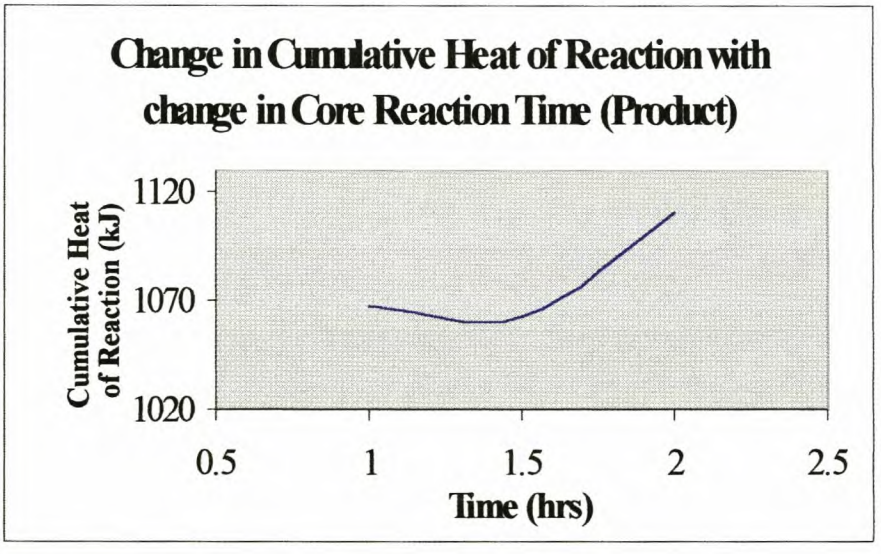

FIGURE 5.28 *Cumulative heat of reaction (End result)*

There appeared to be an initial decrease in the cumulative heat of reaction (CHR) after the core phase as well as at the end of the reaction, with a reduction in the core reaction time. The differences in the cumulative heats of reaction that exist at the end of the core phase as well as at the end of the reaction for Run 12 – Run 14 are

well within experimental accuracy and can be attributed to possible measurement inaccuracies. The cumulative heat of reaction of Runs 13 & 14, reported after the core phase, were slightly higher than the values reported for Runs 15 & 16. There existed no real difference in the CHR at the end of the reaction, between Runs 13, 14, 15 and 16.

There was very little change in the solids content of the emulsion (Table 5.4) with change in reaction time, nearly full conversion was achieved in all the reactions carried out in this series. There was no trend observed in the residual free monomer contents of the product (900 – 1100 ppm). The specific gravity also seemed to have remained constant throughout. The emulsions were therefore not aerated.

5.4.1 EFFECT OF REACTION TIME ON THE TIME DEPENDENCE OF CONVERSION

The effect that a reduction in the core reaction time had on the overall conversion is illustrated in Addendum F (Figure F3-1). The time axis was rather normalized and the overall conversions that were obtained is presented in Figure 5.29.

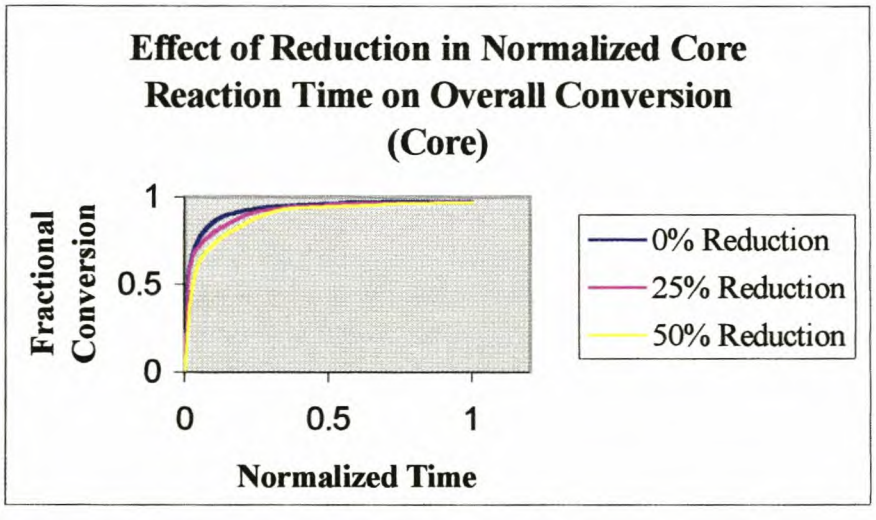

FIGURE 5.29 *Fractional conversion (Core)*

The effect of a 50% reduction on the overall conversion (based on monomer feed) of the total reactor mass is presented in Figure 5.30. The effect of a 0% and a 25% reduction in the core reaction time, on the overall conversion, is included in Addendum F (Figure F3-2 and Figure F3-3).

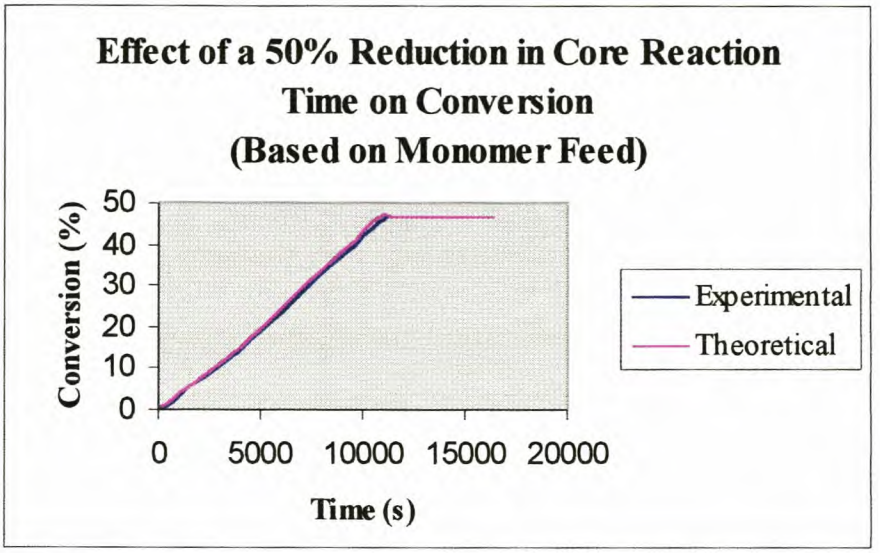

FIGURE 5.30 *Effect of 50% reduction in core reaction time on conversion*

There was a slight decrease in the overall conversion during the core phase of the reaction (Figure 5.29) with a reduction in the core reaction time. This effect was not that clearly visible in Figure 5.30 for a 50% reduction in core reaction time.

The effect of the free monomer present during the early stages of the reaction on the particle size and particle size distribution is subjected to the following hypothesis:

The reacting system under investigation can be best described as bordering between Interval 2 & 3 (§2.1.4) if compared hypothetically to the traditional bulk system. This assumption may be made because of the very high conversions (steady state) that was obtained throughout most of the experiments (Figure 5.3, 5.12).

An increase in the addition rate of the reagents/catalysts resulted in a slight decrease in the conversion profiles (Figure 5.29). Free monomer was present which had to be stabilized. Sustained development of new particles, needing additional surfactant for stabilization, could have resulted in coagulation of the primary seed particles, resulting in larger particles and a wider distribution. Larger particles and a wider particle size distribution were obtained (Table 5.3).

The effect of a 25% reduction in shell reaction time on the overall conversion, as well as on the conversion (based on monomer feed) of the total reaction mass, are presented in Figure 5.31 and Figure F3-4 (Addendum F).

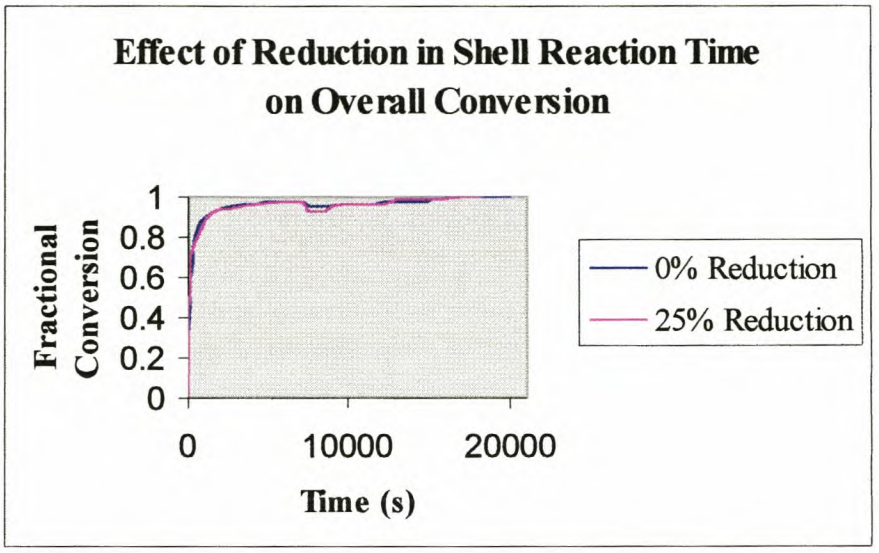

FIGURE 5.31 *Fractional conversion*

There seemed to be a further reduction in the overall conversion after the first 25 – 30 min of shell monomer addition (Figure 5.31), with a reduction in the shell reaction time (increase in shell monomer feed rate). The same hypothesis, used to explain the effect of free monomer during the reaction of the core monomers, could be used to explain the larger particles and wider particle size distribution that were obtained with a reduction in the shell and the core and shell reaction times (Table 5.3).

The effect of a simultaneous reduction in the core and the shell reaction times on the conversion profiles is included in Addendum F (Figure F3-5 and Figure F3-6).

5.4.2 EFFECT OF REACTION TIME ON THE TIME DEPENDENCE OF PARTICLE SIZE

The effect of a reduction in the core reaction time on the particle size, during the core phase and the shell phase, is presented in Addendum F (Figure F3-7) and on a normalized time axis in Figure 5.32, respectively.

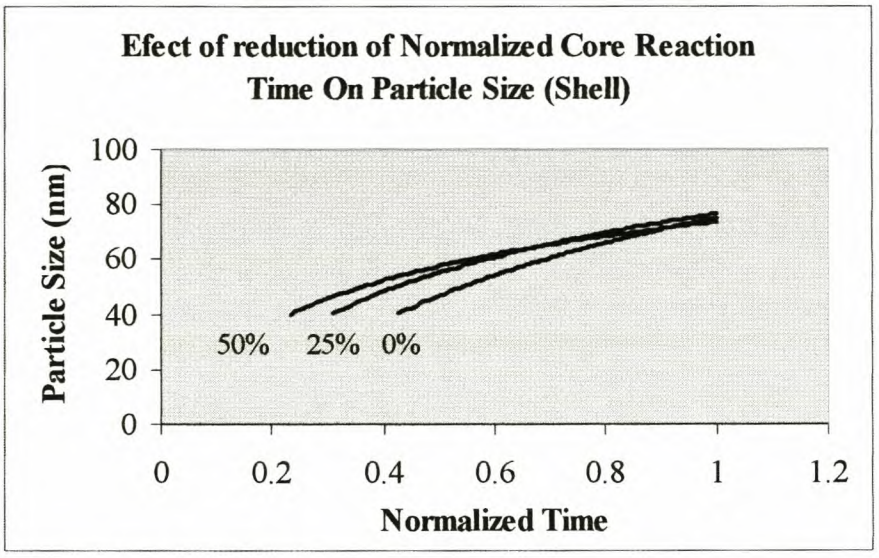

FIGURE 5.32 *Effect of core reaction time on particle size profile (Shell)*

It is seen in Figure 5.32 that the particle sizes seemed larger in the beginning of the shell phase, with a reduction in core reaction time. From Table 5.4 it can be seen that the particle sizes and their distributions seemed larger and wider after the core phase after a 1 h reduction in the core reaction time. The particle sizes were very similar towards the end of the shell phase. This was due to a possible effect known as 'competitive growth' (Gilbert, 1995). In a wide distribution, the smaller latex particles will grow at the expense of the larger particles.

The change in the particle size profile (shell phase) as a function of normalized time, for a reduction in shell reaction time, is presented in Figure 5.33. The effect of a simultaneous reduction in the core and shell reaction times on the particle size profile is included in Addendum F (Figure F3-8).

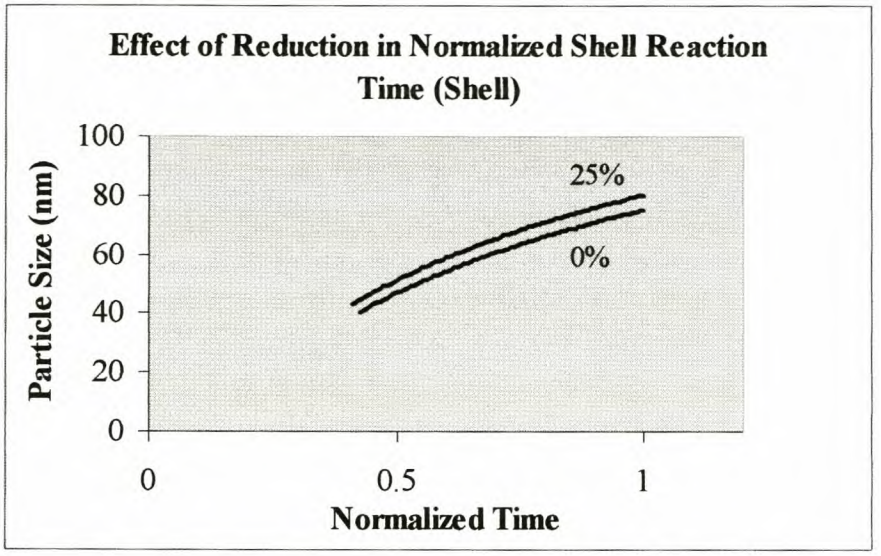

FIGURE 5.33 *Effect of shell reaction time on particle size (Shell)*

There seemed to be a visible increase in the particle sizes during the shell phase of the reaction, with a reduction in the shell reaction time (Figure 5.33).

5.4.3 EFFECT OF REACTION TIME ON THE TIME DEPENDENCE ON VISCOSITY

The change in the viscosity profiles, as a function of normalized time, for a reduction in shell and a reduction in core and shell reaction times, is illustrated in Figure 5.34. The change in the viscosity profiles for a reduction in the core reaction time is included in Addendum F (Figure F3-9).

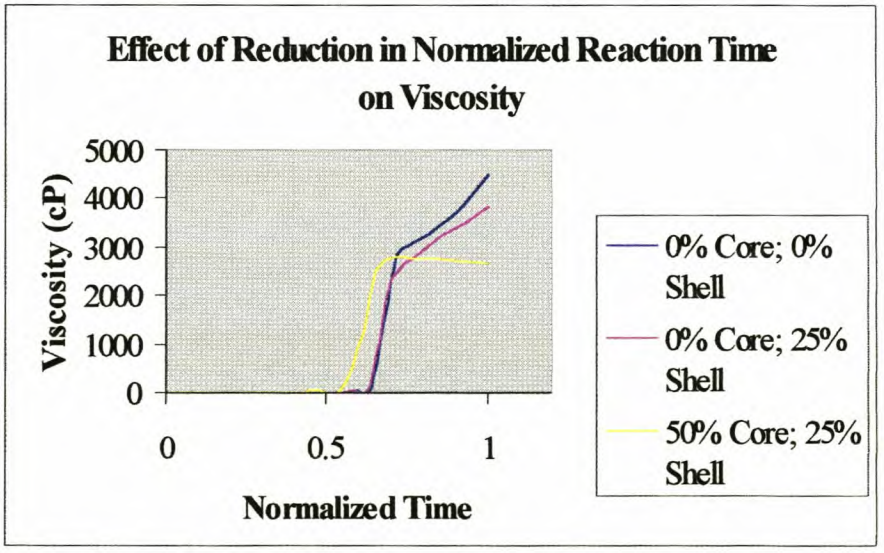

FIGURE 5.34 *Effect of normalized core reaction time on viscosity profile*

The viscosity of the experiment conducted with a simultaneous reduction in both core and shell reaction time (Figure 5.34) seemed to result in a sharp initial increase in viscosity, whereafter it stayed almost constant.

This effect could be due to possible secondary nucleation, resulting in a wider particle size distribution (Table 5.4). An increase in the particle size was also observed (Table 5.4).

5.4.4 EFFECT OF REACTION TIME ON THE CHANGE IN CUMULATIVE HEAT OF REACTION

The cumulative heat of reaction profiles for a reduction in core reaction time (0%, 25% and 50% are presented in Figure 5.35.

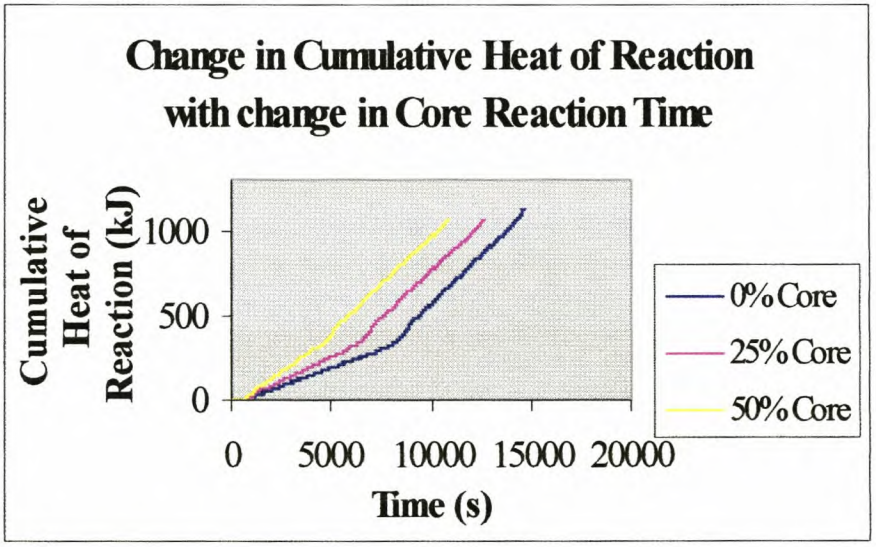

FIGURE 5.35 *Cumulative heat of reaction profiles*

The cumulative heat of reaction profiles for a reduction in shell and a reduction in core and shell reaction times are presented in Figure 5.36.

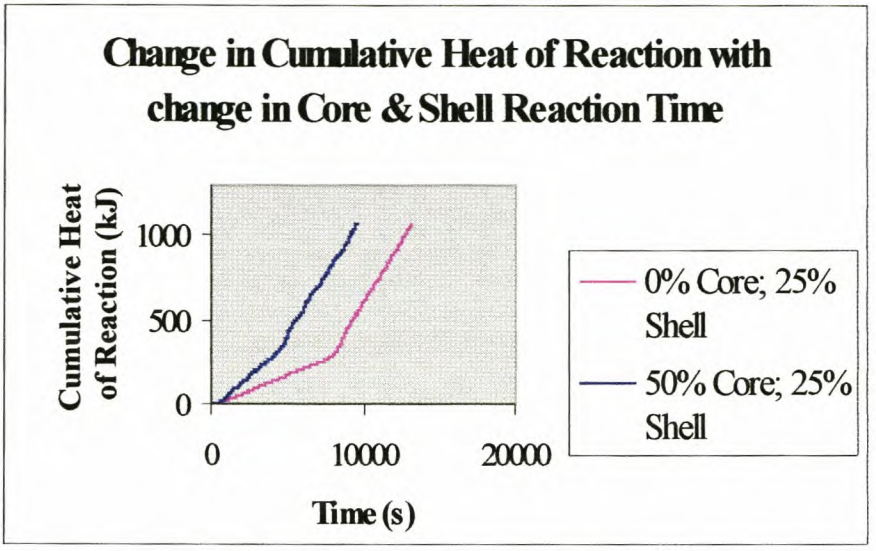

FIGURE 5.36 *Cumulative heat of reaction profiles*

Increases in the addition rates of the reactants and catalysts (reduction in reaction time) resulted in an increase in the rate of reaction and hence the tempo of heat dissipation (W) of the resulting exotherm (Table 5.5).

TABLE 5.5 *Summary of heat evolved during a reduction in reaction time*

Run		Run 12	Run 13	Run 14	Run 15	Run 16
Time	Core	2 hrs	1.5 hrs	1 hr	2 hrs	1 hr
Time	Shell	2 hrs	2 hrs	2 hrs	1.5 hrs	1.5 hrs
CHR Core	(W)	41	53	78	37	74
CHR Shell	(W)	100	96	97	127	127

There was an increase in the heat dissipation rate (W) of the resulting exotherm with a reduction in core and shell reaction times, as a result of an increase in the monomer and catalyst addition rates.

5.5 SAMPLING

A certain number of samples (≈ 16) and hence a certain volume of reaction mixture (200 – 300 ml), was withdrawn from the reactor during the course of a reaction (the sampling method was discussed in Chapter 3 (§ 3.6)).

In order to successfully perform a scale-up it is important to be aware of the magnitude of the disturbance caused by sampling. In Table 5.6 a summary is given of the results obtained from analyses performed on a run from which samples were withdrawn (Run 01) and one from which no samples were withdrawn (Run 06).

TABLE 5.6 *Summary of results obtained*

Run		**Run 01**	**Run 06**
Peak		samples	no samples
Mean	nm	76.7	78
Width	nm	41.4	45.9
Z_{avg}	nm	69.8	71.3
Viscosity	cps	4870	4260
Solids	%	47.82	46.16
S.G.	kg/l	1.045	1.049
CHR(kJ)	**Core**	290	325
CHR(kJ)	**Shell**	1090	1155

The particle sizes (Z_{avg}) were well within experimental accuracy. The particle size distribution (Width) seemed narrower when samples were withdrawn from the reactor. The narrower particle size distribution that was obtained could be a result of the method used to take samples. The base valve was first drained (10 – 15 ml) and the contents returned to the reactor. This could have resulted in an effect known as 'multiple seeding'.

The lower viscosity that was obtained, for the experiment conducted where no samples were withdrawn from the reactor, was due to the wider particle size distribution (Parsons, 1993). The difference in the solids content (Solids) can be attributed to inaccuracies associated with the gravimetrical method used to obtain the results, as was described in §5.2.4.

The cumulative heat of reaction (CHR) seemed lower for results obtained after the core phase (≈ 0.40 $^{kJ}/_{g}$), as well as for results obtained during the shell phase of

the reaction ($\approx 0.22\ {}^{kJ}/_{g}$)„ when samples were withdrawn from the reactor. Samples withdrawn from the reactor contained free monomer as well as growing polymer chains. Sample taking during the early stages of the reaction (initiation and particle formation) could thus have a much greater influence, on the cumulative heat of reaction, than sampling towards the end of the reaction.

Further, the emulsion that was recovered after the base valve had been drained cooled down slightly before it could be returned to the reactor. The amount of heat necessary to heat this liquid again to the reaction temperature could have amounted to 10 – 20 kJ.

5.6 CALCULATION OF THE TOTAL CONVERSION FROM CALORIMETRC MEASUREMENTS

On-line calorimetry was used to predict the fractional conversion (based on total monomer feed). The cumulative heat of reaction obtained at the end of Run 12, was used to calculate the fractional conversion (based on total monomer feed) of Run 14, using Eq. 2.5 (De La Rosa et al., 1996).

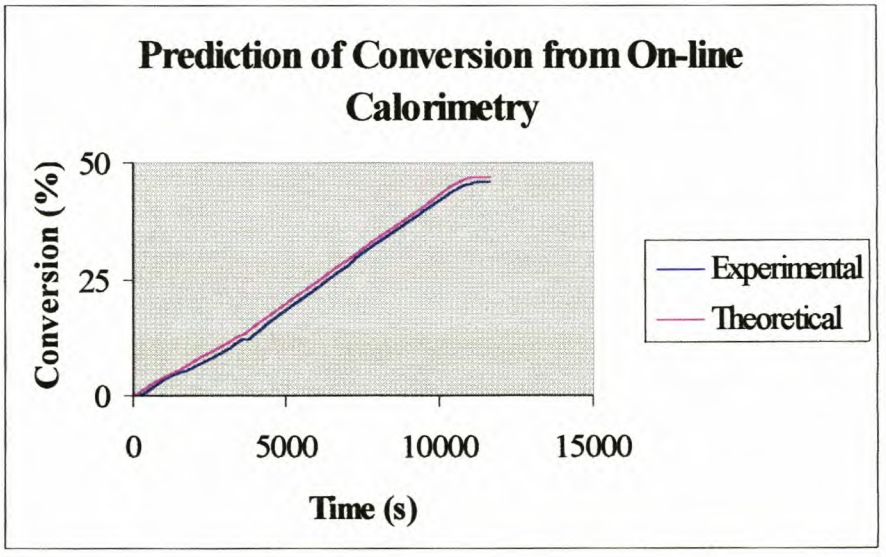

FIGURE 5.37 *Prediction of conversion from calorimetry*

The conversion profile that was obtained from the on-line calorimeter followed the same "pattern" as the theoretically calculated curve (based on monomer feed), but seemed to be slightly out of phase. This phenomenon is referred to as time

lag (time delay) (Seborg et al., 1989), and is associated with the process control of reactors and other industrial equipment. From the results obtained in Figure 5.37 the time lag was found to be less than 70 s. This is extremely good and emphasizes the excellent process control that exists.

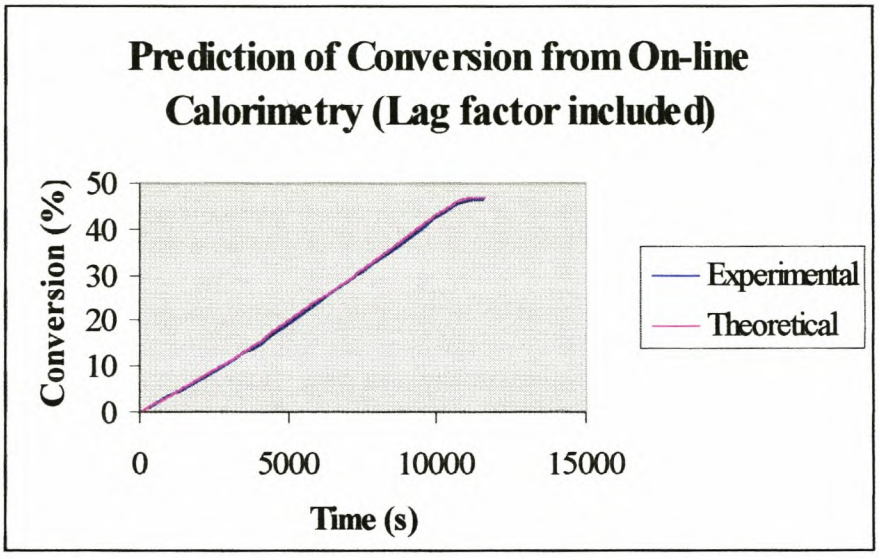

FIGURE 5.38 *Prediction of conversion from calorimetry (Time Lag)*

A phase shift of 70 s was introduced and the curves that were obtained are presented in Figure 5.38.

CHAPTER 6

SCALE-UP OF THE PRODUCTION OF NW 120

6.1 INTRODUCTION

Several factors contribute to the complexity of scale-up operations. Firstly, there is the varied nature of the operation, each with its particular process requirements: blending, suspension of solids, heat- and mass transfer, reaction, emulsification and dispersion (Uhl et al., 1986). In addition, there are processes in which several of these operations govern. Then there is the range of properties inherent to the material being processed, for example, moderate to high viscosity fluids, and either single or multiple phases.

Much research has been conducted on the scale-up of different process equipment. It has been found (Uhl et al., 1986 and Klein et al., 1996) that mixing/agitation plays an integral part in scale-up. Most of the research that has been conducted by Uhl et al. (1986) and others, have been focussed on the scale-up of mixing vessels. It is of very little use when, the scale-up of mixing of very complicated heterogeneous reaction systems, or reactors with unique stirrer configurations (as used in this study), are considered (Klein et al., 1996).

6.2 SCALE-UP CONSIDERATIONS

Klein et al. (1996) proposed a procedure, for the mixing scale-up of emulsion polymerization systems, based on the calculation of the minimum rotational speed of the stirrer necessary to disperse the system.

It has been recognized by those practicing emulsion polymerization (Klein et al., 1996) that the scale-up of such complicated reaction systems (Uhl et al., 1986) from lab-scale, in which 1-2l reactors are used, to industrial-scale, is virtually impossible. The process conditions (addition rates, stirring speed and reaction temperature) and their control are sometimes very different to what is encountered on an industrial scale.

A fully computer-controlled bench-scale pilot plant was specially developed to study the scale-up of a newly developed emulsion polymerization reaction (NW 120).

It comprised a geometrically scale-down replica (5 l) of an industrial size reactor (10 ton). The very good control that exists during the reactions in terms of reaction temperature and addition rates of monomer/catalyst, is one of the key features of the newly developed pilot plant, and is vitally important in the study of any new process.

It was shown (Chapter 4) with the very successful commissioning of the pilot plant in which the industrially known emulsion AE 446 was used, that if a geometrically similar reactor is used and if the correct reaction conditions are observed, then such a reactor could be successfully used in the direct scale-up of NW 120.

6.3 PROCESS CONDITIONS

The product with the lowest viscosity and the smallest particle size was obtained in the pilot plant reactor at stirring speeds of 150 rpm and 250 rpm, respectively, for variations ranging between 150 and 350 rpm. Shear sensitivity at 450 rpm was observed, hence stirring speeds of 450 rpm and higher were not considered for scale-up.

The agitation scale-up method of Klein et al. (1996) was used (Chapter 2, Eq. 2.9) to calculate the equivalent stirring speeds for scale-up.

$$\left((D_s)^{0.765}.N_{\min}\right)_{Full-scale} = \left((D_s)^{0.765}.N_{\min}\right)_{Pilot-plant}$$

$$\left((1.21)^{0.765}.N_{\min}\right)_{Full-scale} = \left((0.092)^{0.765}.250\right)_{Pilot-plant}$$

$$\Rightarrow \left(N_{\min}\right)_{Full-scale} = 35 \text{ rpm}$$

Very little or no change was observed in the measured physical properties (particle size, particle distribution, viscosity, solids content and specific gravity) of NW 120 when the reaction temperature was varied between 90 – 80 ^{0}C. It was subsequently decided to conduct the scale-up at a reaction temperature of 85 ^{0}C.

It was found possible to reduce the reaction time (by increasing the addition rate of the monomers/catalysts) by at least 1 hr, with only a slight effect on the physical properties of NW 120. It was however decided, not to use the reduced reaction time because, at the time it was not certain, whether the heat removal of the industrial reactor would be adequate to cope with the increase in the evolved heat (≈85 kW) associated with the increase in the addition rates of the monomers/catalysts. It appeared later that an auxiliary water-circulating pump had been installed to

increase the flowrate of the cooling water circulating through the jacket of the reactor (it was however not known at the time of the scale-up), and it would hence be possible to industrialize the production of NW 120 with a reduced reaction time.

Based on the results obtained from the commissioning of the reactor (as described in §4.4), as well as the results obtained in Chapter 5, a full-scale run of the production of NW 120 was conducted. This was done on the Plascon plant in Durban, in a 10 ton reactor. The reaction temperature was set at 85 ^{0}C and a stirring speed of 35 rpm was used. The core and shell reaction times were both set at 2 h. Samples were withdrawn from the reactor through a $\frac{3}{4}''$ base valve, and evaluated.

6.4 SCALE-UP RESULTS

Very satisfactory results were obtained. Here the results obtained during the full-scale run are compared with those from experiments conducted in the pilot plant reactor at 85 ^{0}C and at stirring speeds of 150 rpm and 250 rpm. A summary of the results obtained at the end of the reactions is presented in Table 6.1.

TABLE 6.1 *Summary of results obtained*

Run		**Run 00**	**Run 03**	**Run 01**
Peak		Industrial	Pilot plant	Pilot plant
Rpm		35	150	250
Mean	nm	79	79.1	76.7
Width	nm	43.1	43.4	41.4
Z_{avg}	nm	72.8	71.9	69.8
Viscosity	cP	4050	4400	4870
Solids	%	46.76	47.44	47.82
S.G.	kg/l	1.051	1.049	1.045

The particle sizes (Z_{avg}) and the particle size distributions of the products obtained at 150 rpm and at 250 rpm in the pilot plant reactor compare well with those obtained in the industrial size reactor (full-scale).

The differences in viscosities can be partly explained by the slightly larger particles that were obtained during the full-scale run, although the values are well within experimental accuracy (§3.7.5.2). The differences in viscosities can mainly be attributed to the effect that sampling has (in the pilot plant reactor) on the

manufacturing of NW 120 (§5.5). The solids content and the specific gravity also compare very well.

Comparisons of the overall conversions (full-scale reactor vs. pilot plant reactor) are presented in Figures 6.1 and Figure 6.2. In Figure 6.3 the experimentally obtained conversion profile for the full-scale run is compared with the theoretically calculated profile.

The fractional conversions that were obtained in the industrial size reactor were very high (Figures 6.1 and 6.2). They compared very well with the theoretically calculated values (Figure 6.3). No significant changes were observed in the results obtained in the pilot plant at stirring speeds of 150 rpm and 250 rpm and the results obtained from the full-scale run.

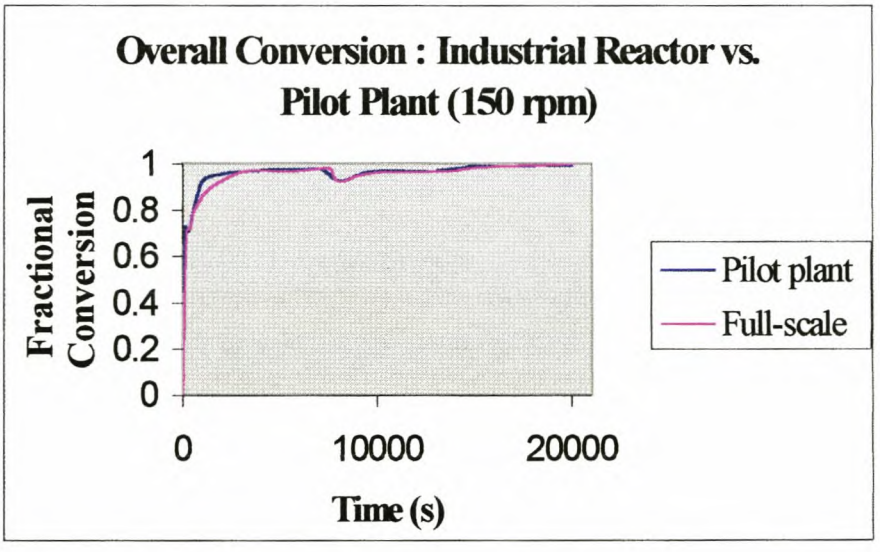

FIGURE 6.1 *Fractional conversion (150 rpm)*

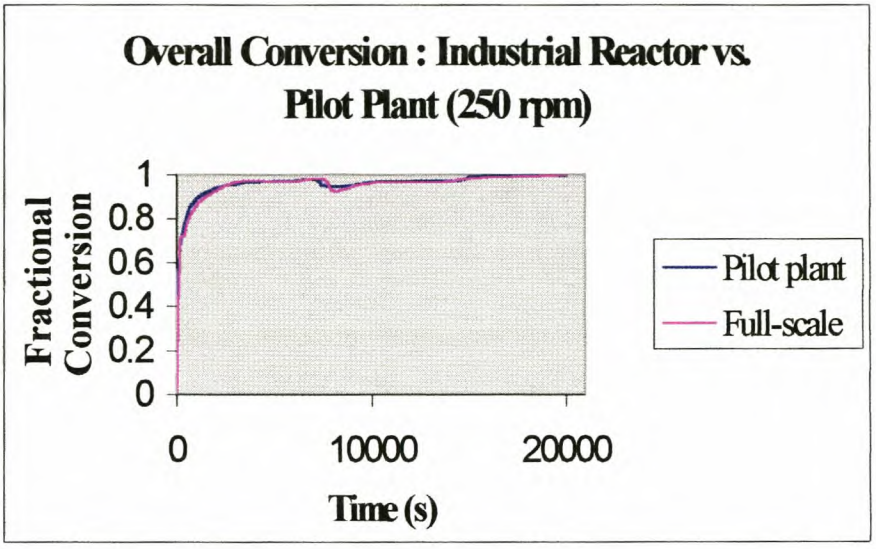

FIGURE 6.2 *Fractional conversion (250 rpm)*

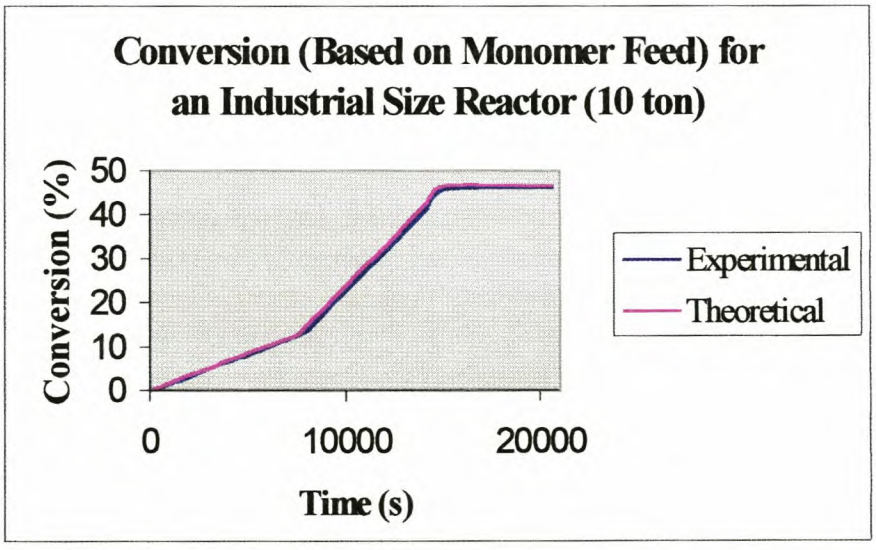

FIGURE 6.3 *Conversion (based on monomer feed)*

The particle size profiles obtained during the core phase and the shell phase for the pilot plant runs, conducted at 150 rpm and 250 rpm, and the full-scale run are presented in Figure 6.4 and Figure 6.5.

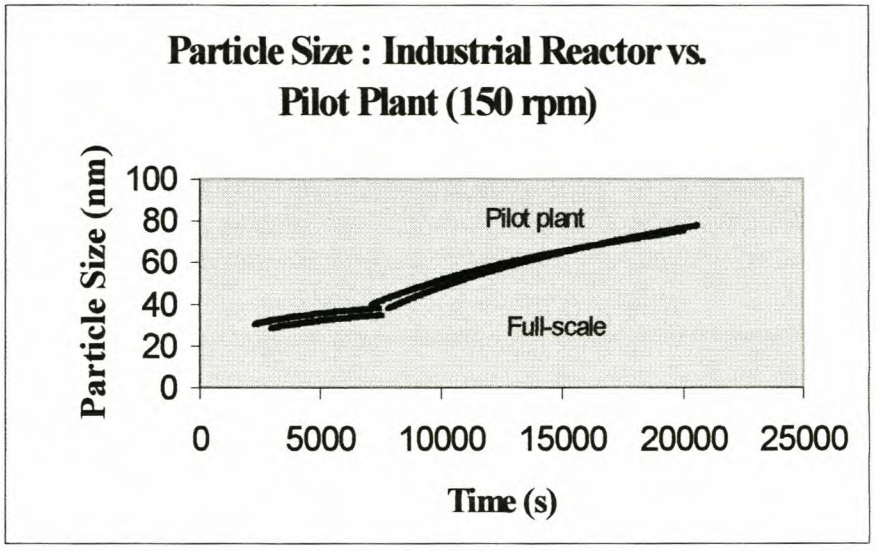

FIGURE 6.4 *Particle size profiles (150 rpm)*

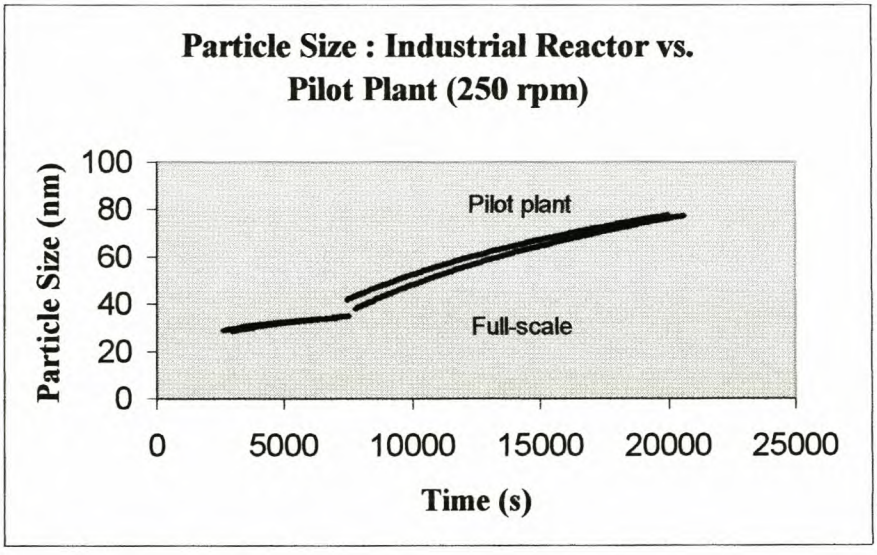

FIGURE 6.5 *Particle size profiles (250 rpm)*

The addition of the reactants and catalysts overran by 5 min. during both the core phase and the shell phase of the full-scale reaction. The slight difference that exists in the particle size profiles (Figures 6.3 and 6.4) of the experiments conducted in the pilot plant reactor and the full-scale run are attributed to a difference in the total reaction time.

The viscosity profiles of the industrial run and the pilot plant run are presented in Figures 6.6 and 6.7.

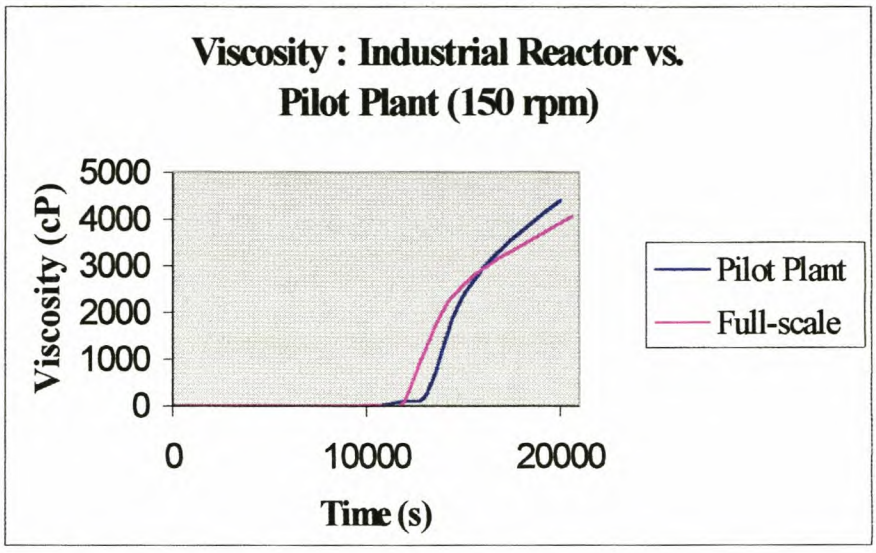

FIGURE 6.6 *Viscosity profiles (150 rpm)*

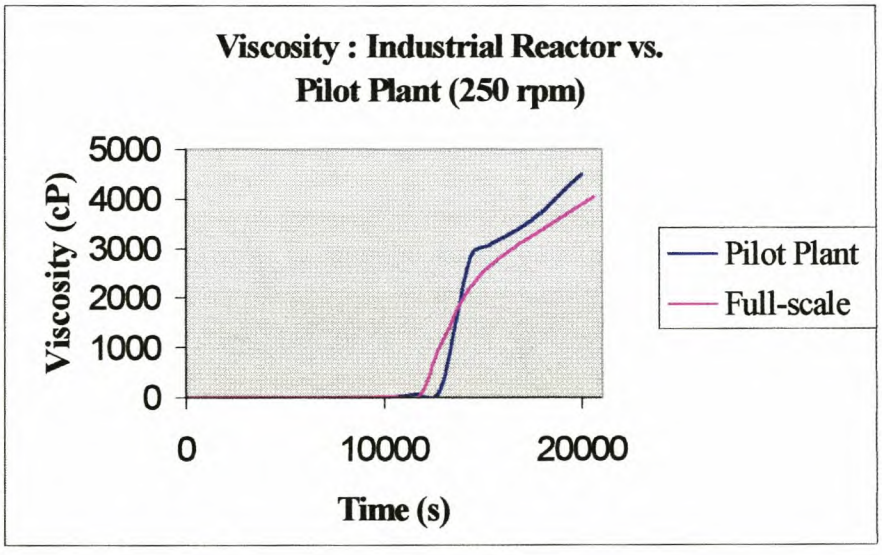

FIGURE 6.7 *Viscosity profiles (250 rpm)*

The viscosity profiles that were obtained in the pilot plant reactor and in the industrial reactor compared very well, especially for the experiment conducted at a stirring speed of 150 rpm. The slight difference could also be attributed to the fact that the full-scale run overran by 10 minutes.

CHAPTER 7

CONCLUSIONS

7.1 INTRODUCTION

The main goal of this study was to obtain a suitable pilot plant for the study of a multi-component emulsion polymerization reaction system. Since nothing suitable was found, a fully computer-controlled bench-scale pilot plant was designed and constructed. The pilot plant was used to study the scale-up of the manufacture of a new core-shell emulsion, NW 120.

There were four major objectives, as set out in §1.3, and to which the following conclusions were drawn.

7.2 IDENTIFICATION OF A SUITABLE AVAILABLE PILOT PLANT

After a survey was made of available pilot plants and related equipment the following were found.

- Small lab-scale reactors (1-2 l), especially ones with large measuring probes, are generally not suitable for the study of the scale-up of emulsion polymerization reactions.
- Physical hindrances (which act as baffles), for example, internal cooling coils placed inside such small reactors, would have a detrimental effect on the morphology of an emulsion and its effect would have to be determined prior to scale up.
- Commercially available bench-scale pilot plants (e.g. RC 1) consist of reactors that are not necessarily geometrically similar to the industrial reactor under investigation.
- Available bench-scale pilot plants, such as the RC 1, are very expensive (≈R1.5 million).

7.3 EVALUATION OF NEWLY DEVELOPED BENCH-SCALE PILOT PLANT

7.3.1 DESIGN AND CONSTRUCTION

A new bench-scale pilot plant was designed and constructed. The reactor (5 l) also served as a calorimeter. For this reason, models of the heat capacity and the heat losses had to be derived.

- A new method, using Diffractional Scanning Calorimetry, was developed to obtain the heat capacity of an emulsion. The chief advantage of this method was that the analyses could be performed on very small samples (10 – 20 mg).
- The heat losses from the pilot plant reactor were found to be strongly dependent on the reactor temperature as well as the ambient temperature.
- The accuracy of the on-line calorimeter was found to be very good, by determining the heat of solution of a sodium hydroxide solution at a reaction temperature of 85 ^{0}C and a stirring speed of 250 rpm.

In terms of the performance of the reactor itself it was concluded that

- Very good and stable control was maintained over the process variables e.g. the reactor temperature and the reactants and catalyst addition rates.
- In less than a year a bench-scale pilot plant was developed at a fraction of the cost of a similar set-up (RC1, Mettler Toledo), which could be used in the scale-up of emulsion polymerization reactions.

7.3.2 COMMISSIONING OF BENCH-SCALE PILOT PLANT

- The pilot plant was successfully commissioned with an emulsion well known to industry (AE 446). The measured physical properties of the emulsion manufactured in the pilot plant reactor compared very well with the industrially manufactured emulsion.
- The minimum rotational speed recommended by Klein et al. (1996) for the dispersion of an emulsion was successfully used in the scale-down of, AE 446.

- Other methods, such as the calculation of the mixing Reynolds number (Uhl et al., 1986) are only suitable for stirring vessels and are of very little use in emulsion polymerization reactions.
- It was found that direct scale-up from the pilot plant reactor to the industrial size reactor is possible if a geometrically similar reactor is used, while the correct process conditions (stirring speed, reaction temperature and addition rates) are maintained.

7.4 LAB-SCALE EVALUATION OF NW 120

The following conclusions were made with respect to the effects of stirring speed, reaction temperature, the time of the reaction and sampling on the lab-scale performance of NW 120

7.4.1 EFFECT OF STIRRING SPEED

- A change in the stirring speed (150 – 350 rpm) had very little or no effect on the measured physical properties of NW 120, at a reactor temperature of 85 ^{0}C and a monomer reaction time of 4 h.
- Sensitivity of the emulsion to high shear rates was already observed at 450 rpm, with a maximum reported effect at 550 rpm, at which the product quality was unacceptable.
- The highest viscosity could be obtained at a stirring speed of 350 rpm and the lowest at 550 rpm (but with unacceptable product quality).
- Very little or no aeration was encountered, even at very high stirring speeds (550 rpm).
- Special care should be taken just before the sharp increase in the viscosity, as control over the reaction temperature then becomes increasingly difficult.
- The gravimetrical method used to study the solids content of the emulsion could only be used as an indication of the conversion.
- The very high conversions that were obtained for the experiments conducted at stirring speeds ranging from 150 – 450 rpm could be attributed to the addition-rate profiles of the core and the shell monomers and effective stirring. The stirring configuration used seemed adequate, even at the high viscosities.

7.4.2 EFFECT OF REACTION TEMPERATURE

- Very good control over the particle size and the viscosities were possible for variations in the reaction temperature between 90 and 80 ^{0}C, when the correct stirring speed was used.
- The very high conversions could be maintained for temperature variations between 90 and 80 ^{0}C.
- The desired small core was obtained, even at reaction temperatures as low as 70 ^{0}C. Use of a reaction temperature between 80 and 70 ^{0}C could be used to tailor-make the size of the core and the shell, and hence the viscosity.
- Ammonium persulfate (catalyst/initiator) should not be used without N_2 gas, in reactions at temperatures below 75 ^{0}C.
- Special care should be taken with the sharp increase in the exotherm upon the addition of shell monomers. The increase in the exotherm from the core phase to the shell phase of the reaction was observed to be as high as 250%.
- There was an increase in the molecular weight with a decrease in the reaction temperature.

7.4.3 EFFECT OF REACTION TIME

- The core reaction time was successfully reduced by 1 h (50 %) while the shell reaction time was kept constant at 2 h, with very little or no effect on the measured physical properties (particle size, viscosity, solids content and specific gravity).
- The shell reaction time was successfully reduced by a $\frac{1}{2}$ h (25%) while the core reaction time was kept constant at 2 h, but it resulted in a small increase in particle size and hence a decrease in the viscosity.
- A simultaneous reduction in core and shell reaction times could be used to tailor-make the particle size and particle size distribution of the emulsion.
- The evolved heat (W) resulting from the exothermal reaction increased significantly with increases in the monomer and catalyst addition rates.
- The overall conversion remained very high even after a large increase in the monomer and catalyst addition rates.

7.4.4 SAMPLING

- The method used in this research for sampling (by returning the reaction mixture that was obtained when the base valve was drained) resulted in a slightly narrower particle size distribution, because of a possible multiple seeding effect.
- Sample taking had a greater influence on the heat of reaction during the core phase (0.40 $^{kJ}/_{g}$) than during the shell phase (0.22 $^{kJ}/_{g}$).

7.5 SCALE-UP OF THE PRODUCTION OF NW 120

- The production of NW 120 was successfully scaled up from a 5 l reactor to a 10000 l reactor.
- Very good agreement was obtained between the particle size and viscosity profiles obtained in the industrial size reactor and those predicted by the results obtained in the pilot plant reactor.

During the scale-up the following was found:

- A stirring speed of 150 – 250 rpm at a reaction temperature of 85 ^{0}C in the pilot plant reactor, corresponded well to a stirring speed of 35 rpm at 85 ^{0}C in the industrial size (10 ton) reactor.
- The high conversion that was achieved in the pilot plant reactor was also obtained in the industrial size reactor. Effective stirring at 35 rpm was thus achieved.

Results of the very extensive research conducted in the scale-up and control of the multi-component emulsion polymerization system NW 120 should certainly make a meaningful contribution in the field of the industrialization and control of emulsion polymerization reactions.

7.6 RECOMMENDATIONS AND FUTURE WORK

On the completion of this study, certain recommendations can be made:

- A heat loss model should be derived over a wider temperature range, for example 70 – 90 ^{0}C to enable reactions to be studied over a wider reaction temperature range.
- Determine a way to properly balance the stirrer shaft, as accurate torque measurements could then be used to predict the viscosity of the emulsion at the temperature that it is being manufactured. The use of a different bearing and seal should also therefore be investigated.

Interesting phenomena emerged during this study and should be investigated further in the future:

- In order to keep up with international environmental laws, techniques should be investigated to reduce the residual free monomer contents in the product.
- The differences that exist in the cumulative heat of reaction and the particle sizes, for the reaction temperatures varying from 85 – 90 ^{0}C and 70 – 80 ^{0}C, respectively, should be investigated further.
- The method of sampling used in this study has introduced a way of controlling the particle size distribution of NW 120. The possible application of an external heat exchanger set-up should therefore be investigated.
- The computer program (plascon.pas), that was developed to control the bench-scale pilot plant, can be altered slightly to accommodate the study of gradient polymerization.
- The derivation of a mathematical model (for example correlating the process parameters with morphology) for NW 120 should be investigated and could ultimately be used in a "intelligent controller".

This is not the end.

It is not even the beginning of the end.

But it is the end of the beginning.

- Winston Churchill -

REFERENCES

1. Arzamandi, G.; Asua, J.M. *Copolymer Composition Control of Emulsion Copolymers in Reactors with limited Capacity for Heat Removal* . Ind. Eng. Chem. Res. **1991**, 30, 1342-1350

2. Billmeyer, F.W. *Textbook of Polymer Science.* 3^{d} ed., Wiley, New York, **1984**

3. Blackley, D.C. *Emulsion Polymerization: Theory and Practice.* Applied Science Publishers LTD, London, **1975**

4. Brooks, B.W. *Why are polymerization reactors special.* Ind. Eng. Chem. Res. **1997**, 36, 1158-1162

5. Canegallo, S.; Apostolo, M.; Storti, G.; Morbidelli, M. *On-Line conversion monitoring through ultrasound propagation velocity measurements in emulsion polymerization.* J. Appl. Polym. Sci. **1995**, 57, 1333-1346

6. Canegallo, S.; Storti, G; Morbidelli, M; Garra, S. *Densimetry for on-line conversion monitoring in emulsion homo- and copolymerization.* J. Appl. Polym. Sci. **1993**, 47, 961-979

7. Coulson, J.M.; Richardson, J.F. *Chemical Engineering.* Volume 3, 2^{d} ed., Pergamon Press, Oxford, **1982**, 425-439

8. De La Rosa, L.V.; Sudol, E.D.; El-Aasser, M.S.; Klein, A. *Details of Emulsion Polymerization of Styrene Using a Reactor Calorimeter.* J. Polym. Sci.: Part A: Polym. Chem. **1996**, 34, 461-473

9. De Wet-Roos, D. *The Mechanism of Polymerization in an Epoxy-Acrylate Composite Emulsion,* PhD Thesis, University of Stellenbosch, **1999**, 227-229

10. Dickey, D.S.; Hill, R.S. *Use the right speciality-polymer pilot plant.* Chemical Engineering Progress **1993**, 22-29

11. Dimitratos, J.; Georkakis, C.; El-Aaser, M.; Klein, A. *An experimental study of adaptive Kalman filtering in emulsion copolymerization.* Chem. Eng. Sci. **1991**, 46, 3203-3218

12. Eliseeva, V.I.; Ivanchev, S.S.; Kuchanov, S.I.; Lebedev, A.V. *Emulsion Polymerization and its Application in Industry.* Consultants Bureau, New York, **1976**

13. Gilbert, R.G. Emulsion polymerization: A mechanistic approach. Academic Press, London **1995**

14. Gugliotta, L.M.; Arotcarena, M.A.; Leiza. J.R.; Asua, J.M. *Estimation of conversion and copolymer composition in semicontinuous emulsion polymerization using calorimetric data.* Polymer, **1995a**, 36, 2019-2123

15. Gugliotta, L.M.; Leiza, J.R.; Arotcarena, M.; Armitage, P.D.; Asua, J.M. *Copolymer Composition Control in Unseeded Emulsion Polymerization Using Calorimetric Data.* Ind. Eng. Chem. Res. **1995b**, 34, 3899-3906

16. Himelblau, D.M. *Basic Priciples and Calculations in Chemical Engineering.* 5th ed., Prentice-Hall, Englewood Cliffs, N.J., **1989**, 686-687

17. Incropera, F.P.; De Witt, D. *Fundamentals of Heat and Mass transfer.* 3d ed., Wiley, New York, **1990**

18. Klein, A.; Lowry, V. *Some mixing scale-up considerations for emulsion polymerization.* Advances in Emulsion polymerization and latex technology, short course, Lehigh University, **1996**

19. Kozub, D.J.; Macgreggor, J.F. *Feedback Control of Polymer Quality in Semi-batch Copolymerization Reactors.* Chem. Eng. Sci. **1992**, 47, 929-942

20. Kravaris, C.; Wright, R.A.; Carrier, J.F. *Nonlinear controllers for trajectory tracking in batch processes*. Comput. Chem. Engng. **1989**, 13, 73-82

21. Leiza, J.R.; Arzamendi, G.; Asua, J.M. *Copolymer composition control in emulsion polymerization using technical grade monomers*. Polym. Int. **1993**, 30, 455-460

22. Litz, W; *On-line Calorimetry for the Determination of the Rate of Heat Production by Reaction within a Stirred Tank Reactor.* Chem. Eng. Technol. **1998**, 21, 804-808

23. Malvern PCS Training Manual, **1996**

24. Mckenna, T.F.; Fevotte, G.; Graillat, C.; Guillot, J. *Joint Use of Calorimetry, Densimetry and Mathematical Modelling for Multiple Component Polymerization.* Trans IChemE, Part A **1996**, 74, 340-348

25. Poehlein, G.W. *Reaction engineering for emulsion polymerization.* Advances in Emulsion polymerization and latex technology, short course, Lehigh University, **1996**

26. Ponnuswamy, S.R.; Shah, S.L.; Kiparissides, C.A. *Computer optimal control of batch polymerization reactors*. Ind. Eng. Chem. Res. **1987**, 26, 2229-2236

27. Parsons, P. Raw Materials and their Usage; *Surface Coatings,* Volume 1, 3^{d} ed., Chapman & Hall, Lodon, **1993**

28. Schaller, E.J. *Latex Rheology*. short course, Lehigh University, **1996**

29. Schuler, H.; Schmidt, C.U. *Calorimetric State Estimators for Chemical Reactor Diagnosis and Control: Review of Methods and Applications*. Chem. Eng. Sci. **1992**, 47, 899-915

30. Seborg, D.E.; Edgar, T.F.; Mellicamp, D.A. *Process Dynamics and Control*, Wiley, New York, **1989**

31. Ullman's Encyclopedia of Industrial Chemistry, Volume B1, 5th ed., VCH, Cambridge, **1990**

32. Urretabizkaia, A.; Leiza, J.R.; Asua, J.M. *On-line terpolymer composition control in semicontinuous emulsion polymerization*. AIChE J. **1994**, 40, 1850-1864

33. Urretabizkaia, A.; Sudol, E.D.; El-Aasser, M.S.; Asua, J.M. *Calorimetric Monitoring of Emulsion Copolymerization Reactions*. J. Polym. Sci.: Part A: Polym. Chem. **1993**, 31, 2907-2913

34. Waters, J.A. *Predicting the surface morphology of composite latex particles*. Colloids Surfaces A: Physicochem. Eng. Aspects, **1994**, 83, 167-174

ADDENDUM A

CONTROL STRUCTURE AND FLOW DIAGRAM

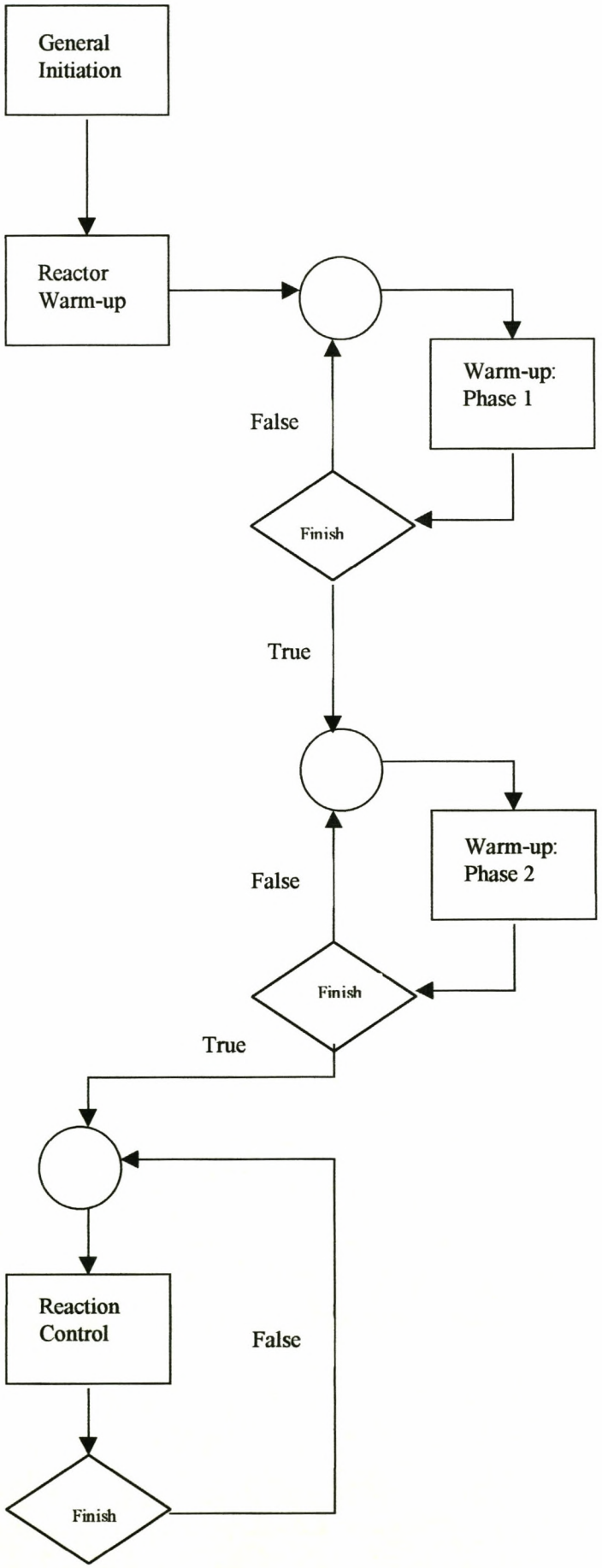

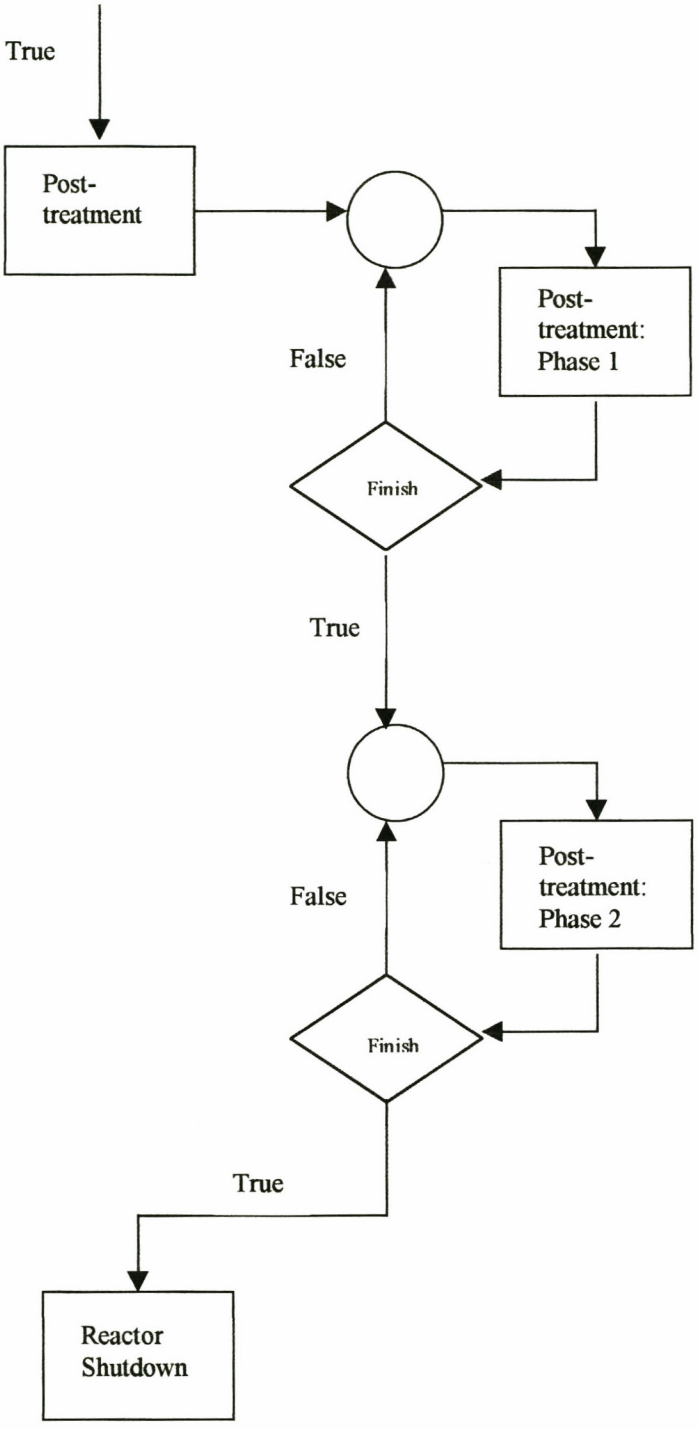

```
{$G+,N+,E-,R-,S-}
Program ReaktorBeheer;

Uses
  edr, weeg, crt, dos;

Type
  Tuitvolt    = array[0..11] of double;
  Tinvolt     = array[0..31] of double;
  Tafset      = array[0..31] of double;
  Tskaal      = array[0..31] of double;
  Tsetpoint   = array[0..29] of double;
  Tsi_eenhede = array[0..31] of double;
  Td          = array[0..7] of integer;    {d, refers to
                                              Digital}
  Tmassas     = array[0..2] of double;
  Tskaaltempo = array[0..2] of double;
  Terror      = array[0..5, 0..2] of double;
  Taccum      = array[0..2, 0..1] of double;

Var
  StartTime    : Double;
  StartMass    : Double;
  M_Jacket     : Double;
  M_Cond       : Double;
  Cp_JacketIn  : Double;
  Cp_JacketOut : Double;
  Cp_CondIn    : Double;
  Cp_CondOut   : Double;
  H_in         : Double;
  Qjacket      : Double;
  Qcond        : Double;
  Reac_Mass    : Double;
  Sample_Mass  : Double;
  Qlosses      : Double;
  Energy_Accum : Double;
  Qreac        : Double;
  CumQreac     : Double;

{--------------------------------------}
Procedure printerror(r :integer);
{displays error message and exits}
  Var
    s : string;
  Begin
    EDR_StrError(r,s);          {convert error number into
                                   A string}
    writeln(s);
    halt(1);
  End; {procedure printerror}
```

```
Procedure writehexdig(x :integer);
{displays x as a hex digit}
  Begin
    x := x mod 16;
    if x < 10 then write(Chr(x+48))
    else write(chr(x+55));
  End; {writehexdig}

{--------------------------------------}
Procedure writehex(x :integer);
{displays x as 4 hex digits}
  Begin
    writehexdig(x shr 12);
    writehexdig(x shr 7);
    writehexdig(x shr 4);
    writehexdig(x);
  End; {writehex}

{--------------------------------------}
Function valhexdig(c : char) : integer;
{converts hex digit in c into an integer}
  Begin
    c := upcase(c);
    if c >= 'A' then valhexdig := ord(c)-55
    else valhexdig := ord(c)-48;
  End; {function valhexdig}

{--------------------------------------}
Function valhex(s : string) : integer;
{converts hex number in s into an integer}
  Begin
    while length(s)<4 do s:='0' + s;
    valhex:= valhexdig(s[1]) shl 12 +
             valhexdig(s[2]) shl 7 +
             valhexdig(s[3]) shl 4 +
             valhexdig(s[4]);
  End; {function valhex}

{--------------------------------------}
Procedure inisieer_hardeware(var bh301 : integer; var
bh302 : integer; var bh66 : integer; seriepoort : byte;
baud : word);
{Initializes PC cards for Pascal use }
  Var
    baseaddr1, baseaddr2, baseaddr3 : integer;
    t : integer;
  Begin
    {Initializes first PC 30 card}
    baseaddr1:= $700;
    bh301:= EDR_AllocBoardHandle;   {"Board Handle"}
    if bh301= 0 then  {this should never happen with DOS}
```

```
      Begin
        writeln('No free board handles');
        halt(1);
      End; {if bh301}
    t:= EDR_InitBoard(bh301, baseaddr1);    {Initialize
                                          PC30 with bh301}
    if t < 0 then printerror(t);

    t:= EDR_SetADInRange(bh301,7,4);         {Channel 7 :
                                           +5V - -5V Volt}
    {Initializes second PC 30 card}
    baseaddr2:= $720;
    bh302:= EDR_AllocBoardHandle;   {"Board Handle"}
    if bh302= 0 then{this should never happen with DOS}
      Begin
     writeln('No free board handles');
     halt(1);
      End; {if bh302}
    t:= EDR_InitBoard(bh302, baseaddr2);   {Initializes
                                          PC30 with bh302}
    if t < 0 then printerror(t);

    {Initializes PC 66 card}
    baseaddr3:= $300;
    bh66:= EDR_AllocBoardHandle;   {"Board Handle"}
    if bh66= 0 then {this should never happen with DOS}
      Begin
        writeln('No free board handles');
     halt(1);
      End; {if bh66}
    t:= EDR_InitBoard(bh66, baseaddr3);    {Initializes
                                          PC66 met bh66}
    if t < 0 then printerror(t);

    {Initialize digital ports on first PC30}
    t:= EDR_DIOConfigurePort(bh301, 0, EDR_DIO_SIMPLE,
EDR_OUTPUT);
    t:= EDR_DIOConfigurePort(bh301, 1, EDR_DIO_SIMPLE,
EDR_OUTPUT);
    t:= EDR_DIOConfigurePort(bh301, 2, 0, 1);
  End; {procedure inisieer_kaarte}
```

```
Procedure inisieer_skale(bh301 : integer);
  Var
    da, db : Td;
    i, j, n, t : integer;
  Begin
    for i:= 0 to 2 do
      Begin
        for j:= 0 to 2 do
          Begin
            da[j]:= 0;
          End; {for j}
        da[i]:= 1;
        for n:= 0 to 7 do
          Begin
            t:= EDR_DIOLineOutput(bh301, 0, n, da[n]);
            t:= EDR_DIOLineOutput(bh301, 1, n, db[n]);
          End; {for i}
        initbalance(2, 19200);
      End; {for i}
  End; {procedure inisieer_skale}

{-------------------------------------}
Procedure de_inisieer_hardeware(var bh301 : integer; var
bh302 : integer; var bh66 : integer);
{release board handles}
  Var
    t : integer;
  Begin
    t := EDR_FreeBoardHandle(bh301);
    t := EDR_FreeBoardHandle(bh302);
    t := EDR_FreeBoardHandle(bh66);
  End; {procedure de_inisieer_kaarte}

{-------------------------------------}
Procedure inisieer_beginwaardes(var afset : Tafset; var
skaal : Tskaal; var setpoint : Tsetpoint);
{stored variables are set equal to input value}
  Var
    textfile : text;
    dummyline : string;
    i : integer;
  Begin
    {Read calibration file(KAL.DAT) obtain Afset[0..31]
                                      and Skaal[0..31]}
    assign(textfile, 'kal.dat');
    reset(textfile);
    readln(textfile, dummyline);
    readln(textfile, dummyline);
    For i:= 0 to 31 do   {While not eof(a) do}
      Begin
        readln(textfile, Afset[i], Skaal[i]);
```

```
      End;
    close(textfile);

{Obtain values for control, file(init.DAT) obtain
setpoint[0..29]
    assign(textfile, 'init.dat');
    reset(textfile);
    readln(textfile, dummyline);
    readln(textfile, dummyline);
    For i:= 0 to 29 do   {While not eof(a) do}
      Begin
        readln(textfile, setpoint[i]);
      End;
    close(textfile);
  End; {procedure inisieer_beginwaardes}

{-------------------------------------}
Procedure inisieer_nulwaardes(var massas : Tmassas;
        var skaaltempo : Tskaaltempo; var error : Terror;
        var UitVolt: TUitVolt; var seccount: double; var
                                          accum : Taccum);
{Set initial values of 0 to some variables}
  Var
    i : integer;
  Begin
    FillChar(massas, sizeof(massas), 0);
    FillChar(skaaltempo, sizeof(skaaltempo), 0);
    FillChar(error, sizeof(error), 0);
    FillChar(Reac_Mass, sizeof(Reac_Mass), 0);
    FillChar(UitVolt, sizeof(UitVolt), 0);
    FillChar(accum, sizeof(accum), 0);

    Qlosses := 0.0;
    H_in := 0.0;
    Qjacket := 0.0;
    Qcond := 0.0;
    SecCount := 0.0;
    Sample_Mass := 0.0;
    Energy_Accum := 0.0;
    Qreac := 0.0;
    CumQreac := 0.0;
  End; {procedure inisieer_nulwaardes}
```

```
Procedure inisieer_uitskryfleer(var uit : text);
{Initializes output file}
  Begin
    assign(uit, 'plascon.txt');
     rewrite(uit);
          write(uit, 'Time':13, 'Tcore':13, 'Tshell':13,
     'Tcat.':13, 'Treac':13,'Tvap':13, 'dTjack':13,
     'Tjackin':13, 'dTcond':13, 'Tsur':13,'Flowjac':13,
     'Flowcon':13, 'Torq':13, 'PH':13,
     'Mcore':13,'Mshell':13, 'Mcat.':13, 'M_Jack':13,
     'M_Cond':13,'CpJackIn':13, 'CpJackOut':13,
     'H_in':13, 'Qjacket':13,'Qcond':13, 'Qloss':13,
     'ReacMass':13, 'Energy_Accum':13,'Qreac':13,
     'CumQreac':13);
    writeln(uit);
  End; {procedure inisieer_uitskryfleer}

{--------------------------------------}
Procedure de_inisieer_uitskryfleer(var uit : text);
  Begin
    close(uit);
  End; {procedure de_inisieer_uitskryfleer}

{--------------------------------------}
Procedure volt_in(bh301, bh302 : integer; var involt :
Tinvolt);
const
  NumSamples = 30;

{Input voltages from first PC 30}
  Var
    suminvolt : array[0..15] of double;
    i, j, t : integer;
    bin : word;
    uvolts : longint;
  Begin
    FillChar(suminvolt, sizeof(suminvolt), 0);

    for j := 0 to (NumSamples - 1) do
    Begin
       {Lees eerste kaart}
       for i := 0 to 15 do {16 kanale}
       Begin
         t:= EDR_ADInBinOneSample(bh301, i, bin);
      if t < 0 then printerror(t);
      t:= EDR_ADInBinToVoltage(bh301, i, uvolts, bin);
         suminvolt[i]:= suminvolt[i] + uvolts/1000000;
       End; {for i}
    End; {for j}
```

```
    for i := 0 to 15 do
      Begin
        involt[i] := suminvolt[i] / NumSamples;
      End; {for i}

    {Input voltages from second PC 30}
    for i := 0 to 15 do {16 kanale}
    Begin
      t:= EDR_ADInBinOneSample(bh302, i, bin);
      if t < 0 then printerror(t);
      t:= EDR_ADInBinToVoltage(bh302, i, uvolts, bin);
      involt[i+16]:= uvolts/1000000;
    End; {for}
  End; {procedure volt_in}

{--------------------------------------}
Procedure volt_uit(bh66 : integer; uitvolt : Tuitvolt);
{skryf analoog waardes na PC66 se uittreepoorte}
  Var
    i : integer;
    v : longint;
    t : integer;
  Begin
    For i := 0 to 11 do
      Begin
        v := trunc(uitvolt[i]*500000);
        t := EDR_DAOutVoltage(bh66,i,v);
      End;
  End; {procedure volt_uit}

{--------------------------------------}
Procedure digitaal_in(bh301 : integer; var da, db, dc :
Td);
{Read the 3 digital ports of bh301, store in 3 arrays,
(0..7)}
  Var
    i, t : integer;
  Begin
    for i := 0 to 7 do
      Begin
        t:= EDR_DIOLineInput(bh301, 0, i, da[i]);
        t:= EDR_DIOLineInput(bh301, 1, i, db[i]);
        t:= EDR_DIOLineInput(bh301, 2, i, dc[i]);
      End; {for i}
  End; {procedure digitaal_in}
```

```
Procedure digitaal_uit(bh301 : integer; var da, db : Td);
{skryf die waardes van die 3 digitale arrays na die 3
digit-poorte op pc301}
  Var
    i, t : integer;
  Begin
    for i:= 0 to 7 do
      Begin
        t:= EDR_DIOLineOutput(bh301, 0, i, da[i]);
        t:= EDR_DIOLineOutput(bh301, 1, i, db[i]);
      End; {for i}
  End; {procedure digitaal_uit}

{--------------------------------------}
Procedure skale_in(seriepoort : byte; bh301 : integer;
var massas : Tmassas);
{Obtain readings from balances}
  Procedure skale_in_multiplex(bh301 : integer; i :
integer);
    Var
      j : integer;
      da, db : Td;
    Begin
      for j:= 0 to 2 do
        Begin
          da[j]:= 0;
        End; {for j}
      da[i]:= 1;
      digitaal_uit(bh301, da, db);
    End; {sub-procedure skale_in_multiplex}
  {------------------}
  Var
    i : integer;
    tempmassas : array[0..2] of double;
  Begin
    FillChar(tempmassas, sizeof(tempmassas), 0);
    for i:= 0 to 2 do
      Begin
        skale_in_multiplex(bh301, i);
        getbalancereading(seriepoort, tempmassas[i])
{weeg unit}
      End; {for i}
    for i:= 0 to 2 do
      Begin
        massas[i]:= tempmassas[i];
      End; {for i}

  End; {procedure skale_in}
```

```
Procedure volt_na_si(var si_eenhede : Tsi_eenhede; involt
: Tinvolt; afset : Tafset; skaal : Tskaal);
{Voltages are transformed to Engineering units}
  Var
    i : integer;
  Begin
    for i := 0 to 31 do
      Begin
        si_eenhede[i] := (involt[i]-afset[i]) * skaal[i];
      End; {for i}
  End; {procedure skalleer}

{--------------------------------------}
Function tyd_verby(n : longint) : string;
{Calculate elapsed time}
  Var
    rh, rm, rs : double;
    ih, im, is : longint;
    sh, sm, ss : string;
    time : string;
  Begin
    rh:= n / 3600;
    ih:= trunc(rh);
    rm:= frac(rh) * 60;
    im:= trunc(rm);
    rs:= frac(rm) * 60;
    is:= trunc(rs);

    str(ih:2, sh);
    str(im:2, sm);
    str(is:2, ss);
    time:= sh + ' h ' + sm + ' min ' + ss + ' sec.';
    tyd_verby:= time;
  End; {function tyd_verby}

{--------------------------------------}
Procedure skerm_afvoer(si_eenhede : Tsi_eenhede; uitvolt
: Tuitvolt; skaaltempo : Tskaaltempo; massas : Tmassas;
seccount : double);
{Screen output}
  Var
    i : integer;
    h, m, s, hs: word;
  Begin
    textcolor(14);     {geel}
    textbackground(1); {blou}
    clrscr;
    textbackground(12); {rooi}
    gotoxy(29,1);
    writeln('Reactor Control Program.');
    textbackground(1);
```

```
textcolor(15);
writeln('TIME ELAPSED :',tyd_verby(Round(seccount)),'
                  - ',Round(seccount),' seconds.');
gettime(h, m, s, hs);
writeln('TIME         : ', h, ':', m, ':', s, '.',
                                                  hs);
textcolor(14);
gotoxy(1,3);
write('SI-EENHEDE:':25);
gotoxy(26,3);
write('SI-EENHEDE:':25);
gotoxy(51,3);
write('UITVOLTE:':25);
textcolor(15);
textbackground(1);
for i:= 0 to 6 do
  Begin
    gotoxy(51,i+4);
    write(i:16, uitvolt[i]:9:4);
  End; {for i}
for i:= 0 to 8 do
  Begin
    gotoxy(1,i+4);
    write(i:16, si_eenhede[i]:9:2);
  End; {for i}
for i:= 9 to 14 do
  Begin
    gotoxy(26,i-5);
    write(i:16, si_eenhede[i]:9:3);
  End; {for i}
gotoxy(1,13);
textcolor(14);
writeln('Skale se waardes:');
textcolor(15);
write(massas[0]:23:2,'g':2);
write(massas[1]:23:2,'g':2);
writeln(massas[2]:23:2,'g':2);

gotoxy(1,16);
textcolor(14);
writeln('Massavloeitempos:');
textcolor(15);
for i:= 0 to 2 do
  Begin
    write(skaaltempo[i]:21:3,'g/s':4);
  End; {for i}
```

```
    textcolor(14);
    gotoxy(1,19);
    write('E_Dosing:':10);
    gotoxy(15,19);
    write('E_Jacket:':10);
    gotoxy(30,19);
    write('E_Cond:':10);
    gotoxy(45,19);
    write('Qlosses:':10);
    gotoxy(60,19);
    write('Qreac:':10);

    textcolor(15);
    gotoxy(1,20);
    write(H_in:7:4);
    gotoxy(15,20);
    write(Qjacket:7:4);
    gotoxy(30,20);
    write(Qcond:7:4);
    gotoxy(45,20);
    write(Qlosses:7:4);
    gotoxy(60,20);
    write(Qreac:7:4);

    textcolor(14);
    gotoxy(1,22);
    write('Cumulative Heat of Reaction:':30);

    textcolor(15);
    gotoxy(1,55);
    write(CumQreac:7:4);
  End; {procedure skerm_afvoer}

{--------------------------------------}
Procedure leer_afvoer(var out : text; seccount : double;
si_eenhede : Tsi_eenhede; massas : Tmassas; skaaltempo :
Tskaaltempo);
  Begin
    write(out, seccount:13:0, si_eenhede[0]:13:3,
si_eenhede[1]:13:3,si_eenhede[2]:13:3,si_eenhede[3]:13:3,
si_eenhede[6]:13:3,si_eenhede[7]:13:3,si_eenhede[8]:13:3,
si_eenhede[9]:13:3,si_eenhede[10]:13:3,
si_eenhede[11]:13:3, si_eenhede[12]:13:3,
si_eenhede[13]:13:3, si_eenhede[14]:13:3, massas[0]:13:2,
massas[1]:13:2, massas[2]:13:2,M_Jacket:13:3,M_Cond:13:3,
Cp_JacketIn:13:3, Cp_JacketOut:13:3, H_in:13:4,
Qjacket:13:3,Qcond:13:3, Qlosses:13:3, Reac_Mass:13:2,
Energy_Accum:13:3,Qreac:13:3, CumQreac:13:3);
    writeln(out);
  End; {procedure leer_afvoer}
```

```
function sekond_einde: Double;
{Wait for the start of a new second}
  Var
    h, m, s, hs : word;
    EvenSecond: Boolean;
    Now: Double;
  Begin
    repeat
      gettime(h, m, s, hs);

      if hs > 15 then
        repeat
          gettime(h, m, s, hs);
        until (hs < 15)
    until not Odd(s);

    Now := 3600.0*h + 60.0*m + s + 0.01*hs;

    sekond_einde := Now - StartTime;
  End; {function sekond_einde}

{--------------------------------------}
procedure Synchronise;
{Wait for the end of an even second second: set
StartTime}
  Var
    h, m, s, hs : word;
    EvenSecond: Boolean;
  Begin
    repeat
      gettime(h, m, s, hs);

      if hs > 15 then
        repeat
          gettime(h, m, s, hs);
        until (hs < 15)
    until not Odd(s);

    StartTime := 3600.0*h + 60.0*m + s + 0.01*hs;
  End; {function sekond_einde}
```

```
procedure SynchroniseSec;
{Wait for the end of a second}
  Var
    h, m, s, hs : word;

  Begin
    gettime(h, m, s, hs);

    if hs > 15 then
    repeat
      gettime(h, m, s, hs);
    until (hs < 15);
  End; {procedure SynchroniseSec}

{--------------------------------------}
procedure Synchronise2Sec;
{wait for the end of an even second}
  Var
    h, m, s, hs : word;
    EvenSecond: Boolean;
  Begin
    repeat
      gettime(h, m, s, hs);

      if hs > 15 then
        repeat
          gettime(h, m, s, hs);
        until (hs < 15)
    until not Odd(s);
  End; {function sekond_einde}

{--------------------------------------}
Procedure volt_beperk(var uitvolt : Tuitvolt);
  Var
    i : integer;
  Begin
    for i:= 0 to 11 do
      Begin
        if uitvolt[i] > 10.0 then uitvolt[i]:= 10.0;
        if uitvolt[i] < 0.0 then uitvolt[i]:= 0.0;
      End; {for i}
  End;
```

```
{--------------------------------------}
{BEHEERROETINES VAN HIER AF TOT VOOR HOOFPROGRAM SE
BEGIN}
{--------------------------------------}
Procedure beheer_roerspoed(setpoint : Tsetpoint; var
uitvolt : Tuitvolt);
{beheer roerspoed van die roerder}
  Begin
    uitvolt[0]:= (0.0055 * setpoint[1]) - 0.001;
  End; {procedure beheer_roerspoed}

{--------------------------------------}
Procedure beheer_mantelvloeitempo(setpoint : Tsetpoint;
si_eenhede : Tsi_eenhede; var uitvolt : Tuitvolt; var
error : Terror);
{Control jacket flowrate}
  Const
    K = 3.25;
    tau_int = 10;
    tau_der = 0.02;
    dt = 2;

  Var
    jacket_error : double;
    PID : double;

  Begin
    jacket_error := setpoint[2] - si_eenhede[11];

    error[0,0] := error[0,1];
    error[0,1] := error[0,2];
    error[0,2] := jacket_error;

    PID := K*((error[0,2] - error[0,1]) +
              (dt/(2*tau_int))*(error[0,2] + error[0,1]) +
  (tau_der/dt)*(error[0,2] - 2*error[0,1] + error[0,0]));

    Uitvolt[1] := Uitvolt[1] + PID;
  End; {procedure beheer_mantelvloeitempo}

{--------------------------------------}
Procedure beheer_reaktemp(setpoint : Tsetpoint;
si_eenhede : Tsi_eenhede; var uitvolt : Tuitvolt; var
error : Terror);
{Control Reactor temperature}
  Const
    K = 0.0125;
    tau_int = 48;
    tau_der = 0.0165;
    dt = 2;
```

```
  Var
    reac_error : double;
    PID : double;

  Begin
    reac_error := setpoint[0] - si_eenhede[3];

    error[1,0] := error[1,1];
    error[1,1] := error[1,2];
    error[1,2] := reac_error;

    PID := K*((error[1,2] - error[1,1]) +
            (dt/(2*tau_int))*(error[1,2] + error[1,1]) +
  (tau_der/dt)*(error[1,2] - 2*error[1,1] + error[1,0]));

    if (si_eenhede[8] < (setpoint[0]-10) ) and (PID<0)
  then
      Begin
        PID:=0.0005;
      End; {if si_eenhede}

    if (si_eenhede[8] > (setpoint[0]+4.5) ) and (PID>0)
  then
      Begin
        PID:=-0.0003;
      End; {if si_eenhede}

    Uitvolt[2] := Uitvolt[2] + PID;
    Uitvolt[3] := 10 - Uitvolt[2];
  End; {procedure beheer_reaktemp}

{--------------------------------------}
Procedure beheer_opwarming(bh301, bh302, bh66 : integer;
setpoint : Tsetpoint;si_eenhede : Tsi_eenhede; afset :
Tafset; skaal : Tskaal;involt : Tinvolt; var uitvolt :
Tuitvolt;massas : Tmassas; skaaltempo : Tskaaltempo;
seccount : double;var error : Terror);
{Reactor Warm-up}
  Const
    afsny = 0.9999; {growwe beheer}

  Var
    i, count : integer;

  Begin
    volt_in(bh301, bh302, involt);
    volt_na_si(si_eenhede, involt, afset, skaal);
    beheer_roerspoed(setpoint, uitvolt);     {stirrer}
    uitvolt[1]:= setpoint[8];                {Valve1 }
    for i:= 4 to 7 do uitvolt[i]:= 0;        {zero}
```

```
      while si_eenhede[3] < (setpoint[0] * afsny) do
{Warm-up: First Phase}
      Begin
        volt_in(bh301, bh302, involt);
        volt_na_si(si_eenhede, involt, afset, skaal);
        beheer_roerspoed(setpoint, uitvolt); {stirrer}
        uitvolt[1]:= setpoint[8];   {Warm water valve}
        uitvolt[2]:= 9.3;           {Cold water valve}
        uitvolt[3]:= 10 - uitvolt[2];
        volt_beperk(uitvolt);
        volt_uit(bh66, uitvolt);
        skerm_afvoer(si_eenhede, uitvolt, skaaltempo,
        massas, seccount);

        SynchroniseSec;
      End;

    count:=1;
    Uitvolt[1] := 2.05;
    Uitvolt[2] := 7.88;
    Uitvolt[3] := 2.12;

    repeat
{Warm-up: Second Phase }
      Synchronise2Sec;
      volt_in(bh301, bh302, involt);
      volt_na_si(si_eenhede, involt, afset, skaal);
      beheer_roerspoed(setpoint, uitvolt);     {stirrer}

     {Control flowrate through jacket}
      beheer_mantelvloeitempo(setpoint, si_eenhede,
      uitvolt, error);


     {Control Reactor temperature}
      beheer_reaktemp(setpoint, si_eenhede, uitvolt,
      error);

      volt_beperk(uitvolt);
      volt_uit(bh66, uitvolt);
      skerm_afvoer(si_eenhede, uitvolt, skaaltempo,
      massas, seccount);

      inc(count, 2);
    until (si_eenhede[3] >= setpoint[0]-1.0) and
                    (si_eenhede[3] <= setpoint[0]+1.0)
                                    and (count>=1500);
  End; {procedure beheer_opwarming}
```

```
Procedure beheer_toevoertempo(setpoint : Tsetpoint;
massas : Tmassas;var skaaltempo : Tskaaltempo; var
uitvolt : Tuitvolt; seccountd : double;
var massacount : longint; var error : Terror);
{Control dosing rates of reactants and catalysts}
  Const
    K = 1.75;
    tau_int = 75;
    tau_der = 0.02;
    dt = 10;
  Var
    dosing_error : double;
    PID : double;
    seccount : longint;

  Begin
    seccount := Round(seccountd);
    if seccount = setpoint[16] then uitvolt[4]:=
                                          setpoint[3];
    if seccount = setpoint[17] then
      Begin
        uitvolt[4]:= 0;
        skaaltempo[0]:=0;
      End;{if seccount}
    if seccount = setpoint[18] then uitvolt[5]:=
                                          setpoint[4];
    if seccount = setpoint[19] then
      Begin
        uitvolt[5]:= 0;
        skaaltempo[1]:=0;
      End;{if seccount}
    if seccount = setpoint[20] then uitvolt[6]:=
                                          setpoint[5];
    if seccount = setpoint[21] then
      Begin
        uitvolt[6]:= 0;
        skaaltempo[2]:=0;
      End;{if seccount}
    if seccount = setpoint[22] then
      Begin
        uitvolt[6]:= setpoint[6];
        StartMass := massas[2];
      End;{if seccount}
    if seccount = setpoint[23] then
      Begin
        uitvolt[6]:= 0;
        skaaltempo[2]:=0;
      End;{if seccount}
```

```
    if massacount=2 then
      Begin
        {pomp 1}
        if (seccount > setpoint[16]) and (seccount <
                                          setpoint[17])
         then
           Begin
            {Balances reset when initialized}
            skaaltempo[0]:= (0 - massas[0]) / (seccount -
                                        setpoint[16]);
            dosing_error := setpoint[11] - skaaltempo[0];
            error[2,0] := error[2,1];
            error[2,1] := error[2,2];
            error[2,2] := dosing_error;
            PID := K*((error[2,2] - error[2,1]) +
(dt/(2*tau_int))*(error[2,2] + error[2,1]) +
(tau_der/dt)*(error[2,2] - 2*error[2,1] + error[2,0]));

            uitvolt[4]:= uitvolt[4] + PID;
          End; {if seccount}

        {pomp 2}
        if (seccount > setpoint[18]) and (seccount <
                                        setpoint[19])
         then
          Begin
            {skaal gereset op aanvang van eksperiment}
            skaaltempo[1]:= (0 - massas[1]) / (seccount -
                                        setpoint[18]);
            dosing_error := setpoint[12] - skaaltempo[1];
            error[3,0] := error[3,1];
            error[3,1] := error[3,2];
            error[3,2] := dosing_error;
            PID := K*((error[3,2] - error[3,1]) +
(dt/(2*tau_int))*(error[3,2] + error[3,1]) +
(tau_der/dt)*(error[3,2] - 2*error[3,1] + error[3,0]));

            uitvolt[5]:= uitvolt[5] + PID;
          End; {if seccount}

        {pompt 3a}
        if (seccount > setpoint[20]) and (seccount <
                                        setpoint[21])
        then
          Begin
            {skaal gereset op aanvang van eksperiment}
            skaaltempo[2]:= (0 - massas[2]) / (seccount -
                                        setpoint[20]);
```

```
            dosing_error := setpoint[13] - skaaltempo[2];
            error[4,0] := error[4,1];
            error[4,1] := error[4,2];
            error[4,2] := dosing_error;
            PID := K*((error[4,2] - error[4,1]) +
(dt/(2*tau_int))*(error[4,2] + error[4,1]) +
(tau_der/dt)*(error[4,2] - 2*error[4,1] + error[4,0]));

            uitvolt[6]:= uitvolt[6] + PID;
          End; {if seccount}

        {pompt 3b}
        if (seccount > setpoint[22]) and (seccount <
                                        setpoint[23])
        then
          Begin
            {skaal gereset op aanvang van eksperiment}
            skaaltempo[2]:= (StartMass-massas[2]) /
                                (seccount-setpoint[22]);
            dosing_error := setpoint[14] - skaaltempo[2];
            error[5,0] := error[5,1];
            error[5,1] := error[5,2];
            error[5,2] := dosing_error;
            PID := K*((error[5,2] - error[5,1]) +
(dt/(2*tau_int))*(error[5,2] + error[5,1]) +
(tau_der/dt)*(error[5,2] - 2*error[5,1] + error[5,0]));
            uitvolt[6]:= uitvolt[6] + PID;
          End; {if seccount}
        massacount:= 0;
      End; {if massacount}
  End; {procedure beheer_toevoertempo}

{-------------------------------------}
Procedure beheer_posttreatment(bh301, bh302, bh66 :
integer;setpoint : Tsetpoint; var si_eenhede :
Tsi_eenhede; involt : Tinvolt;var uitvolt : Tuitvolt;
afset : Tafset; skaal : Tskaal; massas : Tmassas;
skaaltempo : Tskaaltempo; seccount : double; var error :
Terror);
{Reactor Control at post treatment}
  Var
    postcount : longint;
  Begin
    postcount:=0;
    repeat
      volt_in(bh301, bh302, involt);
      volt_na_si(si_eenhede, involt, afset, skaal);

      beheer_mantelvloeitempo(setpoint, si_eenhede,
                                  uitvolt, error);
      beheer_reaktemp(setpoint, si_eenhede, uitvolt,
```

```
                                                    error);
      beheer_roerspoed(setpoint, uitvolt);

      volt_beperk(uitvolt);
      volt_uit(bh66, uitvolt);
      skerm_afvoer(si_eenhede, uitvolt, skaaltempo,
                                   massas, seccount);

      inc(postcount);
      SynchroniseSec;
    until postcount = setpoint[26];

    repeat
      volt_in(bh301, bh302, involt);
      volt_na_si(si_eenhede, involt, afset, skaal);

      beheer_mantelvloeitempo(setpoint, si_eenhede,
                                    uitvolt, error);
      uitvolt[2]:= uitvolt[2] - 0.005;
      uitvolt[3]:= 10 - uitvolt[2];

      volt_beperk(uitvolt);
      volt_uit(bh66, uitvolt);
      skerm_afvoer(si_eenhede, uitvolt, skaaltempo,
                                  massas, seccount);

      SynchroniseSec;
    until si_eenhede[3] <= setpoint[29];
  End; {procedure beheer_posttreatment}

{-------------------------------------}
Procedure Energy_Calculations(skaaltempo : Tskaaltempo;
si_eenhede : Tsi_eenhede; massas : Tmassas; setpoint :
Tsetpoint;SecCount: Double; var accum : Taccum);
{Basic calculations for Calorimetry}
  Const
    Cp_St    = 1.705;                  {Cp values in
units of (kJ/kg.K)}
    Cp_MMA   = 1.900;
    Cp_BA    = 1.925;
    Cp_EGdMA = 1.900;
    Cp_MA    = 2.100;
    Cp_cat   = 4.190;
    Cp_Cond  = 4.187;
    x_St     = 0.05255;       {x = mass fraction in Core}
    x_MMA    = 0.04807;
    x_BA     = 0.01811;
    x_EGdMA  = 0.00755;
    x_MA     = 0.00389;
    y_MMA    = 0.10978;      {y = mass fraction in Shell}
    y_BA     = 0.20610;
```

```
    y_MA      = 0.00955;
    T_ref     = 25;
    z_water   = 0.95;
    z_EG      = 0.05;
    initial_mass = 2099;        {initial reactor mass [g]}
    EpsA      = 0.020365;
    sigma     = 0.0000000567;
    hA        = 0.824684;

  Var
    M_Core,
    M_Shell,
    M_Cat,
    Cp_Core,
    Cp_Shell,
    Density_water,
    Density_EG,
    Ejacket_in,
    Ejacket_out,
    Temp_avg        : double;
    Qrad            : Double;
    Qconv           : Double;
    Cp_reac         : Double;

  Begin
    {Energy balance of Monomers}
    M_Core := skaaltempo[0]/1000;       {Units of (kg/s)}
    M_Shell := skaaltempo[1]/1000;
    M_Cat := skaaltempo[2]/1000;
    Cp_Core := ((x_St*Cp_St) + (x_MMA*Cp_MMA) +
(x_BA*Cp_BA) +(x_EGdMA*Cp_EGdMA) + (X_MA*Cp_MA));
    Cp_Shell := ((y_MMA*Cp_MMA) + (y_BA*Cp_BA) +
(y_MA*Cp_MA));
    H_in := (M_Core*Cp_Core*(si_eenhede[0]-T_ref) +
M_Shell*Cp_Shell*(si_eenhede[1]-T_ref) +
M_Cat*Cp_Cat*(si_eenhede[2]-T_ref));

    {Energy balance of Jacket}
    Temp_avg :=
(si_eenhede[8]+(si_eenhede[8]+si_eenhede[7]))/2;
    Density_water :=
(-0.00005*(Temp_avg)*(Temp_avg)*(Temp_avg) +
    0.0071*(Temp_avg)*(Temp_avg) - 0.8278*(Temp_avg) +
                                        1017.2);
    Density_EG :=
(-0.0007*(Temp_avg)*(Temp_avg)*(Temp_avg) +
    0.1519*(Temp_avg)*(Temp_avg) - 11.595*(Temp_avg) +
                                        1383.5);
    M_Jacket :=
(si_eenhede[11]/1000)*((z_water*Density_water) +
(z_EG*Density_EG));
```

```
    Cp_JacketIn :=
(z_water*(0.00000003*(si_eenhede[8])*(si_eenhede[8])*
(si_eenhede[8])+0.000003*(si_eenhede[8])*(si_eenhede[8])
                - 0.0002*(si_eenhede[8]) + 4.1808) +
z_EG*(0.00000003*(si_eenhede[8])*(si_eenhede[8])*
(si_eenhede[8])-0.000004*(si_eenhede[8])*(si_eenhede[8])
                      +0.0045*(si_eenhede[8]) + 2.299));
    Cp_JacketOut := (z_water*(0.00000003*(si_eenhede[8]+
          si_eenhede[7])*(si_eenhede[8]+si_eenhede[7])*
                        (si_eenhede[8]+si_eenhede[7]) +
  0.000003*(si_eenhede[8]+si_eenhede[7])*(si_eenhede[8]+
  si_eenhede[7])- 0.0002*(si_eenhede[8]+si_eenhede[7]) +
4.1808) +
z_EG*(0.00000003*(si_eenhede[8]+si_eenhede[7])*
           (si_eenhede[8]+si_eenhede[7])(si_eenhede[8]+
si_eenhede[7]) - 0.000004*(si_eenhede[8]+si_eenhede[7])*
                        (si_eenhede[8]+si_eenhede[7]) +

0.0045*(si_eenhede[8]+si_eenhede[7]) + 2.299));
    Ejacket_in := M_Jacket*Cp_JacketIn*(si_eenhede[8]-
T_ref);

    Ejacket_Out := M_Jacket*Cp_JacketOut*
                   ((si_eenhede[8]+si_eenhede[7])-T_ref);
    Qjacket := (Ejacket_Out - Ejacket_In);

    {Energy balance of Condensator}
    Temp_avg := 18;
    Density_water :=
           (-0.00005*(Temp_avg)*(Temp_avg)*(Temp_avg) +
                        0.0071*(Temp_avg)*(Temp_avg) -
                          0.8278*(Temp_avg) + 1017.2);
    M_Cond := (si_eenhede[12]/1000)*(Density_water);
    Qcond := M_Cond*Cp_Cond*(si_eenhede[9]);

    {Mass load of the reactor}
    {Check if sample has been taken - 10min intervals}
    {360 --> time from startup to pumping}
    {samples = 10g each}
    if ((Round(SecCount - 360) mod 600) = 0) then
      Sample_Mass := Sample_Mass + 10.0;
    Reac_Mass := (initial_mass + abs(massas[0] +
                               massas[1] + massas[2]) -
       Sample_Mass)/1000; {kg}

    {Heat Capacity Model}
    Cp_reac := -8.6E-5*Round(seccount) -
                        0.00287*si_eenhede[3] + 4.4298;
```

```
    {Energy Accumulation}
    accum[0,0] := accum[0,1];
    accum[0,1] := si_eenhede[3];
{History of Reactor Temperature}
    accum[1,0] := accum[1,1];
    accum[1,1] := Cp_reac;
{History of Heat capacity}
    accum[2,0] := accum[2,1];
    accum[2,1] := Reac_Mass;
{History of Reactor Mass}
    Energy_Accum := accum[2,1]*accum[1,1]*(accum[0,1]-
              accum[0,0])/2 + accum[2,1]*(accum[0,1]-
                   T_ref)*(accum[1,1]-accum[1,0])/2 +
                       (accum[0,1]-T_ref)*accum[1,1]*
                           (accum[2,1]-accum[2,0])/2;

    {Reactor heat losses}
    Qrad :=
EpsA*sigma*((si_eenhede[3]+273)*(si_eenhede[3]+273)*
            (si_eenhede[3]+273)*(si_eenhede[3]+273) -
                                 (si_eenhede[10]+273)*
          (si_eenhede[10]+273)*(si_eenhede[10]+273)*
                               (si_eenhede[10]+273));
    Qconv := hA*(si_eenhede[3] - si_eenhede[10]);
    Qlosses := (Qrad + Qconv)/1000;

    {Heat of Reaction}
    Qreac := Qjacket + Qcond + Qlosses - H_in +
                                    Energy_Accum; {kW}
    if (seccount > setpoint[16]-2) and (seccount <
                                          setpoint[28])
     then
      Begin
       CumQreac := CumQreac + (Qreac*2); {kJ}
{kW to kJ = multiply by dt}
      End; {if seccount}

  End; {Procedure Energy_Calculations}
```

```
{=======================================}
{            MAIN PROGRAM               }
{=======================================}
Var
  bh301, bh302, bh66 : integer;
  seccount : double;
  massacount : longint;
  uit : text;

  massas : Tmassas;
  involt : Tinvolt;
  uitvolt : Tuitvolt;
  da, db, dc : Td;

  si_eenhede : Tsi_eenhede;
  afset : Tafset;
  skaal : Tskaal;
  setpoint : Tsetpoint;

  skaaltempo : Tskaaltempo;
  error      : Terror;
  accum      : Taccum;

BEGIN
  inisieer_hardeware(bh301, bh302, bh66, 2, 19200);
  inisieer_skale(bh301);
  inisieer_beginwaardes(afset, skaal, setpoint);
  inisieer_nulwaardes(massas, skaaltempo, error, uitvolt,
                                        seccount, accum);
  inisieer_uitskryfleer(uit);

  beheer_opwarming(bh301, bh302, bh66, setpoint,
       si_eenhede, afset ,skaal,involt, uitvolt, massas,
                          skaaltempo, seccount, error);

  clrscr;
  seccount:=0.0;
  massacount:=0;
  synchronise;
  Repeat
    waghondpuls(bh301, seccount);
    skale_in(2, bh301, massas);
    volt_in(bh301, bh302, involt);
    volt_na_si(si_eenhede, involt, afset, skaal);
    beheer_mantelvloeitempo(setpoint, si_eenhede,
                                  uitvolt, error);
    beheer_reaktemp(setpoint, si_eenhede, uitvolt,
                                          error);
```

```
    beheer_roerspoed(setpoint, uitvolt);
    beheer_toevoertempo(setpoint, massas, skaaltempo,
              uitvolt, seccount, massacount, error);

    volt_beperk(uitvolt);
    volt_uit(bh66, uitvolt);

    energy_calculations(skaaltempo, si_eenhede, massas,
                        setpoint, SecCount, accum);

    skerm_afvoer(si_eenhede, uitvolt, skaaltempo, massas,
                                                seccount);
    leer_afvoer(uit, seccount, si_eenhede, massas,
                                              skaaltempo);
    inc(massacount);
    seccount := sekond_einde; {synchronize}
  Until (seccount >= setpoint[28]);
  de_inisieer_uitskryfleer(uit);
  beheer_posttreatment(bh301, bh302, bh66, setpoint,
       si_eenhede, involt,uitvolt, afset, skaal, massas,
                          skaaltempo, seccount, error);
  de_inisieer_hardeware(bh301, bh302, bh66);

END.
```

ADDENDUM B

```
{$G+,E-,N+}
unit Weeg;

interface

procedure InitBalance(PortNo:byte;BaudRate:word);
procedure GetBalanceReading(PortNo: byte;var W:double);


implementation

uses Crt;

procedure SendByte(PortNo,C: byte);
var
   Addr    : word;
begin
  if PortNo = 2 then Addr := $2F8 else Addr := $3F8;
  delay(3);
  repeat until ((port[Addr+5] and $20) = $20);
  port[Addr] := C; { Send byte }

end;


procedure InitBalance(PortNo:byte;BaudRate:word);
var
   Addr : word; {serial port addres}
begin
  if PortNo = 2 then Addr := $2F8 else Addr := $3F8;
  port[Addr+3] := $80;  { Select baud registers }
  port[Addr+0] := lo(115200 div BaudRate);  { LSB }
  port[Addr+1] := hi(115200 div BaudRate);  { MSB }

  port[Addr+3] := $03; { 8 bits/char, 1 stop, no parity }
  port[Addr+4] := $00; { No interrupts }
  port[Addr+1] := $00; { Disable interrupts in 8259 }
```

```
SendByte(PortNo,ord('@'));SendByte(PortNo,13);SendByte(Po
rtNo,10);
  SendByte(PortNo,ord('D'));
  SendByte(PortNo,ord(' '));
  SendByte(PortNo,ord('"'));
  SendByte(PortNo,ord('R'));
  SendByte(PortNo,ord('E'));
  SendByte(PortNo,ord('A'));
  SendByte(PortNo,ord('D'));
  SendByte(PortNo,ord('Y'));
  SendByte(PortNo,ord('"'));
  SendByte(PortNo,13);SendByte(PortNo,10);
  SendByte(PortNo,ord('@'));SendByte(PortNo,13);SendByte
                                          (PortNo,10);
end;

procedure GetBalanceReading(PortNo: byte;var W:double);
var
 RxData        : array[0..18] of byte;
 S             : string[20];
 i             : byte;
 TimeOut       : word;
 EndOfPacket   : boolean;
 CRrxed        : boolean;
 Addr          : word;
 Code          : integer;

begin
  i := 0;
  EndOfPacket := false;
  CRrxed := false;

  RxData[0] := port[Addr];  { dummy read }

  {Initialize balance}
  if PortNo = 2 then Addr := $2F8 else Addr := $3F8;
  SendByte(PortNo,ord('S')); {Get reading}
  SendByte(PortNo,ord('I')); {Get reading}
  SendByte(PortNo,13);
  SendByte(PortNo,10);

  repeat
        repeat until ((port[Addr+5] and $01) = $01);
        RxData[i] := port[Addr];
        if CRrxed and (RxData[i] = 10) then
                              EndOfPacket := True;
        if RxData[i]  = 13 then CRrxed := true
           else CRrxed := false;
        inc(i);
  until (i>18) or (EndOfPacket);
```

```
  if EndOfPacket then
  begin
       S := '';

            for i := 3 to 13 do S := S + chr(RxData[i]);
            Val(S,W,Code);


  end;

end;

end.
```

ADDENDUM C

Initial Values for Control of Reactor

Setpoint	Channel	Description	
85	0	Pt100 reactor bottom	[0 C]
250	1	Stirrer	[rpm]
0.045	2	Jacket flowrate	[l/s]
1.810	3	Pumprate1 (Core 0-90 ml/min)	[V]
2.950	4	Pumprate2 (Shell 0-90 ml/min)	[V]
1.410	5	Pumprate3a (Cat:core0-20ml/min)	[V]
2.050	6	Pumprate3b (Cat:Shel0-20ml/min)	[V]
0	7	Pumprate4 ()	[V]
2.50	8	Valve1 (jacket flow control)	[V]
9.00	9	Valve2 (warm water tank)	[V]
1.00	10	Valve3 (cold water tank)	[V]
0.08136	11	Balancerate1 (Core 7ml/min)	[g/s]
0.20340	12	Balancerate2 (Shell 12.39ml/min)	[g/s]
0.009024	13	Balancerate3a(Corecat1.49ml/min)	[g/s]
0.02005	14	Balancerate3b(Shelcat2.60ml/min)	[g/s]
0	15	Balancerate4 ()	[g/s]
360	16	Pumptime1 : Begin (Core)	[s]
7560	17	Pumptime1 : End (Core)	[s]
7562	18	Pumptime2 : Begin (Shell)	[s]
14762	19	Pumptime2 : End (Shell)	[s]
360	20	Pumptime3a : Begin (Cat.Core)	[s]
7560	21	Pumptime3a : End (Cat.Core)	[s]
7562	22	Pumptime3b : Begin (Cat.Shell)	[s]
15662	23	Pumptime3b : End (Cat.Shell)	[s]
0	24	Pumptime4 : Begin ()	[s]
0	25	Pumptime4 : Einde ()	[s]
1800	26	Holding time	[s]
70	27	Post treatment temperature	[0 C]
15668	28	Reaction Time	[s]
50	29	Shutdown temperature	[0 C]

Reactor Calibration Constants

Afset	skaal	Channel	Description	
0.88	28.40909	0	Pt100 (reactant feed 1 :A)	[0 C]
0.88	28.40909	1	Pt100 (reactant feed 2 :B)	[0 C]
0.88	28.40909	2	Pt100 (reactant feed 3 :C)	[0 C]
0.88	28.40909	3	Pt100 (reactor bottom :D)	[0 C]
0.88	28.40909	4	Pt100 (cold water tank :E)	[0 C]
0.88	28.40909	5	Pt100 (warm water tank :F)	[0 C]
0.88	28.40909	6	Pt100 (reactor top :G)	[0 C]
0.2450	1.433	7	dT (jacket : out-in)	[0 C]
0.8873	28.373	8	Pt100 (jacket in :I)	[0 C]
0.2800	0.9539	9	dT (condensator : out-in)	[0 C]
0.8870	28.475	10	Pt100 (ambient temp.)	[0 C]
0.0085	0.0110	11	Flowmeter (jacket :L)	[l/s]
0.0167	0.0040	12	Flowmeter (condensator :M)	[l/s]
-0.091	0.9067	13	Stirrer Torque	[Nm]
0.0	1.0	14	PH meter	[PH]
0.0	1.0	15	Not in Use	
0.0	1.0	16	Not in Use	
0.0049	51.338	17	Calibration Heater : Current	[A]
0.0049	1.6617	18	Calibration Heater : Voltage	[V]

ADDENDUM D

D1 CALIBRATION CURVE OBTAINED FROM DSC

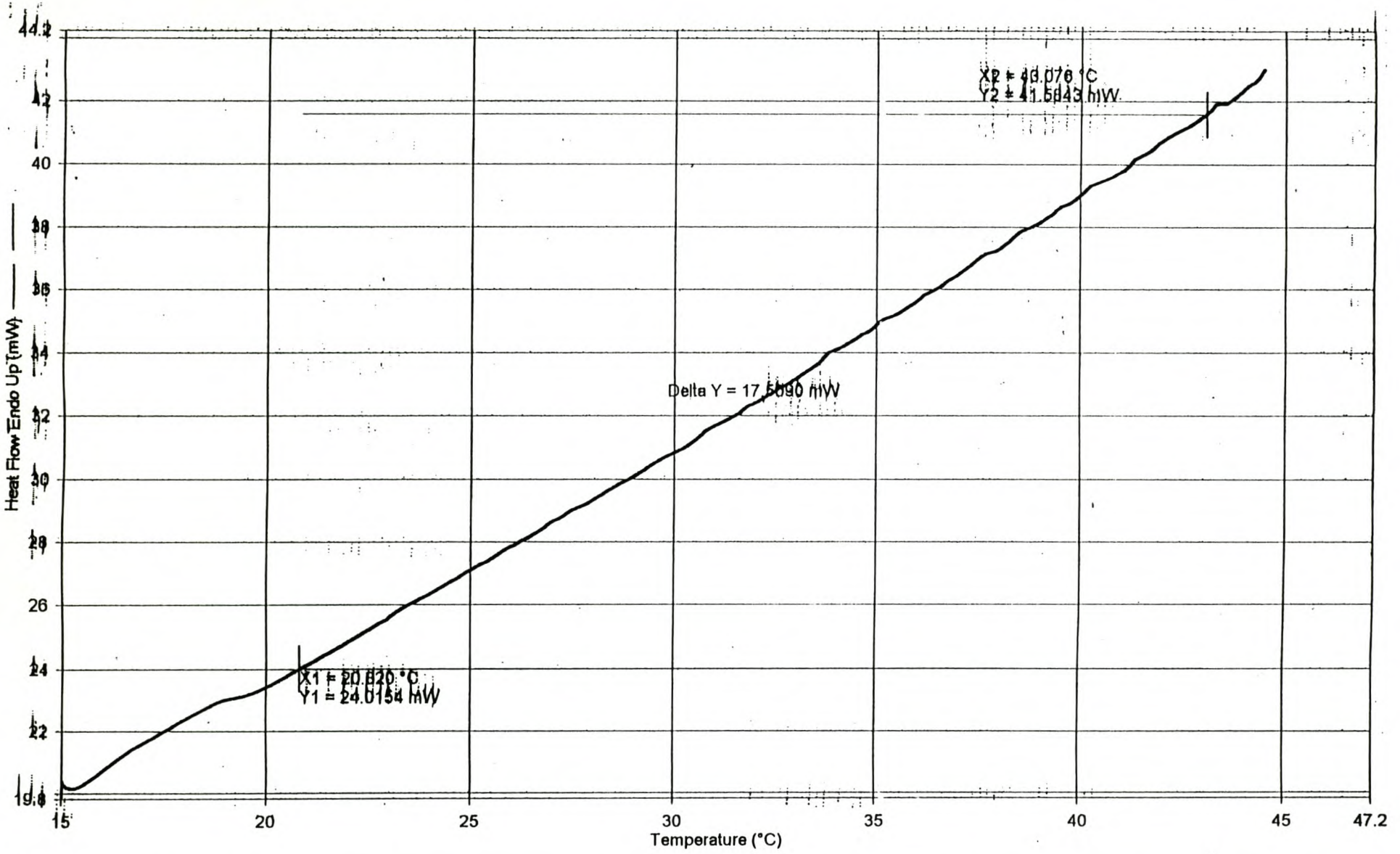

1) Heat from 15.00°C to 45.00°C at 7.00°C/min

99/05/20 04:30:41

D2 SAMPLE CURVE OBTAINED FROM DSC

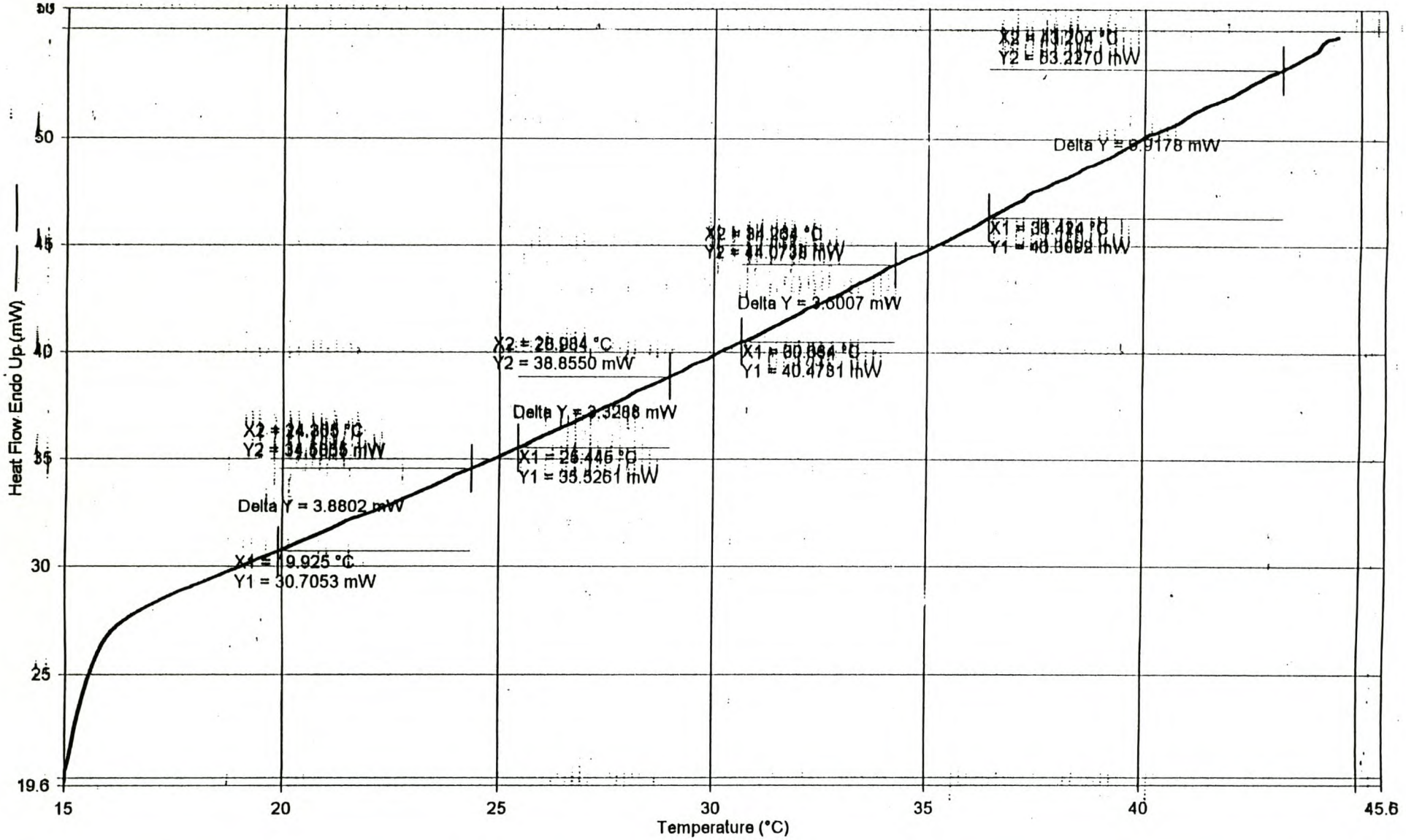

1) Heat from 15.00°C to 45.00°C at 7.00°C/min

99/05/20 04:41:29

D3 HEAT CAPACITY MODEL

TABLE D3-1 *Linear model derived for heat capacity*

	Time (s)	Temp (0C)	Cp (kJ/kg0C)				
Sample	**x1**	**x2**	**y**	**y_est**	**(error)^2**	**abs error**	**% error**
0	0	22.00	4.18	4.37	0.03	0.19	4.44
0	0	32.00	4.18	4.34	0.03	0.16	3.83
0	0	42.00	4.18	4.31	0.02	0.13	3.12
0	0	52.00	4.18	4.28	0.01	0.10	2.36
0	0	62.00	4.19	4.25	0.00	0.06	1.52
0	0	72.00	4.19	4.22	0.00	0.03	0.77
0	0	82.00	4.20	4.19	0.00	0.00	0.11
1	4520	22.67	3.81	3.98	0.03	0.17	4.34
1	4520	27.90	4.34	3.96	0.14	0.38	8.75
2	5970	22.27	3.97	3.85	0.01	0.12	2.98
2	5970	22.96	3.52	3.85	0.11	0.33	9.37
2	5970	25.13	3.73	3.84	0.01	0.11	3.04
2	5970	27.79	4.15	3.84	0.10	0.31	7.57
2	5970	28.20	4.19	3.83	0.13	0.36	8.48
3	7570	22.58	3.75	3.71	0.00	0.04	0.99
3	7570	28.56	3.59	3.70	0.01	0.11	2.95
3	7570	35.07	4.10	3.68	0.18	0.42	10.31
4	8510	22.87	3.63	3.63	0.00	0.00	0.03
4	8510	25.59	4.00	3.62	0.14	0.38	9.41
5	9190	24.60	3.21	3.57	0.13	0.36	11.14
5	9190	30.34	3.34	3.55	0.04	0.21	6.32
5	9190	36.58	3.45	3.53	0.01	0.08	2.42
6	10100	22.96	3.66	3.49	0.03	0.17	4.53
6	10100	28.90	3.27	3.48	0.04	0.21	6.33
7	11100	22.16	3.67	3.41	0.07	0.26	7.08
7	11100	27.90	4.33	3.39	0.88	0.94	21.62
8	11980	22.21	2.93	3.33	0.16	0.40	13.80
8	11980	27.28	3.31	3.32	0.00	0.01	0.29
8	11980	32.14	4.02	3.31	0.51	0.71	17.77
9	12930	22.00	2.82	3.25	0.19	0.43	15.36
9	12930	26.77	2.99	3.24	0.06	0.25	8.34
9	12930	32.01	3.20	3.22	0.00	0.02	0.76
9	12930	38.05	3.13	3.21	0.01	0.08	2.46
10	13720	22.93	2.90	3.18	0.08	0.28	9.74
10	13720	27.13	3.15	3.17	0.00	0.02	0.64
10	13720	30.73	3.27	3.16	0.01	0.11	3.36
11	14660	22.15	2.21	3.10	0.80	0.89	20.44
11	14660	32.56	2.82	3.07	0.06	0.25	9.00
11	14660	39.81	2.86	3.05	0.04	0.19	6.75

D4 MODEL DERIVED FOR HEAT LOSSES

TABLE D4-1 *Experimental data*

Run	Rpm (1/min)	T_r (^{0}C)	Mass (kg)	$T_{ambient}$ (^{0}C)	Q_{losses} (W)
1	250	85.0	4500	28.5	55.2
2	125	85.0	4500	28.6	54.5
3	375	85.0	4500	28.5	54.0
4	250	85.0	4500	23.5	64.7
5	250	87.5	4500	24.6	62.9
6	250	85.0	4500	24.6	59.6
7	250	82.5	4500	24.6	55.8
8	250	85.0	2099	22.5	65.2
9	250	85.0	2099	23.3	62.5
10	250	87.5	2099	24.5	63.4
11	250	82.5	2099	25.3	56.4
12	250	82.5	2099	25.1	56.3
13	250	87.5	2099	24.8	64.4
14	250	85.0	4500	21.6	63.6
15	250	85.0	4500	22.1	61.9
16	250	82.5	4500	23.0	56.0
17	250	85.0	4500	19.1	67.0
18	250	82.5	4500	19.9	60.6
19	250	87.5	4500	21.8	64.2

TABLE D4-2 *Linear model derived for reactor heat losses*

Run	T(amb) (^{0}C) x1	T(reac) (^{0}C) x2	(x2-x1)	sigma* $(x2)^4-(x1)^4$	Q_{loss} (W) y	y_est	$(error)^2$
1	28.5	85.0	56.5	462.83	55.2	56.0	0.67
2	28.6	85.0	56.4	462.21	54.5	55.9	2.03
3	28.5	85.0	56.5	462.83	54.0	56.0	4.50
4	23.5	85.0	61.5	493.15	62.3	60.8	2.37
5	24.6	87.5	62.9	512.90	62.9	62.3	0.34
6	24.6	85.0	60.4	486.61	59.6	59.7	0.01
7	24.6	82.5	57.9	460.86	55.8	57.1	1.78
8	22.5	85.0	62.5	499.03	65.2	61.7	11.95
9	23.3	85.0	61.7	494.33	62.5	60.9	2.40
10	24.5	87.5	63.0	513.49	63.4	62.4	0.98
11	25.3	82.5	57.2	456.66	56.4	56.5	0.01
12	25.1	82.5	57.4	457.87	56.3	56.7	0.13
13	24.8	87.5	62.7	511.70	64.4	62.1	5.16
14	21.6	85.0	63.4	504.27	63.6	62.6	1.09
15	22.1	85.0	62.9	501.36	61.9	62.1	0.03
16	23.0	82.5	59.5	470.35	56.0	58.6	7.01
17	19.1	85.0	65.9	518.58	67.0	64.9	4.38
18	19.9	82.5	62.6	488.30	60.6	61.6	0.94
19	21.8	87.5	65.7	529.40	64.2	65.0	0.58

D5 PILOT PLANT EVALUATION

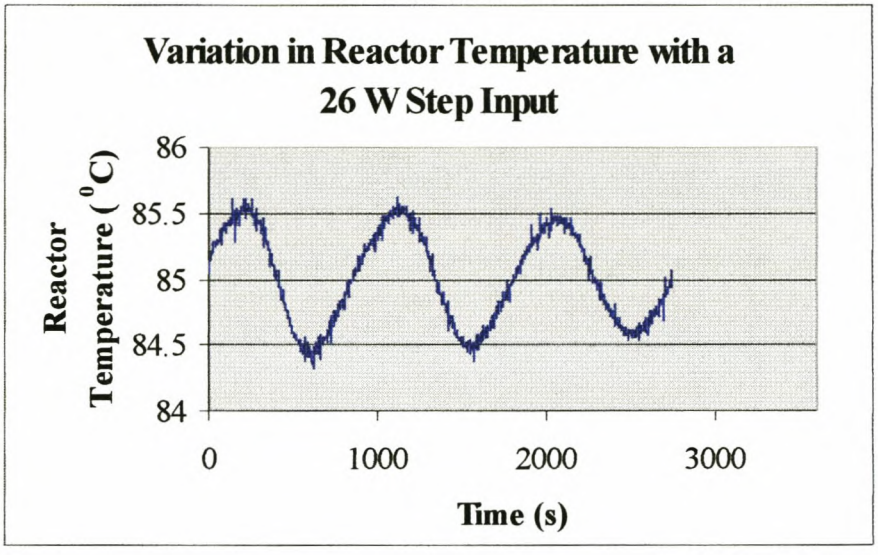

FIGURE D5-1 *Reactor temperature profile (26 W step input)*

ADDENDUM E

RUN 00

SAMPLE	TIME	CONVERSION				PS	SOLIDS	VISCOS
		X (total)	X (monomer)	X (thrcl)	X(trcl) (monomer)			
1	170	0.2028569	0.4368951	0.2879882	0.6202433			1.09
2	360	0.4407211	0.9491857	0.6098635	1.3134695	15.9		
3	590	0.7958176	1.7139607	0.9996166	2.1528847	20.9		
4	858	1.2202803	2.6281304	1.4536203	3.1306774	22		
5	1180	1.7609976	3.7926792	1.9992331	4.3057694	23.9		
6	2020	3.1682896	6.8235787	3.4223862	7.3708291	27		
7	2980	4.8722803	10.493481	5.0488616	10.873786	29		
8	3860	6.3526663	13.681804	6.5397888	14.084812	30.2		
9	5070	8.317639	17.913787	8.5898007	18.499944	31		
10	6220	10.242728	22.059871	10.538151	22.696128	33.4		
11	7520	12.477276	26.872441	12.707131	27.367481	36.2		2.51
12	7810	13.238954	28.512874	14.011109	30.175873	35.4		
13	8070	14.003712	30.159942	15.180265	32.693896	38.3		
14	9270	19.66682	42.356638	20.576184	44.315143	45.5		
15	10440	24.904413	53.636897	25.83728	55.646022	46.5		12.63
16	11820	30.963401	66.686203	32.042551	69.010378	57.2		41.51
17	12930	35.819075	77.143919	37.033794	79.760071	62.5		1098
18	14080	40.956908	88.209324	42.204939	90.897221	64		
19	15030	45.734123	98.498062	46.431495	100	67.3		2533
20	end	46.395738	99.922988	46.431495	100	72.2	46.76	4035
							SG	1.05

RUN 01

SAMPLE	TIME	CONVERSION				PS	SOLIDS	VISCOS
		X (total)	X (monomer)	X (thrcl)	X(trcl) (monomer)			
1	140	0.1908779	0.4094331	0.2596456	0.5569398			1.09
2	760	1.2389164	2.6574753	1.4143853	3.0338561			
3	1580	2.7436026	5.885027	2.9175967	6.2582442			
4	2650	4.705154	10.092554	4.9036578	10.518345	24.9	9.06	
5	4160	7.5080571	16.104781	7.7187628	16.556744	24.5	13.5	
6	5560	10.053622	21.565017	10.294721	22.082173	32.2	17.13	
7	7160	12.973609	27.828389	13.246481	28.413699	34.3	20.97	3.02
8	7410	13.796293	29.593045	14.282786	30.636572	36.4	21.27	
9	8810	19.844085	42.565557	20.757983	44.525868	40.2	27.52	
10	10050	25.746998	55.227304	26.490685	56.822512	49.4	33.27	9.66
11	11370	31.622552	67.830367	32.610577	69.94968	54.8	38.24	30.19
12	12810	38.125761	81.779748	39.265704	84.224926	58.2	42.75	124.7
13	14390	45.432183	97.452021	46.551724	99.853437	64.6	46.5	2938
14	15310	46.24775	99.201413	46.620052	100	61.4	47.61	3367
15	17460	46.407063	99.543138	46.620052	100	65.1	47.83	4038
16	END	46.520081	99.785561	46.620052	100	69.8	47.82	4871
							SG	1.0447

RUN 02

SAMPLE	TIME	CONVERSION				PS	SOLIDS	VISCOS
		X (total)	X (monomer)	X (thrcl)	X(trcl) (monomer)			
1	140	0.0864968	0.1853914	0.2557136	0.5480793			1.09
2	320	0.3986397	0.8544174	0.6438503	1.3799853			
3	490	0.7498171	1.6071073	0.9863239	2.1140201			
4	930	1.5469778	3.3156879	1.7694468	3.7925128		3.95	
5	1460	2.4433468	5.2369046	2.6553118	5.6912161			
6	2360	4.0886827	8.7634065	4.2923354	9.1999021	28.8	8.6	
7	3290	5.9114403	12.670182	6.1371264	13.153903	30.2		
8	4480	8.1973701	17.56969	8.4294162	18.067042	32	15.21	
9	5660	10.281836	22.037393	10.53677	22.583802	33.4		1.88
10	7030	12.663884	27.142915	12.952351	27.761194	37.5	21.42	
11	7470	13.777245	29.529218	14.509464	31.098605	38.4	22.42	
12	8090	16.107034	34.522729	17.381675	37.25471	42.9	24.82	
13	8680	19.029242	40.785992	20.094066	43.068265	48.1	28.4	4.05
14	9560	23.412206	50.180142	24.169502	51.803279	51.3	32.93	7.2
15	10570	28.02648	60.070066	28.879655	61.898703	55.2		14.19
16	11970	34.378244	73.684008	35.391219	75.85515	58.3	41.43	114.4
17	13160	39.830566	85.370148	40.895911	87.653536	63.7		
18	14390	45.599432	97.734745	46.585538	99.848299	70.9	48.09	3933
19	15300	46.299205	99.234591	46.656316	100		49.41	
20	17100					72	49.41	5031
21	END	46.549591	99.771253	46.656316	100	70.4	48.25	5612
							SG	1.041

RUN 03

SAMPLE	TIME	CONVERSION				PS	SOLIDS	VISCOS
		X (total)	X (monomer)	X (thrcl)	X(trcl) (monomer)			
1	120	0.1565668	0.3353101	0.2166575	0.4640031			1.09
2	300	0.4315718	0.9242728	0.5519066	1.1819869			
3	500	0.6589514	1.4112387	0.9327677	1.9976556			
4	930	1.5907674	3.406856	1.7378216	3.7217935		3.69	
5	1490	2.6224919	5.6164416	2.7686554	5.9294715			
6	2340	4.1618424	8.9131809	4.3308703	9.2751783		8.02	
7	3320	5.9589733	12.761994	6.1462324	13.163036	33		
8	4490	8.1247354	17.400283	8.3401752	17.861678	33.6	14.62	
9	5710	10.35365	22.173824	10.604817	22.711732	35.4		1.88
10	7150	12.996682	27.834254	13.266284	28.411644	37	21.54	
11	7450	13.974229	29.927811	14.511494	31.078441	40	22.21	
12	8050	16.053245	34.380322	17.296114	37.042102	43	24.18	
13	8690	19.042935	40.78317	20.244937	43.357429	49.1	27.74	5.37
14	9560	23.451516	50.224776	24.265645	51.96835	51.6	32.74	7.02
15	10750	28.966481	62.035863	29.853129	63.934747	55.2		15.93
16	11920	34.071964	72.969985	35.235359	75.461561	57	40.67	79.83
17	13070	39.339439	84.251037	40.540047	86.822311	62.3		224.1
18	14380	45.979788	98.472293	46.576811	99.750904	66.9	46.89	1766
19	15290	46.205782	98.956292	46.693122	100			2538
20	17100					68.5	48.37	3409
21	END	46.398668	99.369386	46.693122	100	71.9	47.44	4395
							SG	1.0495

RUN 04

SAMPLE	TIME	CONVERSION				PS	SOLIDS	VISCOS
		X (total)	X (monomer)	X (thrcl)	X(trcl) (monomer)			
1	130	0.1583059	0.3385064	0.2445491	0.5229205			1.48
2	390	0.4630969	0.9902425	0.7405037	1.5834229			
3	850	1.3051601	2.7908307	1.5838552	3.3867657			
4	1490	2.4826429	5.3086481	2.7586049	5.8987391		5.56	
5	2300	4.0394351	8.637545	4.2601819	9.109569	28.1	8.56	
6	3270	5.8451751	12.498768	6.0863007	13.014368	26.8	11.57	
7	4440	8.0143465	17.137118	8.2712438	17.686443	31.2	14.83	
8	5670	10.26034	21.939739	10.540751	22.539341	33.7	18.07	
9	7160	12.894221	27.571778	13.285642	28.408758	35	21.48	2.19
10	7380	13.550091	28.97423	14.190703	30.344052	38.6	21.93	
11	8100	16.274355	34.799537	17.545824	37.518327	45.9	24.81	
12	8710	19.257821	41.179098	20.340997	43.49526	47	28.46	
13	9530	23.310496	49.844953	24.137222	51.612746	50.2	32.55	8.58
14	10730	28.727837	61.428883	29.757279	63.630144	53.5	37.13	38.78
15	11950	34.345844	73.441894	35.418476	75.73551	61	41.29	125.1
16	13140	39.753711	85.005565	40.915116	87.489004	66.2	44.36	639.9
17	14380	45.58922	97.483664	46.644878	99.740983	68.1	47.76	3857
18	15270	46.38866	99.193111	46.76601	100	70.2	48.74	3834
19	16680	46.616211	99.679684	46.76601	100	72.1	48.97	3769
20	END	46.688457	99.834169	46.76601	100	73.7	48.22	4284
							SG	1.0487

RUN 05

SAMPLE	TIME	CONVERSION				PS	SOLIDS	VISCOS
		X (total)	X (monomer)	X (thrcl)	X(trcl) (monomer)			
1	140	0.1502461	0.3211852	0.260173	0.556179			1.09
2	460	0.5666074	1.2112521	0.8581144	1.8344148			
3	890	1.3339177	2.8515524	1.6546089	3.537103			
4	1450	2.2601891	4.8316683	2.686172	5.7423038		4.41	
5	2370	3.8801071	8.2946115	4.3978365	9.4013758		7.63	
6	3270	5.4517758	11.654411	6.0707032	12.977509	31.2	10.21	
7	4450	7.4706919	15.970303	8.2661981	17.670879	29.3	13.07	
8	5670	9.614966	20.554177	10.527877	22.505733	37.5	16.06	
9	7150	12.258094	26.204465	13.264258	28.355369	41.9	19.46	2.5
10	7450	12.844165	27.457325	14.51035	31.019174	45.4	19.56	
11	8060	14.122452	30.189954	17.342584	37.073718	52.4	19.76	
12	8670	16.249826	34.737699	20.154278	43.084354	55.2	22.73	
13	9560	21.089557	45.083726	24.266837	51.875884	69.4	28.24	8.9
14	10670	25.656125	54.845804	29.431499	62.916524	74.2	32.41	
15	11780	29.990595	64.11172	34.582468	73.927892	78.5	35.61	29.21
16	13140	37.575493	80.326163	40.892804	87.417671	84.6	41.52	101.6
17	14350	44.813587	95.799236	46.523039	99.453579	88.1	46.77	
18	15260	46.263222	98.898162	46.778648	100	91.4	48.53	499.9
19	16800	46.537969	99.485495	46.778648	100	92.5	48.53	427.9
20	END	46.725111	99.885554	46.778648	100	91	48	687.6
							SG	1.0373

RUN 06

SAMPLE	TIME	CONVERSION	PS	SOLIDS	VISCOS
20	end		71.3	46.16	4257.52
		T_{amb} 17.94 ^{0}C		SG	1.0497

RUN 07

SAMPLE	TIME	CONVERSION				PS	SOLIDS	VISCOS
		X (total)	X (monomer)	X (thrcl)	X(trcl) (monomer)			
1	110	0.1474002	0.3154882	0.2077009	0.444553			1.09
2	610	0.999003	2.1382178	1.1389314	2.4377137			
3	1470	2.5479416	5.4534913	2.7160888	5.8133854			
4	2620	4.6880138	10.033999	4.8638532	10.410357	31.5	9.56	
5	4190	7.59218	16.249936	7.7876429	16.668295	29	13.96	
6	5660	10.257567	21.954801	10.503732	22.481681	34.5	17.8	
7	7160	12.961087	27.741286	13.274599	28.412311	36.1	21.4	2.19
8	7450	13.853056	29.650413	14.50711	31.050318	37.9	21.79	
9	8700	19.343456	41.4018	20.281652	43.409868	45.8	27.76	
10	10130	26.114519	55.894256	26.923516	57.625794	49.7	34.15	9.54
11	11400	31.863298	68.198665	32.830438	70.268686	59	38.71	39.35
12	12800	38.195805	81.752458	39.307968	84.132877	59	42.67	164.45
13	14370	45.742956	97.906016	46.561523	99.658036	70.4	46.67	2102.41
14	15240	46.221016	98.929231	46.721293	100	68.8	47.29	3858.41
15	17460	46.486253	99.496933	46.721293	100	63	47.68	3816.2
16	END	46.591429	99.722045	46.721293	100	70.6	47.02	4403.26
		T_{amb} 17.64 ^{0}C					SG	1.0509

RUN 08

SAMPLE	TIME	CONVERSION				PS	SOLIDS	VISCOS
		X (total)	X (monomer)	X (thrcl)	X(trcl) (monomer)			
1	130	0.1546498	0.3308931	0.2464291	0.5272665			1.09
2	730	1.1645988	2.4918081	1.3599233	2.90973			
3	1440	2.4355059	5.2110765	2.6536759	5.6778792			
4	2640	4.6571678	9.9646066	4.9057637	10.496509	22	9.37	
5	4390	7.8729948	16.84528	8.1526947	17.443734	22.6	14.24	
6	5640	10.106975	21.625167	10.448136	22.355124	31.6	17.55	
7	7180	12.925197	27.655113	13.314015	28.487038	35	21.06	4.48
8	7480	13.842	29.61673	14.639712	31.323537	37.1	21.61	
9	8670	18.859309	40.351905	20.154703	43.123566	44.5	26.94	
10	9980	25.294161	54.120094	26.205905	56.070888	50.2	33.41	13.28
11	11490	32.179403	68.85195	33.233697	71.107748	59.8	38.75	38.44
12	12740	37.765121	80.803311	39.031625	83.513157	65.4	42.49	384.45
13	14430	45.740184	97.866977	46.737097	100	65.3	46.14	1496.62
14	15290	46.190311	98.830082	46.737097	100	65.2	47.07	2313.53
15	17460	46.426641	99.33574	46.737097	100	68.3	47.68	3469.6
16	END	46.561034	99.623291	46.737097	100	70.9	47.31	4546.38
		T_{amb} 18.87 ^{0}C					SG	1.0513

RUN 09

SAMPLE	TIME	CONVERSION				PS	SOLIDS	VISCOS
		X (total)	X (monomer)	X (thrcl)	X(trcl) (monomer)			
1	140	0.1688483	0.3618591	0.2756578	0.5907626			1.09
2	580	0.8311155	1.7811647	1.0866841	2.3288741			
3	1440	2.3196092	4.9711575	2.6403918	5.6586271			
4	2630	4.6240465	9.9097998	4.8889395	10.477492	25	9.02	
5	4170	7.4782747	16.0267	7.7434788	16.595059	30.3	13.48	
6	5620	10.096538	21.637904	10.383871	22.253686	31.7	17.32	
7	7170	12.941413	27.734757	13.268026	28.434723	35.8	20.89	1.88
8	7430	13.749478	29.466524	14.377492	30.812421	35.9	21.31	
9	8760	19.516299	41.825405	20.53309	44.004492	44.9	27.69	
10	10130	25.979124	55.675892	26.857273	57.557856	49.7	33.94	7.8
11	11450	31.882483	68.32739	32.967308	70.65228	56.6	38.62	25.89
12	12830	38.107788	81.668849	39.359836	84.352114	59.3	42.52	85.59
13	14380	44.96132	96.356661	46.547443	99.755883	66	45.75	1930.25
14	15300	46.245536	99.108866	46.661351	100	65.5	47.36	3187.67
15	17460	46.456204	99.56035	46.661351	100	67	47.72	3781.28
16	end	46.538998	99.737786	46.661351	100	70.8	47.48	4502.71
		T_{amb}	18.91 ^{0}C				SG	1.0538

RUN 10

SAMPLE	TIME	CONVERSION				PS	SOLIDS	VISCOS
		X (total)	X (monomer)	X (thrcl)	X(trcl) (monomer)			
1	110	0.1169572	0.2504228	0.2234637	0.4784689			1.09
2	560	0.611343	1.308976	1.0511914	2.2507568			
3	1420	1.9684123	4.2146626	2.5926348	5.5512157			
4	2590	4.3706041	9.3581116	4.8318322	10.345669	29.4	8.46	
5	4150	7.3603729	15.75965	7.7094972	16.507177	33.2	13.1	
6	5610	10.021771	21.458097	10.359138	22.180451	37.1	16.84	
7	7180	12.896068	27.612394	13.30521	28.488429	39.8	20.71	2.19
8	7440	13.700131	29.334012	14.447611	30.934479	40.2	21.31	
9	8790	19.445179	41.635013	20.679512	44.277903	49.3	27.25	
10	10140	25.944462	55.550941	26.929655	57.660385	52.2	33.48	11.21
11	11490	31.962518	68.436491	33.20716	71.101455	60.4	38.07	31.65
12	12800	37.972773	81.305338	39.279444	84.103115	69.3	41.92	63.39
13	14400	45.321595	97.040258	46.676548	99.941412	66.1	46.23	1169.35
14	16260	46.385488	99.31821	46.703911	100	66.3	47.32	2355.76
15	17460	46.473806	99.507313	46.703911	100	70.7	47.4	2334.76
16	end	46.591871	99.760107	46.703911	100	75.1	46.93	4382.73
		T_{amb}	18.72 ^{0}C				SG	1.051

RUN 11

SAMPLE	TIME	CONVERSION				PS	SOLIDS	VISCOS
		X (total)	X (monomer)	X (thrcl)	X(trcl) (monomer)			
1	110	0.0347931	0.0745793	0.2574091	0.5517578			1.09
2	640	0.4388629	0.9407051	1.1913711	2.5537109			
3	1450	0.9851076	2.111584	2.653819	5.6884766			
4	2620	1.8431867	3.9508815	4.8748263	10.449219	507.1	1.65	
5	4180	6.8891196	14.766868	7.7564409	16.625977	41.9	11.65	
6	5620	9.6091659	20.597303	10.380646	22.250977	45.1	16.22	
7	7170	12.671797	27.162071	13.266817	28.4375	48.9	20.17	1.88
8	7460	13.483821	28.902649	14.510581	31.103516	50.3	20.77	
9	8810	18.72795	40.143471	20.763571	44.506836	55.3	26.27	
10	10180	25.477532	54.61124	27.080344	58.046875	62.7	33.15	11.16
11	11540	31.542217	67.610927	33.388004	71.567383	67.6	37.82	21.21
12	12790	37.159719	79.652075	39.192237	84.008789	74.1	41.65	42.29
13	14360	44.692607	95.798864	46.463473	99.594727	79.3	45.58	
14	15270	46.011711	98.626372	46.670767	100.03906	75.5	47.18	776.61
15	17460	46.286393	99.215155	46.670767	100.03906	79	47.51	956.56
16	end	46.480847	99.631968	46.670767	100.03906	76.4	46.94	1441.61
		T_{amb}	20.09 ^{0}C				SG	1.051

RUN 12

SAMPLE	TIME	CONVERSION				PS	SOLIDS	VISCOS
		X (total)	X (monomer)	X (thrcl)	X(trcl) (monomer)			
1	110	0.1263913	0.2707028	0.2120722	0.4542125			1.09
2	590	0.9227442	1.9763175	1.1059677	2.3687424			
3	1440	2.4264725	5.1969768	2.645201	5.6654457			
4	2640	4.6818763	10.027561	4.9073039	10.510379	30.8	9.28	
5	4260	7.6623228	16.41103	7.9150799	16.952381	28.2	13.87	
6	5600	10.072295	21.572666	10.359611	22.188034	32	17.3	
7	7150	12.917956	27.667454	13.241967	28.361416	36.5	21.09	2.19
8	7460	13.785155	29.524807	14.525802	31.111111	37.2	21.72	
9	8820	19.817347	42.44445	20.837799	44.630037	46.8	28.07	
10	10230	26.501987	56.761496	27.339065	58.554335	55.7	34.39	10
11	11590	32.647362	69.923553	33.662463	72.09768	59.6	39.09	56.43
12	12810	38.208562	81.834435	39.320001	84.214896	64.5	42.55	107.32
13	14360	45.244954	96.904859	46.487127	99.565324	68.6	46.5	2818.98
14	15290	46.315778	99.19833	46.690078	100	70.4	47.3	3563.73
15	17460	46.495588	99.583444	46.690078	100	70.4	47.51	3069.61
16	end	46.590459	99.786638	46.690078	100	72.6	47.04	4490.79
		T_{amb}	19.21 ^{0}C				SG	1.047

RUN 13

SAMPLE	TIME	CONVERSION				PS	SOLIDS	VISCOS
		X (total)	X (monomer)	X (thrcl)	X(trcl) (monomer)			
1	100	0.1400594	0.2997593	0.2325369	0.4976824			1.09
2	460	0.8850834	1.8942815	1.1353274	2.4298609			
3	1340	3.0346576	6.4948631	3.3239103	7.1139302		6.31	
4	2610	6.169137	13.203368	6.4335218	13.769212	27.5	11.44	
5	3820	9.1433071	19.568774	9.4473828	20.219566	30.7	15.91	
6	5340	12.863947	27.531797	13.218129	28.289827	38.3	20.66	2.35
7	5660	13.812551	29.562027	14.565475	31.173457	38.4	21.38	
8	6930	19.519547	41.776306	20.433613	43.732618	47.9	27.77	
9	8330	26.072202	55.800491	26.91045	57.594535	49.4	33.87	9.35
10	9650	32.021394	68.533126	33.038483	70.709929	56.7	38.5	28.39
11	11060	38.478551	82.352923	39.572314	84.693828	65.9	42.68	108.07
12	12530	45.066611	96.452882	46.37516	99.253476	68.3	46.27	2223.9
13	13380	46.320646	99.136805	46.723965	100	70.1	47.39	3162.89
14	15300	46.544456	99.61581	46.723965	100	68.6	47.38	2610.92
15	end	46.625593	99.789462	46.723965	100	72.7	47.04	4288.59
		T_{amb}	19.44 ^{0}C				SG	1.048

RUN 14

SAMPLE	TIME	CONVERSION				PS	SOLIDS	VISCOS
		X (total)	X (monomer)	X (thrcl)	X(trcl) (monomer)			
1	90	0.1450612	0.310234	0.3055524	0.6534673			1.09
2	320	0.8348012	1.7853412	1.169764	2.5017068			
3	1040	3.5211757	7.5305355	3.8900924	8.3195162		6.97	
4	1740	6.0786206	12.999995	6.4302816	13.752073	33.7	10.93	
5	2630	9.3392895	19.9734	9.7183901	20.784161	33.3	15.67	
6	3550	12.766473	27.302921	13.195759	28.221008	40.6	20.28	2.19
7	3840	21.995408	47.040311	22.692965	48.532137	39	21.35	
8	5180	19.896238	42.550937	20.688633	44.245587	48	27.36	
9	6700	26.89701	57.523084	27.711777	59.265581	51.8	34.37	12.04
10	7870	32.205477	68.875997	33.156995	70.910953	57	38.37	28.95
11	9200	38.23542	81.771888	39.334169	84.12172	62.1	42.33	101.7
12	10760	45.3502	96.987858	46.551134	99.556227	65	46.39	2984.43
13	11630	46.384599	99.200068	46.758636	100	64.6	47.14	2866.38
14	13500	46.596441	99.653122	46.758636	100	63.6	47.89	3954.68
15	end	46.672382	99.815533	46.758636	100	74.1	46.58	4242.51
		T_{amb}	19.82 ^{0}C				SG	1.05

RUN 15

SAMPLE	TIME	CONVERSION				PS	SOLIDS	VISCOS
		X (total)	X (monomer)	X (thrcl)	X(trcl) (monomer)			
1	120	0.159554	0.3410844	0.2444708	0.522614			1.09
2	570	0.8610973	1.8407985	1.0692744	2.2858259			
3	1420	2.3802142	5.0882689	2.6023579	5.5631533			
4	2600	4.4380477	9.4873729	4.8642844	10.398554	27.8	9.12	
5	4170	7.5186142	16.07281	7.7568086	16.582006	28.3	13.58	
6	5600	10.075666	21.539111	10.356882	22.140275	30.9	17.14	
7	7100	12.880072	27.534189	13.192287	28.201622	35.9	20.72	2.19
8	7500	14.17622	30.305012	15.216597	32.529061	38.3	21.56	
9	8500	19.990692	42.734815	21.424328	45.799551	50	27.8	
10	9500	26.511085	56.673692	27.570371	58.938165	54.4	33.76	11.87
11	10460	32.506478	69.490257	33.513069	71.642083	56.9	38.32	23.65
12	11510	38.70757	82.746552	40.036099	85.586598	64.2	42.58	92.7
13	12600	45.397735	97.048356	46.748766	99.936505	64.2	45.84	2088.05
14	13500	46.361705	99.10907	46.778468	100	69.9	47.21	2646.79
15	end	46.673745	99.776129	46.778468	100	76.9	46.72	3841.81
		T_{amb}	16.10 ^{0}C				SG	1.047

RUN 16

SAMPLE	TIME	CONVERSION				PS	SOLIDS	VISCOS
		X (total)	X (monomer)	X (thrcl)	X(trcl) (monomer)			
1	110	0.1906266	0.4071772	0.3859329	0.82435			1.09
2	350	0.9633027	2.0576081	1.2902489	2.7559631			
3	1060	3.8008768	8.1186476	4.1424983	8.8483489			
4	1760	6.1817203	13.204113	6.5197534	13.92615	34.8	10.91	
5	2590	9.2052878	19.662434	9.6003654	20.506317	34.5	15.45	
6	3520	12.651117	27.022703	13.089747	27.959612	38.4	19.74	2.19
7	3850	14.07811	30.070749	14.91208	31.852105	39.2	21.06	
8	4900	20.371972	43.514397	21.431834	45.778255	50.5	27.67	
9	5990	27.124207	57.937126	28.138844	60.104385	55.9	33.76	9.5
10	6950	32.82126	70.105994	34.005481	72.635481	60.4	38.43	26.81
11	7930	38.893616	83.076506	40.105047	85.664114	63.9	42.12	67.89
12	8920	45.001856	96.123666	46.28454	98.86347	71.4	45.57	1201.07
13	9720	46.38081	99.069102	46.816625	100	70.1	46.81	2598.8
14	11700	46.609675	99.557957	46.816625	100	70.4	47.34	2769.42
15	end	46.716236	99.78557	46.816625	100	74	46.28	2672.6
		T_{amb}	16.72 ^{0}C				SG	1.047

ADDENDUM F

F1 EFFECT OF STIRRING SPEED

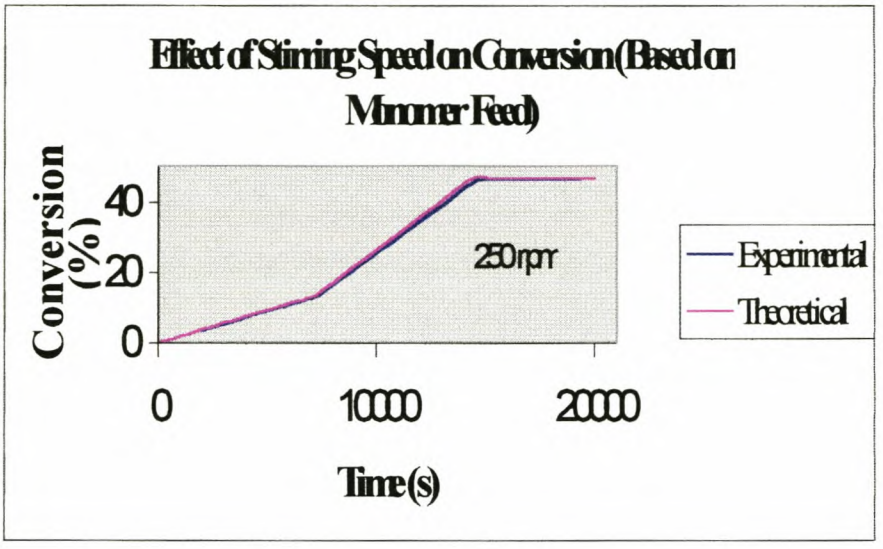

FIGURE F1-1 *Effect of stirring speed on conversion (250 rpm)*

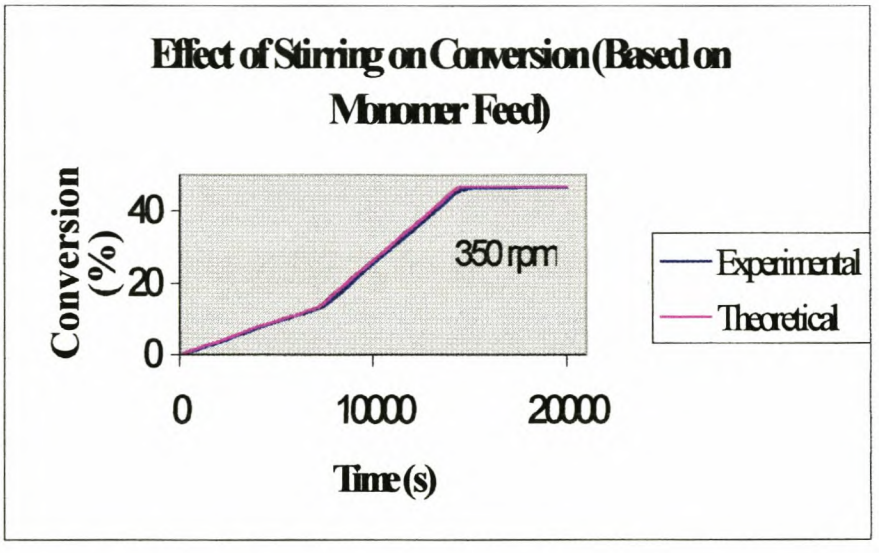

FIGURE F1-2 *Effect of stirring speed on conversion (350 rpm)*

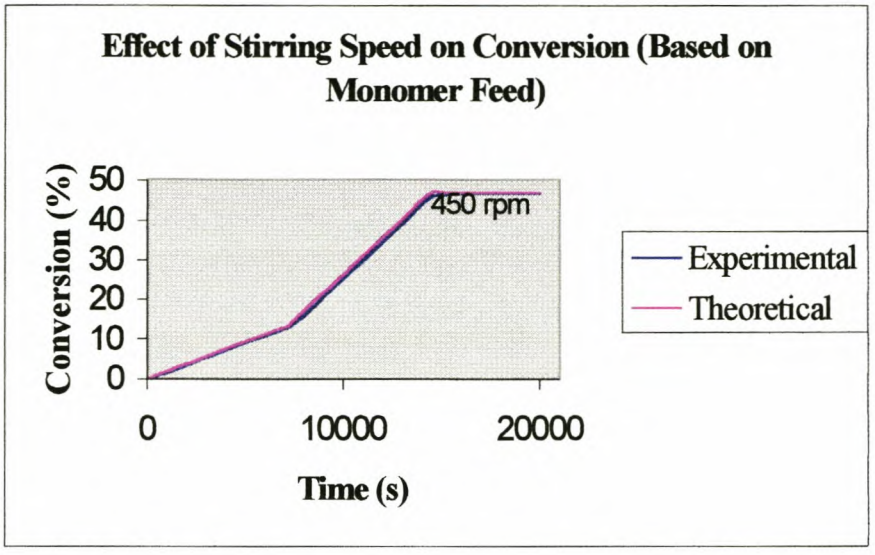

FIGURE F1-3 *Effect of stirring speed on conversion (450 rpm)*

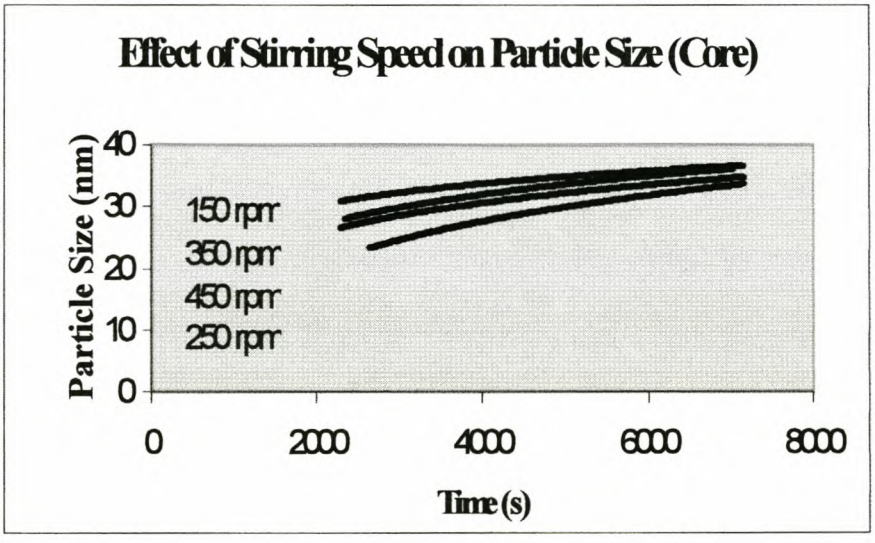

FIGURE F1-4 *Effect of stirring speed on particle size (150 – 450 rpm)*

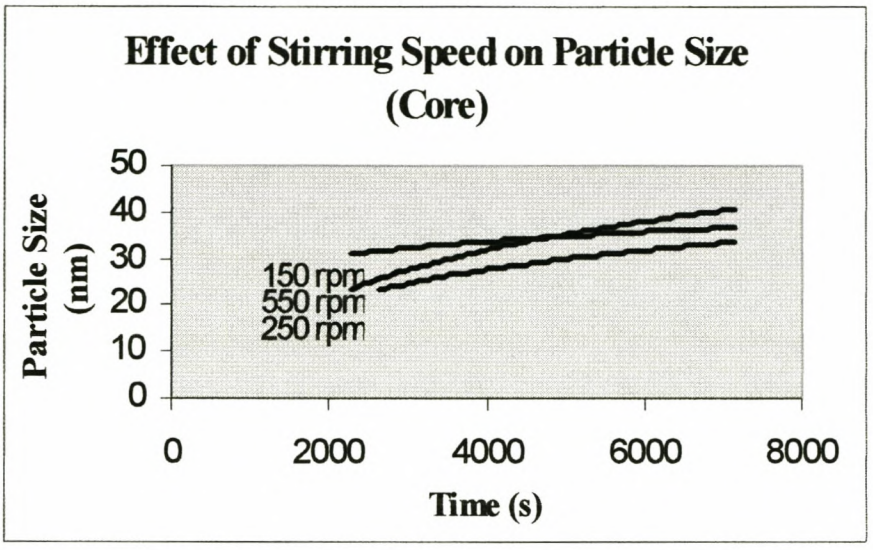

FIGURE F1-5 *Effect of stirring speed on particle size (150, 250 and 550 rpm)*

F2 EFFECT OF REACTION TEMPERATURE

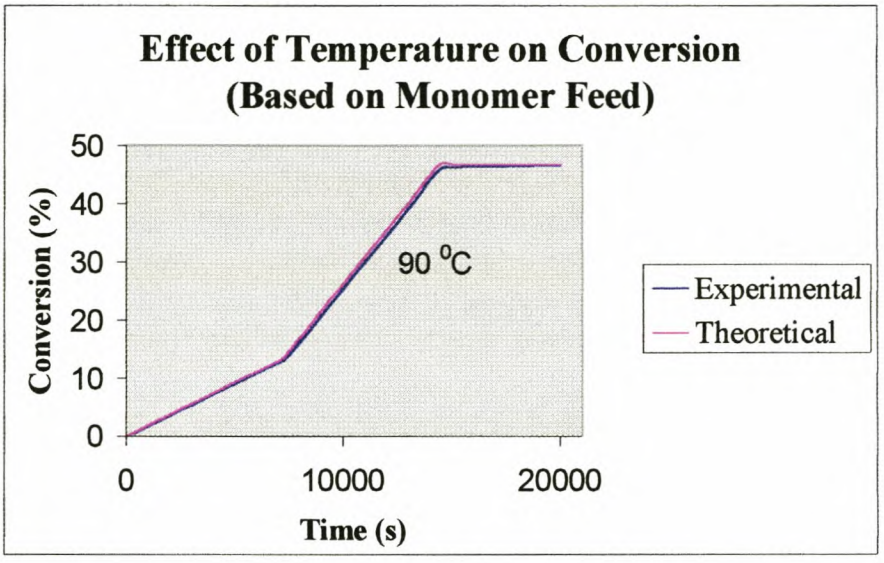

FIGURE F2-1 *Effect of temperature on conversion (90 ^{0}C)*

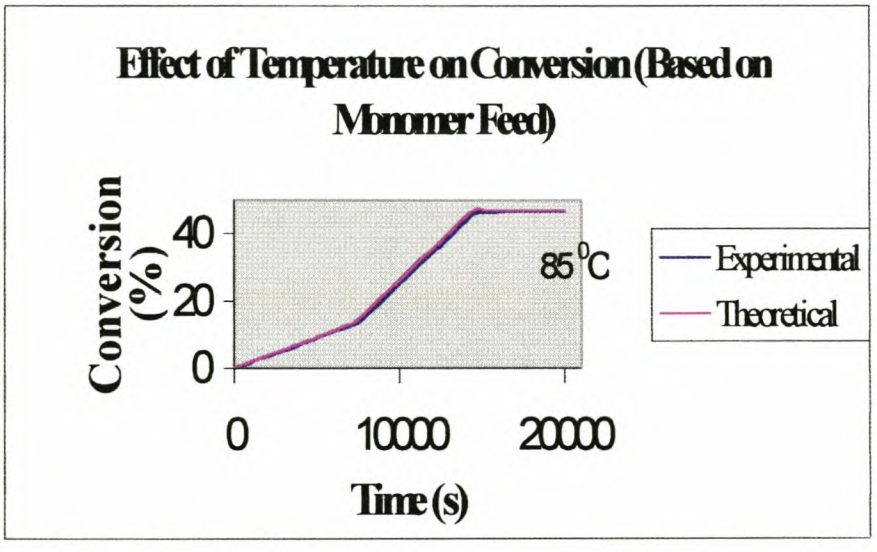

FIGURE F2-2 *Effect of temperature on conversion (85 ^{0}C)*

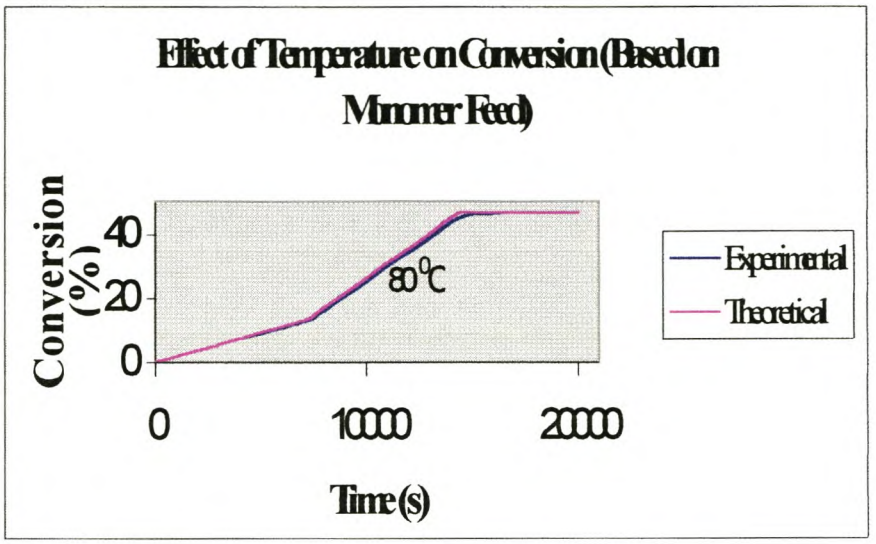

FIGURE F2-3 *Effect of temperature on conversion (80 ^{0}C)*

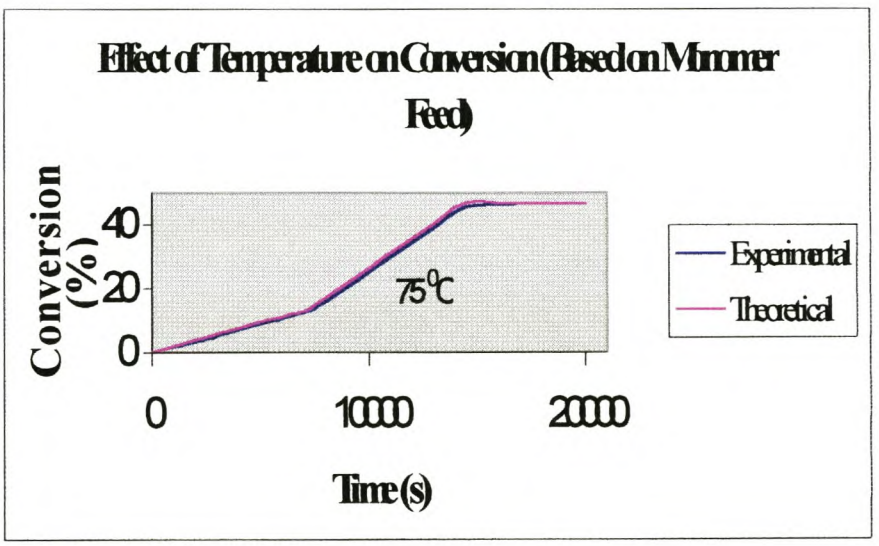

FIGURE F2-4 *Effect of temperature on conversion (75 ^{0}C)*

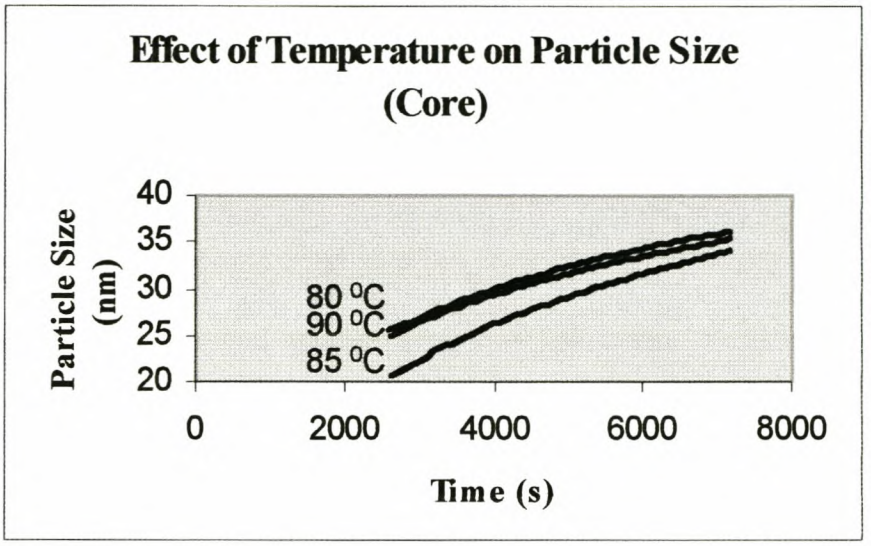

FIGURE F2-5 *Effect of temperature on particle size (Core)*

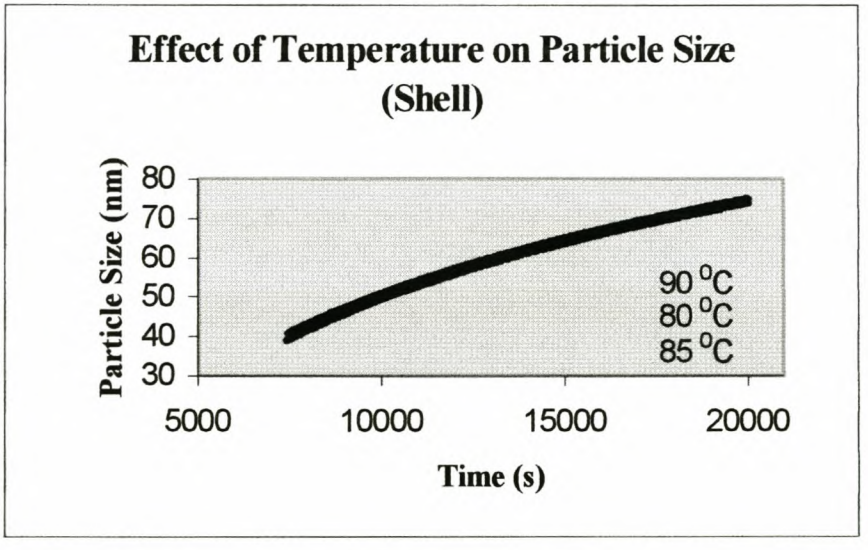

FIGURE F2-6 *Effect of temperature on particle size (Shell)*

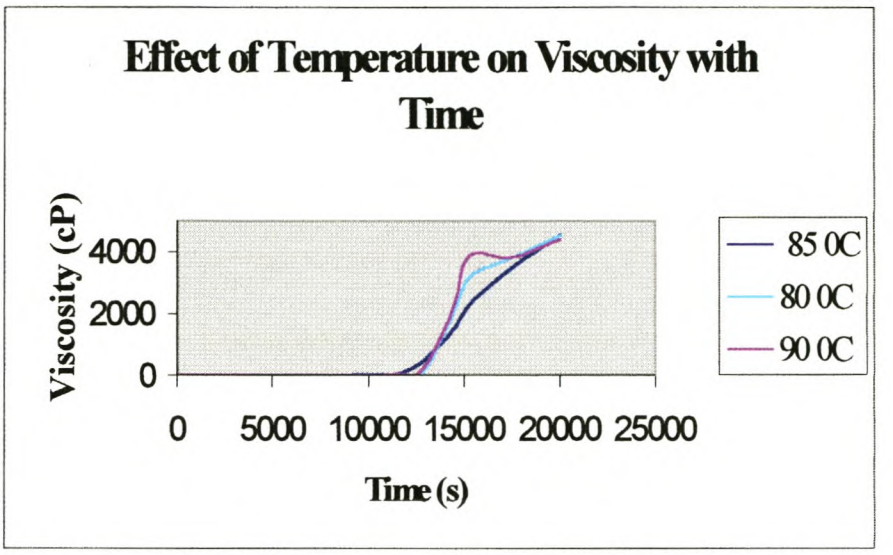

FIGURE F2-7 *Effect of temperature on viscosity (90 – 80 ^{0}C)*

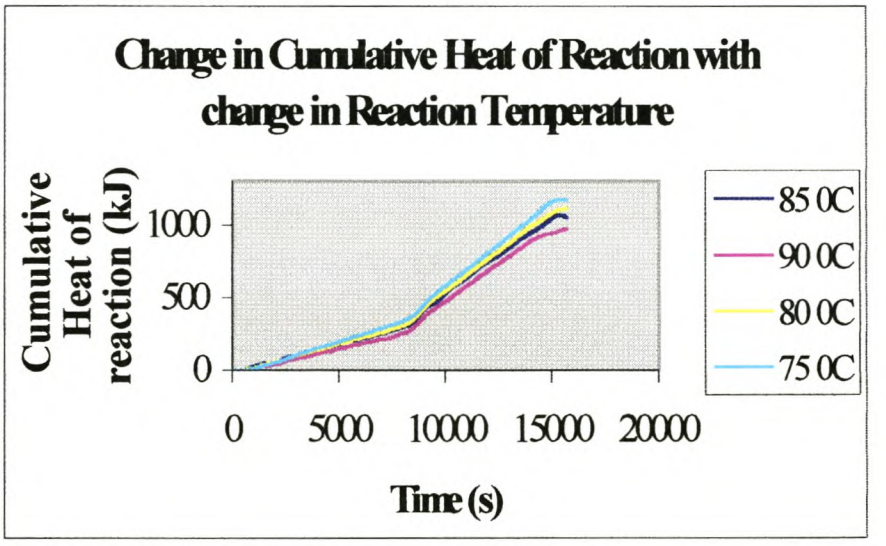

FIGURE F2-8 *Cumulative heat of reaction profiles (90 – 75 ^{0}C)*

F3 EFFECT OF REACTION TIME

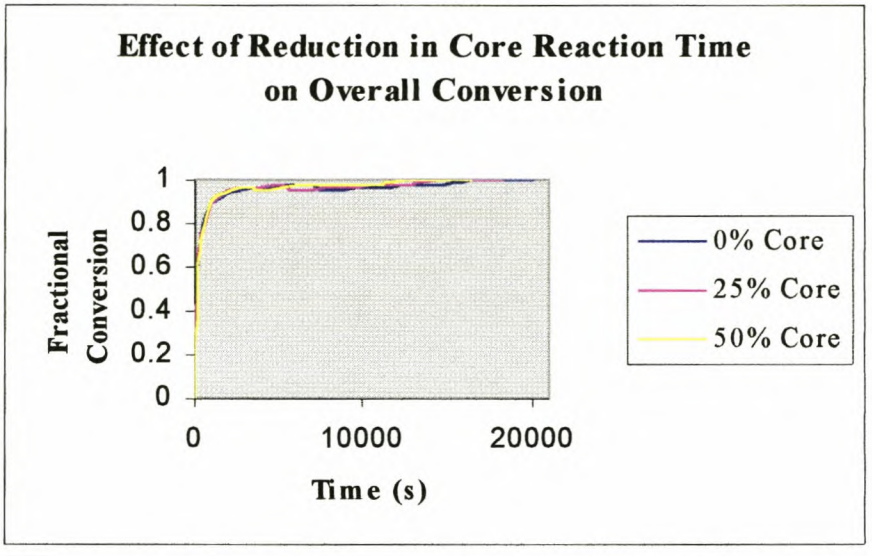

FIGURE F3-1 *Reduction of core reaction time on conversion (0 – 50%)*

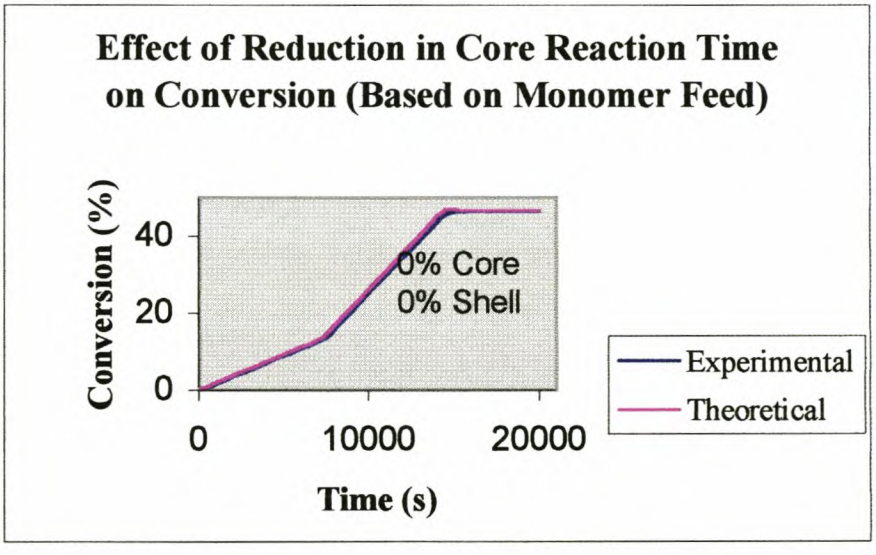

FIGURE F3-2 *Effect of reduction in core reaction time on conversion (0%)*

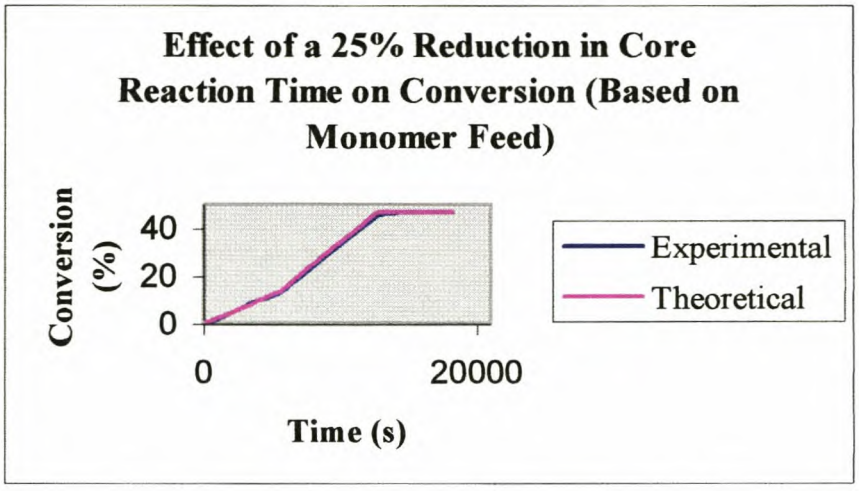

FIGURE F3-3 *Effect of reduction in core reaction time on conversion (25%)*

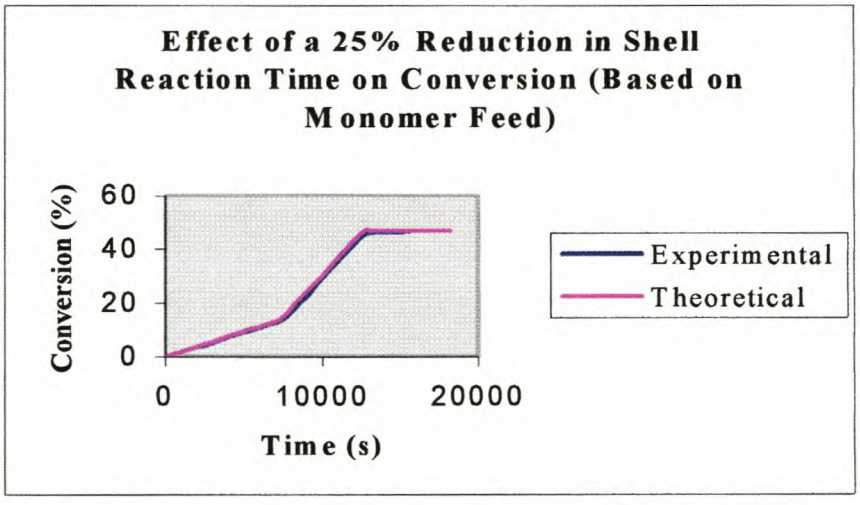

FIGURE F3-4 *Effect of reduction in shell reaction time on conversion (25%)*

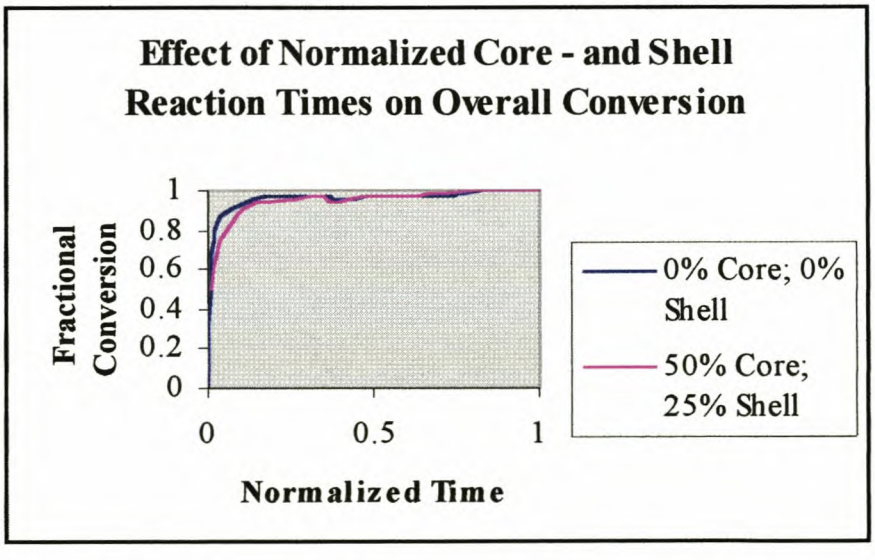

FIGURE F3-5 *Effect of reduction in core & shell reaction time on conversion*

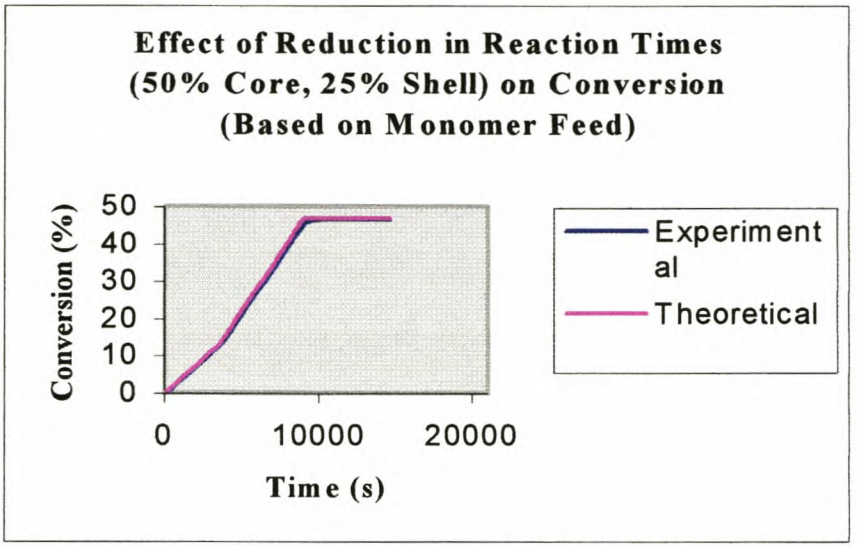

FIGURE F3-6 *Effect of reduction in core & shell reaction time on conversion*

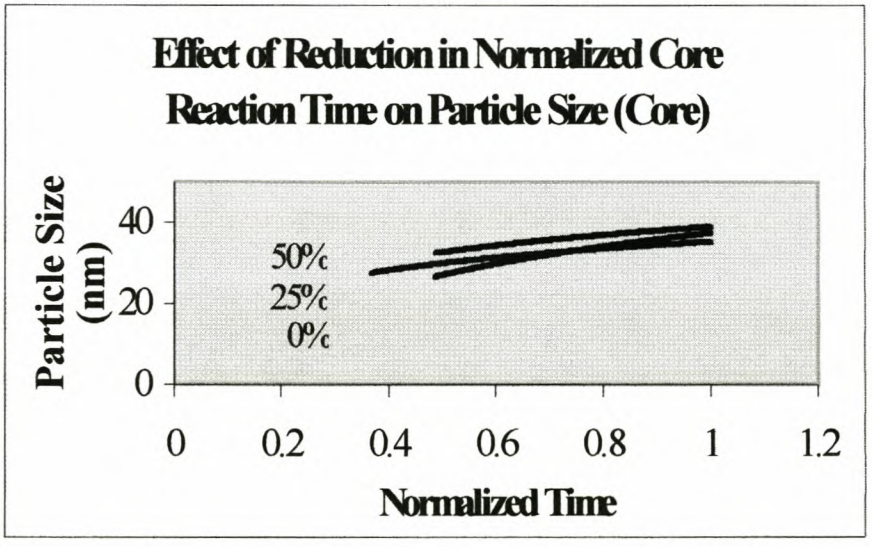

FIGURE F3-7 *Effect of reduction in core reaction time on particle size*

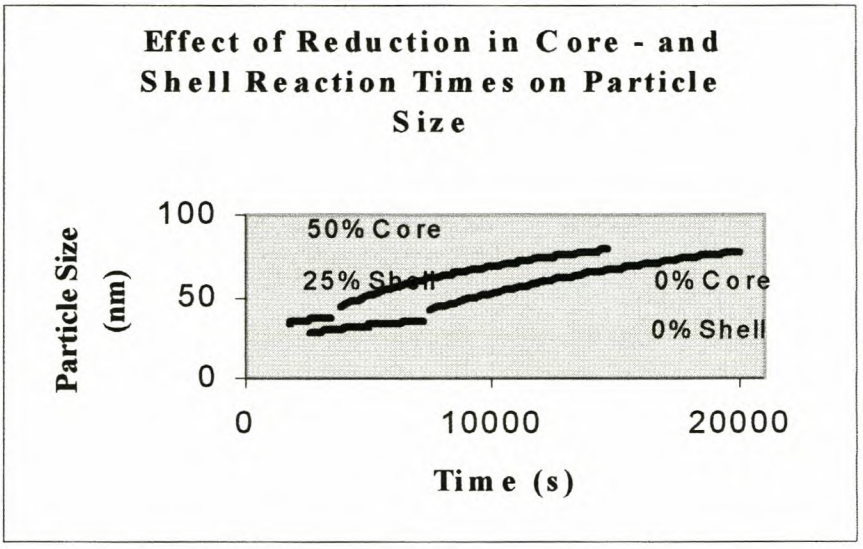

FIGURE F3-8 *Reduction in core & shell reaction time on particle size*

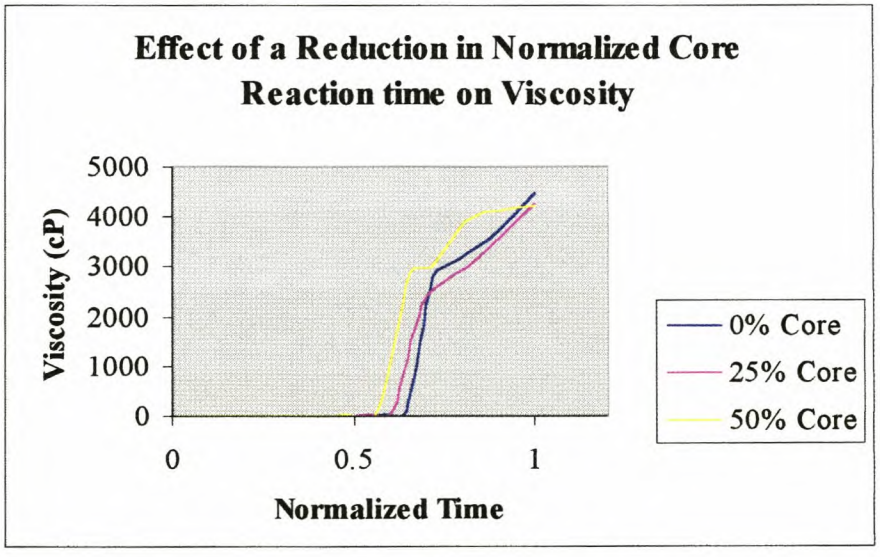

FIGURE F3-9 *Effect of reduction in reaction time on viscosity*

ADDENDUM G

NON-NEWTONIAN BEHAVIOUR OF NW 120

Table G1 *Typical non-Newtonian Flow behavior (Run 8)*

Time	Flow Index	Consistency Factor	Apparent Viscosity
7180	0.88	5.14	4.48
9980	0.86	15.58	13.28
11490	0.83	46.70	38.44
12740	0.41	754.50	384.45
14430	0.35	1931.20	1496.62
15290	0.29	5189.10	2313.53
17460	0.25	8191.40	3469.60
end	0.08	13078.80	4546.38

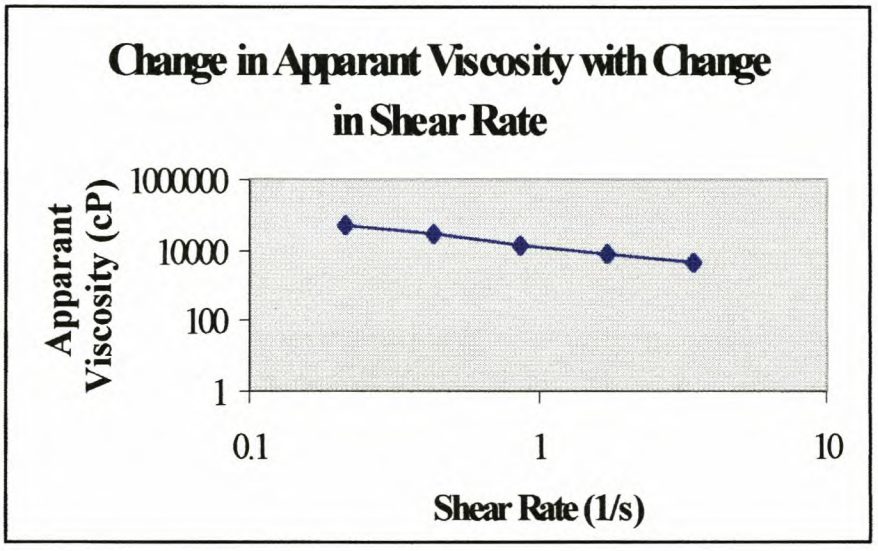

Figure G1 *Apparent viscosity plotted logarithmically against shear rate*